Investigation of Seepage Induced Internal Instability in Dense Gap-graded Soils under Complex States of Stress

Author:

FAHED GABER

A thesis submitted in fulfilment of the requirements for the degree of Doctor of Philosophy

The University of Sheffield

Faculty of Engineering

Department of Civil and Structural Engineering

April, 2021

Declaration of Authorship

I, FAHED GABER, declare that this thesis titled, "Investigation of Seepage Induced Internal Instability in Dense Gap-graded Soils under Complex States of Stress" and the work presented in it are my own. I confirm that this work was done wholly or mainly while in candidature for a research degree at The University of Sheffield, where I have quoted from the work of others, the source is always given, with the exception of such quotations, this thesis is entirely my own work and I have acknowledged all main sources of help.

Fahed Gaber

April 2021

Acknowledgements

I would like to express my sincere gratitude to my supervisor, Dr. Elisabeth Bowman, for her guidance through each stage of the process. I would also like to acknowledge all the technical assistance given to me by Mark Foster.

To my grandparents, parents, beloved wife, and kids, thank you for your support and belief in me. Without your tremendous understanding and encouragement in the past few years, it would be impossible for me to complete my PhD.

Finally, I would like to extend my thanks to all family members, friends, and colleagues for their support throughout my PhD.

Abstract

Investigation of Seepage Induced Internal Instability in Dense Gap-graded Soils under Complex States of Stress

by FAHED GABER

As well as providing and storing water and regulating flows, hydroelectric dams function as a sustainable and clean source of energy and energy storage. However, many large embankment dams were constructed before engineers had a sound understanding of filter design. As a result, seepage induced internal erosion of fines through the coarser matrix is the biggest challenge to existing embankment dams, such that nearly 50% of embankment dam stability problems are due to internal instability. The initiation and later effects of internal erosion depend on a combination of both geometric and hydromechanical criteria, with the complex stress states that the soil is subject to being one of the determinant factors.

The fact that internal erosion is stress state dependent has been recently recognised and reported. Therefore, this thesis aims to develop an understanding of the role that the critical stress condition plays in the erosion process. This research investigates the influence of varying different hydraulic gradient, fines content, stress path and finally, shearing rate. All erosion tests were conducted while changing the stress state (continuously shearing while eroding). To attain this objective, a triaxial permeameter was developed to study the effect of seepage flow through a dense gap-graded samples under controlled stress conditions. This enables the permeability to be examined, as well as the quantity of eroded soil. The triaxial permeameter is equipped with a pressurised water supply system, fine particles collection system and water collection system. The pore pressure differential across the sample, volume change, outflow rate of water and the mass of eroded particles were recorded during all tests. This allowed the hydro-mechanical parameters including hydraulic gradient, seepage velocity, permeability and the internal erosion rate to be determined.

The tests reveal that shearing under seepage results in fines being released continuously from the soil, with the rate of release depending on hydraulic gradient, initial fines content, stress path and shear strain developed. However, shear strain rate did not affect the rate of fines release. In all tests, permeability decreased under downward seepage, irrespective of fines loss. It was also concluded that the intensity of fines erosion could affect the shear strength of the soil.

Contents

List of Figures

xviii

List of Tables

List of Abbreviations

AS	Anisotropic Stress
CD	Consolidated Drained
CS	Critical State
CSL	Critical State Line
CU	Consolidated Undrained
DEM	Discrete Element Methods
DF	Downward Flow
ES	External Strain
HCHG	High Critical Hydraulic Gradient
IE	Internal Erosion
IS	Isotropic Stress
LCHG	Low Critical Hydraulic Gradient
LS	Local Strain
LVDT	Linear Variable Differential Transformer
NMT	Numerical Modelling Testing
PPT	Pore-Water Pressure Transducer
PSD	Particle Size Distribution
SS	Stable Sample
UF	Upward Flow
US	Unstable Sample
UU	Unconsolidated Undrained

List of Symbols

m_{fa}	Accumulated erosion mass	g
m_{fap}	Accumulated erosion percent	%
ϵ_a	Axial strain	%
D'	Coarse fraction	%
m_{ci}	Coarse particles initial mass	g
A_c	Corrected area	mm^2
L_c	Corrected length	mm
S^*	Critical fines content	%
i_c	Critical hydraulic gradient	-
ρ_w	Density of water	g/cm^3
σ'_f	Effective stress level in the fines content	kPa
h_2	Filtering between the coarse and fine particles	-
d'	Fine fraction	%
m_{fi}	Fine particles initial mass	g
F	Fines composition	%
α	Fines stress reduction factor	-
i	Hydraulic gradients	-
L_i	Initial length	mm
D_{Ri}	Initial relative density	%
e_0	Initial void ratio	-
H	Mass fraction exists between diameter D and $4D$	%

q_{max}	Max deviatoric stress	kPa
ρ_{max}	Maximum density	g/cm^3
e_{max}	Maximum void ration	-
p'	Mean effective stress	kPa
p'_{qmax}	Mean effective stress at q_{max}	kPa
i_m	Mean hydraulic gradient	-
$\overline{\sigma_{vm}}'$	Mean normalised overburden stress	kPa
ρ_{min}	Minimum density	g/cm^3
e_{min}	Minimum void ration	-
q_n	Normalised deviatoric stress	kPa
d_x	Percentage passing a given grain size by mass	%
k	Permeability	m/s
D_r	Relative density	%
K_0	Rest earth pressure	kPa
v_D	Seepage flow Darcy's velocity	mm/s
v_T	Seepage flow true velocity	mm/s
v	Seepage flow velocity	mm/s
ϵ_s	Shear strain	%
h_1	Slope of the PSD for coarse particles	-
G_s	Specific gravity	-
p	Total mean stress	kPa
γ'	Unit weight of soil	kN/m^3
γ_w	Unit weight of water	kN/m^3
σ'_v	Vertical effective overburden stress	kPa
e	Void ratio	-
ϵ_v	Volumetric strain	%

Half of the knowledge is (having ability) to say I don't know - Imam Ali (AS)

Chapter 1

Introduction

1.1 Motivation

As resources are shifting towards more environmentally-friendly construction materials and natural solutions, dam engineering has to focus less on the traditional concrete gravity, arch, or buttress dams, and more towards embankment dams produced of entirely natural or engineered soil (Bonelli, 2013).

Research in embankment dams is still lagging behind, especially considering that the problems faced by embankment dams are often times of very a different nature than those faced by other forms of dam construction (Chang and Zhang, 2011). Internal erosion is a problem that is virtually non-existent for all types of concrete dams – this being one of the main reasons why in comparison to concrete dam construction, there exists much less systematised knowledge about embankment dam construction and maintenance. Nevertheless, most of the embankment dams built to date have as their most frequent cause of failure processes involving internal erosion (Bonelli, 2013).

Internal erosion is a very complex phenomenon, involving a multitude of factors, from the fines content of the soil, to the stress state present. This change in stress state (non-zero shearing rate) could be experienced during an earthquake or if the geotechnical structure was altered externally by excavation, wall height increase, or changes in water level.

In order to develop a framework capable of better dealing with the phenomena that embankment dams are exposed to during their lifetime, it is important to develop a means of analysing the soil in laboratory conditions which mirrors as closely as possible the conditions to be found in-situ (Chang et al., 2012).

Internal erosion can cause a variety of problems for an embankment dam, such as loss of fines, change in the soil skeleton structure, change in porosity, settlement, differential movement, and even structural failure. Settlement in particular is problematic for an embankment dam as it decreases the maximum water level it can hold and thus makes the dam more prone to overtopping. In particular, settlement which occurs locally in only one region of the dam, often known as differential settlement, can pose additional structural stability issues. For this reason, the geotechnical aspects of the soil have to be better understood so as to enable the design and maintenance of a wide variety of embankment dams which can fulfil local needs safely.

Internal instability is caused by internal erosion which is particularly dangerous and widespread for embankment dams. A large share of the currently existent embankment dams are susceptible to internal instability(Kenney

and Lau, 1985; Bonelli, 2013) , and about 50% of embankment dam failures worldwide are due to such instability. It is necessary to understand the conditions under which these dams may actually become unstable in order to prevent failure incidents that can lead to the destruction of nearby infrastructure or loss of lives (Deutsches-Talsperrenkomitee, 2007).

To achieve maximum stability in geotechnical structures, it is a common practice to aim for maximum in-situ density. Therefore this category is of importance in investigating internal erosion. For the purpose of this research, it was decided to investigate dense samples attempting to replicate in-situ density as closely as possible.

This research focuses on suffusion and suffosion, and in particular, on the role suffosion may have in affecting embankment dams. This study proposes to investigate the commencement and progression of suffosion in gap-graded soils and to develop a triaxial permeameter apparatus capable of assessing the effects of the complex stress states often present in the soil of dams. This knowledge will be used to investigate the effects of internal erosion with the aim of developing a better understanding of the geotechnical behaviour of embankment dams prone to internal instability.

The main motivation of this thesis is to answer the following set of questions:

- What is the role of shearing rate and stress path on internal erosion progression as determined by loss of fines?

- How does the initial fines content affect the outcome of mass loss during erosion and shearing?

- How does internal erosion relate to hydraulic gradient during shearing?

- How does disturbance of the soil fabric under monotonic shearing result in release and erosion of fine particles?

- How does the progression of internal erosion affect permeability?

- Is there a relationship between loss of fines and shear strength?

1.2   Aim and objectives

The aim of this research is to examine the role of seepage flow on internal instability in dense gap-graded soils under complex states of stress. Based on the aim, several objectives were set out as follows:

- To develop a triaxial permeameter to investigate the internal erosion in gap-graded soil under complex stress states.

- To study the behaviour of soil erosion while changing the stress state (continuously shearing), i.e. propensity to erode, volume loss of fines, permeability, and soil strength.

- To investigate soil erosion behaviour under complex stress states, i.e. using stress path testing (changing radial and axial stress leading to non-standard stress paths in q-p space) and using different shear rate.

- To investigate the influence of different seepage flow and initial fines content on internal erosion progression.

- To use all findings from this research to develop an understanding of the geotechnical behaviour of embankment dams more generally, prone to internal instability.

1.3   The novelty of the research

The novelty of the research presented in this work is centred around developing an understanding of the role the stress condition plays in the erosion process in embankment dams. Figure 1.1 illustration of the factors affecting internal erosion. It shows the three factors needed to produce internal erosion (at the nexus of the overlapping circles), according to Garner and Fannin (2010) which is discussed further in Chapter 2.

The novelty of the research lies in the following facts: There are many dams around the world which are deemed to be unstable based on an investigation of their material susceptibility (bottom right circle) and hydraulic conditions (bottom left circle), therefore it is necessary to uncover what is the future of such dams. Critical stress is a relatively neglected area of research (top circle) when it comes to internal erosion, with very little research performed to date.
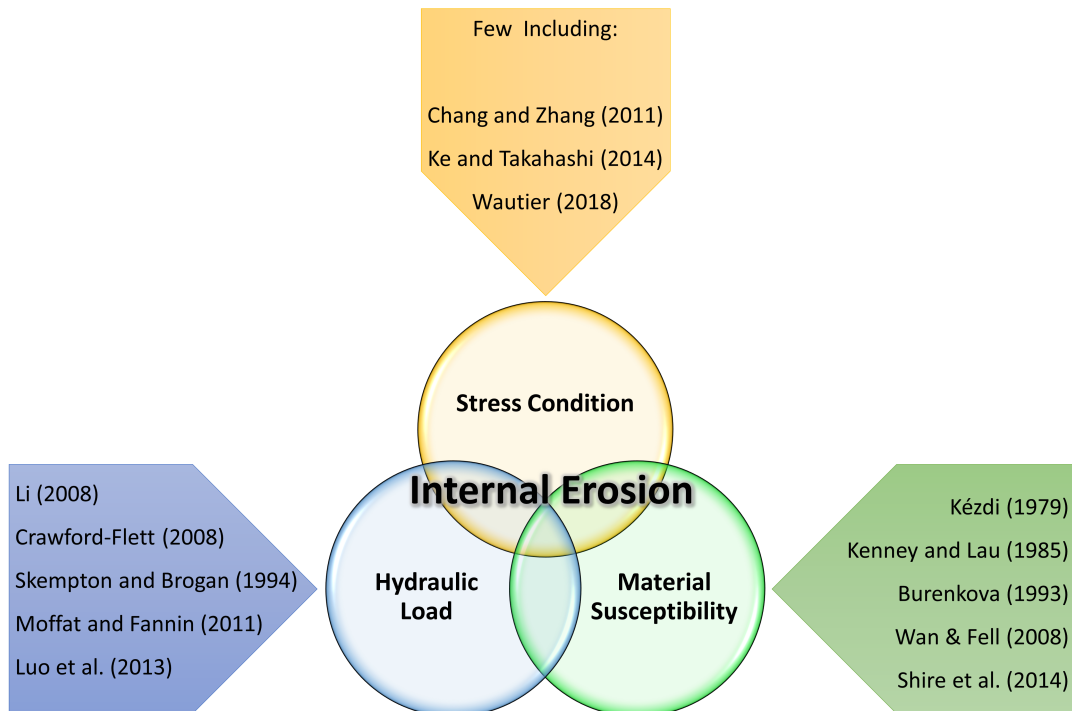
FIGURE 1.1: Illustration of the factors affecting internal erosion
modified after Garner and Fannin (2010)

For this reason, this project will improve on previous triaxial erosion test-ing apparatuses in order to study different materials under complex states of stress.

For the first time, the internal erosion process was studied under three dif-ferent stress paths (changing radial and axial stress leading to non-standard stress paths in q-p space). As well as studying the influence of the shear rate on internal erosion by shearing the testing samples using three differ-ent axial displacement rates.

This can model the change in stress state under constant fluid flow in a geotechnical structure, which could be experienced during an earthquake

or if the geotechnical structure was altered (loaded/unloaded) externally via, for example, excavation or wall height increase which applies to tailings dams (since they are built continuously upwards). This change in load scenario could also occur due to changes in water level behind the geotechnical structure. The loading experienced by the geotechnical structure can be cyclic or monotonic loading, for the purpose of this research, only monotonic loading was used.

This will enable a better understanding of internal erosion behaviour and may shed light on the reason for the failure of some dams and the ongoing stability of others.

1.4   Thesis layout

This thesis comprises eight chapters. In Chapter 1, the motivation and the novelty of this study were introduced, including the main aim and objectives.

Chapter 2 reviews past and recent research on internal instability in embankment dams, including geometric and hydromechanical constraints on this field. Moreover, a comparison of experimental investigations on internal erosion is included.

Chapter 3, provides a description of the material used, characterisation tests, the development of the triaxial permeameter, the testing program and the testing procedures.

Chapter 4 discusses a series of tests to qualify and quantify the influence of the hydraulic gradient on the progression of internal erosion of a dense gap graded soil.

Chapter 5, presents the second set of tests performed to study the influence of the initial fines content on the onset and progression of internal erosion under a constant aimed-for initial hydraulic gradient of 10.

In Chapter 6, the third set of tests is presented to investigate the effect of the stress path on the onset and the progression of internal erosion on gap-graded soil. The experimental tests were carried out on six samples of gap-graded soil under three different stress paths while shearing.

Chapter 7 examines the influence of different shearing rates on the internal erosion behaviour of different samples of dense gap-graded soil.

Chapter 8 provides discussion and conclusions drawn from this research and recommendations for further research.

Chapter 2

Literature Review

2.1 Internal instability in embankment dams

2.1.1 Definitions

The following definitions are given with respect to embankment dams, although may be applied to other hydro-geotechnical structures such as levees, dykes and retaining walls.

Internal instability

A term used to describe a soil element's potential for loss of fine particles as a result of suffusion or suffosion (Kenney and Lau, 1985; Moffat, 2005; Crawford-Flett, 2014).

Internal erosion

In geotechnical structures, internal erosion refers to fine particles loss. There is a series of different processes which can initiate internal erosion, the

most common being suffusion, concentrated leak erosion, backward erosion, and contact erosion (Deutsches-Talsperrenkomitee, 2007; Bonelli, 2013).

Suffusion

Sometimes separated into internal suffusion and external suffusion. Internal suffusion is the movement of particles within the soil skeleton (also called fines migration), which may cause changes in hydraulic conductivity but no change in the overall particle size distribution of the soil (Crawford-Flett, 2014). External suffusion involves fine particles being transported from the soil's coarse particle matrix to the outside of the soil block (Crawford-Flett, 2014). Recently theorists have assigned external suffusion to represent solely the flow of fine particles from a coarse particle matrix only if there are no structural changes (no total volume change) in the soil skeleton due to this process (Moffat and Fannin, 2011).

Suffosion

Researchers have identified suffosion as being the same process as external suffusion, with the sole difference that in suffosion the soil skeleton changes or collapses, leading to a reduction in total soil element volume (Moffat and Fannin, 2011). This is likely to occur when the skeleton deformation critical hydraulic gradient is reached. Suffosion usually occurs when the soil is overfilled with fines, i.e. finer particles are partially or fully in contact with coarse particles and provide support to them. Where suffusion usually occurs when the soil is underfilled, i.e. finer particles are fully confined within voids between coarse particles and provide no support to the coarse particles.

Contact erosion

The phenomenon of erosion that happens in the base soil at the interface between the base and filter, illustrated in Figure 2.1.

Concentrated leak erosion

The phenomenon that can occur once a crack is formed within an embankment dam or its foundation. The crack could originate from a variety of processes, such as differential settlement during or after construction, freeze-thaw damage, hydraulic fracture, or desiccation (Deutsches-Talsperrenkomitee, 2007; Bonelli, 2013). Once the crack is formed, it can be expanded by seeping water to form a pipe. The process can be self-limiting if any one of the following conditions holds true: the soil doesn't have adequate strength parameters to hold the crack/pipe open, the hydraulic gradient present is limited, adequate dam filters are present to prevent erosion, seepage causes the soil to swell, thereby closing the crack (Bonelli, 2013).

Backward erosion

A form of erosion, illustrated in Figures 2.2, which begins at the point where seepage flow exits the dam, and gradually moves backward as more particles are eroded (Chang et al., 2012). Backward erosion is often associated with piping (Bonelli, 2013; Chang et al., 2012).

Backward erosion piping

A phenomenon happening when an erosion pipe forms, starting at the free surface. It occurs most commonly underneath an existing embankment dam through its foundation (Deutsches-Talsperrenkomitee, 2007; Bonelli, 2013).

Piping

A term used to describe a 'pipe' that forms in a local area of the dam where internal erosion occurs (Bonelli, 2013). Piping is often associated with other phenomena, in particular with suffusion (Ke and Takahashi, 2014).

Heave

A phenomenon which occurs when the effective weight of the soil becomes negligible due to rising pore water pressures within the soil (Bonelli, 2013). This causes the seepage flow to move the surface of the soil in its direction of flow. The soil also loses its structure in the process, i.e. particles lose contact with each other, and so the phenomenon can also be known as liquefaction, although this term is more often associated with seismic shaking or shearing collapse of loose cohesionless soil (Deutsches-Talsperrenkomitee, 2007; Crawford-Flett, 2014; Bonelli, 2013).
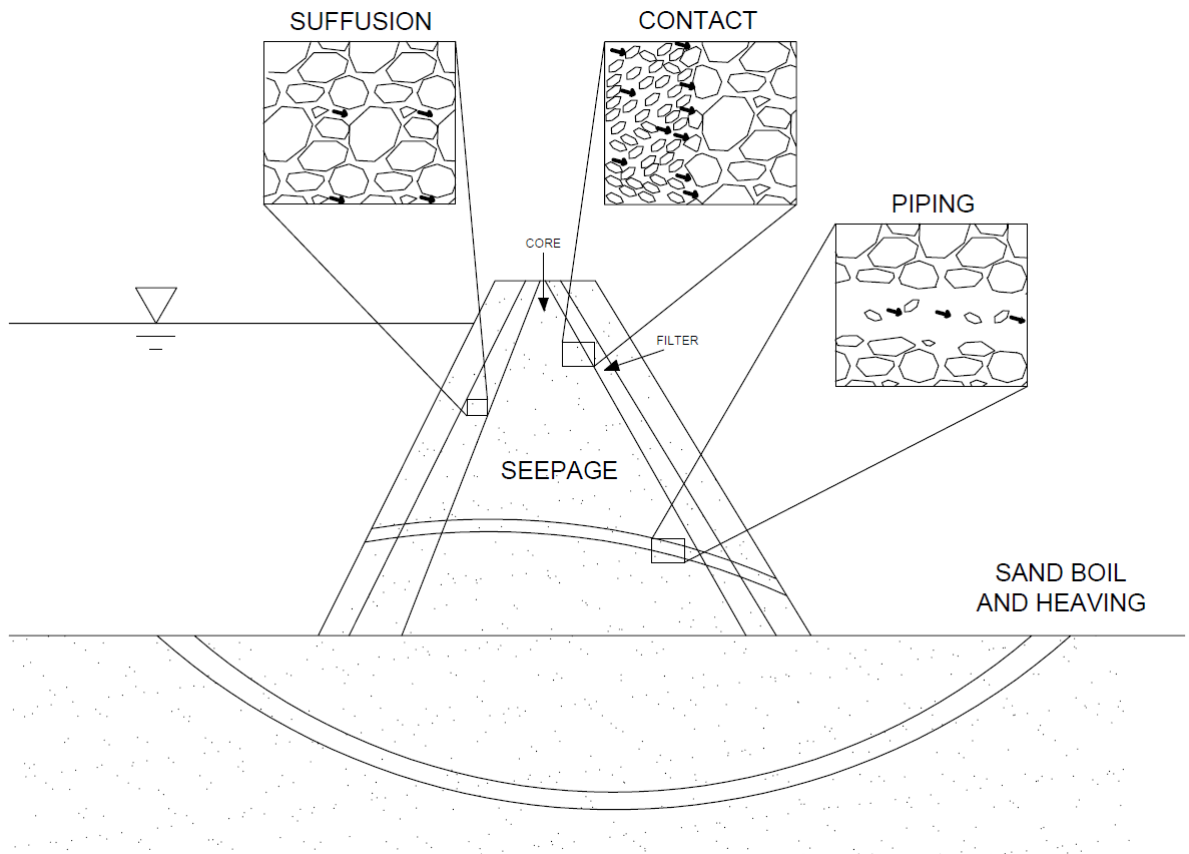
FIGURE 2.1: An illustration of erosion in earthen embankment
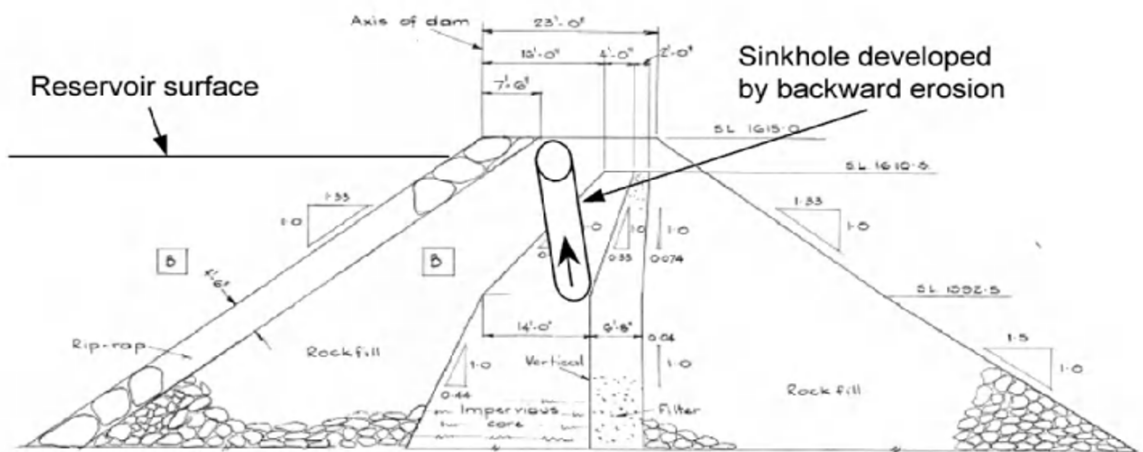
FIGURE 2.2: Backward Erosion forming a sinkhole; from Bonelli (2013)

2.1.2   Modes of failure due to internal instability

The primary modes of failure associated with internal instability are due to the effects of external suffusion and suffosion (Bonelli, 2013). Indeed, the two processes are linked to each other, and in most situations, a dam can undergo both of them. Generally, a classification of the progression of this erosion process is shown below.

Stage 1: No loss of fines

The embankment dam is in a stable soil configuration, with no fine particles being eroded (Deutsches-Talsperrenkomitee, 2007; Bonelli, 2013). The soil forming the dam or its filter, due to its geometric constraints (to be discussed in greater detail later), is prone to internal instability.

Stage 2: Initiation of loss of fines

A factor such as increasing hydraulic gradient due to an increased reservoir level behind the dam, or increasing deviatoric stress initiates the erosion process (Chang et al., 2012). This stage is associated with increasing permeability, which often results in higher seepage velocities and may therefore increase internal erosion even further (Bonelli, 2013; Chang and Zhang, 2013).

Stage 3: Massive loss of fines and change of structure (suffosion)

If either deviatoric stress or hydraulic gradient increase such that the skeleton-deformation hydraulic gradient is reached, then a massive loss of fine particles , coupled with a large increase in permeability, settlement and deformation and a collapse of the soil-skeleton will occur (Chang et al., 2012; Bonelli, 2013). This stage terminates very quickly, and is generally followed by a re-organisation of the soil under a different matrix, with an altered voids ratio. This newer matrix, in theory, has its own skeleton-deformation hydraulic gradient, which when reached will cause another re-arrangement (Luo et al., 2013; Chang and Zhang, 2013). Nevertheless, it is possible for another stage to happen if the migration paths of the fine particles are clogged or blocked.

Stage 4: Hydraulic fracture

Assuming that the remaining fine particles are clogged up and cannot easily escape the soil-skeleton, increases in hydraulic gradient may lead to hydraulic fracturing between the coarse particles due to the rising pressure inside the soil, and thus failure of the embankment dam (Bonelli, 2013).

However – it must be noted that a dam is likely to already have failed once stage 3 is reached. The most likely causes of failure in such a scenario would be very large settlements in the embankment dam as well as weakening of its structure which makes the dam a risk to operate. Settlement due to suffosion is indeed a common cause of failure according to the embankment dam literature. Therefore, it should be aimed in its

design that a dam never reaches the third stage under the stress and hydraulic gradient conditions it is likely to experience in its lifetime.

Another important risk of suffosion and suffusion for a dam occurs when its filter is prone to internal instability. If the filter starts to lose fine particles, then the core of the dam often becomes exposed to erosion as well. This loss of fine particles can continue, thereby causing large settlements and ultimately undermining the entire earth structure (Bonelli, 2013). Filter material is therefore key to ensure the structural integrity of an embankment dam.

2.1.3   Requirements in embankment dams to prevent suffosion

There is a series of conditions that can be looked for to ensure that dams are internally stable and thus not prone to suffosion. The first order condition is that the fines content in the filter is greater than 35% (Skempton and Brogan, 1994). If this is the case, all the pores are filled and the structural matrix integrates the fine particles, thereby making it more difficult for them to be removed. The second order condition involves geometrical constraints – primarily the particle size distribution curve of the soils. If the soil is not gap-graded then the probability is that it is internally stable (Kézdi, 1979; Kenney and Lau, 1986).

If neither of these two conditions are met, then the soil is potentially unstable. However, for instability to actually occur it is necessary that the soil be exposed to a critical hydraulic gradient due to seepage flow

(Bonelli, 2013; Chang and Zhang, 2013). The value of this critical hydraulic gradient required for erosion to happen depends on a several factors, the most important being stress state (including stress level and whether isotropic or deviatoric), hydraulic load or water level behind the dam, and relative density (Crawford-Flett, 2014; Chang et al., 2012; Bonelli, 2013)). In general, lower relative density and higher deviatoric stress will lead to lower critical hydraulic gradients (Chang and Zhang, 2013).

This chapter will continue with an investigation of the aforementioned conditions in order to enable an understanding of the behaviour of soils prone to internal instability. Further investigations along this line will yield a better understanding of cohesionless soil behaviour under internal erosion, thereby allowing an assessment of the settlement potential of such soil as part of an embankment dam.

2.2 Geometric constraints on internal erosion

A constraint on internal erosion, for the purposes of this work, will be defined as a physical mechanism capable of influencing the likelihood of internal erosion on the geotechnical and hydraulic integrity of an embankment dam (Kenney and Lau, 1985; Moffat, 2005). Constraints determine the conditions under which fine particles from an embankment's core material or filter may be prevented from, susceptible to, or caused to migrate. According to Moffat (2005), constraints on the internal erosion of dams can be separated in two different categories: geometric constraints, and hydromechanical constraints.

The former constraints include the composition, porosity and particle size distribution of the soil, whereas the latter encompass effects due hydraulic gradient and velocity of seepage flow, as well as effective stress level in the fines content(σ'_f) (Kenney and Lau, 1985; Moffat, 2005; Moffat and Fannin, 2011). In general, the geometric constraints will determine whether particles can move within the soil matrix (which is, at least theoretically, influenced by whether the pores of the primary matrix are sufficiently large for the fine particles to move through) while hydromechanical constraints will determine the flow velocity required to initiate erosion of fine particles (Moffat, 2005; Moffat and Fannin, 2011).

Before investigating the methods commonly used to approximate the geometric constraints of the soil from its particle size distribution curve, it is necessary to explore the macro-conditions that govern the use of these methods. These conditions have to do primarily with the fines fraction by mass out of the entire soil composition, which largely determines the type of soil skeleton formed, its porosity, and how the internal stresses are carried (Skempton and Brogan, 1994; Shire et al., 2014).

The fines composition (*F*) is an important factor to understand internal erosion because it determines how loads are transmitted through the soil. Skempton and Brogan (1994) have defined a critical fines content S^* at, or above which the internal voids between the coarse particles are filled by fine particles. At fines compositions lower than S^*, fine particles are generally held completely within voids between coarse particles and offer no support in carrying the loads. The critical fines content, S^* was calculated to be 24% for densely packed specimens and 29% for loosely packed specimens based on the permeameter seepage studies performed by Skempton

and Brogan (1994). It must be noted that this range seems very general and would change with material, seepage flow and stress condition.

The other important fines content limit is 35%, which represents the fines composition when coarse particles are completely separated from one another, S_{max} (Shire et al., 2014).

As noted from the bottom diagram in Figure 2.3, increasing the fines content up to S^* decreases the porosity as fine particles are used to fill the voids that exist between the coarse ones. Thus, if the fines content is lower than S^* and the geometric criteria indicates that the pore network is sufficiently large for fine particles to pass through, then the soil is internally unstable Shire et al. (2014). If the fines content is larger than S_{max}, the matrix is completely filled and fine particles have no paths to escape and so the soil is internally stable, Table 2.1. If the fines content is between S^* and S_{max}, then it may be prone to instability, but increasing relative density will improve stability (Shire et al., 2014).
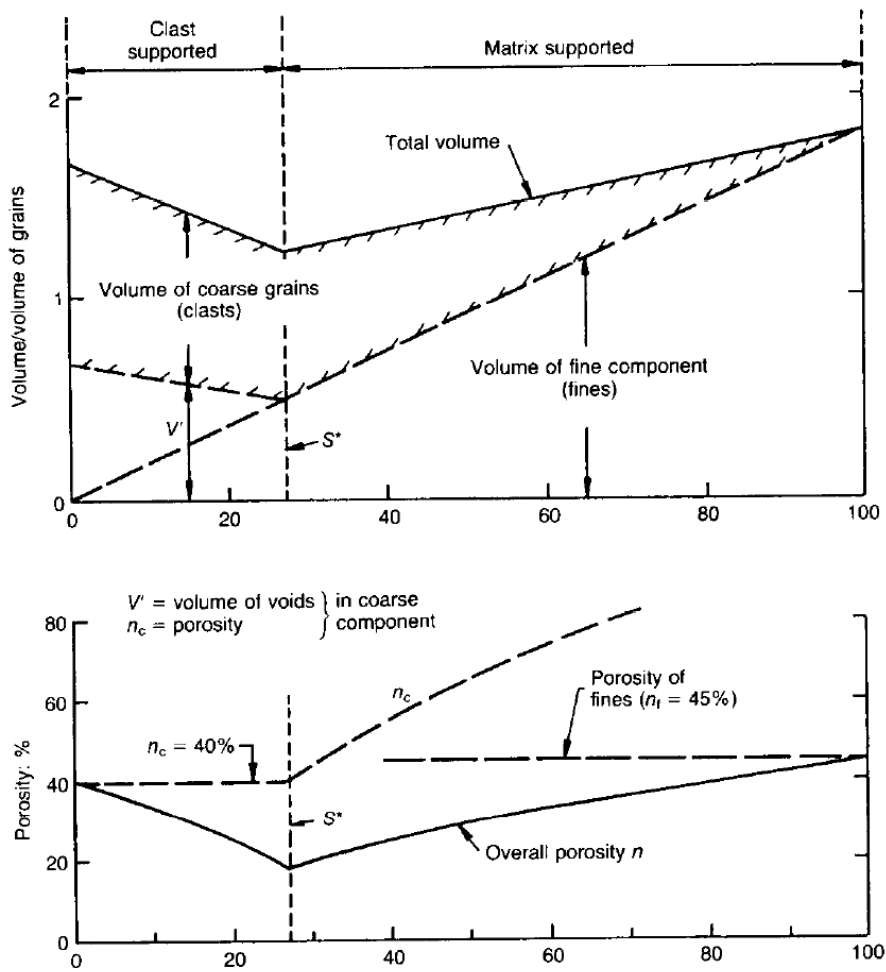
FIGURE 2.3: Illustration of the effect of fines content on the structure of soil and its porosity; from Skempton and Brogan (1994)

Other authors have attempted to separate soil skeletons into different classes in order to further clarify the difference between each. Thevanayagam (1998) have classified particles in four different classes, as illustrated in Table 2.1; as cited in Shire et al. (2014).

TABLE 2.1: Different classes of soil skeleton cases as classified by
Thevanayagam (1998); images from Shire et al. (2014).

Case	Description	Illustration
1 **and** **3** **(F<S$_f$)**	**Case 1:** -Fine particles carry no load/stress -Fine particles are trapped in pores -Prone to internal instability. **Case 3:** -Most fine particles are trapped in pores -some fine particles separate coarse particles from one another and reduce their load carrying ability -Prone to internal instability.	
2 **(F<S$_f$)**	**Case 2:** -Fine particles carry limited load/stress -Prone to internal instability, but less so than case 1 and 3.	
4(a) **and** **4(b)** **(F>S$_{max}$)**	**Case 4 (a):** -Both type of particles carry loads/stresses -Internally stable, but may be prone to piping **Case 4 (b):** -Soil skeleton created by fine particles governs strength -Internally stable, but may be prone to piping	

Thus, for soils with fines content below 35%, it is necessary to determine whether the pore sizes in the network are sufficiently large to allow the migration of fine particles, which, under the right hydromechanical conditions, can cause erosion. This is done by investigating geometric constraints based on the particle size distribution of the soil, which governs the behaviour of the pore network. This review will analyse the three most common methods used in practice for investigating whether a filter is stable or unstable, and their developments. These are the Kenney and Lau (1985), the Kézdi (1979) and the Burenkova (1993). These methods remain the most widely used, however, there have been recent improvements that have occurred in their usage, which will also be discussed. Such improvements do appear to offer better predictive power, and certainly offer a more thorough variety in the assessment of internal instability (Li and Fannin, 2008).

2.2.1   Kenney and Lau method

Kenney and Lau (1985) describes the primary geometrical constraint in granular filter materials to be given by the particle size distribution, PSD of the soil. The method categorises the granular material as being composed of three different elements: the primary matrix, which is responsible for carrying stresses and which is generally stable and not prone to movement, the loose particles present which are prone to being transported in the soil skeleton, and the constrictions generated by the presence of different size particles which can prevent the aforementioned particle transportation (Kenney and Lau, 1985).

This makes it evident that cohesionless filters which are gap-graded, such

that there is an absence of sufficient particles of the size required to block traveling paths of fines in-between the much larger coarse particles, are more likely to be internally unstable. Indeed this hypothesis has been verified by a few research studies (Kenney and Lau, 1985; Skempton and Brogan, 1994). This is also supported by Kenney and Lau (1985) calculations for compacted filter material which indicate that uniformly graded materials have a higher relative mass content of maximum loose particles (30%) than widely-graded materials (20% maximum loose particles).

Generally, according to Kenney and Lau (1985), stable filters will be characterised by particle displacement paths smaller than the thickness of the filter. The paper then provides both an empirical and a theoretical framework for assessing the internal stability of a filter material based on these considerations.

Empirically, their proposal is a seepage test having the material setup illustrated in Figure 2.4. The specimen would be exposed to vibration and flow velocity characterised by a hydrodynamic flow number greater or equal to 10 (Kenney and Lau, 1985). The test involves measuring the grading of the soil sample prior to the test, and afterwards, to enable identifying losses or changes that occur due to seepage in the PSD curve. Assuming no losses and/or changes occurred, the filter in question is deemed stable (Kenney and Lau, 1985).
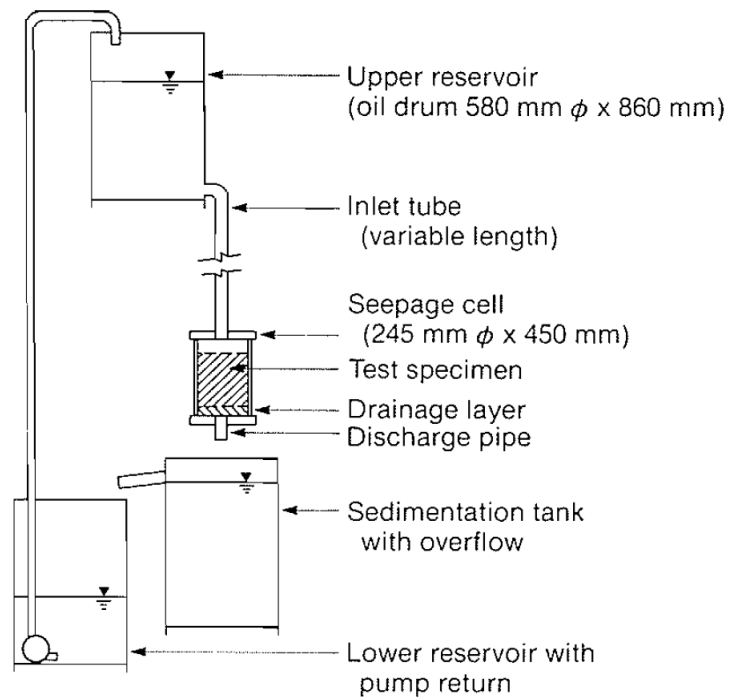
FIGURE 2.4: Material setup in a seepage test according to Kenney
and Lau (1985)

In this testing methodology, it is proposed to compact the specimen prior to testing and use a coarse drainage layer, as well as use vibrational forces to increase the likelihood of particle motion (Kenney and Lau, 1985). The settings recommended therefore act to maximise internal erosion, and therefore are likely to be conservative in determining whether, in practice, an embankment dam's filter is internally stable based on its PSD. Indeed, it has been found by the authors that 23 out of 45 dams that were retroactively studied had filters that were, according to their empirical methodology inadequate, although their performance in practice showed no issues (Kenney and Lau, 1985). Nevertheless, the empirical seepage tests can provide a lower bound solution to the problem of determining potential for internal stability.

Theoretically, Kenney and Lau (1985) propose that a soil may be assessed by ensuring that for all particle diameters D chosen, corresponding to points on the PSD curve with a cumulative fines content by mass smaller than 30% for uniformly graded material and smaller than 20% for a widely-graded material, the fines content F at that diameter is smaller than or equal to the mass fraction H that exists between diameter D and $4D$ (Kenney and Lau, 1985). Initially it was thought that H had to be larger than 1.3 F, however, this proved to be overly conservative, and it was readjusted to H having to be bigger than $1F$ (Kenney and Lau, 1986). The reason cited by Kenney and Lau (1985) for picking the range of D to $4D$ is that particles in this range are required to block the migration paths of particles of size D between the larger particles out of this range. This can be simplified mathematically into the formula below:

$$\frac{H}{F} > 1 \; (previously \; 1.3) \tag{2.1}$$

This is also shown graphically in Figure 2.5, and it is seen that the material in question is unstable, as there are fines contents below 30% for which H/F is smaller than 1 as shown on the right.
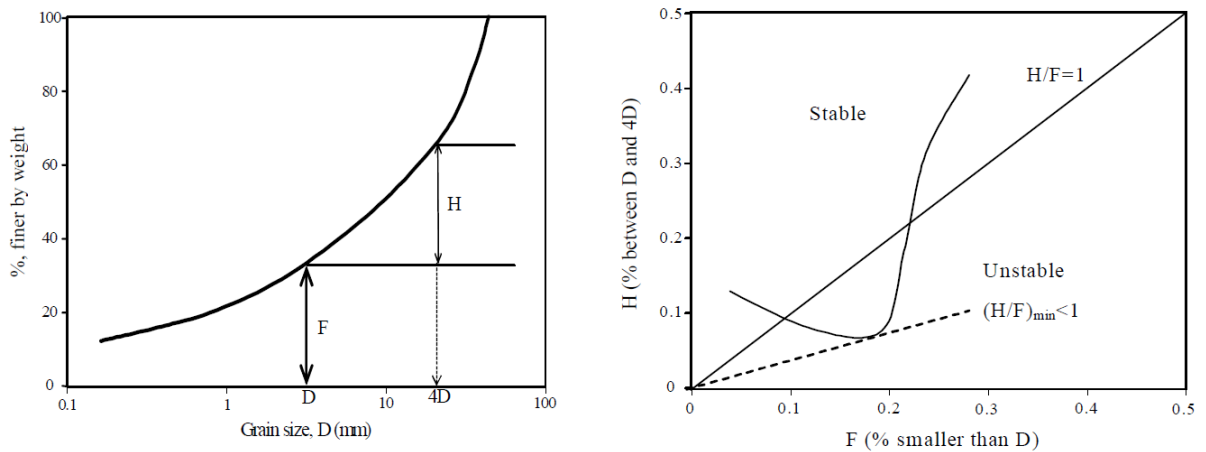
FIGURE 2.5: Kenny and Lau Method as illustrated by Li (2008)

The Kenney and Lau method appears to be best suited for widely graded soils, where it has been found to have better predictive power than the other two methods investigated below (Moffat, 2005; Li and Fannin, 2008). On the other hand, in soils containing significant contents of silt the method may be overly conservative, finding such soils to be internally unstable, when experimentally they are in fact stable (Bonelli, 2013). The method was improved by Li and Fannin (2008) when they created dual criteria by combining the Kenney and Lau criteria with an extension of the Kezdi criteria (to be discussed next) as follows:

$$If \ \ F < 15\% \ \ \Rightarrow \ \ H \geq F \tag{2.2}$$

$$If \ \ F \geq 15\% \ \ \Rightarrow \ \ H \geq 15\% \tag{2.3}$$

The improved Kenney and Lau method shows better agreement with empirical results than its first version, nevertheless both methods have shown

validation and continue to be used (Kenney and Lau, 1985; Moffat, 2005; Li and Fannin, 2008; Brown and Bridle, 2008).

However, actual behaviour may be more difficult to predict, as there certainly are flow, hydraulic gradient and stress conditions under which samples which are deemed internally unstable by the Kenney and Lau method do prove to be stable in practice (Li and Fannin, 2008). Skempton and Brogan (1994) illustrate that there exists, depending on the stability index which is quantified by the ratio of H/F and the porosity of the sand, a certain critical hydraulic gradient, i_c which needs to be met in order for migration to start. This is illustrated by the relationship sketched in Figure 2.6.

As shown in the figure, the critical hydraulic gradient lowers significantly below $(H/F)_{min}$ = 1.3. This brings in the important point that some soils are prone to erosion due to the geometrical constraints they have, however, whether erosion actually takes place in those soils will be the result of the hydromechanical constraints imposed on them, such as the critical hydraulic gradient, which will be further explored later.
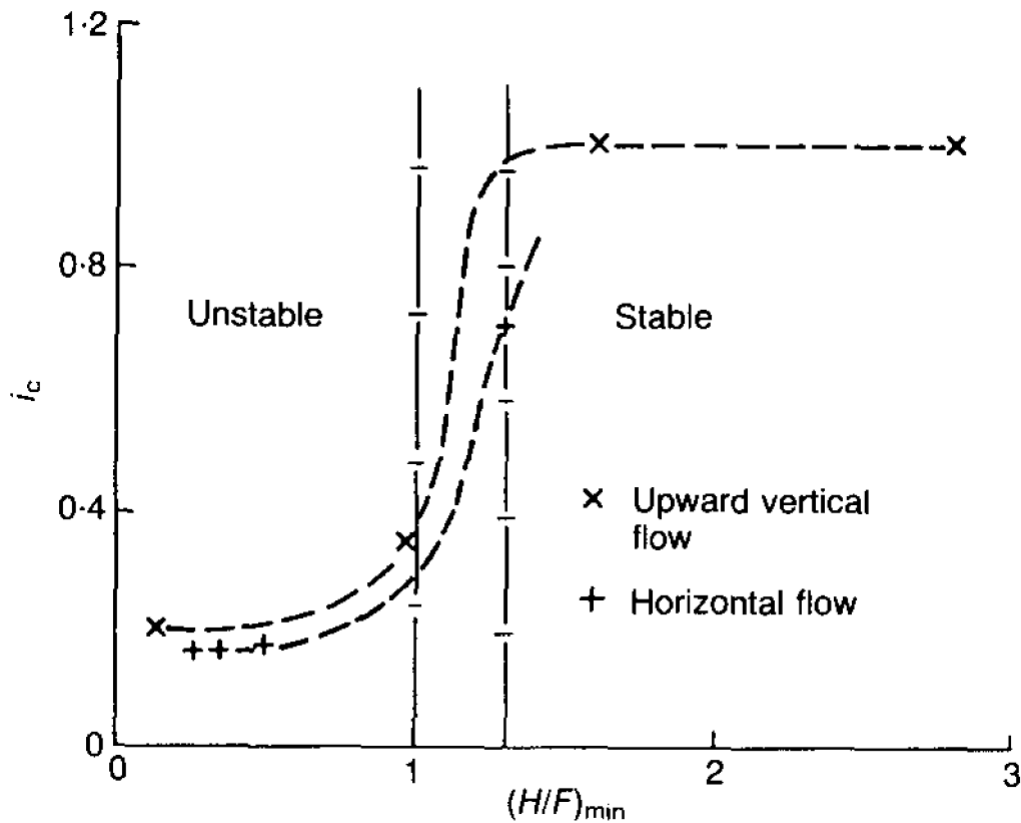
FIGURE 2.6: Relationship between ratio of $(H/F)_{min}$ and i_c according to Skempton and Brogan (1994)

2.2.2 Kezdi method

The Kezdi Method is based on the division of the particles of the filter into fines and coarse, with the expectation that each component should obey Terzaghi's filter law, which states that the ratio of the diameter of 15% by mass of coarse passing particles, D_{15} to the diameter of 85% by mass of fine passing particles, d_{85} should not be greater than 4 to ensure internal stability (Kézdi, 1979; Skempton and Brogan, 1994; Moffat, 2005; Shire et al., 2014; Li, 2008). This is mathematically simplified as shown below:

$$\frac{D_{15}}{d_{85}} < 4 \tag{2.4}$$

The procedure is also illustrated graphically, with the separation of the fines and coarse particles in two different PSD curves and the two diameters calculated by Li and Fannin (2008) in Figure 2.7.
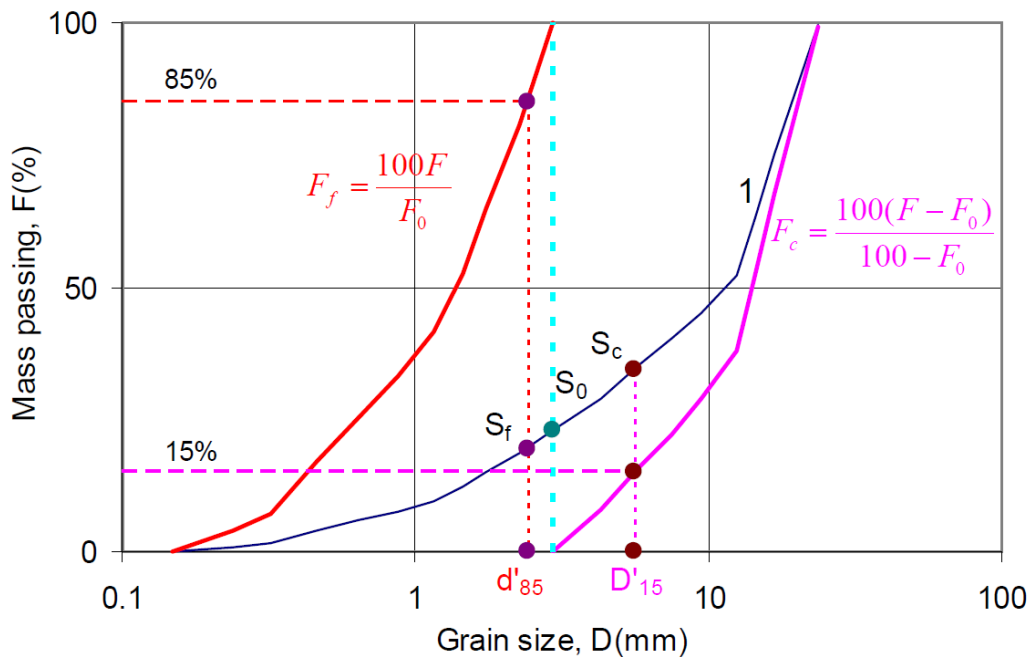
FIGURE 2.7: Li (2008) illustration of the Kezdi Method

The Kezdi Method has very strong empirical backing, and is especially suited to the analysis of gap-graded cohesionless soils compared to the other two methods presented here (Skempton and Brogan, 1994; Moffat, 2005; Li, 2008; Moffat and Fannin, 2011). However, care must be taken that the percentage of the finer fraction isn't greater than 35% of the filter by mass, because in that case the coarse particles would possess a porosity higher than the maximum required to be in contact with each other

and thus they would be suspended in a soil skeleton formed of fine particles (Skempton and Brogan, 1994; Moffat, 2005). This would mean that the coarse particles won't be able to act as a filter even if the Terzaghi equation is fulfilled (Skempton and Brogan, 1994).

The empirical backing of the method is illustrated in Figure 2.8. As can be noted, the method is useful to predict whether a soil may be internally unstable, however, as it can be seen, there are some soils with a D_{15}/d_{85} factor greater than 4 who yet show a low total loss by mass similar to the one found in those with a D_{15}/d_{85} smaller than 4. This illustrates that more conditions may need to be met for a soil to be unstable.
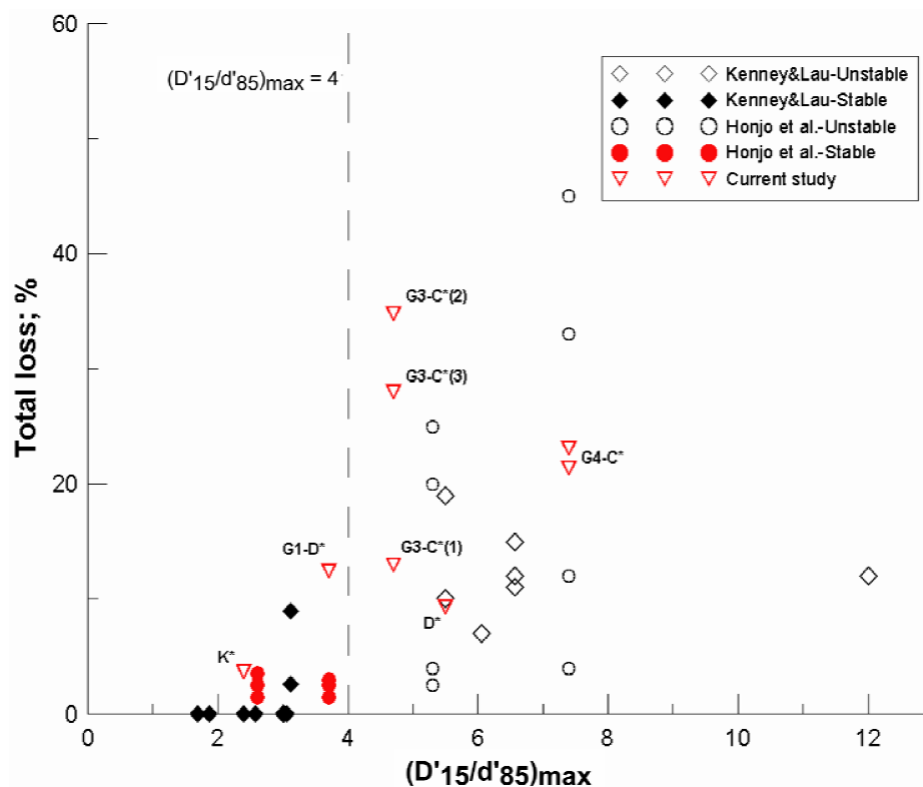
FIGURE 2.8: Loss of particles by mass for specimens of different D_{15} to d_{85} ratio as compiled by Li (2008)

2.2.3 Burenkova method

For materials with coefficients of uniformity up to 200, Burenkova determined another method to assess internal instability caused by suffosion (Li, 2008; Wan and Fell, 2004). This was done by calculating two factors of uniformity:

$$h_1 = \frac{d_{90}}{d_{60}} \tag{2.5}$$

$$h_2 = \frac{d_{90}}{d_{15}} \tag{2.6}$$

Where d_{90}, d_{60} and d_{15} are the sizes of the sieves under which 90%, 60%, and 15% respectively of the soil by mass pass (Wan and Fell, 2008). h_1 is regarded as a measure of the slope of the PSD for coarse particles while h_2 is an estimation of the filtering between the coarse and fine particles (Wan and Fell, 2008). The calculation of these factors enabled each material to be assigned to a certain zone as shown below – where zone I and III represent internally unstable soils, zone II represents stable soils, and zone IV represents artificial soils (Li, 2008): Burenkova used the presence of the zones to develop a formula to account for when a certain soil is in the stable zone based on h1 and h2 , Figure 2.9 (Li, 2008):

$$0.76\,log(h_2) + 1 < h_1 < 1.86\,log(h_2) + 1 \tag{2.7}$$

Burenkova's Method was further adapted to the study of widely-graded and gap graded cohesionless soils by Wan and Fell (2008), who reported that the method did not give conclusive information on the stability/instability

of soil. They used a logistic regression in order to define a probability of internal instability P based on Burenkova's Method (Wan and Fell, 2008):

$$P = \frac{e^z}{1 - e^z} \qquad (2.8)$$

Where Z is a parameter that is calculated differently depending on the conditions and type of the soil. Wan and Fell (2008) defined a Z value (Z1) for soils containing clay or silt particles as well as sand/gravel particles and having a plasticity index and clay size fraction lower than 13% and 10% respectively and another (Z2) for cohesionless soils containing predominantly sand and gravel where there existed less than 10% non-plastic fines smaller than 0.075mm diameter (Wan and Fell, 2008). These are mathematically illustrated below:

$$Z_1 = 2.378 \, log(h_2) - 3.648 \, h_1 + 3.701 \qquad (2.9)$$

$$Z_2 = 3.875 \, log(h_2) - 3.591 \, h_1 + 2.436 \qquad (2.10)$$

The Burenkova method has been reported as being less conservative than either of the other two methods presented before (Wan and Fell, 2008; Li, 2008; Bonelli, 2013). For this reason, it will be useful to treat it as providing an upper bound probabilistic solution.
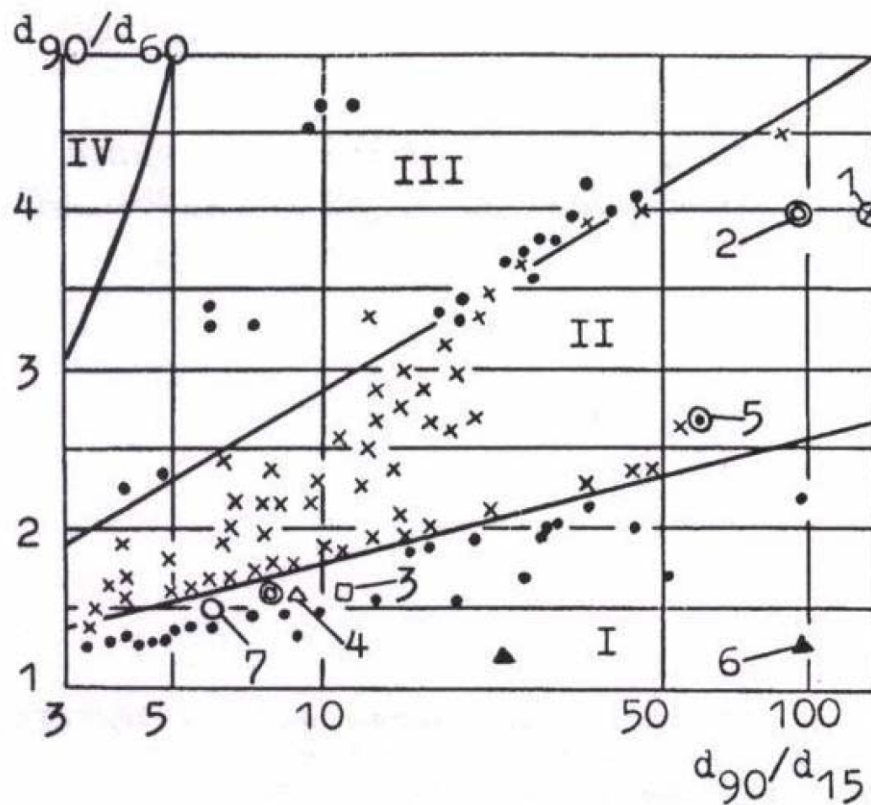
FIGURE 2.9: Illustration of the zones based on the Burenkova
Method as shown by Li (2008)

2.3 Hydromechanical constraints on internal erosion

So far, the literature review has determined that for filters to be suscep-
tible to erosion, their fines content must be lower than 35% (and if their
fines content is between the critical fines content and 35%, then relative
density is also a factor) and the particle size distribution must be such
that it proves potentially unstable according to one or more of the three
criteria previously discussed. If these conditions are met, then the soil is
potentially unstable. However, for instability to actually occur in such a

soil, and for the erosion process of fine particles to be initiated, hydromechanical conditions must also be met. These conditions primarily have to do with hydraulic gradient or seepage flow, and with the effective (mean and deviatoric) stress on the fine particles, which determines how the flow may move and transport fine particles within the voids. In general, the higher the hydraulic gradient and the lower the mean effective stress on the fine particles, the easier it will be for internal erosion to occur (Skempton and Brogan, 1994; Shire et al., 2014; Moffat, 2005).

2.3.1   Hydraulic gradient and vertical effective stress

Understanding of hydromechanical constraints started with Terzaghi's analysis of the critical hydraulic gradient, i_c in 1939 which was defined as being the hydraulic gradient which, when reached, would cause the soil to undergo failure through piping and/or heave (Skempton and Brogan, 1994; Crawford-Flett, 2014; Fannin, 2008; Li and Fannin, 2012; Terzaghi, 1939):

$$i_c = \frac{\gamma'}{\gamma_w} \tag{2.11}$$

This followed from an observation made by Terzaghi (1935) that as the hydraulic gradient experienced by a sample of sand with water flowing vertically upwards increased, so did the velocity, v, of the seepage flow, while the vertical effective stress decreased (Fannin, 2008). As this happened at a constant ratio, the increase in seepage flow was in accordance with Darcy's law (Skempton and Brogan, 1994; Fannin, 2008):

$$v = ki \tag{2.12}$$

Where

v is the seepage flow velocity

k is the coefficient of permeability

i is the hydraulic gradient

However, when the vertical effective stress reached zero, the permeability and velocity of the soil increased exponentially until failure (Fannin, 2008; Crawford-Flett, 2014). This is illustrated graphically in Figure 2.10.
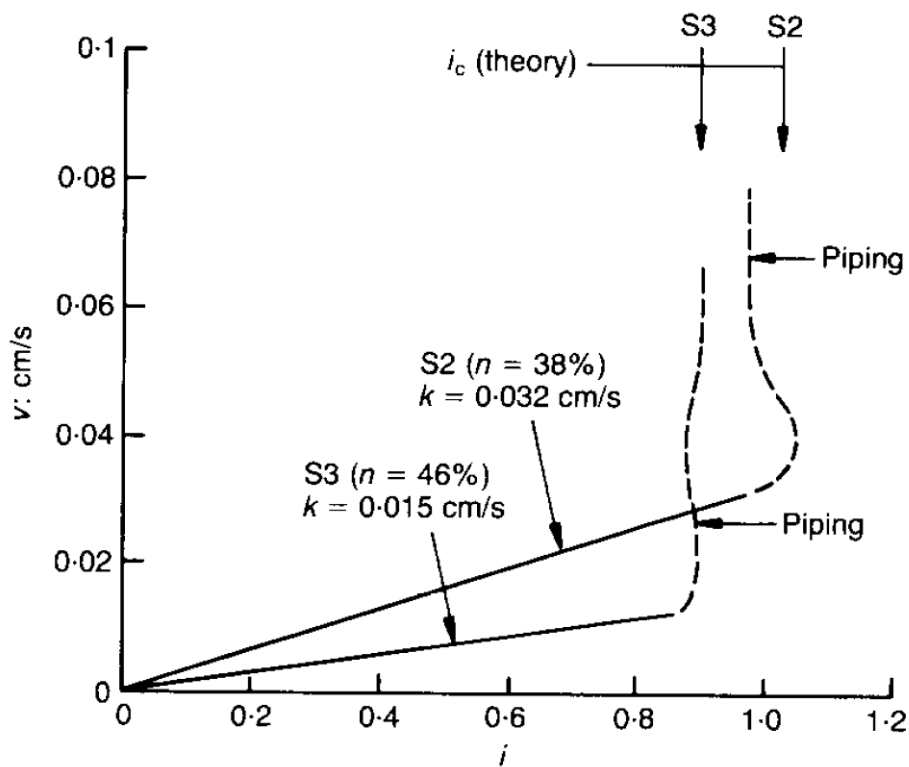
FIGURE 2.10: Illustration of the change in seepage flow velocity with increasing hydraulic gradient; from Skempton and Brogan (1994)

Terzaghi's theory proved to be adequate at predicting the behaviour of soils which were geometrically stable. However, experimental results indicated that the theory predicted much higher critical hydraulic gradients for geometrically unstable soils than were actually seen in practice. This was explained by Skempton and Brogan (1994) who, based on their observations of seepage experiments in a rigid walled permeameter, considered that in these unstable soils, the effective stress taken by the fine particles was much lower than the average effective stress taken by the entire sample, with most of the stress being taken by the coarse particles. This offers further support to Thevanayagam (1998) classification of soil based on its matrix structure; typically soil with a fine's content smaller than 35%, having a structure of case 1-3, has most of the load taken by the coarse particles, with the fines being relatively unstressed. This means that the real effective stress that matters in the calculation of the critical hydraulic gradient is the effective stress felt by the component of fines (Skempton and Brogan, 1994). For this reason, Skempton and Brogan (1994) introduced an adjustment factor α such that the effective stress of the fines, σ'_f under zero seepage is:

$$\sigma'_f = \alpha \sigma' \tag{2.13}$$

Where σ' is the average buoyant stress of the entire soil skeleton. This meant that the critical hydraulic gradient would become:

$$i_c = \alpha \frac{\gamma'}{\gamma_w} \tag{2.14}$$

The difficulty with this way of resolving the issue is that α is a factor that

needs to be calculated after a permeameter test in the laboratory (α is calculated by finding the critical hydraulic gradient according to Terzaghi's equation, and then dividing it by the actual critical hydraulic gradient as measured), and the calculation cannot be applied without testing (Shire et al., 2014). Nevertheless, it proved to be an empirically valid way of assessing cohesionless filters.

The method was later extended in Li and Fannin (2012), based on their experiments using rigid walled permeameters, where it was adapted to account for samples under a vertical effective overburden stress σ'_v. Thus the critical gradient at the base of the sample would be:

$$i_c = \alpha \left(\frac{\sigma'_v}{\gamma_w h} + \frac{\gamma'}{\gamma_w} \right) \tag{2.15}$$

It is important to note that the effective overburden stress is divided by h, which is the distance over which the hydraulic gradient is calculated in order to account for the fact that the critical hydraulic gradient increases with decreasing h (Shire et al., 2014).

Li and Fannin attempted to produce a unified mathematical expression for the critical hydraulic gradient, taking into account overburden stress, for both stable and unstable soils. They developed an equation relating the mean normalised overburden stress $\left(\overline{\sigma'_{vm}} = \frac{\sigma'_{vm}}{\gamma_w h} \right)$ and the hydraulic gradient i:

$$i = \frac{\alpha}{1 - 0.5\alpha} \left(\overline{\sigma'_{vm}} + \frac{0.5\gamma'}{\gamma_w} \right) \tag{2.16}$$

The paper includes a graphical hydromechanical envelope to illustrate this, shown in Figure 2.11. To use the diagram, the user first establishes the overburden stress. If this stress is 0, then the point chosen is Q_0 on the diagram which corresponds with just the buoyant self-weight of the soil, otherwise it is a point P_0 which accounts for that overburden. This condition represents a hydrostatic situation with no hydraulic gradient. The user will then move upwards at a slope of -2, and stop when the critical gradient is reached which is a function of α. If the user knows either the stress, or the hydraulic gradient the user can use the diagram to determine the other condition.
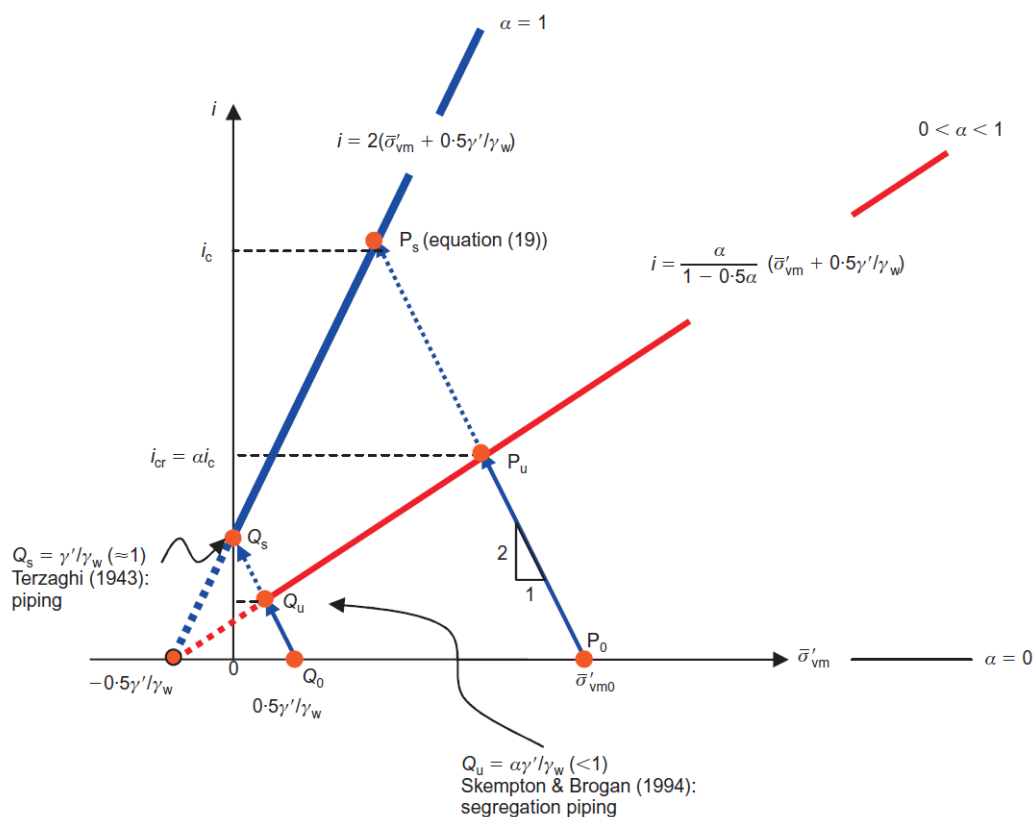
FIGURE 2.11: Hydromechanical envelope for one-dimensional upward flow; from Li and Fannin (2012)

Moffat and Fannin (2011) results investigating the relationship between critical hydraulic gradient (taking effective stress into account) and soil internal instability have revealed the importance of assessing local hydraulic gradients at different depths within the soil, as opposed merely to average hydraulic gradients. They have developed the hydromechanical envelope from their observations that local effective stresses and corresponding critical local hydraulic gradients are related, and further identified that a sudden decrease in local hydraulic gradient at a certain depth indicates the beginning of instability (Moffat and Fannin, 2011). The research also reveals that internal instability may be triggered either by a decrease in effective stress, or an increase in hydraulic gradient such that the hydromechanical boundary is reached. This serves to prove the usefulness of the hydromechanical envelope. Nevertheless, this approach has been developed based on one dimensional seepage flow under rigid walled permeameter conditions (Li and Fannin, 2012), however the reality in embankment dams may be different due to the effects of the complex shear stress states present in core walls and filters (Chang and Zhang, 2011).

Chang et al. (2012), based on experiments conducted in a triaxial permeameter, show that the critical hydraulic gradient of internally unstable soils may lower when the shear stress (or deviatoric stress) increases, and additionally, following the observation made by Moffat and Fannin (2011), that there are two critical hydraulic gradients responsible for different levels of erosion in the same specimen. The next section will focus on understanding the effects of complex stress states, including the K_0 at rest condition, which includes the effects of lateral earth pressure, and relative specimen density on the critical hydraulic gradient and the subsequent erosion.

2.3.2 The initiation of erosion by hydraulic gradient

The hydraulic gradient of the flow can initiate erosion in a given soil at a critical value in accordance with its hydromechanical boundary (Li, 2008; Moffat and Fannin, 2011; Shire et al., 2014). In experiments conducted using rigid walled permeameters, upward and downward seepage direction have different effects on the behaviour of the soil sample in question (Chang et al., 2012). The first difference noticed is in the value of effective stress, especially in the bottom layers of the sample. Under upward flow, vertical effective stress at the bottom is likely to be smaller than under no flow conditions, as upward flow generates an upward pressure which diminishes the effective weight of the soil. Under downward flow, vertical effective stress at the bottom is likely to be greater, as the downward pressure will increase the effective weight of the soil (Moffat and Fannin, 2011). This is illustrated in Figure 2.12:
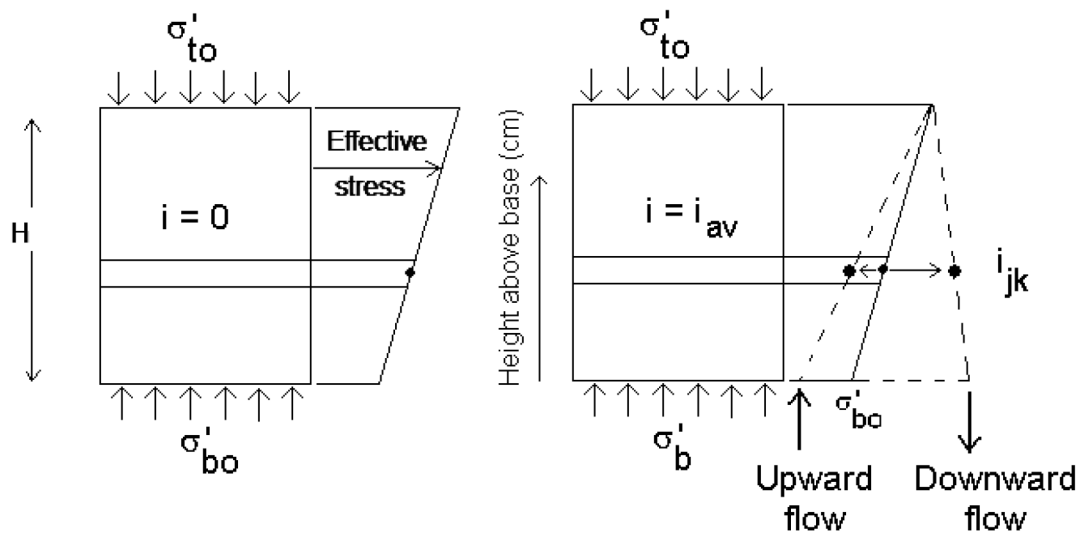
FIGURE 2.12: Illustration of effective stress under (left) no flow conditions, and (right) upward or downward flow; diagram taken from Moffat and Fannin (2011)

The other significant difference has to do with the local critical hydraulic gradient observed, which is higher in the bottom layer than in the top layer for downward flow, and lower in the bottom layer than in the top layer for upward flow (Chang et al., 2012). This is significant because the erosion process always commences from the layer which is hydraulically the "weakest" (smallest critical hydraulic gradient) – for upward flow this would be the bottom layer, and for downward flow this would be the top layer. The explanation for this is that the vertical effective stress – which has a stabilising effect as illustrated by the hydromechanical envelope – is smallest in the bottom layer for upward flow, and smallest in the top layer for downward flow – as shown by Figure 2.13 –necessarily implying that erosion would be greatest in these layers. Further ramifications of this vertical asymmetry suggest that this could account for the greater loss of fines from the top layers than the bottom layers under downward flow conditions, and may provide a possible explanation for the clogging mechanism of particles within the bottom layers of the sample. The process is, however, more complex as the local hydraulic gradient also differs through the sample and changes as the soil skeleton evolves under the effects of seepage (Moffat and Fannin, 2011).
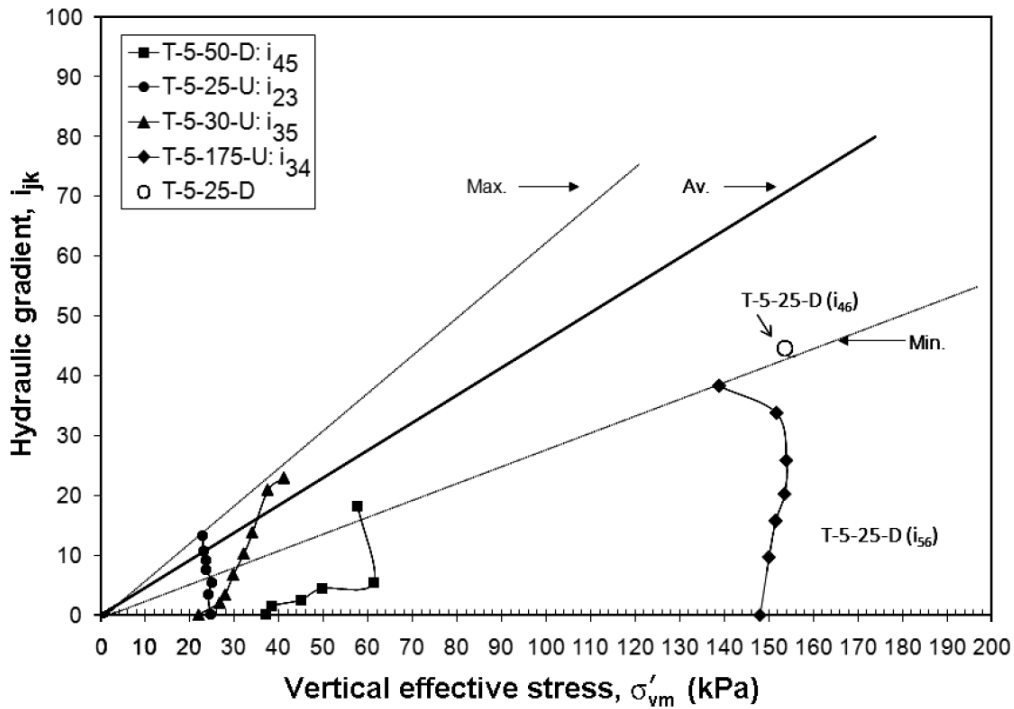
FIGURE 2.13:   Illustration of hydromechanical boundary in gradient-stress space; soils which were tested in upward flow are illustrated with a "U" at the end of their name, and soils tested with downward flow are illustrated with a "D"; diagram from Moffat and Fannin (2011)

At a micro-level, even in downward flow, the fine particles are generally less stressed than the coarse particles and thus more susceptible to erosion. Furthermore, water travels through the path of least resistance, through the gaps in the soil skeleton. It is possible that the uneven flow through the gaps and the vibrations caused by them on the surrounding fine particles cause them to be dislodged (Li, 2008; Crawford-Flett, 2014), and once this process is initiated, more and more fine particles continue to be dragged away. Downward flow has vertical forces applied to the fine particles but that effect combines with lateral forces, breaking the shear connections between particles. Once the shear connections between particles are weakened, the flow will seep through the particles dragging the

fines. Once erosion commences – regardless of whether it is upward, or downward flow – it will start removing fine particles from the soil skeleton and thus lead to a gradual weakening of the material (Li and Fannin, 2012). As the fine particles are removed from in-between the coarse particles, the lateral support of the force chains formed between coarse particles in the soil skeleton is removed, thereby making them more likely to buckle or fail under the weight they are exposed to.

Generally, the higher the hydraulic gradient, the faster and greater the quantity of particles will be removed, thereby weakening the soil skeleton more. This process ultimately leads to failure. In the case of upward seepage, this failure will occur at a smaller critical hydraulic gradient because the average effective stress of the sample is smaller (Li, 2008; Chang et al., 2012). In downward seepage, the critical gradient will be in absolute terms greater due to the greater effective stress (Li, 2008; Chang et al., 2012). However, in relative terms – both gradients will lie on the same hydromechanical boundary (Moffat and Fannin, 2011).

In summary, the hydromechanical boundary in gradient-stress space is independent of flow direction (meaning that the corresponding critical hydraulic gradient lies on the same hydromechanical line, despite the different effective stress conditions that the soil skeleton is exposed to), but the critical hydraulic gradient is greater in the same soil under downward flow than under upward flow due to higher average effective stress conditions.

2.3.3   The effects of complex stress states and relative density

Tests on samples under isotropic stress or K_0 (zero lateral strain) conditions generally find that the higher the stress, the lower the loss of fines and volumetric strain at the same hydraulic gradients (Ke and Takahashi, 2014), in accordance with the relationship postulated by Li and Fannin (2012). However, tests under more complex stress states, involving deviatoric or shear stresses find that the higher the deviatoric stress, the higher the loss of fines, volumetric strain and increase in permeability (Chang and Zhang, 2013). The loss of fines in both stress cases, isotropic and anisotropic, seems to be more accentuated in the top layer of the soil, as opposed to the bottom (Chang and Zhang, 2013; Ke and Takahashi, 2014), most likely due to the fact that, on the way to the bottom starting at the top, the particles have to travel longer distances, and as such, the probability of them becoming clogged and having their migration paths blocked is greater.

Experiments with more complex stress states also reveal that there are two critical hydraulic gradients which are of importance. The first one is the hydraulic gradient at which the initiation of loss of fines begins with a slight increase in permeability, loss of fines and deformation, and the second one, termed the skeleton-deformation hydraulic gradient represents the critical gradient at which the soil skeleton changes its structure, thereby dramatically increasing permeability, loss of fines and total deformation almost instantaneously (Chang and Zhang, 2011). For this reason, for structural purposes in embankment dams, it is this latter skeleton-deformation hydraulic gradient that is of most interest. It has been found

that the higher the deviatoric stress, the greater this increase in permeability, loss of fines (both average erosion rate and maximum erosion rate), and total deformation is (Chang and Zhang, 2013), as illustrated in Figure 2.14.
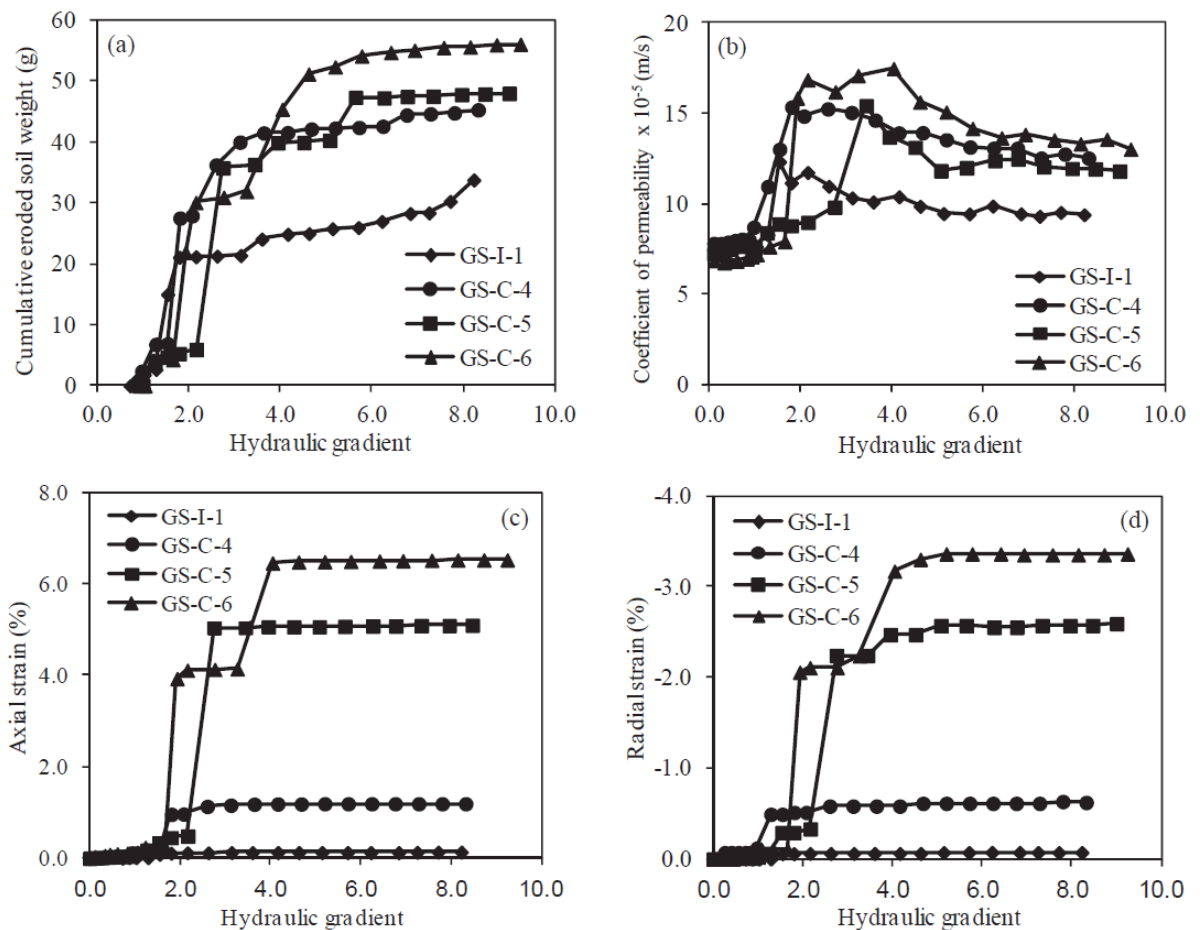
FIGURE 2.14: Illustration of variation of (a) cumulative eroded soil weight, (b) permeability, (c) axial strain, (d) radial strain with hydraulic gradient; GS-I-1 corresponds to isotropic stress, GS-C-4 and onwards to progressively higher deviatoric stresses; from Chang and Zhang (2013)

Furthermore, Chang and Zhang (2011) have found that the higher the deviatoric stress, the smaller the skeleton-deformation hydraulic gradient is,

which suggests that stress state is a controlling factor in the value of the gradient, as shown in Figure 2.15.
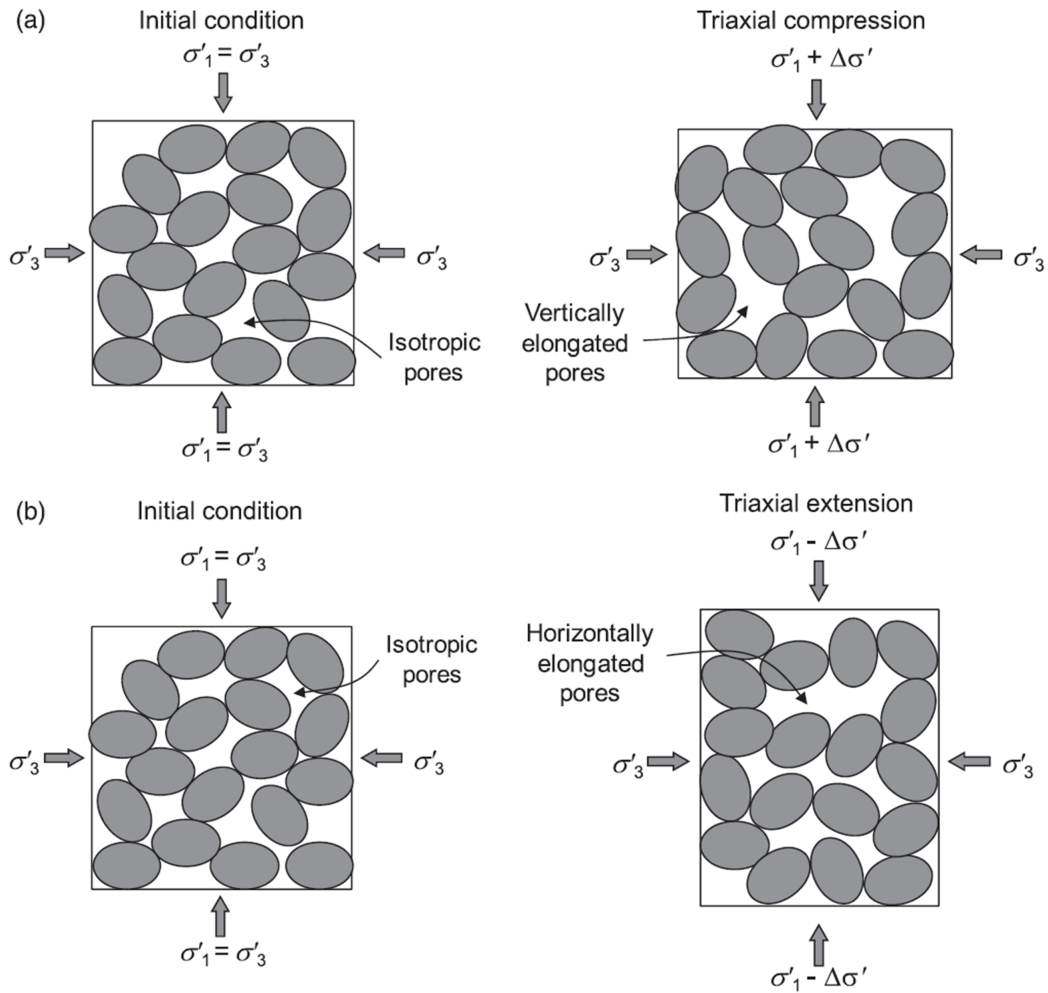
FIGURE 2.15: Illustration of the evolution of pore structure and how they change from isotropic to deviatoric conditions during (a) triaxial compression and (b) triaxial extension; from Chang and Zhang (2013)

Their experiments with relative density at the same deviatoric stress also illustrate that reducing density, thereby making the soil more porous, also decreases the skeleton-deformation hydraulic gradient (Chang and Zhang, 2013).

However – at isotropic conditions the critical hydraulic gradient is still much larger for the same density than at a complex stress state condition (Chang and Zhang, 2013). This can be explained by noting that a more porous skeleton makes it easier for fine particles to be lost, and when fine particles are lost, the stability of the matrix begins to be undermined until the deviatoric stress can produce a sudden change in the soil skeleton – deviatoric stress is more likely than isotropic stress to produce collapse as it acts perpendicular to the force chains, illustrated in Figure 2.16.
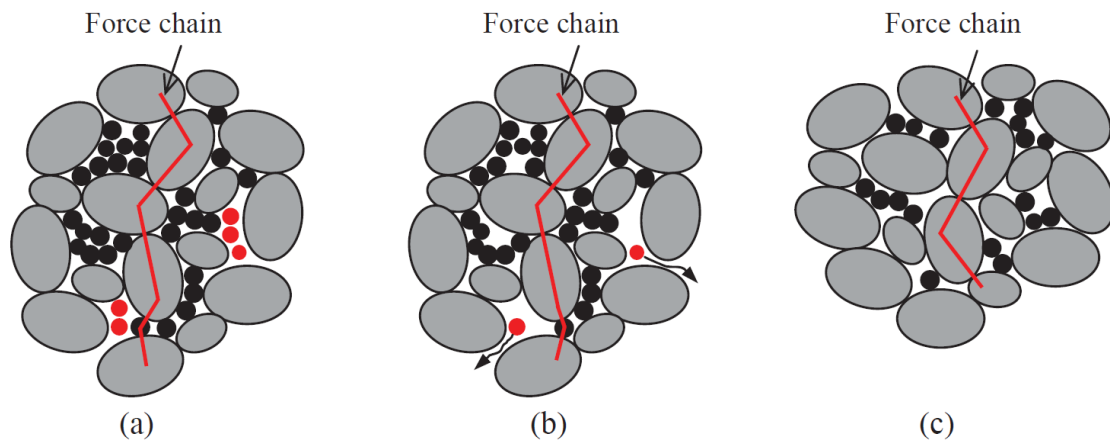
FIGURE 2.16: Transmission of forces in the soil, taken by the coarse matrix in (a) initial state, (b) after the beginning of internal erosion, (c) after the skeleton-deformation hydraulic gradient has been reached. From Chang and Zhang (2013)

The deviatoric stress plays such a role because it alters the structure of the soil. As noted from the Figure 2.16, as particles are removed by internal erosion, moving from (a) to (b) the force chain loses its lateral support and hence becomes prone to a phenomenon alike internal buckling which can be initiated due to the deviatoric stress. The hydraulic gradient at which this buckling and skeleton re-arrangement occurs is the skeleton-deformation gradient.

Chang and Zhang (2013) have also noted that relative density plays an important role on the first critical hydraulic gradient at which loss of fines starts to occur. A more porous material will naturally require less seepage force to commence the erosion of fine particles, with pores in the soil matrix being larger, and thus particles escaping more easily. Thus it is found that erosion rate decreases with increase in relative density at the same deviatoric stress (Chang and Zhang, 2013). The two researchers also identify that the peak stress reached for samples not exposed to erosion is also significantly higher than to those tested after they have been exposed to erosion (Chang and Zhang, 2011).

It is also important to note that non-eroded specimens show a stress-strain relationship of strain-softening and dilative response to deviatoric stress, whereas the eroded samples show a strain hardening and contractive response (Chang and Zhang, 2011). As fine particles are removed from the skeleton, this alters the voids ratio which causes the noted change in the stress-strain relationship. This is similar to the differences observed in loose sand compared to dense sand tested triaxially under conventional drained loading, which suggests that the erosion process leads to a decreasing densification of the sample, which can account for the behaviour changes observed. Thus, it is evident that both relative density and stress state play an important role regarding both the initiation hydraulic gradient and the skeleton-deformation gradient. Furthermore, both these factors alter the response of soils in terms of loss of fines, permeability, and settlement. It is to be expected that higher deviatoric stresses will produce greater settlements in embankment dams, and therefore such dams may be at increased risk of failure. It must be noted that complex stress state analysis is more relevant to the real conditions faced by embankment

dams, and since such analysis reveals that stress state plays an important role in determining the critical hydraulic gradient further research along this line must be carried, which is the purpose of this research.

In order to analyse internal instability under complex stress states a rigid walled permeameter such as was used by Moffat and Fannin (2006) for the study of the impact of axial stress on internal stability is inadequate as such an apparatus cannot measure or generate shear stress within the sample. As most embankment dams are subjected to complex stress states involving shear (**rees2013**; Chang et al., 2012), it is necessary when investigating internal instability as applied to dams to be able to analyse similar situations under laboratory conditions (**rees2016**). As cited in Chang and Zhang (2011), some researchers have already taken steps towards achieving this: Bendahmane et al. (2008) have developed the apparatus required to undertake tests under isotropic stress conditions and Richards and Reddy (2007) used a triaxial system to investigate piping, however the relationship between the soil's stress-strain properties and erosion due to internal instability was largely uninvestigated. Thus, Chang and Zhang (2011) developed an apparatus capable of independently modifying the stress state of the sample as well as the hydraulic gradient it is exposed to. Such a system is formed of four subsystems: a triaxial apparatus, a supply of pressurised water, a water collection system, and a soil collection system (Chang and Zhang, 2011). This, and a history of experimental developments will be discussed next.

2.4   Comparison of experimental investigations on internal erosion

To understand the behaviour of soil under seepage, one may choose to replicate typical site conditions accurately in a laboratory where boundary conditions can be easily controlled. Many factors play a role in soil behaviour, and it is practically impossible to explore all the factors while testing under a single experimental set up. Hence, for different types of erosion, different types of equipment are used to examine specific parameters, based on the aim of the research.

Most of the laboratory tests conducted to explore internal erosion within unstable soils take place under controlled head and flow of water. Permeameters are often used with most apparatuses being rigid walled and some being flexible walled, in order to explore stress states other than K_0. Seepage is generally upward or downward (with some horizontal flow cases). Key examples are given in the following.

2.4.1   Moffat and Fannin (2006)

Moffat and Fannin (2006) developed a large rigid-walled cylindrical permeameter and conducted experiments on uniformly graded and gap graded soils under fixed axial load and increasing hydraulic gradient and reported hydraulic gradient and stress conditions at the onset of failure. The tests were performed using a rigid-wall permeameter made of acrylic tube with a cylindrical test specimen that is 279 mm in diameter and about 450 mm in length with an aluminium top and base plate sealed using O-rings and

six external tie rods, Figure 2.17).

Three specimen configurations were tested. The first configuration was re-constituted entirely by uniformly graded fine glass beads to a length of 430 mm. The second configuration was formed by mixing coarse and fine beads to create a 435 mm length specimen. The third specimen was re-constituted entirely from gap gradation beads to create a 460 mm specimen. All testing specimens were subjected to downward seepage flow under a controlled water head. The local hydraulic gradient variation across the specimen was calculated from the water head distribution, which was measured using pressure transducers. Though the test could not draw a conclusive relationship between effective stress and the critical hydraulic gradient, it focused more on developing suitable apparatus.
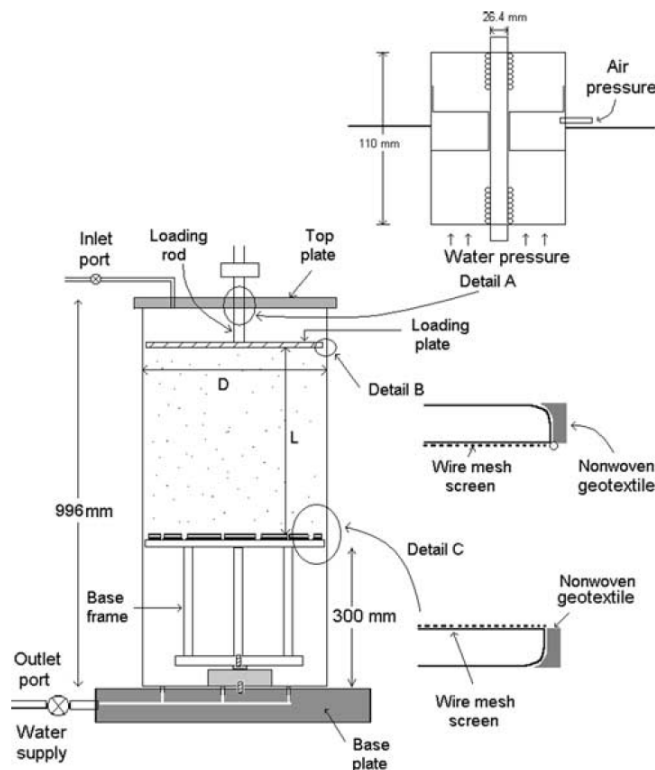
FIGURE 2.17: Permeameter cell used by Moffat and Fannin (2006)

2.4.2   Marot et al. (2011)

An oedo-permeameter (i.e. rigid walled) was used to conduct tests on coarse soils, and a triaxial erodimeter was used for fine soils. The eroded mass was calculated by using a multichannel optical sensor developed by Marot et al. (2011). The oedo-permeameter comprises a cylindrical cell made of a rigid transparent acrylic tube. Specimen diameter was 279 mm with an initial length in the range of 250 mm to 600 mm. The specimen support was a 15 mm thick mesh screen with a 10 mm pore opening size, and different wire meshes can be fixed by a rim on the mesh screen. The piston comprises two perforated plates separated by a 61 mm thick layer of gravel to diffuse the injected fluid uniformly at the top of the specimen. The cell's downstream outlet has a vertical funnel-shaped design and was connected to a soil collecting system. This collecting system has an over-flow outlet with a 0.08mm mesh in order to catch the extracted fine particles, and it was equipped with a rotating sampling system containing several beakers where eroded particles are collected. With the objective to allow only the migration of fine particles, a wire mesh with a 1.25 mm pore opening size was fixed on a wire mesh screen. The tested cohesion-less material was a mixture of glass beads. This mixture was composed of 40% of fine fraction (over-filled) and 60% of coarse fraction. The fine fraction's grain size distribution was within the range of 0.1-0.2 mm, and the grain size distribution of the coarse fraction was within 1.18-3.55 mm.

Six tests were performed with different values of initial specimen length and different histories of hydraulic loading. The applied hydraulic gradi-ent was increased by stages until a strong localised blowout appeared or

the capacity of the device was exceeded. The results reveal that the suffusion characterisation is independent of specimen length and not influenced by the loading history.

2.4.3   Moffat and Fannin (2011)

Moffat and Fannin (2011) present further experiments in continuation of their previous research (Moffat and Fannin, 2006). The emphasis was laid on the local hydraulic gradient. In this study, it was found that under a stable condition, if the effective stress was applied at the top, almost the same stress was noted at the bottom. When seepage flow was introduced in the sample, the bottom stress increased owing to the stress created by water flow.

In stable samples, the average hydraulic gradient (considered between top and bottom) was found to be equal to the local hydraulic gradient (considered between any two points in the sample). However, in samples where suffusion was initiated, a sudden decrease was noticed in the local hydraulic gradient somewhere along the height of the sample.

2.4.4   Xiao and Shwiyhat (2012)

Xiao and Shwiyhat (2012) conducted experimental investigations of the effects of suffusion on physical and geomechanical characteristics on gap-graded samples. The samples were created mixing uniformly-graded river sand and Kaolinite clay, forming a specimen of 51 mm in diameter and 102 mm in height. A triaxial apparatus was used, where the pedestal was

modified to allow water flow and eroded soil to be captured and to monitor changes in total volume. In this experiment, a fixed confining stress (13.2 kPa) and fixed downward hydraulic gradient (20.7) was maintained throughout the erosion procedure. The results were based on the dry mass of eroded solids captured in the collection containers. Volume change, permeability, rate of erosion and cumulative erosion were compared between different samples. Further, undrained compression tests were conducted on eroded samples to assess different samples' post erosion behaviour. The results show an evident influence of suffusion on permeability, compressive strength characteristics, and volume (settlement). A reduction with the progress of suffusion was recorded for the permeability, volume and compressive strength. Gap-graded soils showed more physical and geomechanical changes than uniformly-graded soils, as indicated by the greater erosion rates, permeability reduction, and volume reduction.

2.4.5 Zou et al. (2013)

Zou et al. (2013) designed a large-scale plane-strain permeameter (Figure 2.18) and conducted a study on the behaviour of critical hydraulic gradients under one-dimensional and two-dimensional stresses and different hydraulic load conditions. The apparatus provided a rectangular cubic specimen, 800 mm long, 400 mm wide, and 400 mm high. It was equipped with a horizontal and vertical loading system with a capacity of 1000 kN in the horizontal direction and 2000 kN in the vertical direction coupled with a water pressure system that can provide water head up to 300 m. The test was performed on a gravelly core soil of the Shuangjiangkou Dam, with a grain size attaining 60 mm, and a granular filter of the same

dam, with a maximum grain size of 20 mm. Before installing the specimen, a high plasticity clay layer (5 mm) thick was coated onto the bottom and sidewalls of the specimen container. The test specimens were subjected to incremental water heads applied to the soil specimen by the water pressure pump. The increment of the hydraulic gradient in the soil specimen during the test was about 10.
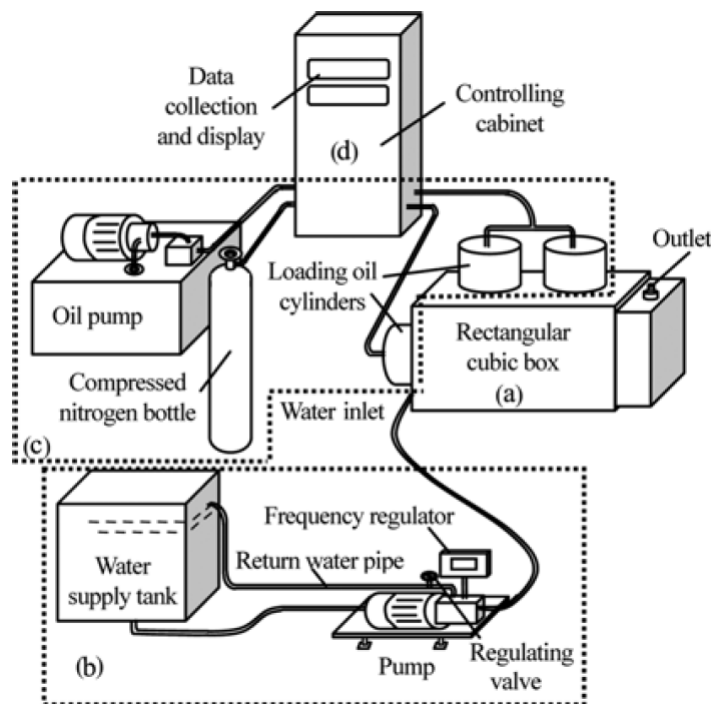
FIGURE 2.18: Layout of the Testing System used by Zou et al. (2013): (a) Rectangular Cubic Box, (b) Water Pressure System, (c) Two-directional Loading System, (d) Data Control and Acquisition System

The results showed that the critical hydraulic gradient increased with the progression of the volumetric compressive strain under one-dimensional stress (vertical loading), and the critical hydraulic gradient first increased and then decreased with the progression of the volumetric compressive strain under two-dimensional stresses increases, as shown in Figure 2.19.
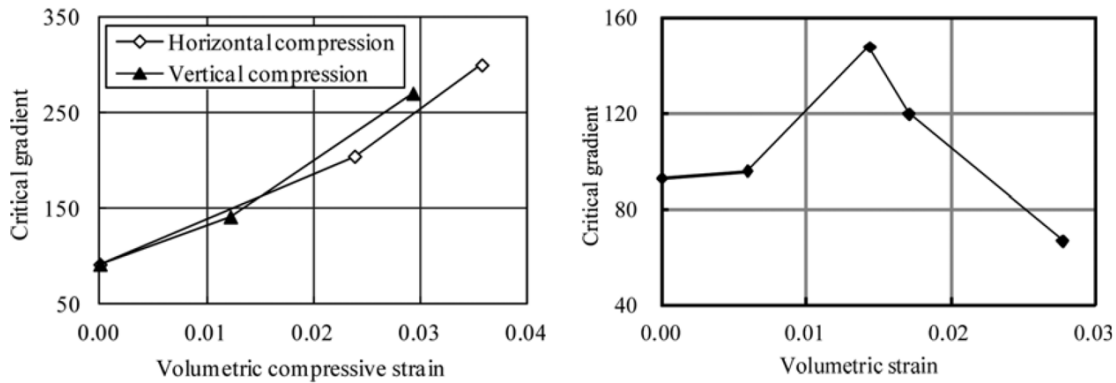
FIGURE 2.19: Critical gradient vs volumetric strain under one dimensional stress and under two-dimensional stress (Zou et al., 2013)

2.4.6   Ke and Takahashi (2014)

In the experimental procedure by Ke and Takahashi (2014), the effect of internal erosion was measured under different confining pressures (50 kPa, 100 kPa and 200kPa) and for gap graded soil samples of different fines percentage (15%, 25% and 35%). Their newly developed triaxial cell (Figure 2.20) mainly consisted of a constant flow-rate control unit, an automated triaxial system and an eroded soil collection unit. A perforated plate with several 1 mm openings was mounted in the top cap, to which the specimen was directly attached, to minimise induced head loss. Another plate was at the base pedestal and served as a filter. A parametric study was performed subjecting the specimens to downward seepage flows. The two variables in this study were the effective confining pressure (50 kPa, 100 kPa and 200 kPa) and initial fines content (35%, 25% and 15%). The tests samples were reconstituted by gap-graded cohesionless soil, which consisted of binary mixtures of silica sands with different dominant grain sizes.

Three main conclusions observed from the results. First, with greater effective confining pressure, there was an apparent reduction in suffusion. With the increase in the confining pressure, it was generally expected that the fines would be packed more densely and inhibit their erosion. Second, with greater initial fines content, more fines eroded. Finally, the monotonic compression tests suggested that suffusion would cause a reduction of the soil strength.
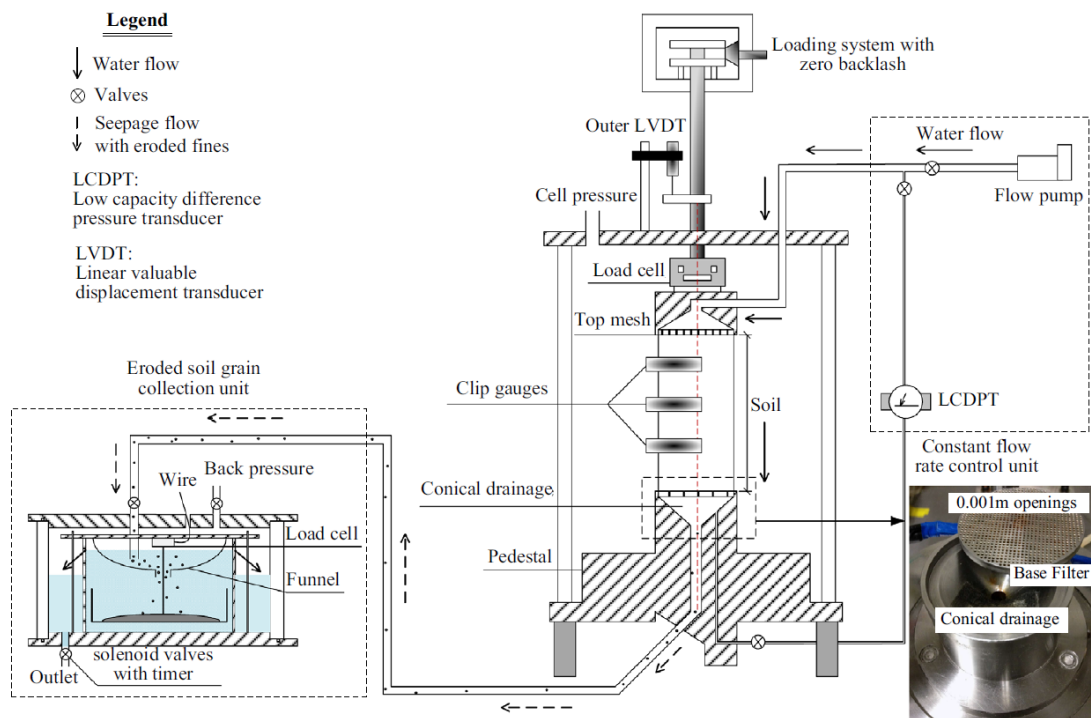
FIGURE 2.20: Schematic diagram of apparatus assembly used by Ke and Takahashi (2014)

2.4.7 Chen et al. (2016)

In the experimental procedure followed by Chen et al. (2016), the effect of erosion on stress-strain response was measured by dissolving salt as

a proxy for fines within the pore space of gap graded material. A gap graded soil samples were created by mixing coarse sand with sand/salt fines. Two different mixtures of soil were tested, group A and B –four tests under group A with 20% of fines content (0, 5, 10 and 15% of particles by mass replaced by salt) and four tests under group B with 35% of fines content (0, 10, 20 and 30% of particles by mass replaced by salt).

The experimental set up consisted of a triaxial apparatus, water supply, water collection, and a data collection system similar to Chang and Zhang (2011). Using the triaxial apparatus, a constant confining stress of 50 kPa was applied to the samples. The artificial effect of erosion was created by dissolving the salt by creating a seepage flow for a long time (36 hours) under a small head (0.1m). The complete dissolution was checked by measuring the concentration of salt in the outflow. Settlement and volume change was noted after the erosion. The stress-strain behaviour of the eroded sample was found by conducting a conventional drained shear test by increasing axial pressure on triaxial apparatus and measuring volume change and settlement.

They concluded that samples with less fines loss showed more dilative response during the drained triaxial shearing test. In addition to that, the shear strength decreased with samples that experienced more fines loss.

The drawback of this approach using artificial fines (salt) might be that no influence of flow path and fines clogging could be examined and all fines would be dissolved in this process (excluding the possibility that any would remain in situ).

2.4.8   Slangen and Fannin (2017)

Slangen and Fannin (2017) developed a double-walled flexible wall perme-ameter device to investigate seepage-induced internal instability by moni-toring volume change during multi-stage seepage flow. By measuring vol-ume change, axial strain and hydraulic conductivity, suffusion and suffos-ion were observed.

The double-walled triaxial cell comprises an inner acrylic tube (Figure 2.21), with an internal diameter of 206 mm and length of 440 mm, and an outer acrylic tube with an internal diameter of 236 mm and length of 440 mm. This device accommodates a cylindrical test specimen (100 mm in diam-eter by 100 mm height). The cavity in the base pedestal was shaped as an inverted cone with mesh. Two bottom wire meshes were placed on the perforated plate: the primary bottom wire mesh had a small opening size of 0.033 mm, to prevent particle loss during specimen reconstitution. A secondary, coarser and stiffer bottom wire mesh, with an opening size of 0.6 mm, kept the primary wire mesh in place. Four gradations of spherical glass beads were tested. A stable gradation was used for the commission-ing of the device and as a base test. Three other gap-graded gradations were prepared by mixing fine and coarse components, one at 20% and two at 35% with different gap ratios D'15/d'85.

From these tests, they considered that if a noticeable increase in the hy-draulic conductivity was found during testing, with no volume change and no increase in axial strain, it could be concluded that this is because of particle migration which indicated suffusion. If this increase in hy-draulic conductivity was accompanied by an increase in volumetric strain,

but axial strain showed no appreciable change, then it was concluded that soil was undergoing suffosion.
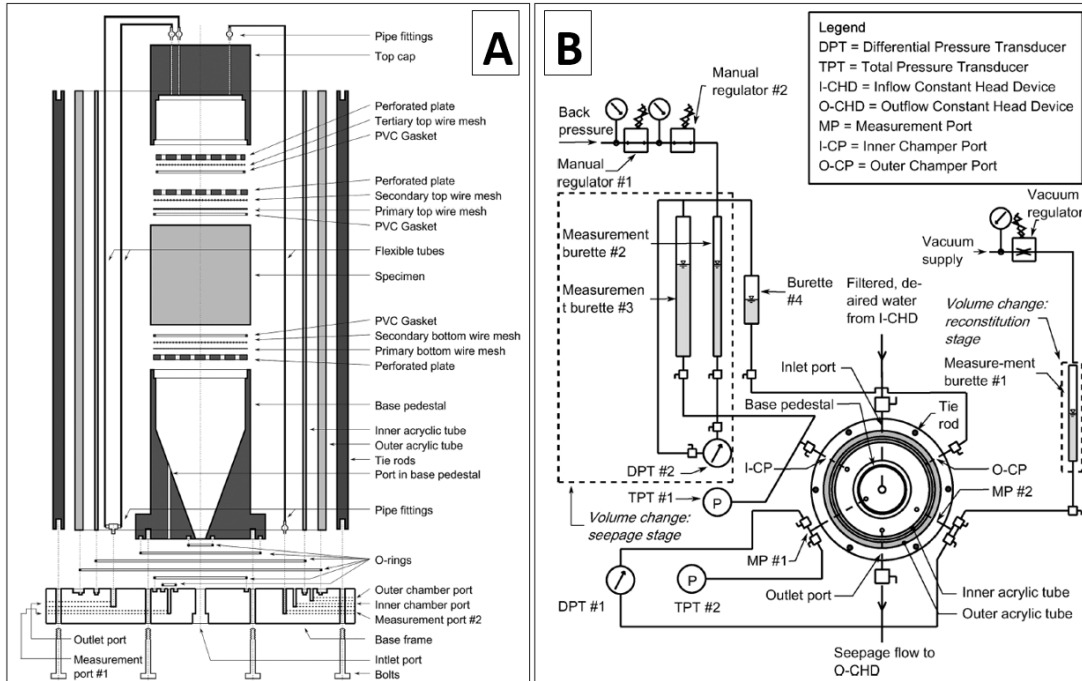
FIGURE 2.21: Overview of flexible wall permeameter arrangement used by Slangen and Fannin (2017), (A) Double-walled triaxial cell and (B) Systematic plan view of double-walled triaxial cell

2.4.9   Liang et al. (2017)

Liang et al. (2017) conducted experiments to assess the effect of isotropic and anisotropic stress conditions on the suffusion behaviour of the soil under upward seepage flow conditions. In their experiments, confining pressure was applied to create an isotropic stress state. Confining and vertical stresses were applied to the saturated specimen using a stress-controlled triaxial apparatus to create an anisotropic stress state.

The apparatus consisted of a loading chamber, a vertical loading system, a confining loading system, an upstream water supply system, a soil-water separating system and a water collecting system. In this research, 36 gap-graded samples were used; all samples were 200 mm in height and 100 mm in diameter. An isotropic stress state was produced using the confining loading system solely, and an anisotropic stress state was achieved by adding axial stress on the confining pressure using the vertical loading system. The specimens were subjected to an increment rate of the hydraulic gradient controlled at about 0.05 per 10 min, and the increment was terminated when sustained erosion was triggered in the specimen. The eroded fines were collected using the soil-water separating system as shown in Figure 2.22.
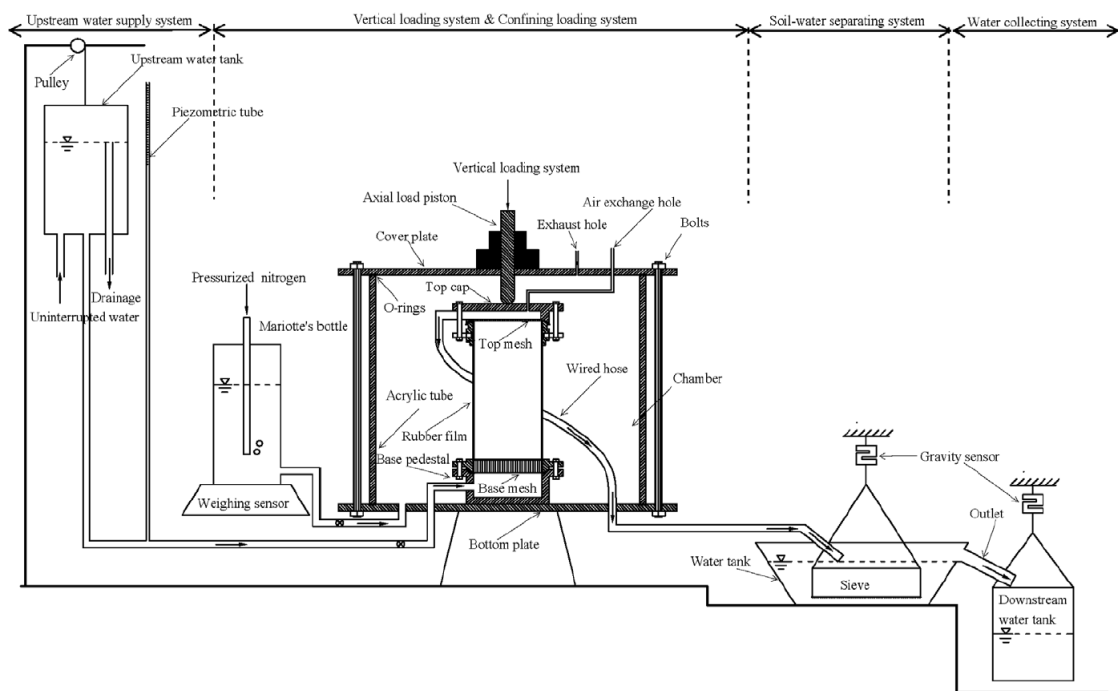
FIGURE 2.22: Sketch map of the designed apparatus by Slangen and Fannin (2017)

The authors defined two different critical hydraulic gradients: low critical

hydraulic gradient LCHG (causing the threshold for the local initiation of suffusion) and high critical hydraulic gradient HCHG (causing the global initiation of the suffusion).

As shown in Figure 2.23, variation of the critical hydraulic gradient was found to be significantly different under the two stress conditions; with a near linear increase in critical hydraulic gradient with isotropic stress, but an increase, then decrease in critical hydraulic gradient as increasing deviatoric stress was applied. Hence, critical hydraulic gradients depend on the magnitude of stress and type of stress (isotropic or anisotropic).
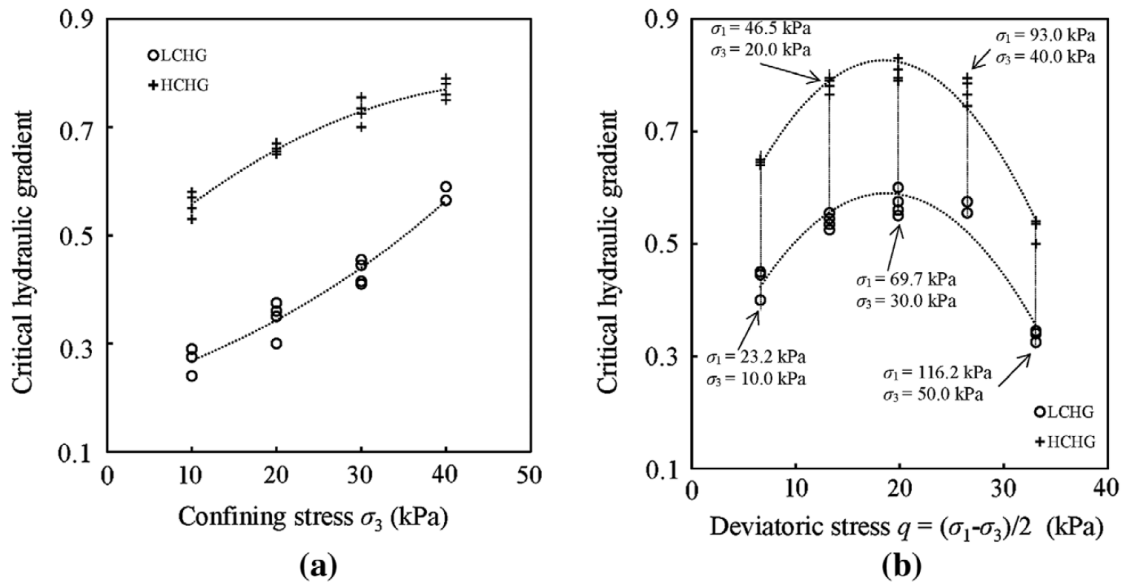
FIGURE 2.23: Influences of stress states on the critical hydraulic gradients: (a) under isotropic stress states; and (b) under anisotropic stress states (Liang et al., 2017)

2.4.10   Prasomsri and Takahashi (2020)

Recently, Prasomsri and Takahashi (2020) conducted an experimental investigation of the contribution of non-plastic fines to the development of

seepage-induced internal instability and its impact on the undrained mechanical response of gap-graded sands using a pressure-controlled triaxial erosion device (flexible wall permeameter), Figure 2.24.

The triaxial erosion apparatus mainly consists of an automated triaxial system, a seepage control system, and an eroded soil collection unit. The seepage system in the current apparatus was based on the principle of hydraulic head control, in which the internal erosion experiments can be performed with high back pressure under pressure controlled condition. The seepage control system was designed to apply the differential hydraulic head between the top and the base of the sample. The hydraulic gradient, i, was calculated using the differential pressure between top pressure and base pressure.

Gap-graded mixtures of silica sand as the coarse fraction and coloured silica sand as the fine fraction were used. Seven mixtures with fines content of 15, 20, 25, 30, 32.5, 35, and 40% were used to construct specimens at the height of 150 mm and a diameter of 75 mm. Eight erosion tests were performed on the medium dense sand, where the inlet tank was used to impose the seepage flow throughout the sample in a downward direction by increasing the inlet tank pressure from 400 to 430 kPa at a rate of 2 kPa/min, keeping it constant for 30 min, and then decreasing it to 400 kPa at the same rate. The base pressure of 400 kPa was maintained throughout the tests. The results indicate that the initial fines content significantly affects the initiation and progress of internal instability. Undrained compression tests on eroded soils reveal that suffusion made the soil looser and more contractive, while suffosion makes the soil more dilative at large strain levels.
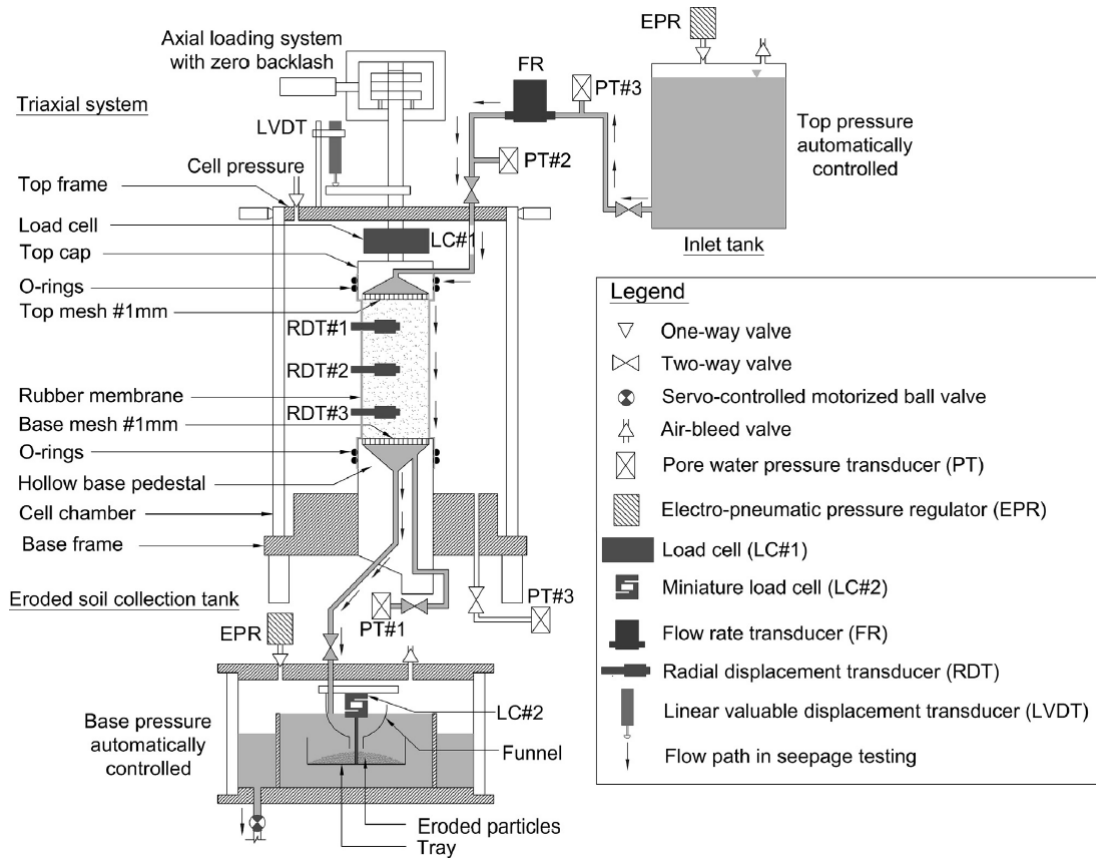
FIGURE 2.24: General configuration of the triaxial apparatus
used by Prasomsri and Takahashi (2020)

A summary of the details of these studies is shown in Table 2.2.

TABLE 2.2: Summary of various experiments on the assessment
of susceptibility and the mechanism of internal erosion.

Research	Equipment	Parameters varied in the experiment	Conclusions
Moffat & Fannin (2006)	Rigid-walled cylindrical permeameter	Gradation Hydraulic gradient	Critical Hydraulic gradient local and global hydraulic gradient identified by a sudden increase in hydraulic conductivity. There is a relation between the effective stress and the critical hydraulic gradient to trigger instability. The exact nature of the effective stress needs further investigations.
Moffat & Fannin (2011)	Rigid-walled cylindrical permeameter	Gradation Hydraulic gradient	Vertical effective stress and corresponding local critical gradients are measured, and a hydromechanical path was proposed to draw a hydromechanical envelope with critical hydraulic gradient and stress values below which that particular soil will be stable.
Marot et al. (2011)	Odeopermeametre	Fines Percentage Initial specimen length Hydraulic gradient	The relation between erosion rate per unit pore area and hydraulic shear stress is inconclusive. Cumulative eroded mass increases with cumulative expended energy.
Marot et al. (2011)	Triaxial erodimeter	Flow rate Hydraulic gradient	The hydraulic shear stress decreases with time (progression of suffusion) under hydraulic gradient controlled conditions and increases underflow rate controlled conditions. The relation between erosion rate per unit pore area and hydraulic shear stress is inconclusive. Cumulative eroded mass increases with cumulative expended energy.
Xiao & Shwiyhat (2012)	Triaxial apparatus	Gradation	Apparent influence of suffusion was obtained on permeability, compressive strength characteristics, and volume (settlement). Gap-graded soils showed more physical and geomechanical changes than uniformly-graded soils, as indicated by the greater erosion rates, permeability reduction, and volume reduction.
Chang & Zhang (2012)	Triaxial apparatus	Hydraulic gradient Stress magnitude stress type (isotropic, compression and extension stresses)	For the same porosity, the initiation gradient is higher for extension stress than compression stress condition. The skeleton-deformation hydraulic gradients are higher under isotropic stress conditions.
Zou, Chen & He (2013)	large-scale plane-strain permeameter	Hydraulic gradient Stress magnitude stress direction (One dimensional and two dimensional)	Under horizontal or vertical stresses (one-directional stress), hydraulic conductivity decreases, and the critical gradient increases with an increase in volumetric compressive strain. Under two-directional stress, hydraulic conductivity decreases and then increases and critical hydraulic gradient increases and then decreases with the increase in volumetric strain.
Ke & Takahashi (2014),	Triaxial permeameter	Confining pressure Gradation	Reduction in suffusion with greater confining pressure. Fines loss was more for the specimens with greater initial fines content (30%, 25% and 15%). The compression tests indicated that suffusion causes a reduction in soil strength.
Lianga et al. (2014)	Triaxial apparatus	Hydraulic gradient Stress magnitude stress type (isotropic and anisotropic)	Low & high critical hydraulic gradients increase with the increase of confining pressure (isotropic state) and increase then decrease with the increase in deviatoric stress (anisotropic state).
Chen, Zhang & Chang (2016)	Triaxial apparatus	Fines content (20 and 35%)	For higher suffusion amounts (i.e., as % loss of particles increases), upon shearing, developed axial strain is higher at the same deviatoric stress. As suffusion progress, for the same axial strain, the volumetric strain increases.
Slagen & Fannin (2017)	double-walled flexible wall permeameter	Hydraulic head (Total dynamic head is increased gradually, thereby increasing seepage flow)	Suffusion: low volume change with the increase of hydraulic conductivity, indicating particle migration. Suffosion: noticeable volume change with the increase of hydraulic conductivity, indicating re-arrangement of particle assembly.
Prasomsri & Takahashi (2020)	Triaxial apparatus	Fines content (15, 20, 25, 30, 32.5, 35, and 40%).	The initial fines content affects the initiation and progress of internal instability. Suffusion made the soil looser and more contractive while more dilative at large strain levels.

2.4.11   Numerical modelling of internal erosion

In the last two decades, numerous studies have introduced the notion of stress as a parameter controlling the internal erosion process (e.g., Tomlinson and Vaid (2000), Fell and Fry (2007), Richards and Reddy (2007), Moffat and Fannin (2011), and Chang and Zhang (2013)).

The advancement of discrete element methods (DEM) is generally credited to Cundall and Strack (1979). DEM can be described as a numerical method that simulates granular materials' behaviour considering the individual particles to be rigid and uses relatively simple models to simulate their interactions (O'Sullivan, 2011). Using the increasingly powerful computing capability, DEM has become widely used in the geomechanics research community as an effective and efficient method to study granular materials' complex behaviour.

Shire et al. (2014)

Shire (2014) started a discrete element modelling DEM based research to investigate the soil fabric and effective stress distribution within 16 gap-graded gradations at three relative density levels (a total of 48 DEM simulations). The DEM simulations were carried out on cubic samples using the open-source DEM code Granular LAMMPS (each simulation had a minimum of 500 coarse particles). The reduction in stress in the finer fraction was quantified by the α-factor, calculated at the microscale using DEM variables.

The results confirmed the hypothesis by Skempton and Brogan (1994), supported experimentally by Moffat and Fannin (2011), that fines erosion initiated at lower hydraulic gradients than would be required for failure by heave or piping as fines carry less stress than would be expected considering the average stress conditions alone. Additionally, the initiation of fines erosion is usually at the weakest layer (most porous layer) if permeability changes through the sample.

Also, from the DEM results, if fines content was less than 25%, fines would sit between voids (underfilled). If fines could fit through the void network, there was a potential for suffusion. In contrast, if the fines content was more than 35%, the soil could be considered overfilled, where the fines fill the voids and stress transfer is shared between coarse and fine particles; in this case, the soil is considered internally stable.

Wautier (2018)

By using a 3D discrete element method, DEM (with open source code YADE), Wautier (2018) investigated the influence of the stress increments on the onset of mechanical instability in cohesionless granular materials by studying interparticle interactions. A cloud of 10,000 non-overlapping spheres surrounded by six bounding planes cube were used in this research.

Afterwards, the existence of mechanical instability was linked to the flow-induced microstructure modifications by exploring flow-grain interactions. A theoretical framework of the second-order work linked to the second-order variation of the kinematic energy was used to detect and assess the existence of the instability at the material point scale.

The results showed that large stress increments have a noticeable destabilising influence on stable granular materials. This influence is more important with the increase of stress increment and can be negligible for small loads. Afterwards, this dependence on the stress increment was explored at the microscale by defining a sliding index for grain contacts, and it was found that high-stress increments had a noticeable impact on the distribution of these contacts and provoked important microstructure re-organisation through gain and loss of contacts. This process was found to lead to a generalised unjamming/rejamming process, leading to force chain renewal occurring in the granular material between the initial and the final state. Whereas the application of small stress increments hardly changed the contact distribution.

Rattlers are fine particles that fail to be incorporated in the force chains. In order to highlight the role played by these particles with respect to mechanical stability in cohesionless granular materials. Wautier (2018) has subjected different samples of these materials to stress probes: a loose sample, where rattlers are removed artificially and naturally. The obtained results showed that the loose sample experienced an important instability during the incremental loading. At the macroscale, this resulted in a larger plastic increment occurring in the depleted sample. Therefore, rattlers, even though they do not contribute to supporting the mechanical loading, play an important role with respect to mechanical stability, and their removal weakens the skeleton of the granular material. Provided that the current contact network fails to withstand an incremental load, the mechanical stability of granular material at the macroscale is closely related to the ability of free particles to get jammed into new force chains.

On the other hand, artificially adding rattlers inside the pores of an unstable granular material is shown to have a stabilising effect, Figure 2.25. This particle enrichment process offers new possibilities in rebuilding contact networks and strengthening the existing force chains. As a result, the sample becomes more stable than the natural and depleted samples (Wautier, 2018).
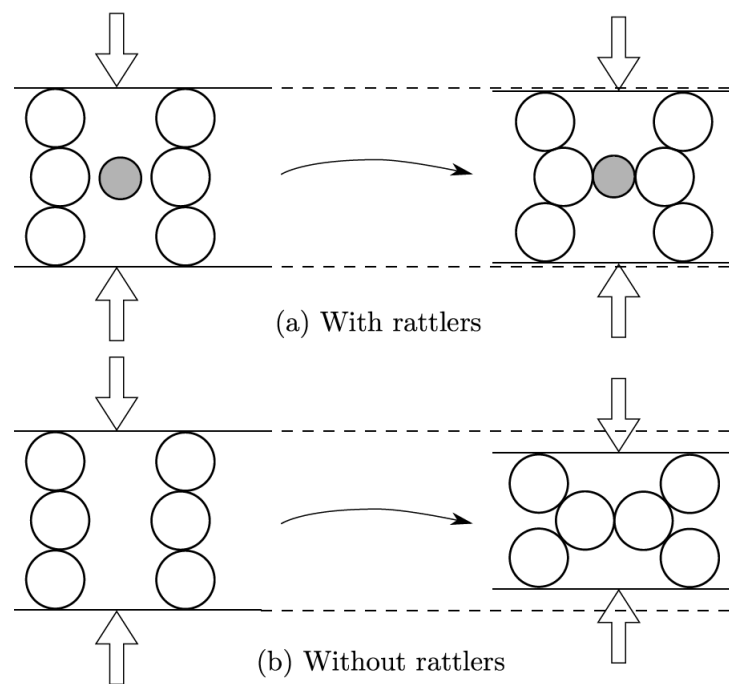
FIGURE 2.25: Schematic diagram comparing a microstructure with rattlers (a) and the same microstructure without rattlers (b) (Wautier, 2018)

A mechanically unstable sample depleted of its rattlers (free particles that are not participating in stress transmission) was subjected to a fluid flow under an incremental loading. The results showed that the internal fluid flow can apply additional forces on the sample at the grain scale. Some contacts will reach their limit of sliding, which may lead to grain detachment following force chain re-organisation. Therefore, the internal flow

acts as a perturbation factor that is sufficient to trigger a local failure of the existing contact network, causing re-arrangement of the existing chain force. Even if the failure remains localised, this can affect the whole contact network as stresses are forced to redistribute. If the new force chain is not able to sustain the stress increment, it can lead the sample to collapse till it finds a new equilibrium. As a result, chained particles can be detached from force chains during these microstructural re-arrangements to either be reincorporated in the new force chains or become a rattler. The second impact of the internal fluid flow is the transport of rattlers and possibly detached particles through the pore network. In this case, the fluid flow can have either a stabilising or a destabilising influence. When the clogging dominates over erosion, the fluid is able to restabilise initially unstable granular materials. This influence was explained by the distribution of the mobilised rattlers in the pores' space, increasing their possibilities of being incorporated in the force chains during microstructural re-arrangements.

In conclusions this literature review has examined experimental research and discrete numerical work on the influence of geometric and hydromechanical constraints on internal erosion. This sets the state of the art for the following experimentally based investigations.

Chapter 3

Methodology

3.1 Introduction

The research presented in this thesis is centred around developing an understanding of the role that the stress condition and the change in stress play in the erosion process in embankment dams. There are many dams around the world which are deemed to be unstable based on an investigation of their material susceptibility and hydraulic conditions, therefore it is necessary to uncover what is the future of such dams. The role of stress state in the erosion process is a relatively neglected area of research when it comes to erosion. Chang et al. (2012) commenced research in this area but the published research was limited to a single material and a limited stress path due to the apparatus used.

This project includes the design and commissioning of a new triaxial erosion testing apparatus in order to study different materials under different stress paths. This new apparatus enables a better understanding of the critical stress condition and its effect on erosion and may shed light

on the reason for internal instability in some dams. As well as the apparatus commissioning, the research investigates the influence of varying the hydraulic gradient, the influence of different fines contents, the role of different stress paths and finally, the influence of the rate of shearing on erosion.

This chapter outlines the tested materials and their characterisation, the testing concept including the development of the triaxial permeameter, the research testing program, and the testing procedures used to prepare and perform the erosion tests.

3.2   Materials and characterisation testing

Prior to undertaking erosion triaxial tests, preliminary tests were undertaken in order to determine the characteristics of the soils to be tested.

The particle size distribution of soils to be tested, their internal stability according to geometric criteria, and more general soil characteristics such as maximum/minimum density and voids ratio, relative density, as well as the behaviour of the soil under conventional drained triaxial conditions are found below.

3.2.1 Soil type

A large number of existing dams have filters made of cohesionless soils, and therefore this category is of importance in investigating internal erosion. For the purpose of this research it was decided to investigate a cohesionless gap-graded sandy soil. Figure 3.1 shows the particle size distribution of the soil tested.

The samples are geometrically unstable according to Kenny & Lau, Burenkova and Kezdi methods (Kenney and Lau, 1986; Burenkova, 1993; Kézdi, 1979). The particle size distribution curve of a typical sample is illustrated in Figure 3.1, more fines percentages have been tested in the following chapters.
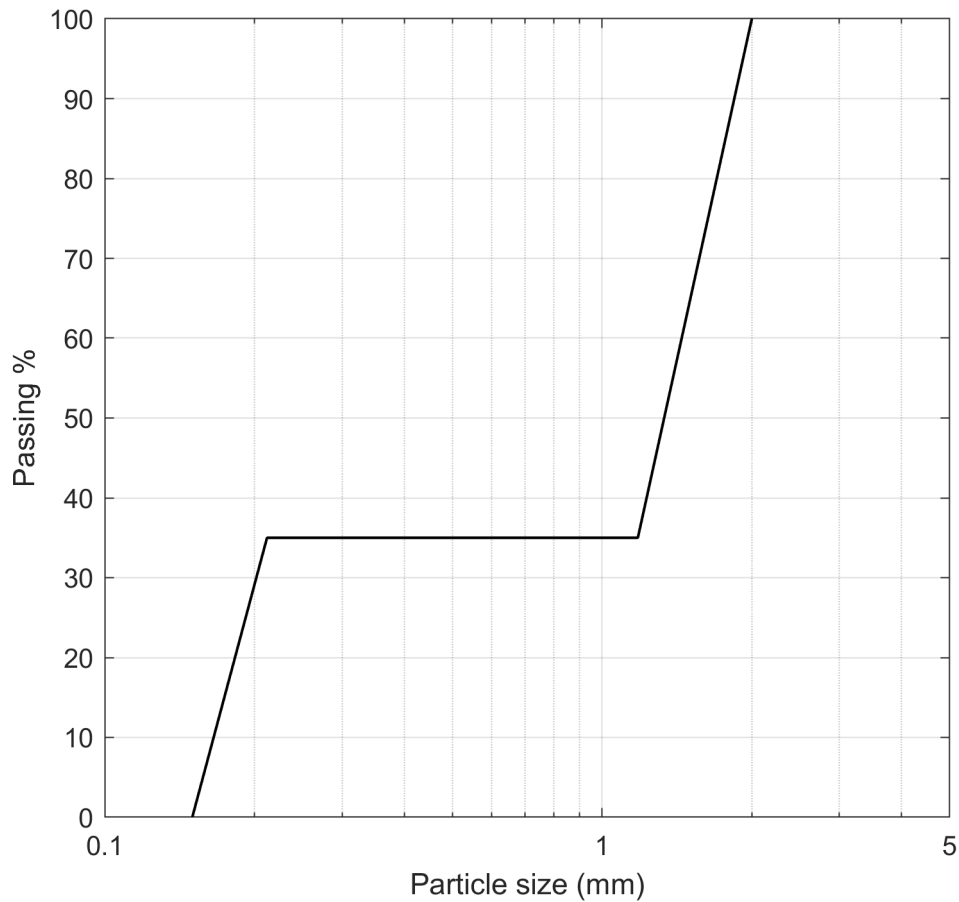
FIGURE 3.1: A typical particle size distribution graph with 35%
fines

The soil gradation is a replication of G4-C which has been used by Moffat
and Fannin (2006) and was originally tested by Honjo et al. (1996). The
fines content used for G4-C was 40% where in this research the fines con-
tent varied from 10% to 50% keeping the same gap ratio of 5.57, Equation
3.1. Leighton Buzzard sand is a standard sand used regularly for the pur-
pose of laboratory testing, and hence in this research the same type of
sand has been used to achieve comparable data in future research, Figure
3.2.

FIGURE 3.2: Leighton Buzzard sand fraction A & D

The soil for this research was obtained by mixing the coarse and fine particles into different proportions. To obtain the correct coarse particles size, Leighton Buzzard sand type 'A' has been sieved and only particles between sieves 1.18mm and 2mm have been used. For the fine particles,

Leighton Buzzard sand type 'D' has been sieved and only particles be-
tween sieves 0.150mm and 0.212mm have been used to achieve the de-
sired gap ratio of 5.57, Figure 3.3 and 3.4.
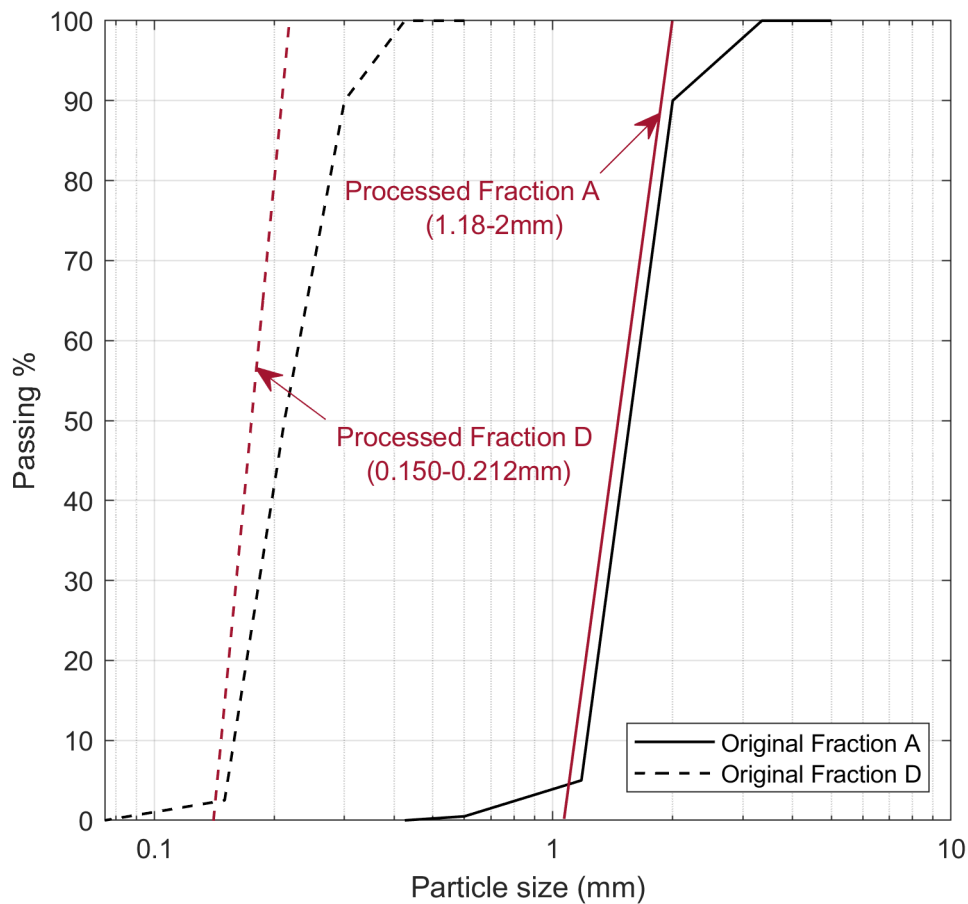
FIGURE 3.3: Leighton Buzzard sand fraction A & D particle size
distribution curves

FIGURE 3.4: Microscopic image of Leighton Buzzard sand fraction A (top) and D (bottom)

The intended gap ratio has been calculated using the following equation:

$$GapRatio = \frac{D'_0}{d'_{100}} \tag{3.1}$$

$$\frac{1.180}{0.212} = 5.57 \tag{3.2}$$

Where

D' represents the coarse fraction

d' represents the fine fraction

3.2.2   Geometric constraints

Six different soil mixes were investigated, Figure 5.1. All six mixes have been checked for internal stability using Kenney & Lau, Kezdi and Burenkova (Kenney and Lau, 1986; Burenkova, 1993; Kézdi, 1979). All samples are geometrically unstable according to these criteria.
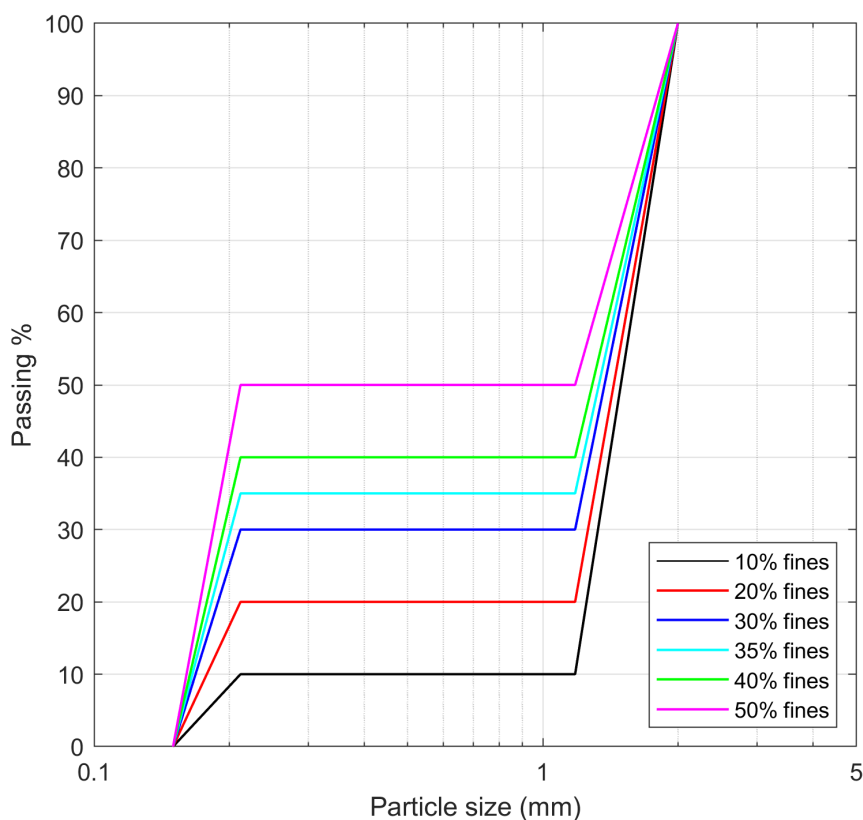
FIGURE 3.5: The particle size distribution curve for the six samples used in this research

It can be seen from Figure 3.6 that all six mixes are unstable according to the combined Kenney & Lau and Kezdi methods (Kenney and Lau, 1986; Kézdi, 1979).
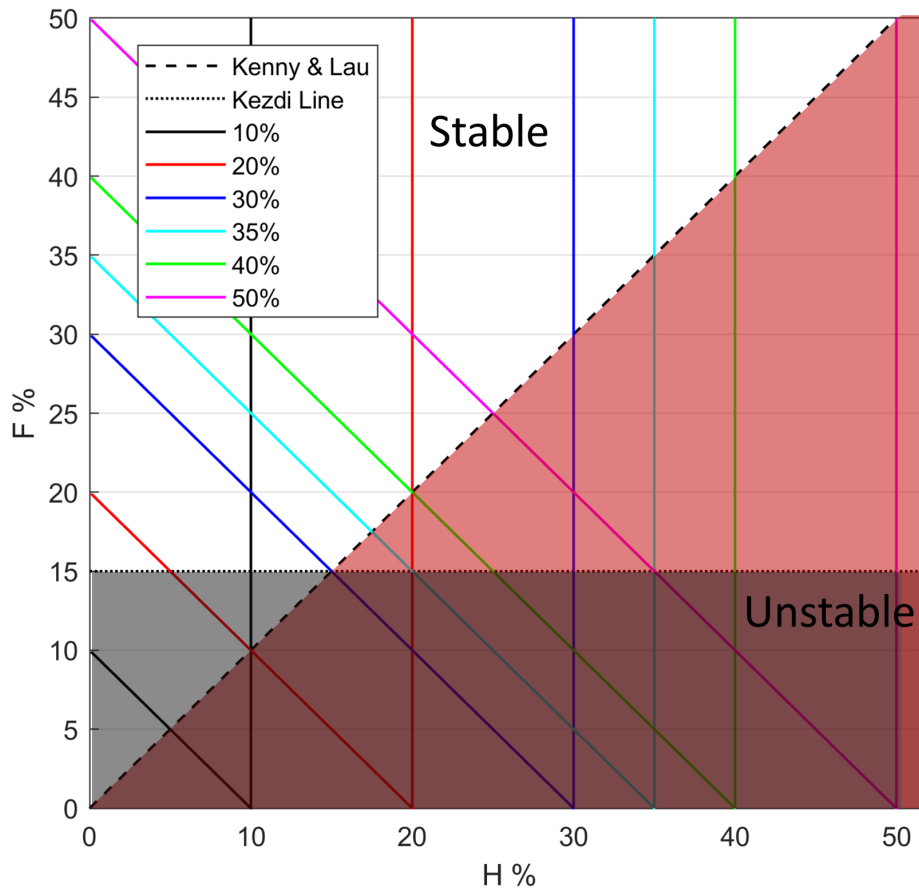
FIGURE 3.6: H against F for, showing the samples fails under the Kenny and Lau and Kezdi boundaries (Kenney and Lau, 1986; Kézdi, 1979).

The Kezdi Method is based on the division of the particles of the filter into fines and coarse, with the expectation that each component should obey Terzaghi's filter law, which states that the ratio of the diameter of 15% by mass of coarse passing particles (D_{15}) to the diameter of 85% by mass of fine passing particles (d_{85}) should not be greater than 4 to ensure

internal stability. This is mathematically simplified as shown below:

$$\frac{D_{15}}{d_{85}} < 4 \tag{3.3}$$

The procedure is also illustrated graphically using the sample with 35% fines content as an example, with the separation of fines and coarse particles in two different PSD curves, Figure 3.7. As shown by the red line, the Kezdi criteria is not satisfied as the ratio of D_{15} to d_{85} is greater than 4 as simplified below.

$$\frac{D_{15}}{d_{85}} = \frac{1.28}{0.20} = 6.4 > 4 \tag{3.4}$$
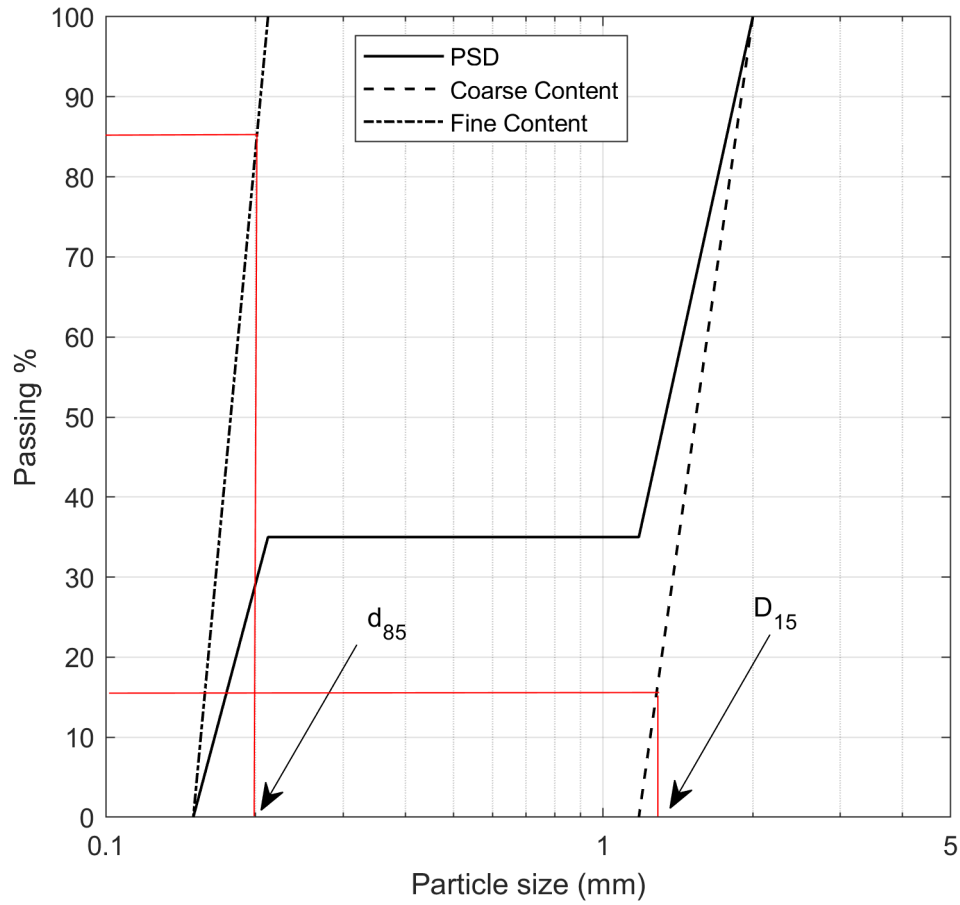
FIGURE 3.7: Illustration of the Kezdi Method (S4-35%)

The third check used in this research is the Burenkova method (Burenkova, 1993). Burenkova determined another method to assess internal instability caused by suffosion, this was done by calculating two factors of uniformity:

$$h_1 = \frac{d_{90}}{d_{60}} \tag{3.5}$$

$$h_2 = \frac{d_{90}}{d_{15}} \tag{3.6}$$

Where

h_1 is a measure of the slope of the PSD for coarse particles

h_2 is an estimation of the filtering between the coarse and fine particles

d_x is the percentage passing a given grain size by mass

The calculation of these factors enabled each material to be assigned to a certain zone as shown in Figure 3.8, where 1st and 3rd zone represent internally unstable soils, 2nd zone represents stable soils, and 4th zone represents artificial soils.

Burenkova developed a formula to account for when a certain soil is in the stable zone based on h_1 and h_2.

$$0.76 \ log(h_2) + 1 \ < h_1 < \ 1.86 \ log(h_2) + 1 \qquad (3.7)$$

A summary of the main three methods used to check the stability of samples has been presented in Table 3.1.
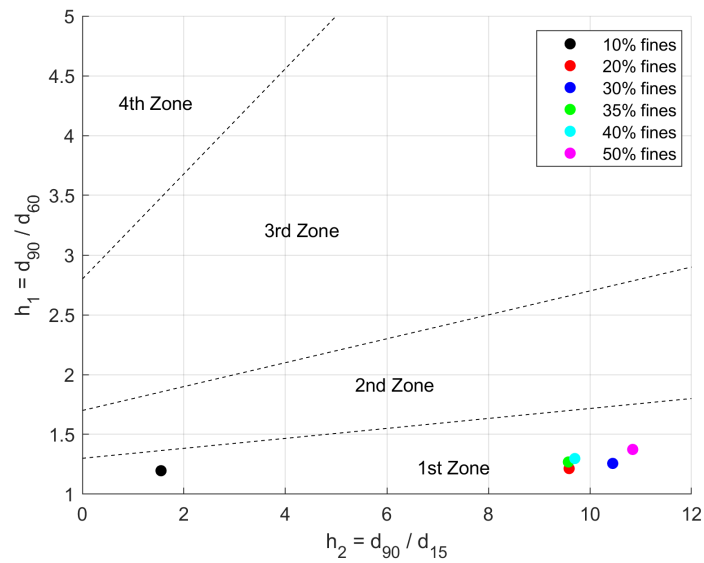
FIGURE 3.8: Illustration of the zones based on the Burenkova
method (Burenkova, 1993)

TABLE 3.1: Summaries of results of Kenney & Lau, Kezedi and
Burenkova methods.

	10%	20%	30%	35%	40%	50%
d_{85} Kezdi	0.20	0.20	0.20	0.20	0.20	0.20
D_{15} Kezdi	1.28	1.28	1.28	1.28	1.28	1.28
D_{15}/d_{85} Kezdi	6.4	6.4	6.4	6.4	6.4	6.4
d_{90} Burenkova	1.890	1.870	1.860	1.840	1.830	1.800
d_{60} Burenkova	1.580	1.540	1.480	1.450	1.410	1.310
d_{15} Burenkova	1.220	0.195	0.178	0.174	0.171	0.166
h_1 Burenkova	1.196	1.214	1.257	1.269	1.298	1.374
h_2 Burenkova	1.549	9.590	10.449	9.575	9.702	10.843
Kenney & Lau	US*	US	US	US	US	US
Kezdi	US	US	US	US	US	US
Burenkova	US	US	US	US	US	US

*US denotes Unstable sample.

3.2.3   Relative density

To achieve maximum stability in geotechnical structures, it is a common practice to aim for a high in-situ density. Therefore this category of density is of importance in investigating internal erosion. For the purpose of this research, it was decided to investigate dense samples attempting to replicate a typically aimed for in-situ density as close as possible.

The voids ratio and density have to be determined as a function of relative density, D_r, for purposes of soil characterisation and also to enable the mass required for the compaction of the soil to a certain relative density to be calculated. The aim is that for erosion testing, the samples are prepared with a uniform relative density. In order to achieve this, the following relationship in Equation 3.8 was used:

$$D_r = \frac{e_{max} - e_o}{e_{max} - e_{min}} \qquad (3.8)$$

Where

D_r is the relative density

e_{max} is the maximum void ratio

e_{min} is the minimum void ratio

e_o is the initial void ratio

Two experiments were set up, one to find the maximum density ρ_{max} and the other to find the minimum density ρ_{min}. This would enable calculation of the maximum and minimum voids ratio for each sample using the

relationship:

$$e_{max} = \frac{G_s \times \rho_w}{\rho_{min}} \quad (3.9)$$

$$e_{min} = \frac{G_s \times \rho_w}{\rho_{max}} \quad (3.10)$$

Where

G_s is the specific gravity taken as 2.67, a typical value for Leighton Buzzard sand (Cavallaro et al., 2001)

ρ_w is the density of water

3.2.4 Minimum and maximum density

Minimum density ρ_{min}

The minimum density of the soil was found using a method adapted from BS1377: Part 4:1990:4.3. A quantity of 500g of room temperature dried soil for each sample was added to a glass cylinder of volume $1000cm^3$. The top of the cylinder was covered with a rubber plug, and the cylinder was shaken three times, afterwards it was turned upside down and then quickly turned to its normal position. The volume of sand displayed on the cylinder was recorded. The cylinder was emptied, and then the same procedure was repeated another two times with new additions of soil for each sample.

A final volume for 500g of soil was recorded for each sample. The mass

M and volume V from the three trials were used to calculate an average value of the minimum density for each soil sample:

$$\rho_{min} = \frac{\frac{M_1}{V_1} + \frac{M_2}{V_2} + \frac{M_3}{V_3}}{3} \tag{3.11}$$

Where

M is the mass in g

V is the volume in cm^3

Maximum density ρ_{max}

The maximum density for each sample was found using a dry method adapted from K.H. Head's Manual of Soil Laboratory Testing (1996). The same method was repeated for each different soil sample. For this method a steel mould of height 115.4mm and inner diameter of 104.5mm was used along with guide sleeves, a surcharge plate, see Figure 3.9, and a vibration deck.

The process began by weighing the empty mould using an electronic mass balance measuring to the nearest 0.1g. This was followed by installing the guide sleeve on top of the mould and using the butterfly wing nuts to ensure that the sides of the mould line together.

Afterwards the sample was divided to 3 portions, each portion was added to the mould, the surcharge base plate was positioned at the surface of the soil and then the surcharge weight was lowered onto the soil. Each portion was vibrated for 10 minutes fixing the mould into the vibration deck

using steel clamps.

At the end, the surcharge weight, excess sand above the mould and guide sleeves were removed, and the soil in the mould was flattened and then the whole ensemble weighed. Subtracting the weight before the soil was added M_m to the weight after the soil was added M_{m+s} yielded the mass of soil added M_m. The volume of the mould was used as the volume of sand V_s to calculate the maximum density ρ_{max} as shown in 3.12 :

$$\rho_{max} = \frac{M_{m+s} - M_m}{V_s} \tag{3.12}$$

Where

M_m is the mass of the mould in g

M_{m+s} is the mass of the mould and the soil in g

V_s is the volume of the mould in cm^3

These results enable the voids ratio at a specific relative density to be calculated. This was done for all samples, Table 3.2 shows the maximum and minimum values for density and void ratio for all samples used in this research.

FIGURE 3.9: Illustration of the steel mould, guide sleeve and sur-
charge plate used

TABLE 3.2: Minimum & maximum density and void ratio

Fines content	ρ_{min}	ρ_{max}	e_{max}	e_{min}
%	g/cm^3	g/cm^3	-	-
10	1.493	1.777	0.788	0.503
20	1.563	1.894	0.709	0.410
30	1.560	1.933	0.711	0.381
35	1.575	1.940	0.695	0.376
40	1.569	1.937	0.702	0.378
50	1.551	1.915	0.721	0.394

3.3 Development of triaxial permeameter

A triaxial permeameter has been developed to study the effect of seepage flow through a gap-graded soil under controlled stress conditions.

The triaxial permeameter, Figure 3.10, enables the permeability to be examined, as well as the quantity of eroded soil, under a complex stress state where axial and radial stress can be controlled.
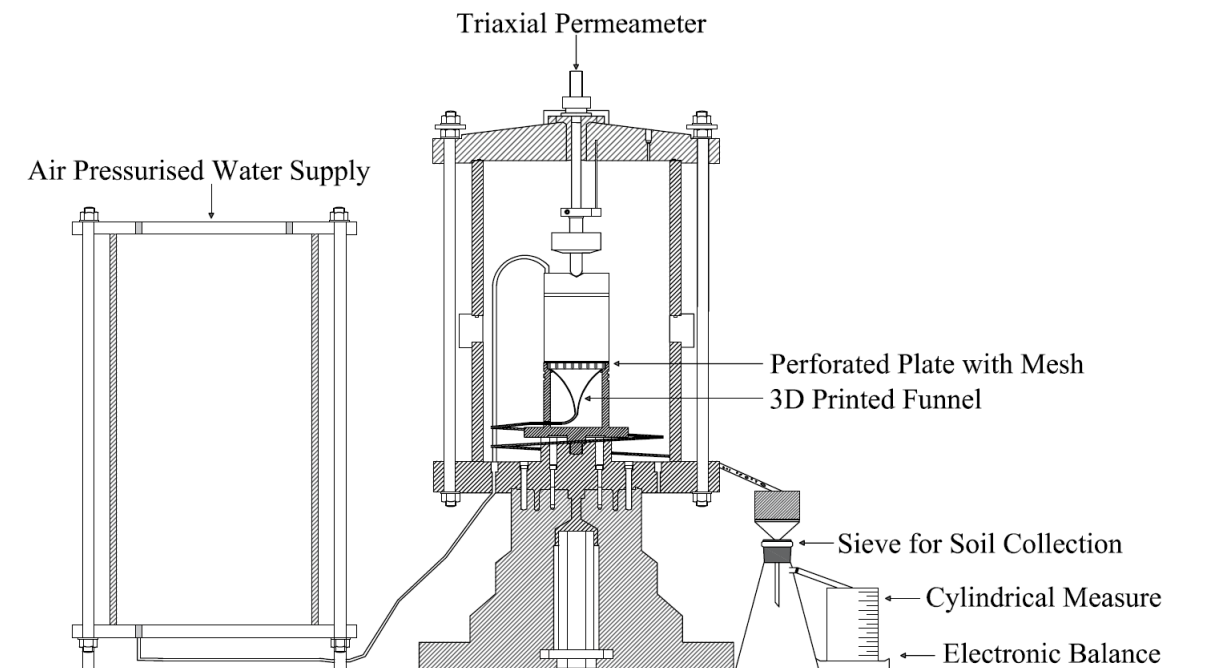
FIGURE 3.10: Schematic of the triaxial permeameter

3.3.1   Main triaxial system

A Bishop and Wesley stress path cell, Figure 3.11, has been adapted to create the triaxial permeameter. The apparatus is computer controlled and pressure controlled by a GDS system allowing independent control of hydraulic gradient and stress state. Figure 3.13 illustrate the main parts of the triaxial permeameter system. The GDS controller has a maximum pressure capacity of 4 MPa and a pressure resolution of 0.1 kPa. A metric load cell with +/- 5 kN capacity was used to record axial load to allow the axial stress to be calculated.

A 3D printed funnel has been added to the base of the triaxial with a wide transparent tube to guide the eroded soil through from the base of the sample to the soil collection system. A pressure sensor was connected to the funnel neck to ensure that the pressure is close to zero (no blockage), as the end of the tube is at atmospheric pressure flowing onto the sieve (soil collection system), see Figure 3.14. The funnel was coated using a seal coating to prevent any leakage.

Typically used porous stones at the bottom and top of the sample have been replaced with a Perspex perforated plate and mesh at the bottom to support the body of the sample while allowing the eroded fine particles to pass through to the soil collection system, see Figure 3.12 and 3.15. A mesh finer than the fine particles was used at the top of the sample to stop any fines migration upwards during the saturation stage.

The perforated solid plastic plate is 10mm thick and 100mm in diameter. Between the specimen and the perforated plate, a mesh with an opening

size of 1mm has been placed in order to screen eroded particles and to ensure that only the fines are removed and not the coarse particles.

When typical top-cap with a single outlet was used, it was visually apparent that fine particles were eroding from one side of the specimen. As a result, the usual top-cap has been replaced with a top-cap with four outlets to ensure that water input is evenly distributed across the specimen. Compared to the usual metal top-cap, the lightweight Perspex top-cap used in this research would reduce the self-weight effect on the total stress, Figure 3.16.

The sample's vertical settlement was measured externally using a linear variable differential transformer, LVDT, with a precision of 0.05 mm. Local on-sample submersible strain transducers (two axial: RDP model D5-400WRA, and one radial, RDP model D5-400W) were mount on the specimen to measure vertical and radial strain internally, removing bedding and apparatus compliance errors, Figure 3.17. The holder of two vertical transducers and one radial was glued (using LOCTITE Super Glue) to the centre of the sample prior to each test. The local strain transducers have a displacement range of +/- 10 mm with a displacement resolution of 4μm.

Each axial submersible LVDT were mounted on the test specimen by means of two diametrically opposed pads glued to the test specimen's membrane and has a weighted rounded end that rests freely on the lower pad anvil. The radial strain belt is positioned at the midpoint of the sample and is hinged at one side, and holds the transducer and pin on the other. The radial submersible LVDT is positioned across the opening of the radial strain belt calliper, where it measures the opening and closing of the jaws.

All submersible LVDTs work with a free-moving internal pin inside the cylindrical barrel, Figure 3.18.

FIGURE 3.11: Fully assembled triaxial permeameter
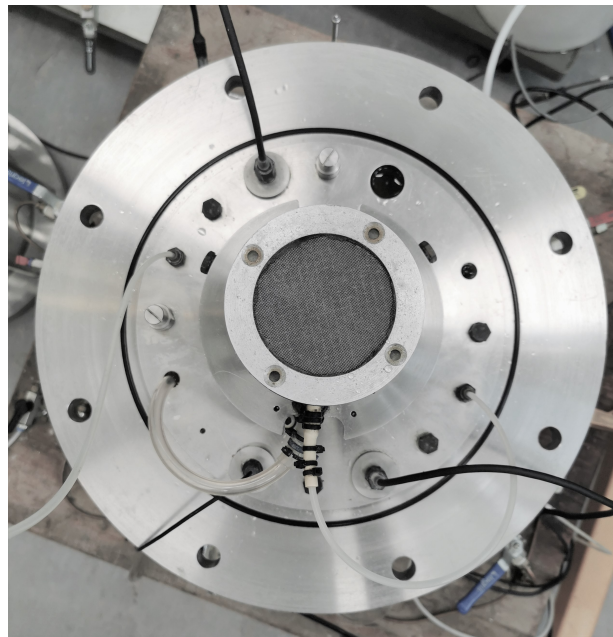
FIGURE 3.12: The triaxial permeameter base with the mesh

cell

sample

funnel

eroded soil
collected

100 mm

100 mm

Sample

GDSLAB Control Software

8 Channel Data Acquisition System

External LVDT

**Local Strain Sensors
and specimen mounts**

GDS Control Chamber Pressure

GDS Control Cell Pressure
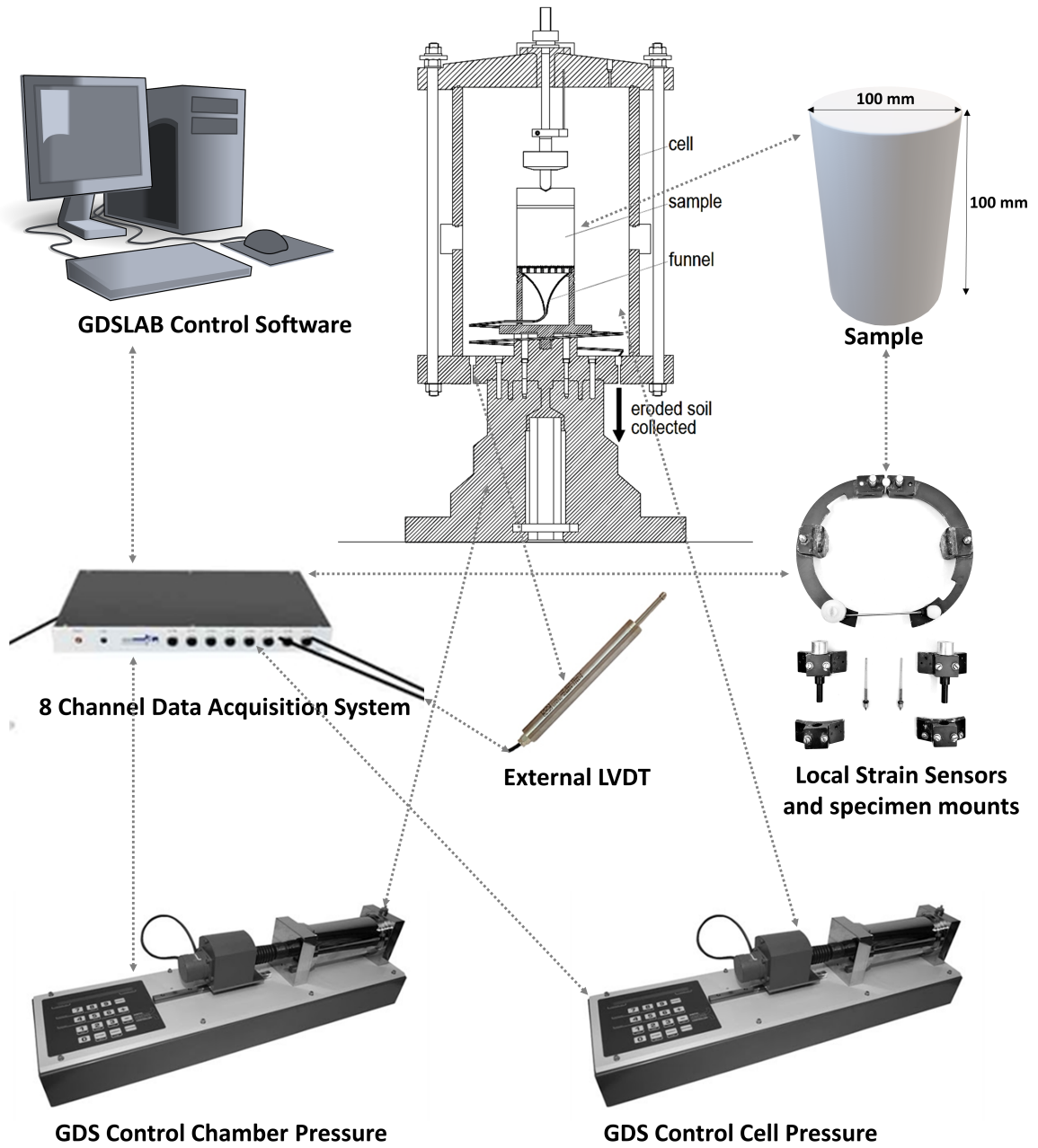
FIGURE 3.13: Main triaxial permeameter system
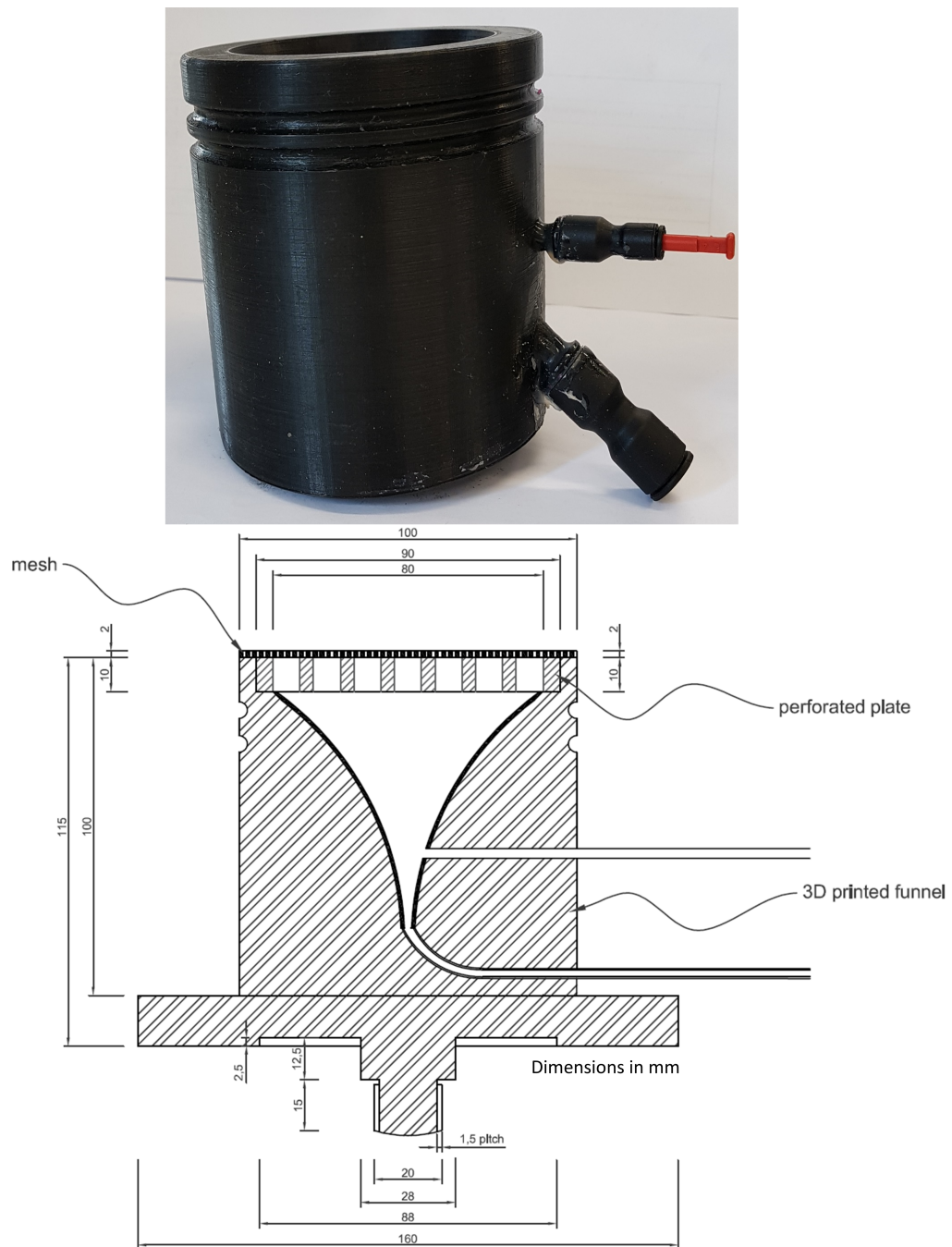
FIGURE 3.14: 3D printed funnel
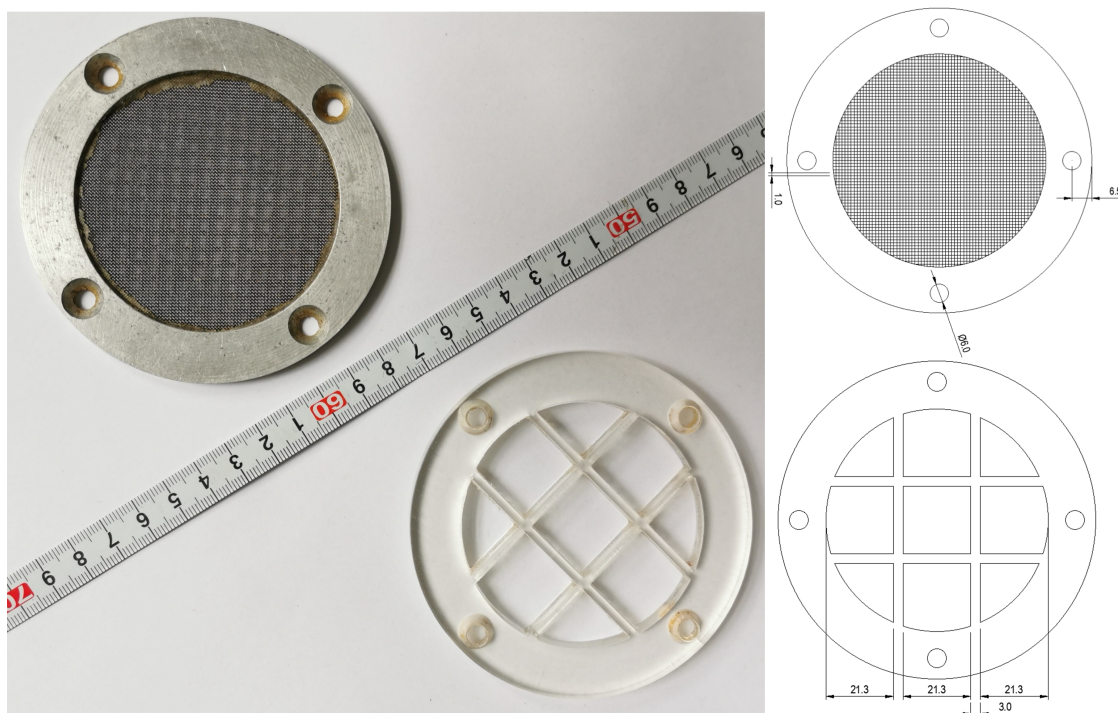
FIGURE 3.15: Perforated plate with 1mm mesh

FIGURE 3.16: Amended top-cap with four outlets

FIGURE 3.17: local strain sensors and specimen attachments (axial mounts and radial strain belt)
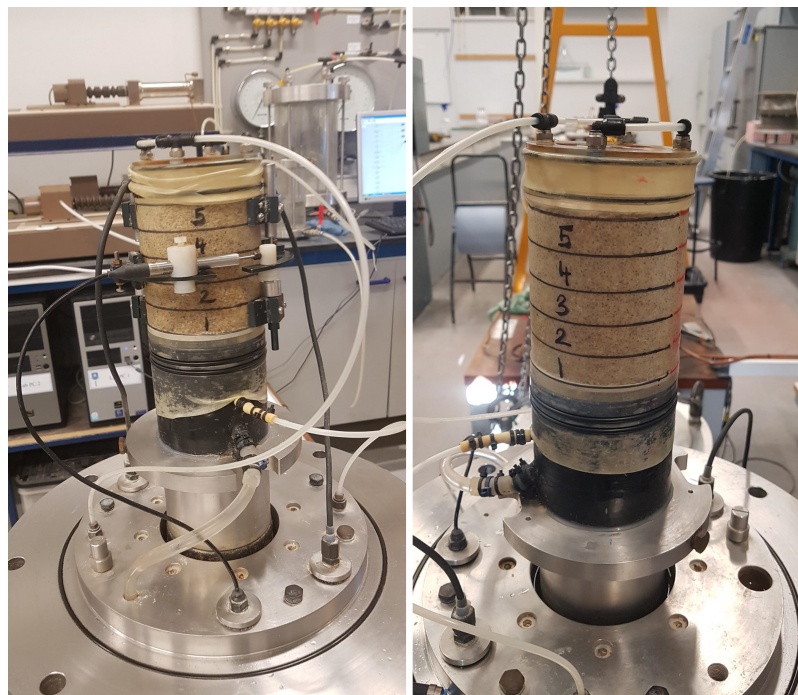
FIGURE 3.18: Sample with and without local strain sensors

3.3.2   Water supply system

The pressurised de-aired water system allowed a steady flow rate to be achieved through the soil. The system was composed of two water tanks formed of a Perspex cell 400 mm in diameter and 600 mm in height and supported on metal bars as illustrated in Figure 3.19.

The pressurised water system had two valves at the top: Valve 1 allowing the hydraulic head to be air pressure controlled through a pressure regulator, and Valve 2 allowing a way to de-pressurise the system when it is desired to reduce pressure. Valve 3 was used to fill the tank with de-aired water which would be used in erosion tests as an outlet valve. The pressure regulator was operated through the pressurised air supply.
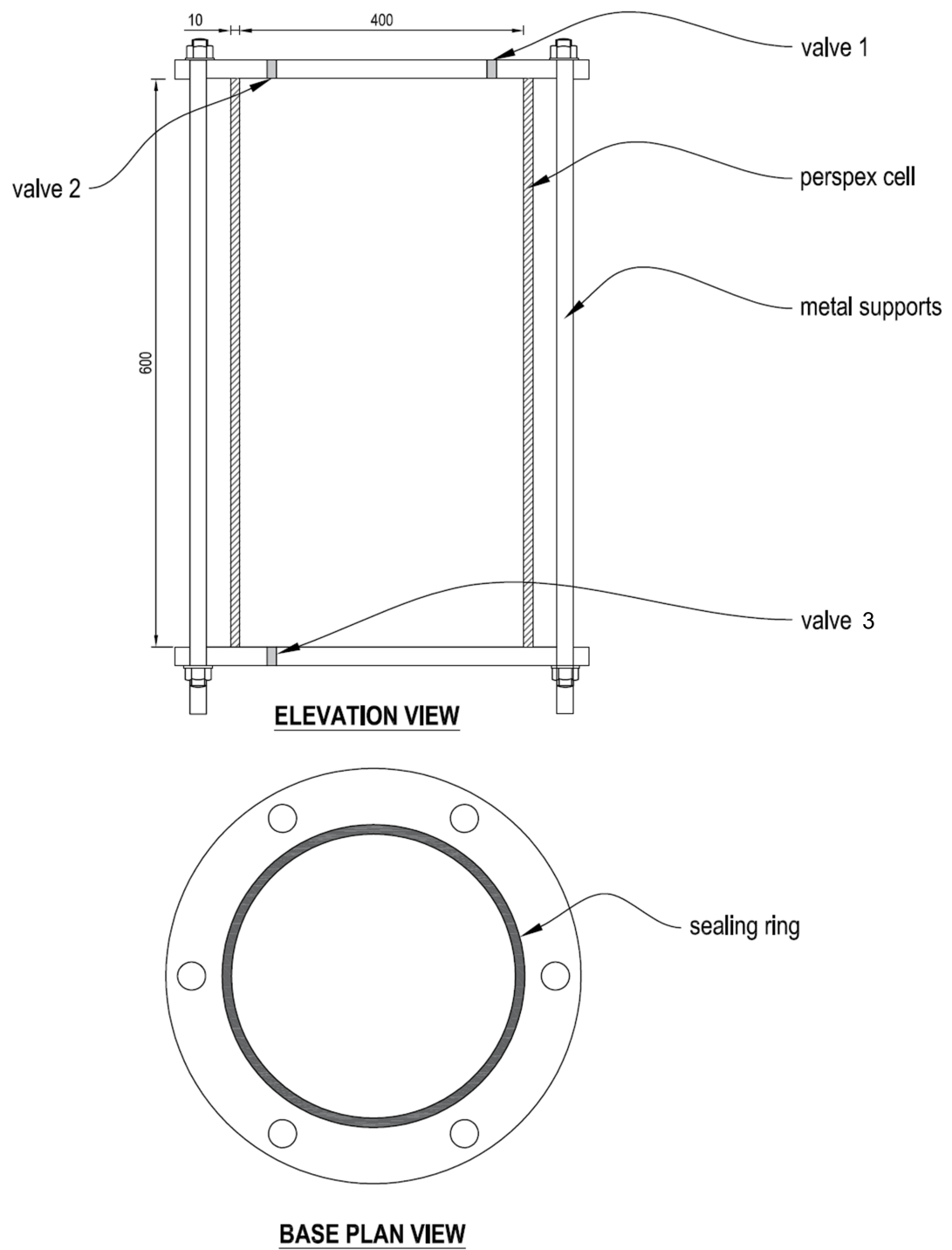
FIGURE 3.19: Pressurised de-aired water system

3.3.3   Fine particle collection system

The fine particle collection system commenced from the 3D printed funnel and its pipe, which guided the eroding soil and accompanying water towards a fine sieve with a 63 micron mesh size. The size of the mesh screen was in accordance with the minimum particle size of the test soil.

Figure 3.20 illustrates the soil collection system from the funnel to the water collection system. The quantity of the eroded fine particles was collected every 10 minutes to study the erosion behaviour.

3.3.4   Water collection system

The water collection system was formed of a downstream reservoir which was fully filled with de-aired water prior to testing, which directed water into a water container sets on an electronic mass balance.

The electronic mass balance was used to periodically log the data to a computer in order to be able to determine the discharge flow rate, seepage flow and permeability of the sample throughout the internal erosion process. The mass balance has a weighing capacity of 6 kg and a resolution of 0.1g.

A software program was developed using Labview to record a reading for the water container every 10 seconds. The software converted the time and weight readings to an excel sheet file.
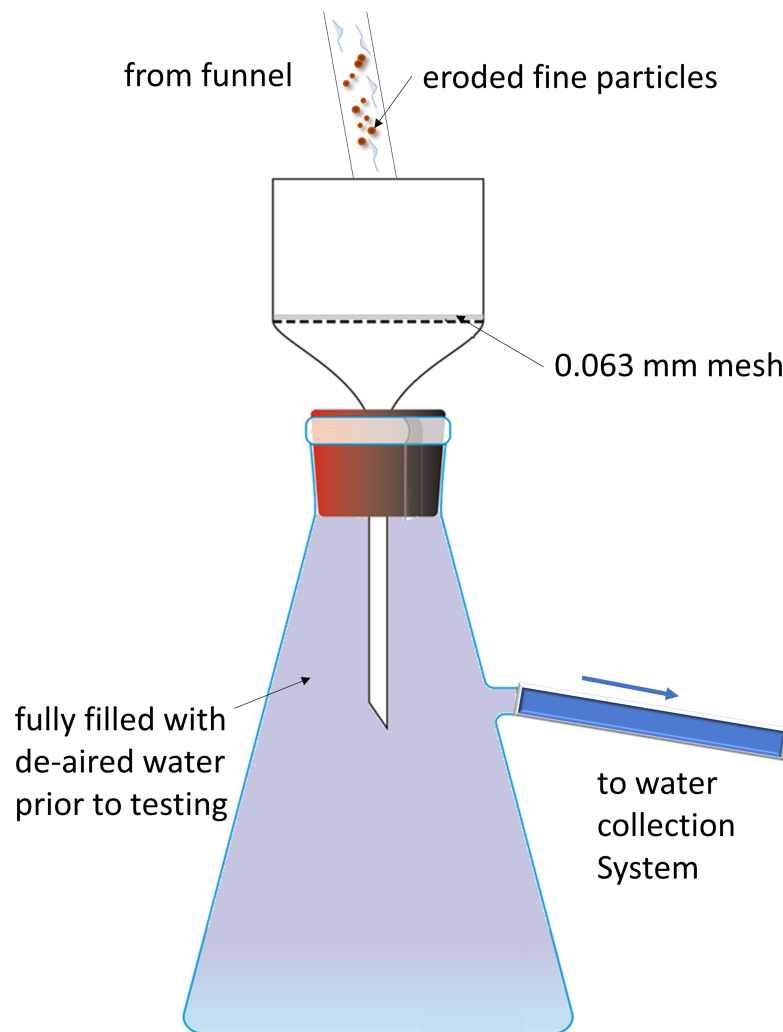
FIGURE 3.20: Fine particles collection system

3.3.5 Previous trials

The design of the 3D printed funnel evolved as a result of two main trials. A detachable plastic funnel located inside a metal pedestal was used for the initial design, Figure 3.21(A). The sharpness of the output neck of the plastic funnel was found to block fine particles, and hence another design was needed.

The second trial, Figure 3.21(b), used a 3D printed funnel with a curved output pipe to avoid fine particles blockage, Figure 3.14. The funnel initially was printed using a low density printing mode. This caused water leakage through the wall of the funnel.

The final design, Figure 3.21(c) used the maximum density setting on the 3D printer to reduce the porosity of the printed medium to the lowest possible value. Moreover, the funnel was then coated using a seal coating (XTC-3D brush-on coating) to prevent any leakage.
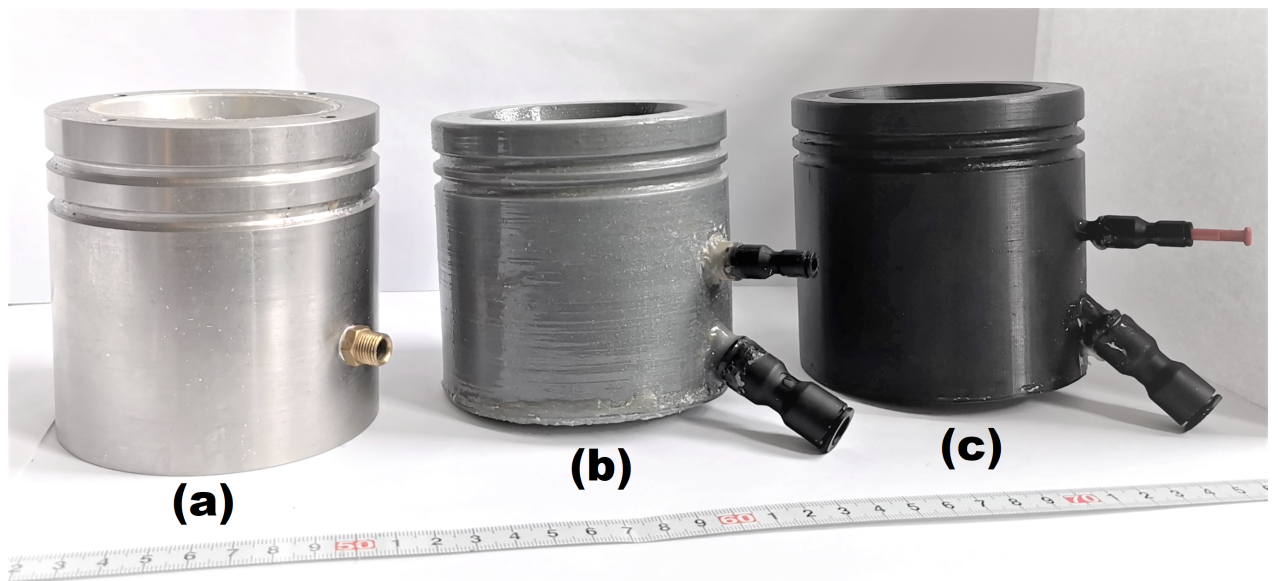
FIGURE 3.21: Fine particles collection system (previous trials)

During the design progress, many perforated plates and meshes were used. Some of the attempts are presented in Figure 3.22.

FIGURE 3.22: Design progress trials

3.4 Testing program

To study the behaviour of fine particles erosion, this research conducted four main testing sets. All four testing sets were tested while shearing the samples.

Firstly to establish a baseline of data, a series of triaxial tests with downward seepage flow at different hydraulic gradients was conducted on a gap-graded soil in order to determine and quantify the influence of the hydraulic gradient on the onset and progression of internal erosion, Chapter 4.

The second set of tests were performed to study the influence of the initial fines content on the onset and progression of internal erosion. To cover a variety of possibilities found in geotechnical structures, from under to overfilled, the erosion tests were performed on six samples with different fines contents in the same conditions under a constant aimed-for initial hydraulic gradient of 10, Chapter 5.

The third set of tests main objective was to investigate the effect of the stress path on the onset and the progression of internal erosion on gap-graded soil. A series of experimental tests was carried out on six samples of gap-graded soil under three different stress paths (two repeats for each path). For stress path 'A', the radial pressure was decreasing, and axial stress was maintained so as to decrease the total mean stress p while increasing the deviatoric stress q, Figure 6.1. For stress path 'B', the radial pressure was decreasing, the axial stress increasing, and hence, deviatoric stress increased while keeping the total mean stress constant (taking a vertical stress path). In stress path 'C', the radial pressure was kept constant, increasing the axial stress and hence, total mean stress while increasing the deviatoric stress (a typical conventional stress path used in triaxial testing).

The influence of different shearing rates on the internal erosion behaviour of different samples of gap-graded soil was studied in the last set of tests. Six samples of internally unstable soil, of a given particle size distribution, were tested in the triaxial permeameter using three different shearing rates, Chapter 7.

Table 3.3 provides a summary of the testing program used in this research. The first segment of the name refers to the specimen number, followed by

the initial fines content and then the intended hydraulic gradient with the stress path used apart from the last set of tests where the third segment represents the shearing rate. All tests in this set used hydraulic gradient of 10 with B stress path (refer to Figure 6.1 for an illustration of the stress paths used in this research).

TABLE 3.3: Summary of the testing program

Test name	Hydraulic gradient	Fines content (%)	Stress path	Shearing rate (mm/min)
Seepage flow study				
S1-35-10B	10	35	B*	0.1
S2-35-15B	15	35	B	0.1
S3-35-20B	20	35	B	0.1
S4-35-25B	25	35	B	0.1
Fines content study				
S5-10-10B	10	10	B	0.1
S6-20-10B	10	20	B	0.1
S7-30-10B	10	30	B	0.1
S1-35-10B	10	35	B	0.1
S8-40-10B	10	40	B	0.1
S9-50-10B	10	50	B	0.1
Stress path study				
S10-35-10A	10	35	A	0.1
S11-35-10A	10	35	A	0.1
S12-35-10B	10	35	B	0.1
S1-35-10B	10	35	B	0.1
S13-35-10C	10	35	C	0.1
S14-35-10C	10	35	C	0.1
Shearing rate study				
S15-20-0.05	10	20	B	0.05
S6-20-0.1	10	20	B	0.1
S16-20-0.2	10	20	B	0.2
S17-35-0.05	10	35	B	0.05
S1-35-0.1	10	35	B	0.1
S18-35-0.2	10	35	B	0.2

*Refer to Figure 6.1 for an illustration of the stress paths used in this research.

3.5 Testing procedures

3.5.1 Test preparation

De-airing water

At the start of any test, a considerable amount of de-aired water needed to be prepared and stored in water tanks, see Figure 3.19. Two de-aired water systems with 8 litres capacity were used to prepare the de-aired water supply, Figure 3.23. It could take to up to 5 hours to fill enough water to start an erosion test. To store de-aired water without introducing any air to the system, the water tank was under negative pressure when storing the de-aired water.

FIGURE 3.23: De-Aired Water system

Soil preparation

Samples were prepared for triaxial testing using the undercompaction method proposed by Ladd (1978). The method helps to ensure an even distribution of particles through the sample. It is very efficient in the compaction of sand, avoiding the issue of having the asymmetrical compaction throughout the sample (bottom layers having a higher relative density in comparison to top layers).

The rubber membrane was visually inspected for tears before each test to avoid any leakage, then a thin layer of silicon grease was applied around the base of the pedestal before the membrane was applied, and the perforated plate with the mesh and O-rings were added to secure the ensemble.

An external 3D printed split compaction mould was used with an internal diameter of 100mm and a height of 100mm, Figure 3.24. The split mould was added around the membrane and sealed using plasticine. A suction vacuum was created between the mould and the membrane in order for the membrane to expand in the mould against its sidewalls. The sample was placed in 5 layers, thus leading to a layer height of 20 mm. Each layer mass was determined by dividing the soil mass, calculated for the desired level of relative density, by the total number of layers. For each layer a moist tamping method was used in order to ensure that the particles would adhere well to each other, and to avoid particle size segregation.

For each layer, the soil mass required for one layer was added and then

compacted with a wooden tamping rod in a circular motion from the periphery towards the centre until the respective layer reached the desired height, as calculated by the formula adapted from Ladd (1978):

$$h_n = 12.5[(n-1) + (1 + U_n)] \tag{3.13}$$

Where

n denotes the layer number (with the layers being counted in the order of placement)

h_n is height of compacted material at the top of the layer being considered

U_n is the percent (as a decimal) of undercompaction

The percentage of undercompaction can be calculated for each layer using the following formula Ladd (1978):

$$U_n = U_{ni} - \left[\frac{U_{ni}}{15} \times (n-1) \right] \tag{3.14}$$

Where

U_{ni} is the percent undercompaction as a decimal chosen, for the first layer to be 5% for this research (recommended to be between 0 and 15% depending on the density of the sand from dense to loose).

After the compaction process was finished, the top cap was added, greased as for the pedestal, and an O-ring was added. The split mould was removed after a negative pressure of 15 kPa had been applied to the sample, in order to ensure that the sample could stand on its own. At this point

the height (100mm) and diameter (100mm) of the sample were measured
in order to ensure that they corresponded to the planned dimensions. The
submerged local strain transducers were mounted and glue left to dry. At
this point the logging of data could be started.

FIGURE 3.24: 3D printed split compaction mould

3.5.2   Soil saturation and consolidation

After preparing the sample, the cell cap was placed and sealed while the
cell was allowed to be filled with water. The negative pressure was slowly
lowered as the cell pressure was increased from 0 to 15 kPa.

The sample was then injected with CO_2 at a slow rate for 1 hour in or-
der to remove air bubbles present in the sample. This process improves

sample saturation as CO_2 dissolves much easier in de-aired water in comparison with air.

The sample was then saturated by very slow de-aired water flow from the bottom upwards. The saturation process was verified by checking the outflow water using a dissolved oxygen meter (inoLab Oxi 730). Totally de-aired water has a reading below 4 mg/L. Aerated water (water fresh from the tap) always gave a reading of above 9 mg/L.

Both the funnel, the base plate and the transparent tube were submerged with de-aired water throughout the test. During all tests, the downward flow was maximum at the top of the sample and very close to atmospheric pressure at the bottom of the sample. The sample sets on the 3D printed base with funnel, a flexible wide transparent tube was used to guide the eroded soil through from the base of the sample to the soil collection system.

The sample was then consolidated to 50 kPa mean total stress by increasing the cell pressure. The consolidation process was complete when the desired cell pressure was reached, and the axial and radial strain of the sample no longer changed with time. Any amount of axial or radial strain before the start of the erosion testing would be considered when determining the initial values of void ratio.

3.5.3   Erosion testing

A hydraulic gradient of 10 was chosen for all tests apart from seepage flow study tests (Chapter 4) to study the behaviour of internal erosion

under the applied stress conditions and material used. This value was used within the chosen hydromechanical boundary which was set following preliminary tests, presented in Chapter 4 and Appendix B.

Before starting to shear the sample, the seepage flow was increased gradually until reaching the intended hydraulic gradient. The amount of eroded fine particles was found to be negligible at this stage. The erosion phase of the test was generally commenced by shearing the sample with the intended shearing rate (either 0.05, 0.1 or 0.2 mm/min - see Chapters 4 to 7). This phase was generally last 1 to 4 hours depending on the shearing rate used.

The eroded particles were collected every 10 minutes, and the water flow was recorded using an electronic balance every 10 seconds.

Once the sample reached failure, the test was stopped and the confining pressure was brought back until it reached atmospheric pressure, the water from the cell was emptied, and the cell was dismantled.

Each stage of collection was numbered for subsequent oven drying to be weighed using an electronic balance with a maximum capacity of 210 g and a very high resolution of 0.1 mg.

3.5.4   Post test grain size distribution analysis

All tested samples was equally divided into three layers, top, middle and bottom after each test. All layers were oven-dried separately and sieved

to analyse the effect of erosion on particle size distribution for each layer, See Chapter 7.

3.6 Summary

This chapter summarises the tested materials and their characterisation, the testing concept including the development of the triaxial permeameter, the research testing program, the procedures used to prepare and perform the erosion tests.

For the purpose of this research, a cohesionless gap-graded sandy soil was used. Characterisation tests were undertaken to determine the characteristics of the soils to be tested.

A triaxial permeameter has been developed to study soil erosion behaviour in a gap-graded soil under controlled stress conditions. The triaxial permeameter enables the permeability to be examined, as well as the quantity of eroded soil, under a complex stress state.

To study the behaviour of fine particle erosion, this research conducted four main testing sets to investigate the effect of seepage flow, initial fines content, stress path and shearing rate on the onset and progression of internal erosion.

Chapter 4

Seepage Flow Study

4.1   Introduction

It has been shown that the potential for internal erosion within a soil is influenced by the geometric, hydraulic and mechanical conditions of the soil (Kenney and Lau, 1985; Tomlinson and Vaid, 2000; Richards and Reddy, 2007; Moffat et al., 2011).

A considerable amount of literature has been published on the influence of seepage flow on the internal erosion process. In this chapter, in order to establish a baseline of data, a series of triaxial tests with downward seepage was conducted on a gap-graded soil in order to determine the influence of the hydraulic gradient on the onset and progression of internal erosion.

Over recent decades, investigating the influence of seepage flow on the onset of internal instability in granular materials has been a constant concern in the literature. Bendahmane et al. (2008) found a gain in the rate

of suffusion with increased hydraulic gradient and with reduced confining stress, from triaxial tests on sand samples with different clay content. Moffat et al. (2011) proposed a hydro-mechanical boundary concept in the stress-hydraulic gradient space to quantify the onset of internal erosion based on the results of erosion.

For a gap graded sand, Chang and Zhang (2013) conducted internal erosion tests under complex stress states and investigated the influence of stress on the critical hydraulic gradient. During erosion testing, the stress state was kept constant while varying the hydraulic gradient. They defined three critical hydraulic gradients which they named 'initiation'- i.e. the critical hydraulic gradient at the onset of erosion or fines loss, 'skeleton-deformation critical hydraulic gradient' when buckling of force chains starts and "failure critical hydraulic gradient" at soil failure. All the above researchers indicated the importance of studying the hydraulic gradient's role in the development of internal erosion.

4.2   Preliminary work

In this research during erosion testing, the hydraulic gradient was kept constant for each test while changing the stress state (i.e. continuously shearing). Initial observational tests were conducted while shearing the sample to determine the ideal range of hydraulic gradients to study the seepage flow behaviour for the soils examined in the thesis at the initial stress state chosen.

The chosen hydraulic gradients needed to be enough to initiate the internal erosion under each set of test conditions but not so high as to enable them to be related to realistic field scenarios. The primary outcomes of the analysis of these preliminary tests were; first, a hydraulic gradient of 10 would be a minimum sufficient gradient to cause measurable fines loss under the initial conditions. Second, a step of 5 in hydraulic gradient (i.e. Δi = 5) would be adequate to observe a physical change in erosional behaviour.

The same experiment was repeated without shearing the sample, and there was no measurable fines loss under the initial conditions. Therefore it has been decided to shear all samples while conducting the erosion testing in this thesis. The preliminary tests details and full observations can be found in Appendix B.

4.3 Results of seepage flow study

Following the preliminary work, this chapter describes a series of triaxial tests performed under different hydraulic gradients, above the threshold of i=10, to investigate the influence of seepage flow on the onset and the development of internal erosion in a gap-grade soil.

Four samples of gap-graded soil, named S1-35-10B, S2-35-15B, S3-35-20B and S4-35-25B with an initial fines content of 35%, were tested under different hydraulic gradients, i, of 10, 15, 20 and 25, respectively. A summary of the testing conditions is shown Table 4.1.

The first segment of the name refers to the specimen number, followed by the initial fines content and then the intended hydraulic gradient with the stress path used. The experimental results are reported in detail and discussed below.

TABLE 4.1: Summary of the testing program and results for seepage flow study.

Test Name*	B2	S1	S2	S3	S4
Finer fraction (%)	35	35	35	35	35
Axial displacement rate (mm/min)	0.1	0.1	0.1	0.1	0.1
Gap ratio	5.57	5.57	5.57	5.57	5.57
Intended relative density, D_R (%)	70	70	70	70	70
Initial relative density, D_{Ri} (%)**	71.3	70.9	69.3	72.5	71.7
Intended void ratio, e	0.472	0.472	0.472	0.472	0.472
Initial void ratio, e_0	0.468	0.469	0.474	0.464	0.467
Coarse particles initial mass, m_{ci} (g)	889	889	889	889	889
Fine particles initial mass, m_{fi} (g)	479	479	479	479	479
Intended Hydraulic Gradient i	-	10	15	20	25
Mean hydraulic gradient i_m	-	11.2	15.6	21.2	25.4
Initial total mean stress, p_i (kPa)	50	50	50	50	50
Max Deviatoric stress, q_{max} (kPa)	102.8	86.4	82.2	78.6	71.6
Mean effective stress at q_{max}, p'_{qmax} (kPa)	51.4	47.4	43.1	41.3	39.4
Shearing resistance internal angle, $\phi_{peak'}$	48.6°	44.3°	46.4°	46.2°	44.3°
Accumulated erosion mass, m_{fa} (g)	-	66.8	68.1	79.8	88.5
Accumulated erosion percent, m_{fap} (%)	-	13.9	14.2	16.7	18.5

*S1=S1-35-10B, S2=S2-35-15B, S3=S3-35-20B, S4=S4-35-25B,and B2=B2-35-0B.

**Initial relative density was measured just before commencing the erosion stage (testing stages are discussed in Chapter 3).

4.3.1 Hydraulic gradient

Figure 4.1 plots the variation of the hydraulic gradient i with respect to local axial strain, ϵ_a for the tested sample during the erosional experiments.

Different initial hydraulic gradients for each test were achieved by controlling the pressure on the air pressurised water tanks, which were pre-filled with de-aired water, prior to the erosion stage. The hydraulic gradient at the start of the test was then set at the desired value using the differential pore pressure across the sample, and the initial corrected length, L_c. The differential pore pressure was assessed using two pore pressure gauges connected at each end of the tested samples and the corrected length, L_c was determined by deducting the length reduction measured by the submerged local strain devices from the original length, as explained in Chapter 3.
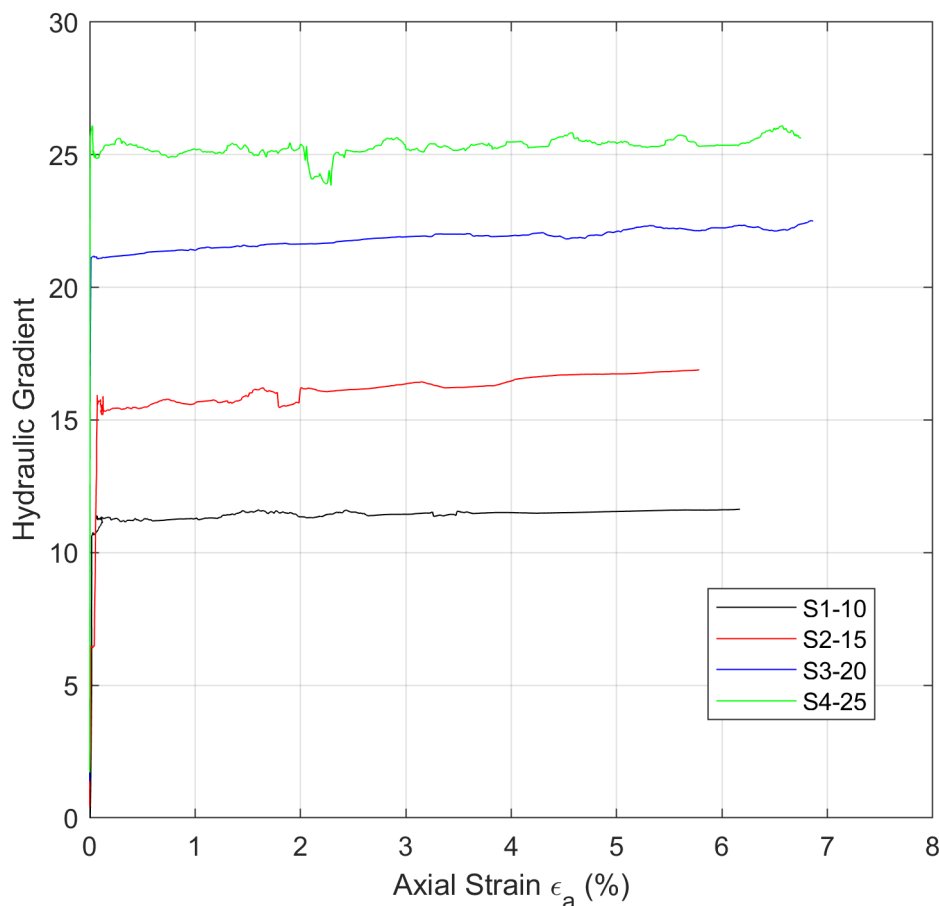
FIGURE 4.1: Relationship between hydraulic gradient and local
axial strain

4.3.2   Drained shear strength

To begin with, a 'baseline' (no erosion) test, named B2-35-0B, was conducted using the same fines content and stress conditions as for the erosional tests, see details in Table 4.1.

In this suite of tests, all were conducted under the stress path 'B' (Figure 6.1), taking a vertical stress path in p-q space to reach failure at or

above the critical state line (with a peak stress expected due to the soils being prepared at a D_R of approximately 70% - i.e. initially 'dense').

In addition to the baseline test, four erosion tests (continuously shearing while eroding) S1 to S4 – with a constant hydraulic gradient for each test of i = 10, 15, 20 and 25, respectively – were conducted. Figure 4.2 demonstrates the initial stress condition for all four tests presented in this chapter. This figure highlights how increasing the hydraulic gradient creates an increasingly non-uniform effective stress within the sample from top to bottom. The mean p′ is reported in the results here.

The failure stress state estimation was taken at the centre of the sample (mid-height), where the radial strain sensors are mounted to give a simplified interpretation.

It is a common practice in triaxial testing to use a 1:2 slenderness ratio (diameter:height) to avoid the effect of end restraint. Bishop and Green (1965) discussed the impact of slenderness ratio and end restraint on the behaviour of sandy soils in triaxial compression testing. They concluded that reducing height to diameter ratio can increase the effect of end restraint leading to an increase in soil strength. However, in this research, it was decided to investigate specimens with 100 mm diameter and 100 mm height (1:1 slenderness ratio) to reduce the differential pore pressure across the sample for a given hydraulic gradient. Since all samples had the same slenderness ratio, this research focuses on analysing comparative values and behaviour and not concentrating on exact values.

The mean stress was kept constant at 50 kPa, Figure 4.3. Note that, because of the seepage within the sample and resultant uncertainties in the local effective stress, the total mean stress p was used, rather than effective mean stress p' to control the stress path.

It is notable that the baseline test B2-35-0B displayed a more consistent and less 'noisy' stress path than the other tests due to the hydraulic controllers being able to maintain the aimed-for stress path far more easily without seepage and erosion taking place. This is more easily seen in Figure 4.4 which shows the deviatoric stress, q against the estimated mean effective stress, p'.
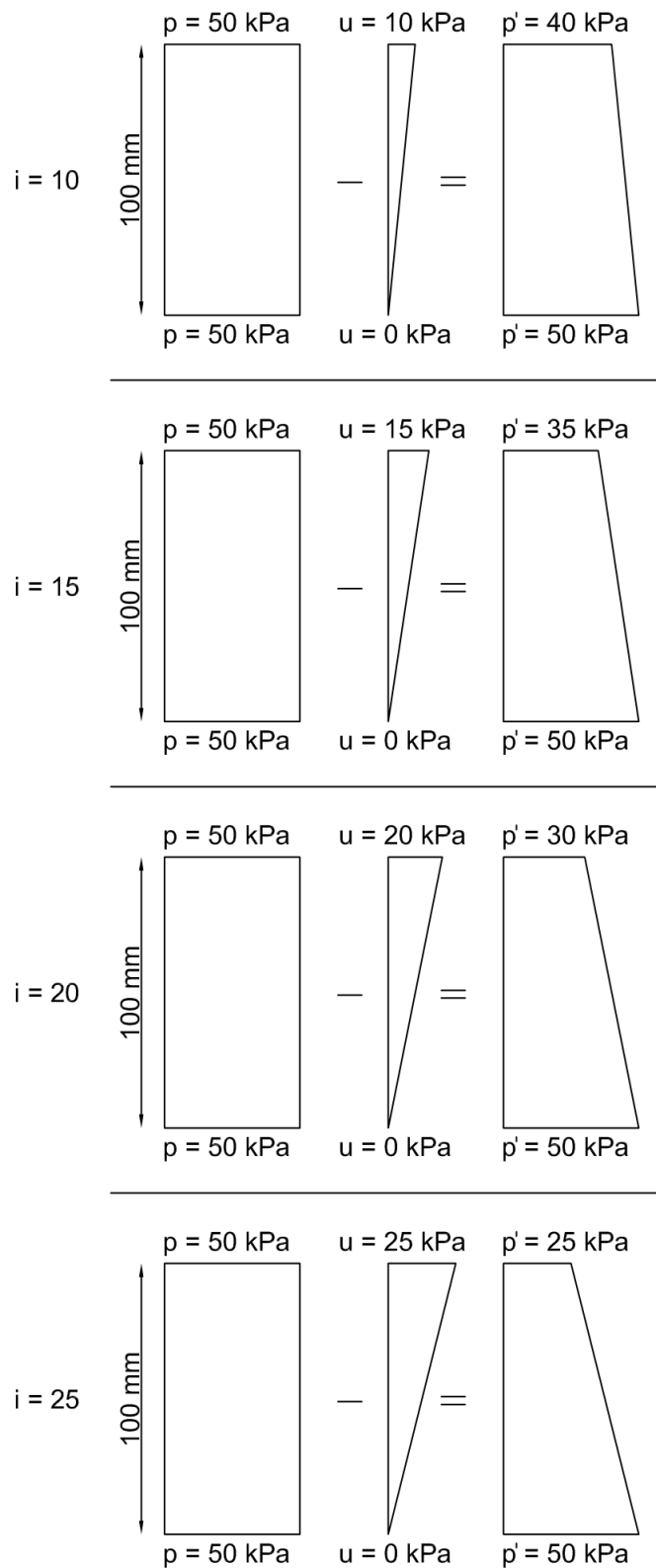
FIGURE 4.2: An illustration of the initial stress conditions
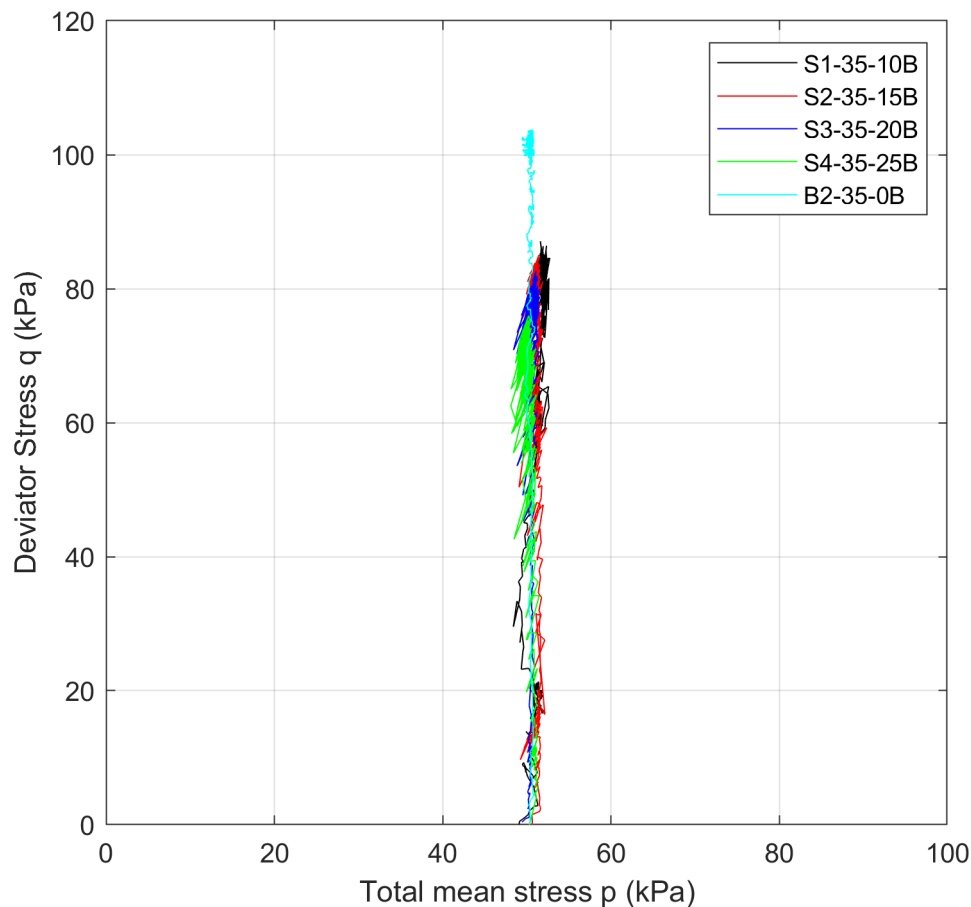
FIGURE 4.3: Deviator stress, q versus total mean stress, p

The mean effective stress was estimated by deducting the average seepage flow pressure across the sample (the pore pressure at mid-point) from the total mean stress, p. In general, all erosion tests recorded lower peak deviatoric stress values comparing to the baseline test (without erosion) B2-35-0B. Also, specimen S4-35-25B recorded the lowest peak deviatoric stress value with specimen S1-35-10B recording the highest of the seepage tests. This may be a result of two processes. The increase in seepage flow rate from test S1-35-10B to S4-35-25B, as denoted by hydraulic gradient, resulted in a higher seepage pressure and hence, lower effective stress at

the specimen midpoint. This would result in less available shear resistance for tests conducted at high flow-rate. In addition, there may be an influence of fines loss, which is discussed later.
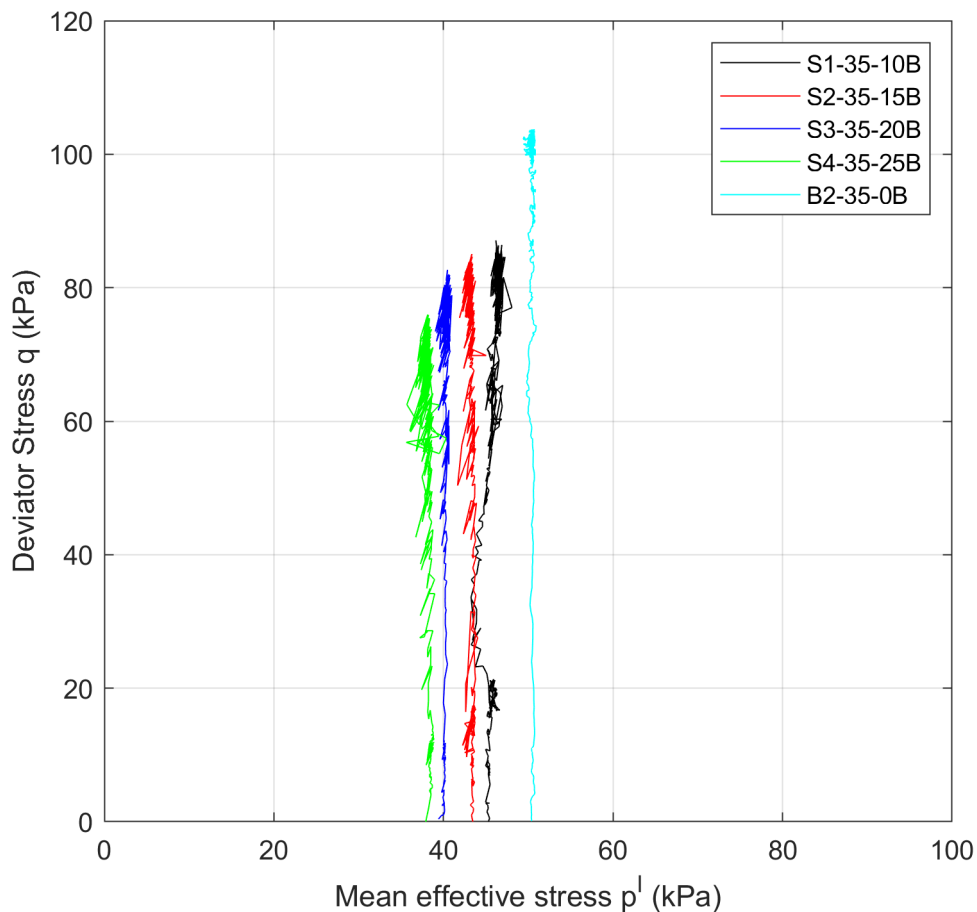
FIGURE 4.4: Deviator stress, q versus mean effective stress, p'

Figure 4.5(a) demonstrates the deviatoric stress, q against the local axial strain, ϵ_a for the tested specimens. As it can be seen from the graph, the peak deviatoric stress, q_{peak} decreases as the hydraulic gradient increases, such that all the specimens recorded lower peak stresses compared to the baseline test B2-35-0B. The reduction in peak stresses varies between 16.4

kPa (16.0%) and 31.2 kPa (30.4%) for tests S1-35-10B and S4-35-10B, respectively.

By increasing the hydraulic gradient from 10 to 25, the peak stress is reduced from 86.4 kPa for test S1-35-10B to 71.6 kPa for S4-35-25B – a reduction of 14.8 kPa in peak deviatoric stress. It is also notable that q_{peak} occurs at a lesser axial strain (by ϵ_a of 6%) for all of the tests experiencing internal erosion than for the no erosion test B2-35-0B, where q_{peak} occurred at ϵ_a of 9%.

Previous literature, wherein Chang and Zhang (2011), Ke and Takahashi (2014), among others, have reported a similar reduction in the soil's strength due to internal erosion/ fines loss. Once again, here it needs to be taken in the context of the fact that seepage was occurring during shearing so that the effective stress was reduced for higher flow-rate.

Figure 4.5(b) illustrates the variation of the volumetric strain with respect to axial strain. All the specimens experienced contractive behaviour followed by dilative behaviour, as expected. Specimens S1-35-10B, S2-35-15B and S4-35-25B display similar dilative behaviour, reaching ϵ_v of approximately 3% at ϵ_a of 6%, while S3-35-20B contracted more and only achieved 2.5% dilative strain at ϵ_a of 6%. Note that S3-35-20B had the largest (and somewhat anomalous) volumetric reduction unlike the other specimens. However, all the specimens have recorded a more dilative response at earlier axial strain in comparison with the no erosion (i=0) test B2-35-0B.
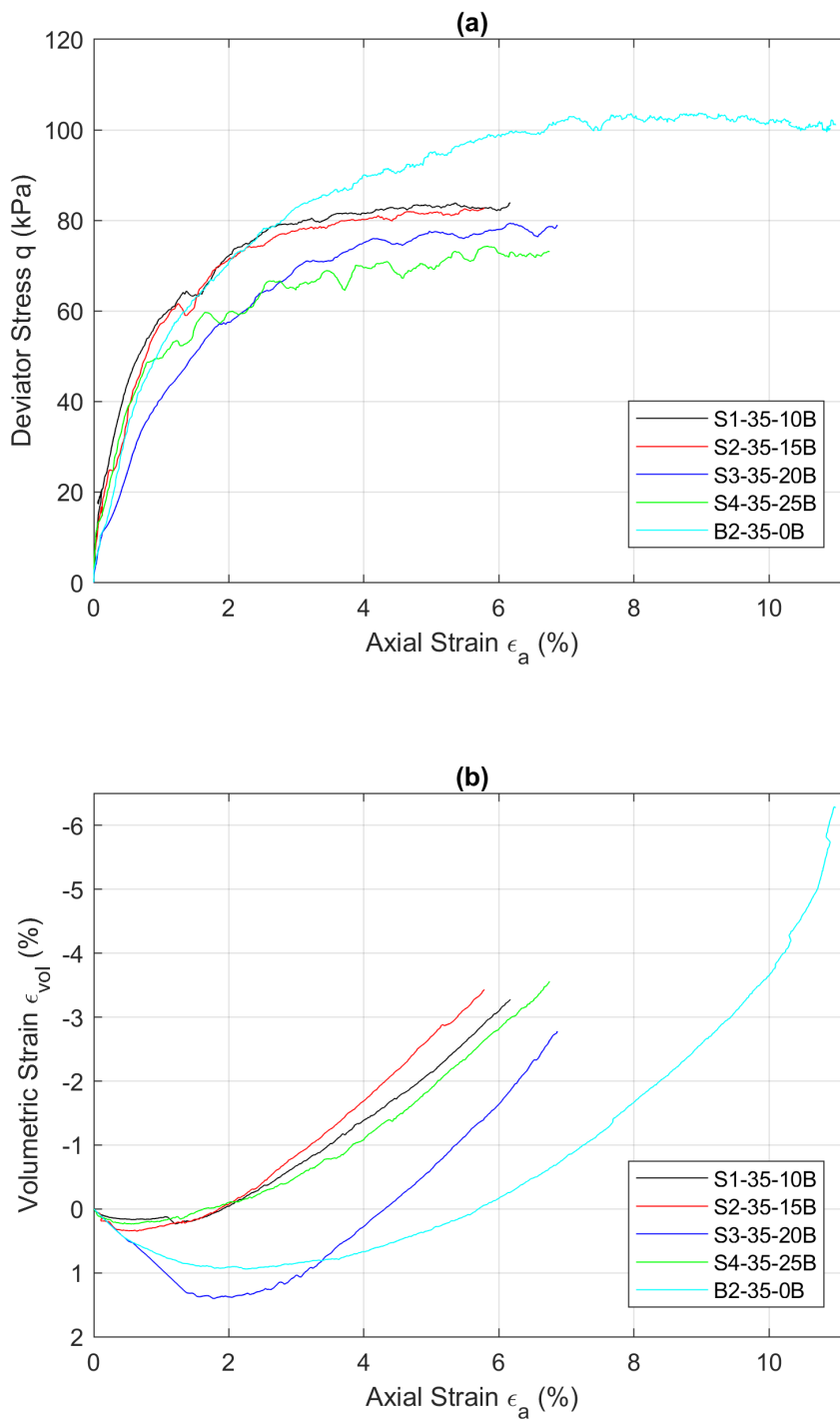
FIGURE 4.5: Relationship between deviatoric stress and volumetric strain vs local axial strain

Figure 4.6(a) demonstrates the normalised deviatoric stress, q_n (q/p') against the local shear strain, ϵ_s for the tested specimens. As it can be seen from the graph, all the specimens recorded lower normalised peak stresses compared to the baseline test B2-35-0B. The reduction in normalised peak stresses varies between 0.3 (13.6%) and 0.5 (22.7%) for tests S4-35-10B and S1-35-10B, respectively. The difference among the eroded tests in normalised peak stresses, q_n was 0.2 (10.5%). Comparing between the tests with erosion, there is no clear difference in the stress-strain curves. Figure 4.6(b) illustrates the variation of the volumetric strain, ϵ_v with respect to shear strain, ϵ_s. All the specimens experienced contractive behaviour followed by dilative behaviour. However, all the specimens have recorded a more dilative response at earlier shear strain in comparison with the no erosion (i=0) test B2-35-0B.
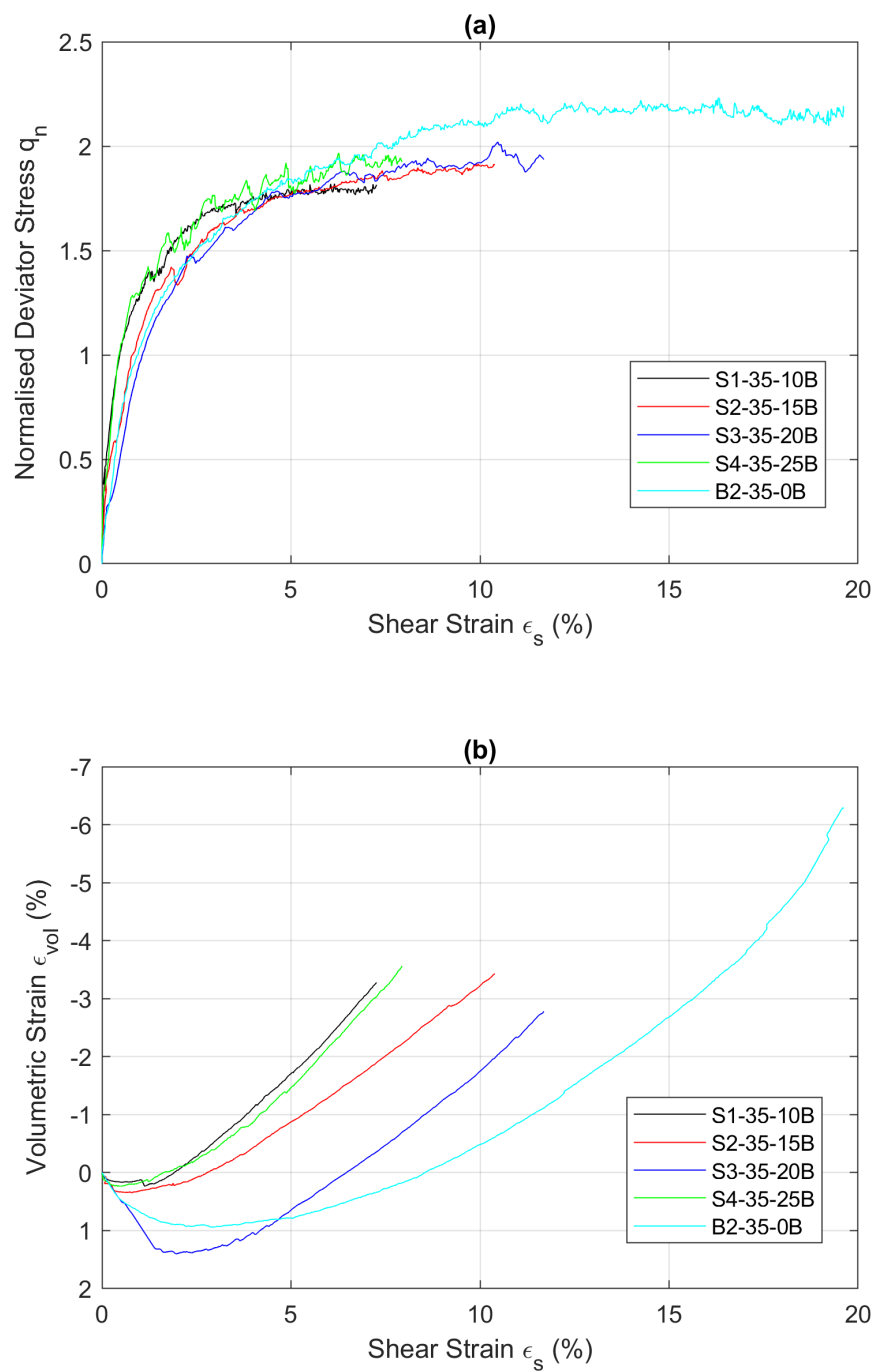
FIGURE 4.6: Relationship between normalised deviatoric stress and volumetric strain with local shear strain

Figure 4.7 illustrates the difference between the peak stress ratio with and without erosion. The peak stress ratio, η_{peak}, has dropped from 2.00 for the baseline test B2-35-0B to 1.86 for the average η_{peak} for tests experiencing internal erosion. This drop can also be seen using the internal angle of shearing resistance, ϕ'. The relation between η and the internal angle of shearing resistance, ϕ' is shown in Equation 4.1 for a soil in triaxial compression (Wood, 1990):

$$sin\phi' = \frac{3\eta}{6+\eta} \tag{4.1}$$

Where

ϕ' is the internal angle of shearing resistance

η is the stress ratio, q/p$'$

From this, ϕ'_{peak} has dropped from 48.6° for the baseline test B2-35-0B to an average of 45.2° for tests experiencing internal erosion, a drop of 3.4° or 7.0%. The graph also shows a slight variation in the peak value of stress ratio between S2-35-15B and S4-35-25B. The value was reduced from 1.91 for the specimen S2-35-15B to 1.82 for the specimen S4-35-25B, a reduction of 0.09 with similar reduction in the internal angle of shearing resistance, ϕ'_{peak}. The value was reduced from 46.4° for S2-35-15B to 44.3° for S4-35-25B, a reduction of 2.1° or 4.5%.
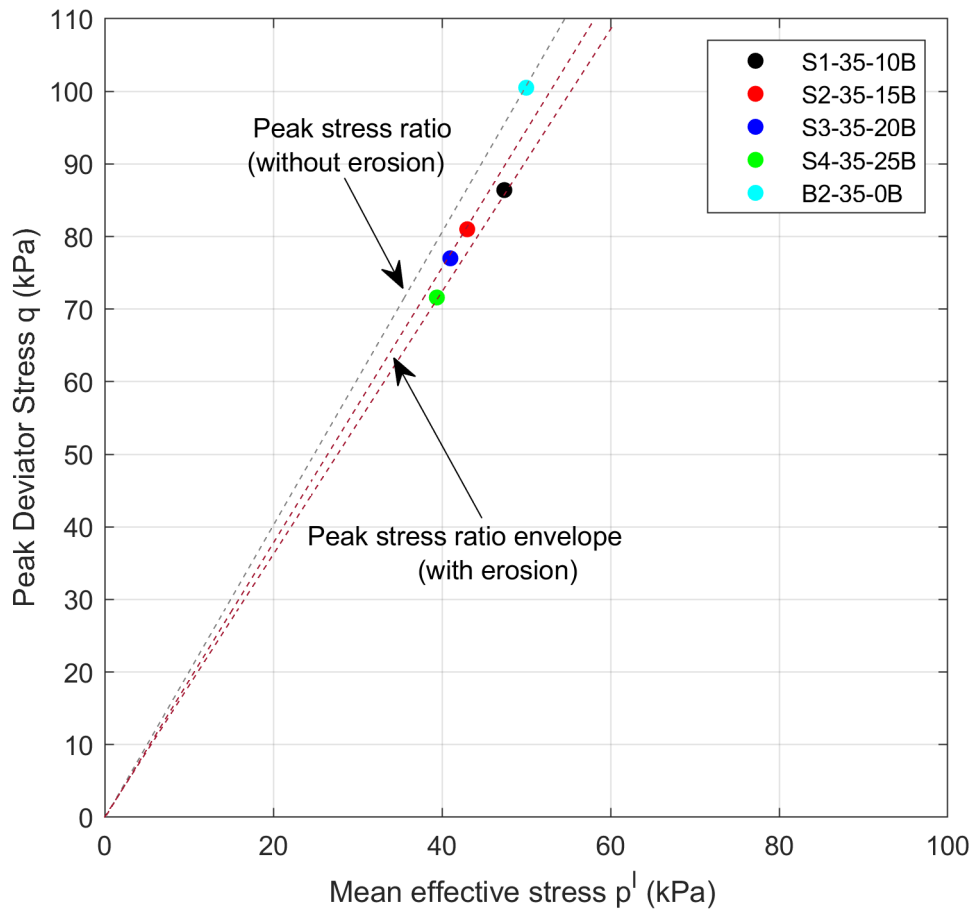
FIGURE 4.7: Maximum deviatoric stress against mean effective
stress

4.3.3 Seepage velocity

The seepage flow velocity, v, was determined by measuring the outflow
rate throughout the specimen test and then dividing the outcome by the
corrected area (determined from the local radial strain) at the midpoint of
the sample. The measurement of seepage flow rate is discussed in Chap-
ter 3.

The variation of seepage flow velocity, v, versus axial strain, ϵ_a, for each test is plotted in Figure 4.8. The seepage flow velocities are strongly correlated to the hydraulic gradient. In theory, for the same material, if the hydraulic gradient value doubles, it is expected that the velocity value would double, maintaining similar permeability.

As expected, test S1-35-10B, with the lowest hydraulic gradient ($i_m = 11.2$) resulted in the lowest seepage velocity with an average velocity of 0.39 mm/s. On the other hand, test S4-35-25B with the highest hydraulic gradient ($i_m = 25.4$) resulted in the highest seepage velocity, with an average of 1.10 mm/s. Tests S2-35-15B and S3-35-20B in between, had intermediate average seepage velocity values of 0.55 and 0.90 mm/s, respectively.

All the tested specimens also exhibited a noticeable decrease in velocity during the erosional tests – typically a drop of 0.11 mm/s over the course of a typical test. With everything else being equal, this would suggest a reduction in permeability throughout testing as discussed next. Some jumps in velocity may be indicative of specific erosion events internal to the specimen.
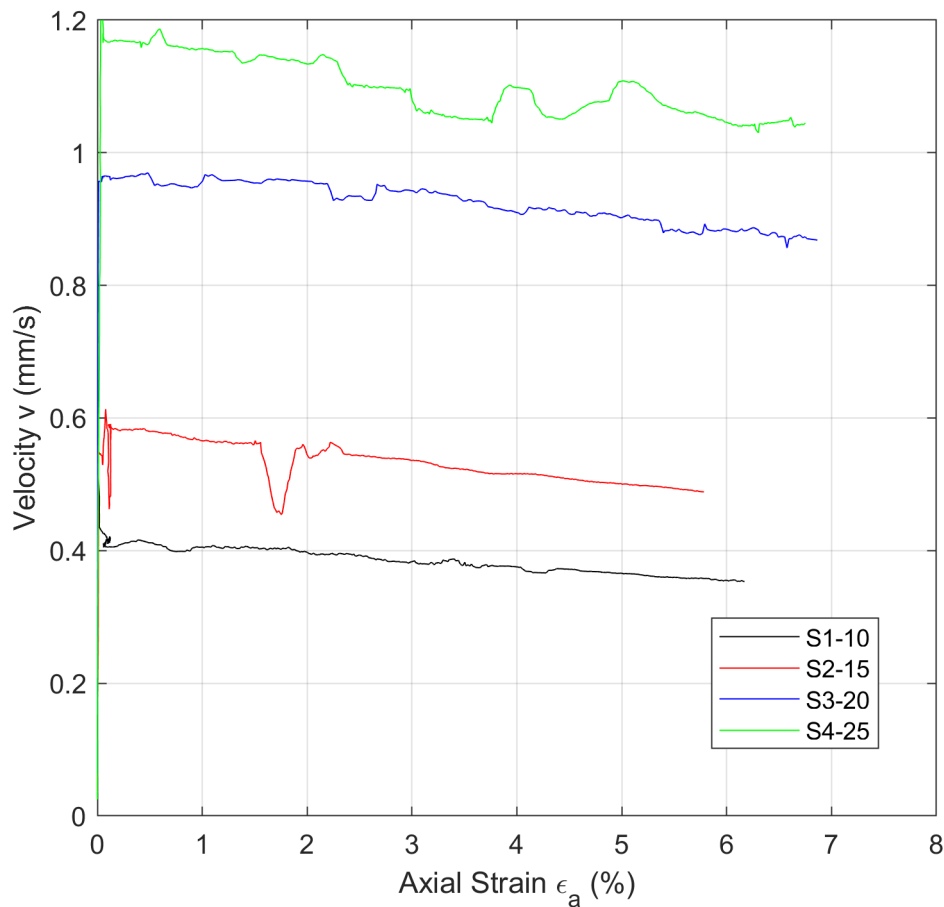
FIGURE 4.8: Seepage velocity versus local axial strain

4.3.4 Permeability

The coefficient of permeability, k, is determined using both the seepage velocity and the hydraulic gradient, which change slightly throughout the test. Figure 4.9 illustrates the variation of the permeability versus the axial strain for the tested specimens.

The average permeability ranges from 3.25×10^{-5} m/s to 4.55×10^{-5} m/s, displaying fairly close values as the same fines content was used. All

specimens experienced a slight decrease in permeability during the erosional tests

Specimens S3-35-20B and S4-35-25B show the highest initial permeability values at 4.60×10^{-5} m/s and 4.70×10^{-5} m/s, respectively with decreases to 3.86×10^{-5} m/s and 4.06×10^{-5} m/s. Specimens S1-35-10B and S2-35-15B recorded the lowest initial permeability values at 3.35×10^{-5} m/s and 3.48×10^{-5} m/s respectively, with decreases to 3.05×10^{-5} m/s and 2.90×10^{-5} m/s. It is notable that the rate of decrease of permeability with axial strain appears to be very similar across all the specimens. While the permeability results seem to be two set of two similar tests, this is likely to be just a coincidence.
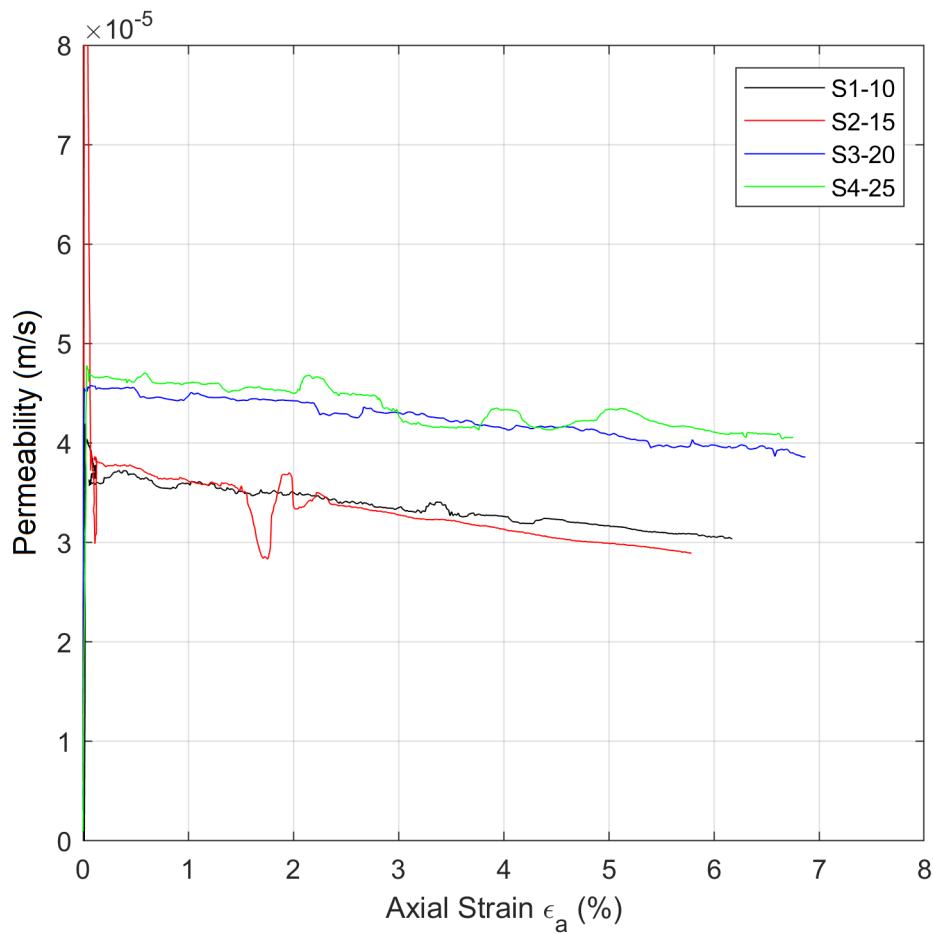
FIGURE 4.9: Relationship between permeability and local axial
strain

4.3.5 Erosion

To study the behaviour of internal erosion, a series of graphs were pre-
sented throughout the thesis to plot erosion versus axial strain. Chapter 7
confirms the importance of shearing amount when studying internal ero-
sion, and hence all graphs were plotted against axial strain.

The accumulated erosion with respect to axial strain is illustrated in Figure 4.10. The mass of eroded particles increases with axial strain for all of the tested specimens. The results also clearly illustrates the effect of the hydraulic gradient on erosion rate with greater erosion at higher hydraulic gradients initially (Figure 4.11), but with a reduction in the difference in the erosion rate subsequently. Note that S3-35-20B, which had the largest (and somewhat anomalous) volumetric reduction also shows a strain range (from 2.0% to 3.6%) over which the erosion rate is maintained, unlike the other specimens.

By the end of the tests, the mass of eroded fines was 66.8g (13.9%) in the specimen with the slowest seepage flow S1-35-10B, 68.1g (14.2%) in S2-35-15B, 79.8g (16.7%) in S3-35-20B and more than 88.5g (18.5%) in the specimen with the greatest seepage flow S4-35-25B.
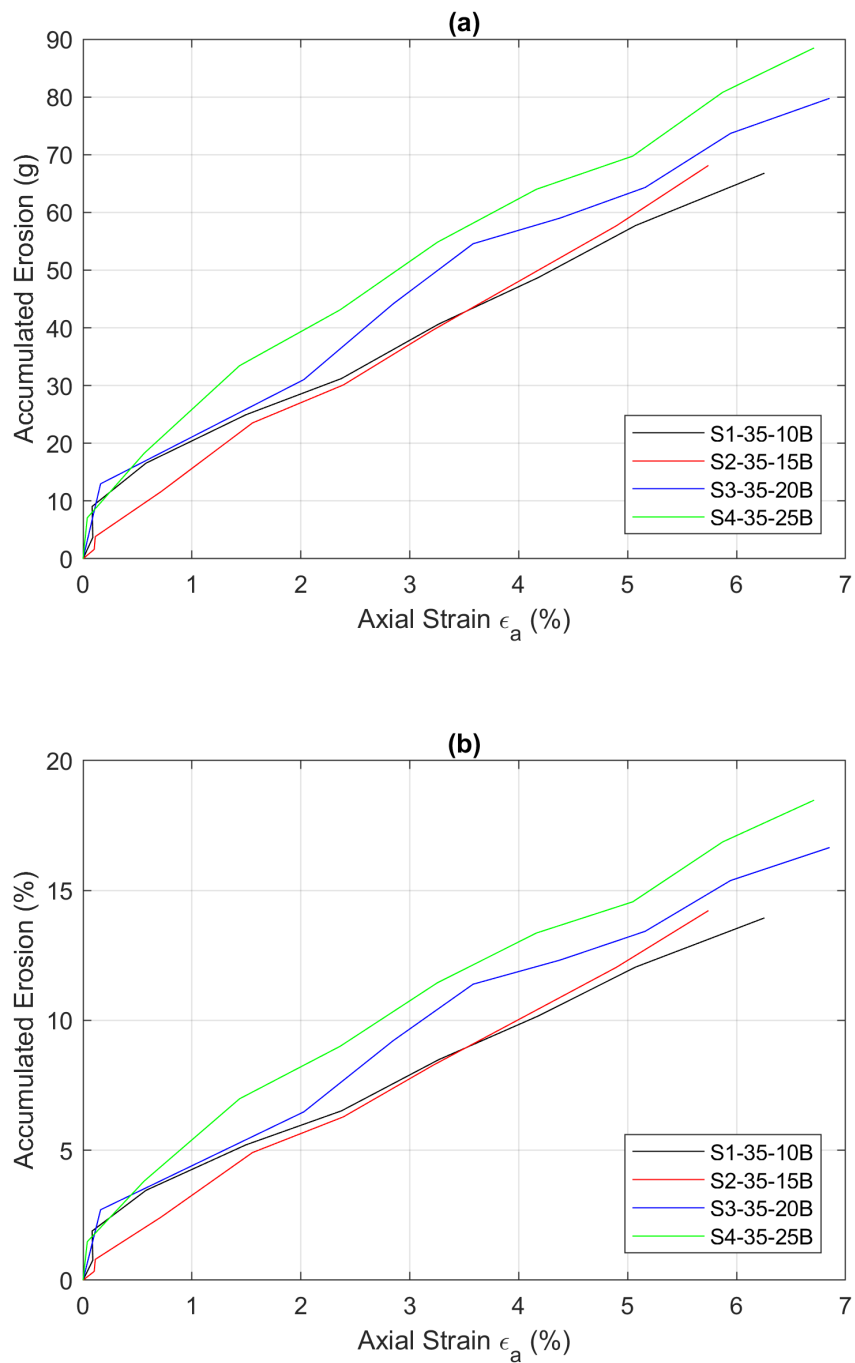
FIGURE 4.10: Accumulated erosion versus local axial strain under different hydraulic gradient, with erosion presented (a) in grams and (b) as a percentage of the initial fines content
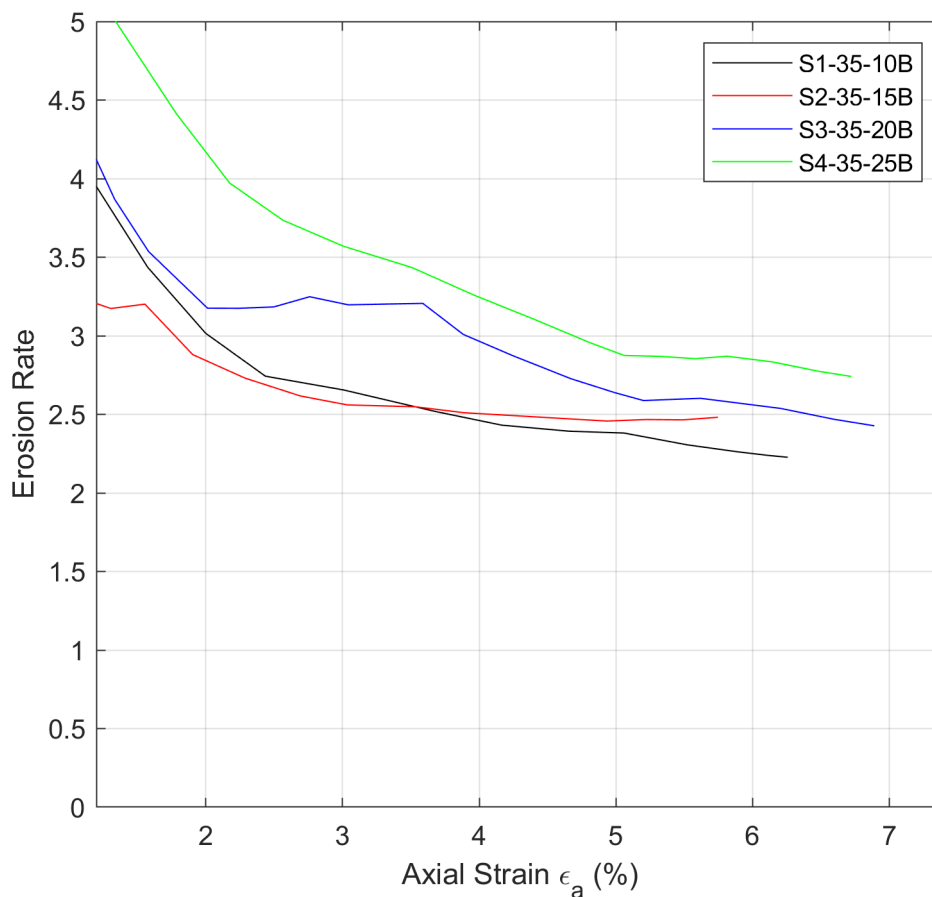
FIGURE 4.11: The erosion rate (accumulated erosion % / axial strain %) versus local axial strain

4.4   Discussion and interpretation

The contribution of seepage flow rate or hydraulic gradient on the on-set and development of internal erosion was apparent in the conducted tests. The purpose of this study is to understand better the influence of such factors on the internal erosion process in gap-graded soil. Therefore, a series of erosional tests were performed on four tests under different hydraulic gradients 10, 15, 20 and 25 with the same initial fines content

percentage at 35%. Drained stress path, hydraulic gradient, seepage velocity, permeability, and erosion results have been reported.

Concerning the shear strength, after analysing the results of the tests, it can be concluded that the shear strength of the tested samples decreases with an an application of seepage resulting in fines loss, however, all samples recorded lower peak stress than the base test B2-35-0B. This can be related to the erosion of particles. Losing fines meant disturbance to the soil fabric and hence weakening the force chains, perhaps irrespective of the exact quantity of that loss. This behaviour can be seen in Figure 7.13 where all tests performed in this thesis are compared.

As for the volumetric strain, all the specimens displayed a contractive behaviour at the first stages of the tests, which is afterwards became dilative behaviour. This dilative behaviour occurred earlier with the increase of the hydraulic gradient from 0 (no erosion) to i = 25. Chang and Zhang (2011) believed that loss of fine particles increased the global void ratio and shifted the soil condition to a looser state, ultimately leading to lower drained shear strength. Recently, Wautier (2018), using discrete element based numerical analysis, referred to rattlers being defined as free particles that provide support for the force chains, although they do not participate in the transfer of the stress. He suggested that the loss of these particles weakens the force chains which become prone to microstructural rearrangements, which favours the development of plastic strain and contractive behaviour. This finding may explain why the base test results recorded higher peak stress compared to the samples that experienced fine particles erosion.

From a hydraulic perspective, the permeability and the seepage velocity values are strongly correlated to the hydraulic gradient. All the tested specimens also exhibited a noticeable decrease in permeability and velocity during the erosional tests. This decrease can be a result of blockages within the seepage flow caused by eroded fines depositing internally. Several researchers reported this decrease in permeability. Shwiyhat and Xiao (2010) explained this behaviour as the clogging of the downstream soil layer by the eroded fine particles. It was found that increasing the hydraulic gradient under which the tests were performed from 10 to 25 led to a slight increase in the amount of eroded fines, with most of the increase occurring at the start of erosion. This positive correlation between the erosion and the hydraulic gradient is evident in all tested specimens.

Overall, these findings are in accordance with findings reported in previous studies wherein Bendahmane et al. (2008) using a fine sand with 10% clay under downward seepage and constant isotropic stress, and a flexible wall permeameter, found a gain in the rate of suffusion with increased hydraulic gradient. Internal instability caused by erosion was found to be significantly influenced by variations in the hydraulic gradient by Moffat et al. (2011). Thus, using a rigid wall permeameter, they found that the suffosion and suffusion processes are triggered by increasing the local hydraulic gradient. Ouyang and Takahashi (2015) using a plane strain apparatus, revealed that when the hydraulic gradient increases, the particle displacement also increases and large amounts of fines are transported. In each of these studies, however, the rate of erosion significantly decreased

at a fixed hydraulic gradient over time. In many cases the erosion rate decreased to zero before the hydraulic gradient was increased in a stepwise procedure.

In this study, the hydraulic gradient was kept constant during the erosion in the four tests under constant shear rate to failure. The tests result demonstrated a notable increase in the amount of eroded soil , which did reduce with both time and axial strain, but not to the degree that was noted in previous research studies conducted under constant stress. Wautier (2018) using Discrete Element Modelling (DEM) simulations investigated the influence of seepage on the internal stability of granular materials and revealed that the seepage flow introduces additional forces in the material, which results in reducing the internal stability of the material. Thus, fine particles are prone to be detached from the force chains to be transported by the internal flow. Here, it is seen that additional forces can be induced also by shear in the soil, which can further detach fines from the force chains to be removed by seepage flow.

Chapter 5

Fines Content Study

5.1   Introduction

Fines content is one of the most important factors controlling internal erosion in cohesionless soils, as the initial fines content controls the internal stability of these materials (Kenney and Lau, 1985). Therefore, a considerable amount of literature has been published on the influence of initial fines content on the internal erosion process.

By performing piping tests on sandy gravels, Skempton and Brogan (1994) proposed a critical fines fraction below which the finer particles will play a diminished role in stress transfer and above which the finer particles would completely separate the coarser particles from one another. The critical fines content was calculated to be 24% for densely packed specimens and 29% for loosely packed specimens based on the permeameter seepage studies performed by Skempton and Brogan (1994). Ke and Takahashi (2014) conducted suffusion tests on three different soil mixtures at 15%, 25% and 35% and found that the fine particle loss was larger for the specimens with larger initial fines content.

In this chapter, in order to ascertain the influence of the initial fines content on the onset and progression of internal erosion, erosion tests were performed on six samples with different fines contents under the same stress conditions and a constant aimed-for initial hydraulic gradient of 10.

5.2   Results of fines content study

There are a few options for comparing the mechanical behaviour of soils that have different fines content but are otherwise the same (Carraro et al., 2009). One option is to test all samples at the same overall void ratio. This would have the effect of reducing the shear strength at higher fines content as interparticle contacts become dominated by the finer soil. Another is to keep the void ratio of the coarse faction the same and vary the quantity of fines. This would have the effect of creating a denser overall soil fabric as the fines content increases. A third option is to test all samples, irrespective of the quantity of fines, at the same relative density, which is an index of state from 0% to 100% (Thevanayagam, 1998). While all methods have advantages and disadvantages, the advantage of using the same relative density is that it defines the soil state in a precise and consistent manner. This is the approach adopted here. Figure 5.1 presents all six samples with different fines content tested in this thesis.
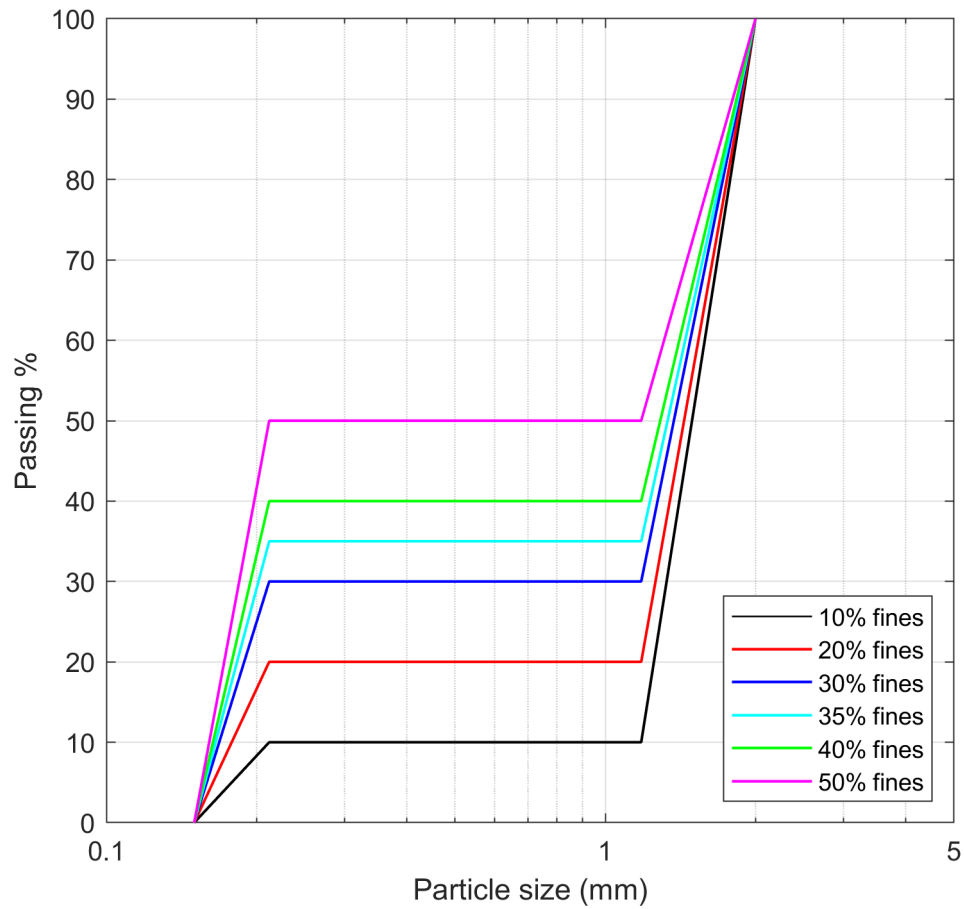
FIGURE 5.1: The particle size distribution curve for the six samples used in this research

Maximum and minimum density tests were performed for each fines content from 0% to 50% to determine the maximum and minimum void ratio, e_{max} and e_{min}, Figure 5.2. Using these values, the overall required void ratio to obtain D_r =70% was determined for each triaxial test specimen.
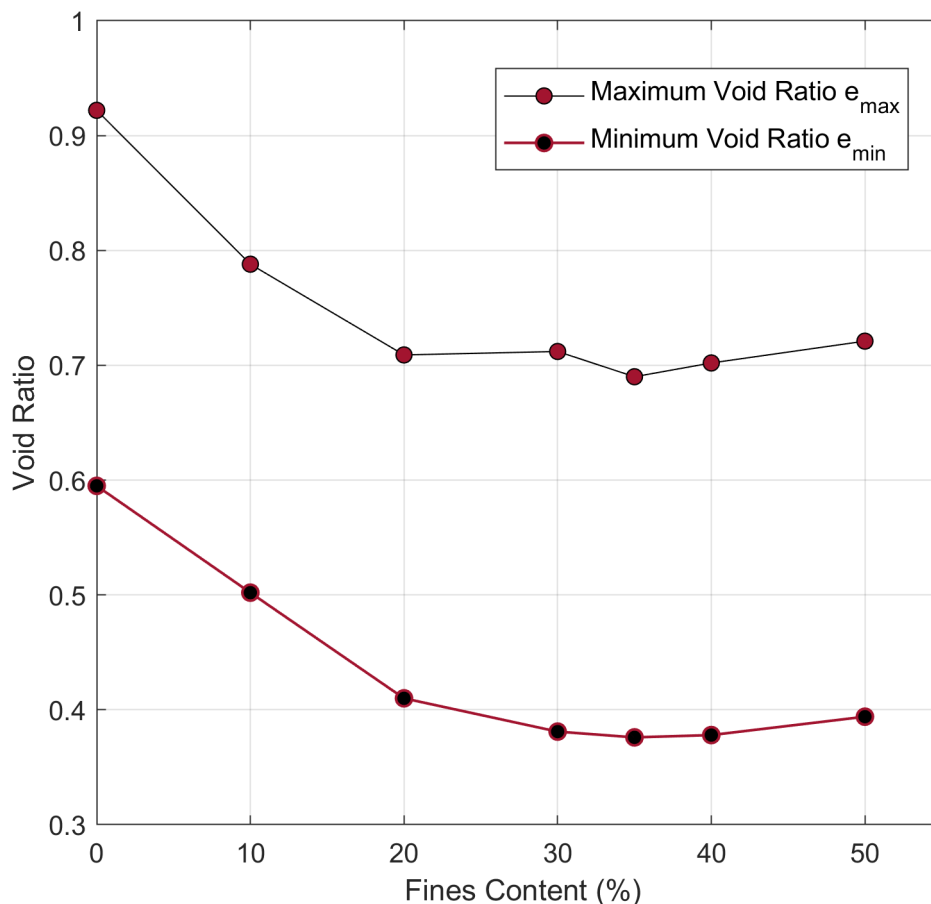
FIGURE 5.2: Maximum void ratio and Minimum void ration versus fines content percentage

Six samples of gap-graded soil were tested at increasing initial fines content 10, 20, 30, 35, 40, 50% named S5-10-10B, S6-20-10B, S7-30-10B, S1-35-10B, S8-40-10B and S9-50-10B, respectively. All six tests were performed in the same conditions under a constant aimed-for initial hydraulic gradient of 10. The six tests were prepared and sheared using the stress path 'B', Figure 6.1, with the total mean stress kept constant at 50 kPa, taking a vertical stress path to reach failure, where the deviatoric stress no longer increased.

The pore pressure differential across the sample, volume change, outflow rate of water and the mass of eroded particles were recorded during all six tests. This allowed the hydro-mechanical parameters including hydraulic gradient, seepage velocity, permeability and the internal erosion rate to be determined. The obtained results are presented and discussed below. A summary of the testing conditions is shown in Table 5.1.

TABLE 5.1: Summary of the testing program and results for fines
content study.

Test Name*	S5	S6	S7	S1	S8	S9
Finer fraction (%)	10	20	30	35	40	50
Axial displacement rate (mm/min)	0.1	0.1	0.1	0.1	0.1	0.1
Gap ratio	5.57	5.57	5.57	5.57	5.57	5.57
Intended relative density, D_R (%)	70	70	70	70	70	70
Initial relative density, D_{Ri} (%)**	71.3	72.3	71.6	70.9	69.2	72.8
Maximum void ratio, e_{max}	0.788	0.709	0.711	0.695	0.702	0.721
Minimum void ratio, e_{min}	0.503	0.410	0.381	0.376	0.378	0.394
Intended void ratio, e	0.588	0.499	0.480	0.472	0.475	0.492
Initial void ratio, e_0	0.585	0.493	0.475	0.469	0.478	0.483
Coarse particles initial mass, m_{ci} (g)	1141	1075	952	889	819	681
Fine particles initial mass, m_{fi} (g)	127	269	408	479	546	681
Intended Hydraulic Gradient i	10	10	10	10	10	10
Mean hydraulic gradient i_m	11.0	9.8	11.4	11.2	11.6	11.5
Initial total mean stress, p_i (kPa)	50	50	50	50	50	50
Max Deviatoric stress, q_{max} (kPa)	97.1	95.1	85.7	86.4	84.8	98.1
Mean effective stress at q_{max}, p'_{qmax} (kPa)	48.8	48.3	46.4	47.4	45.1	49.0
Shearing resistance internal angle, $\phi_{peak'}$	48.1°	47.9°	44.9°	44.3°	45.7°	48.6°
Accumulated erosion mass, m_{fa} (g)	10.8	25.9	50.2	66.8	46.7	18.3
Accumulated erosion percent, m_{fap} (%)	8.5	9.6	12.3	13.9	8.6	2.7

*S5=S5-10-10B, S6=S6-20-10B, S7=S7-30-10B, S1=S1-35-10B, S8=S8-40-10B, and S9=S1-50-10B.

**Initial relative density was measured just before commencing the erosion stage (testing stages are discussed in Chapter 3).

5.2.1   Drained shear strength

The six erosion tests were conducted under the stress path 'B' (see Figure 6.1), taking a vertical stress path in p-q space to reach failure at or above the critical state line with a peak stress expected due to the soils being prepared at a D_R of approximately 70% - i.e. initially 'dense'. The mean stress was kept constant at 50 kPa, Figure 5.3.

Figure 5.4 illustrates the mean effective stress, p' which was estimated by deducting the average seepage flow pressure across the sample (the pore pressure at mid-point) from the total mean stress, p.
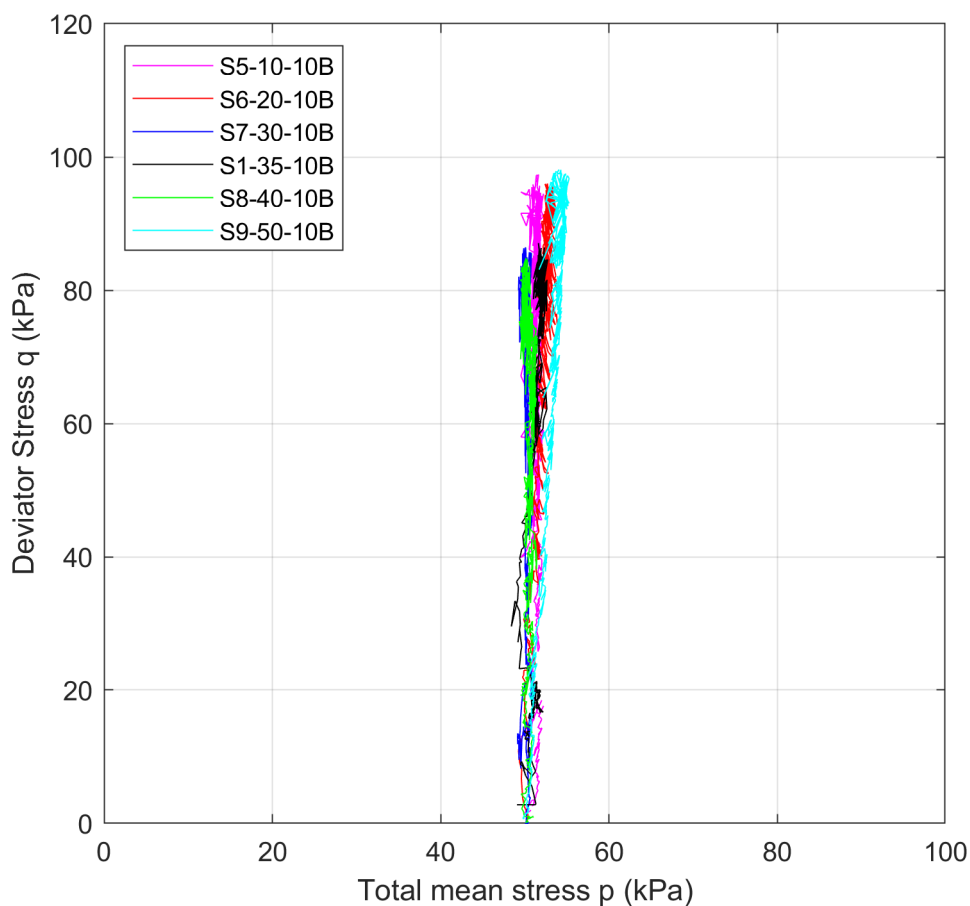
FIGURE 5.3: Deviator stress, q versus total mean stress, p
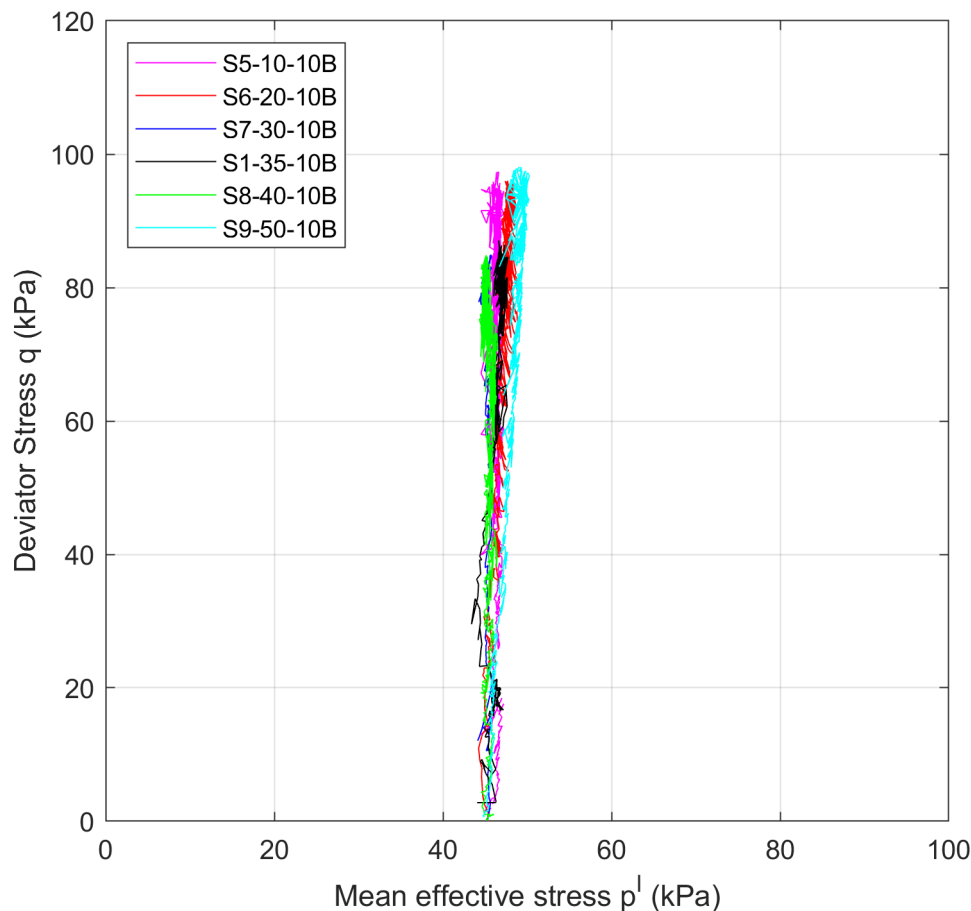
FIGURE 5.4: Deviator stress, q versus mean effective stress, p′

Figure 5.5(a) presents the relationship of deviatoric stress, q with axial strain ϵ_a. The maximum deviatoric stress, q_{max} values ranged from 84.8 kPa to 98.1 kPa represented by specimens S8-40-10B and S9-50-10B, respectively. The highest two values for the maximum deviatoric stress recorded for specimens S9-50-10B and S5-10-10B, which recorded the least accumulated erosion mass loss, m_{fa} 18.3g and 10.8g. Figure 5.3 (b) illustrates the relationship between the volumetric strain and the axial strain. All six samples exhibit a slight contraction at the beginning of the tests followed by dilative behaviour manifested by an increase in their volumes.

The highest two dilative strain values (toward the end of the tests) were recorded with specimens S5-10-10B and S6-20-10B, and contained the least initial fines content, i.e. 10 and 20%.
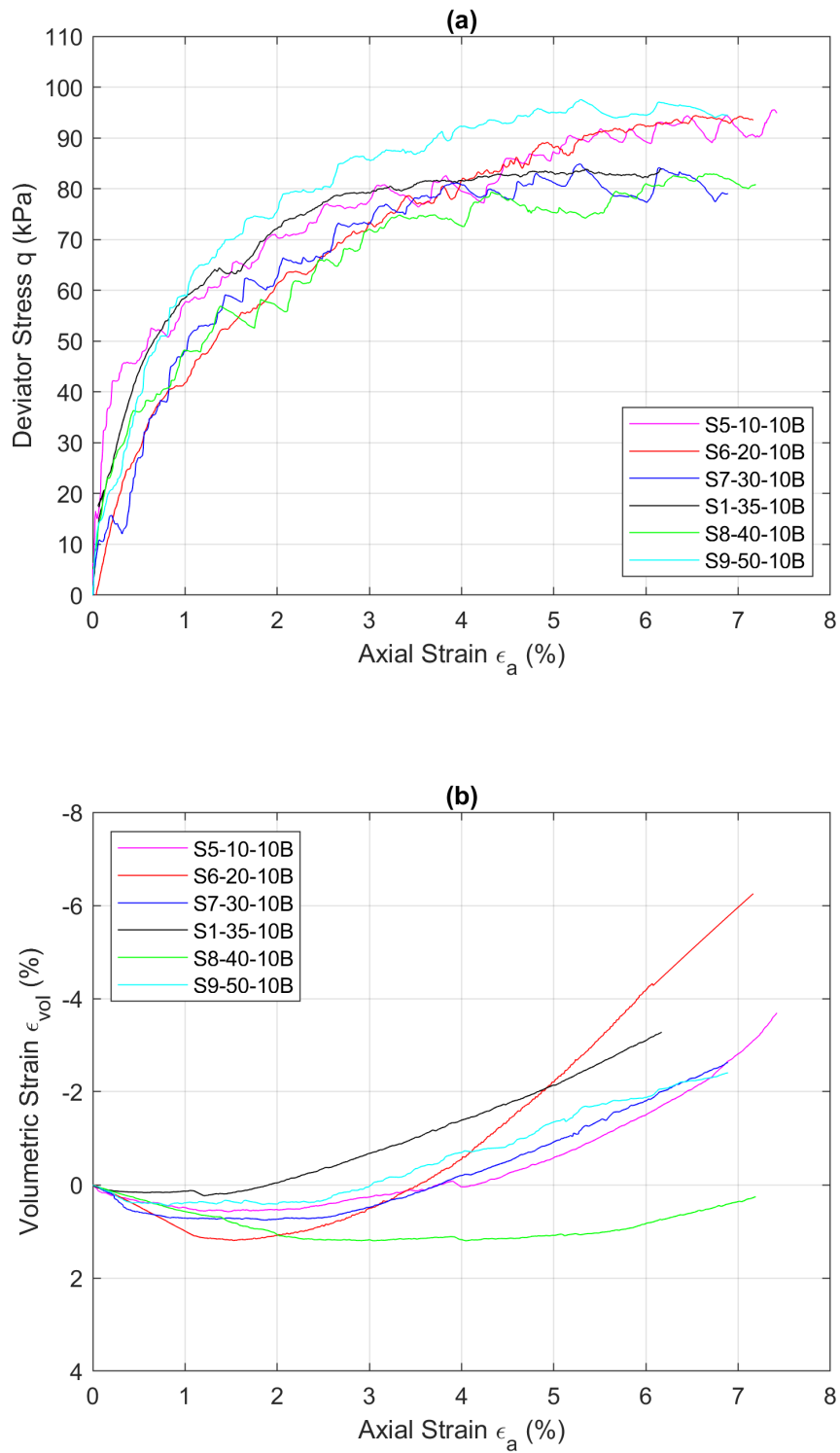
FIGURE 5.5: Relationship between deviatoric stress and volumetric strain vs local axial strain

Figure 5.6(a) demonstrates the normalised deviatoric stress, q_n (q/p') against the local shear strain, ϵ_s for the tested specimens. The variation in the normalised peak stress is 0.28. Again the highest two values recorded for specimens S9-50-10B and S5-10-10B, which recorded the least accumulated erosion mass loss. Comparing all six tests, there is not a significant difference in the stress-strain curves. Figure 5.4(b) illustrates the variation of the volumetric strain $,\epsilon_v$ with respect to shear strain, ϵ_s. All the specimens experienced contractive behaviour followed by dilative behaviour.
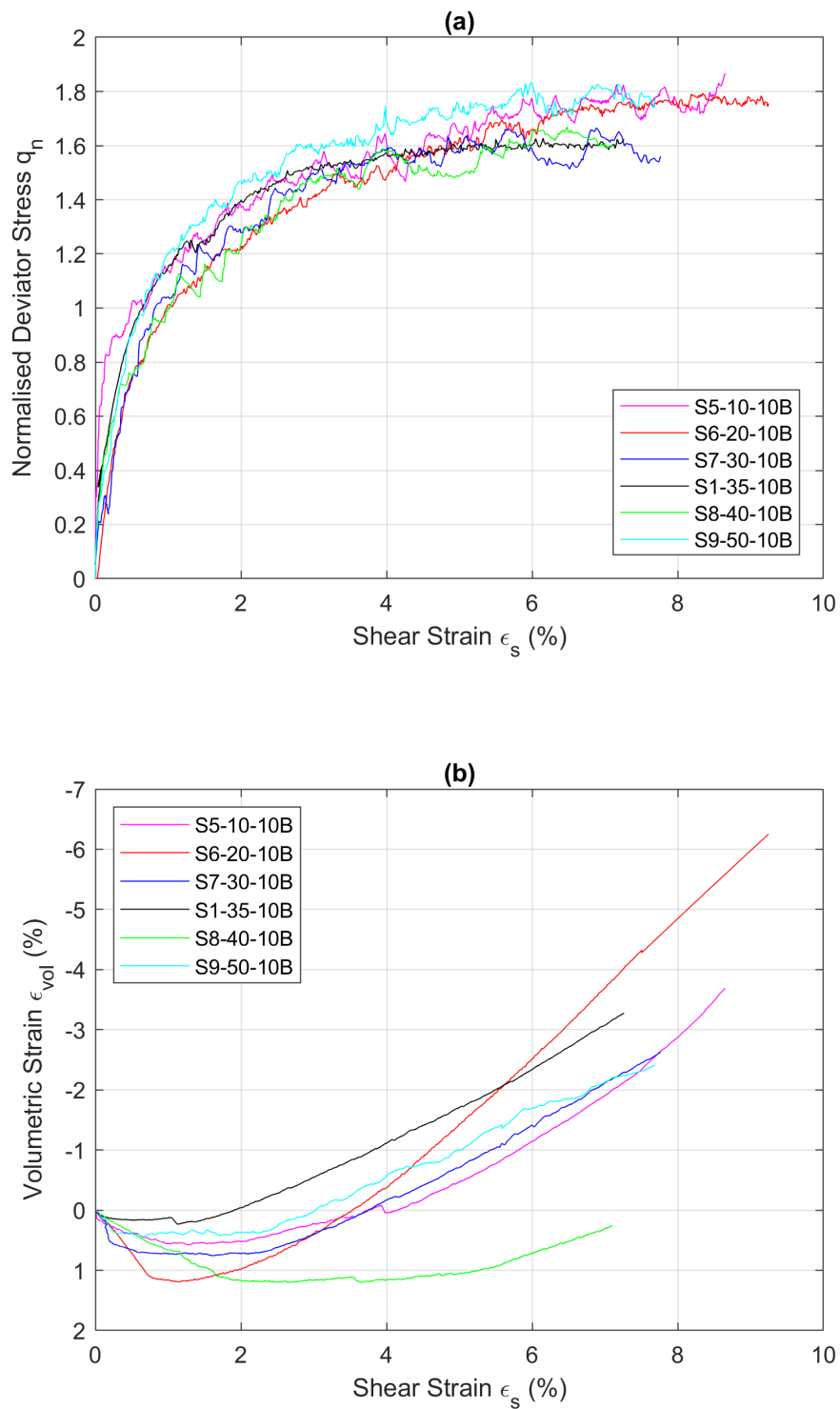
FIGURE 5.6: Relationship between normalised deviatoric stress and volumetric strain with local shear strain

Figure 5.7 illustrates the peak stress ratio, η_{peak} for the different tests. Interestingly, the highest two η_{peak} values were found for S5-10-10B and S9-50-10B with 1.98 and 2.00. Those two tests experienced the least accumulated erosion mass loss percentage at 8.5% and 2.7%, respectively. Correspondingly, the lowest two η_{peak} values were found for S1-35-10B and S7-30-10B with 1.82 and 1.85. Those two tests experienced the most accumulated erosion mass loss percentage at 13.9% and 12.3%, respectively.

This behaviour can also be seen using the internal angle of shearing resistance, ϕ'. The highest peak values, ϕ'_{peak} found was 48.1° in test S5-10-10B and 48.6° for specimen S9-50-10B. Conversely, the lowest two peak internal angle of shearing resistance values were found for S1-35-10B and S7-30-10B with 44.3° and 44.9°, respectively.

The peak stress ratio envelope varies from 1.82 to 2.00, a difference of 0.18 (9%) across all six tests. Alternatively, the peak internal angle of shearing resistance, ϕ'_{peak} varied from 44.3° and 48.6°, a difference of 4.3° (8.8%).
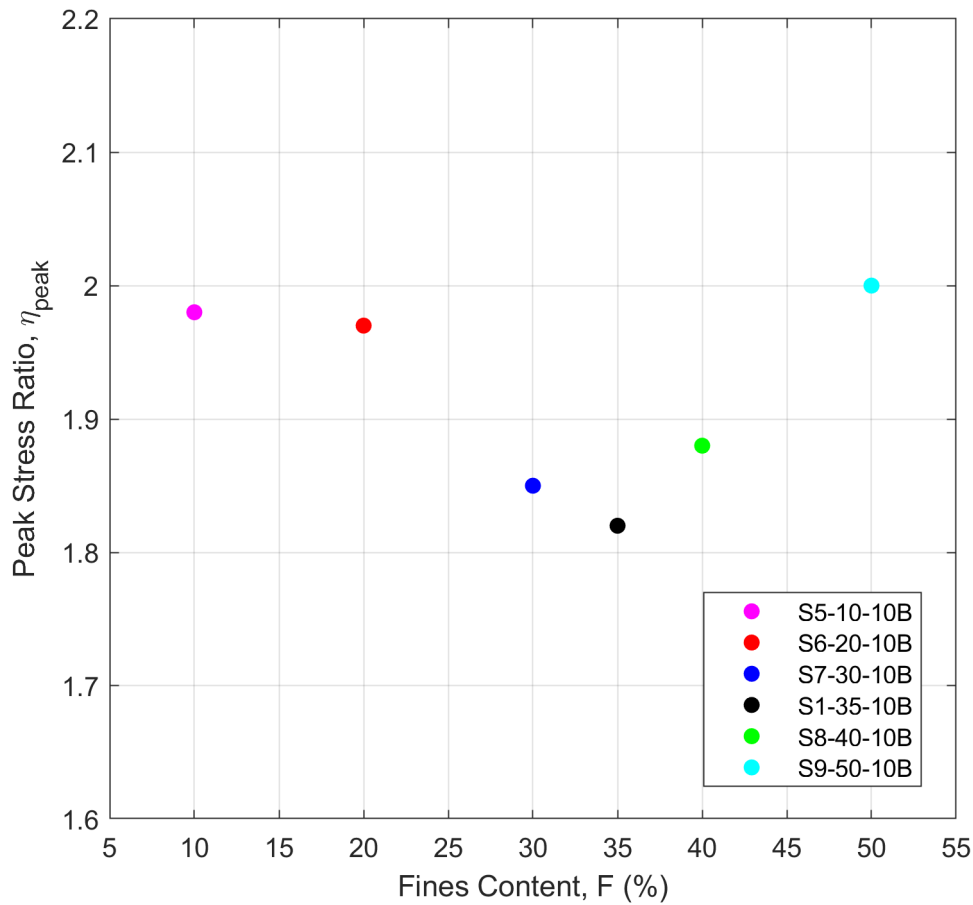
FIGURE 5.7: Fines Content versus Peak Stress Ratio

5.2.2 Permeability

Figure 5.8 plots the coefficient of permeability determined for the six tests as they progressed. The average permeability ranges from 2.73×10^{-5} m/s in S9-50-10B, 3.01×10^{-5} m/s in S8-40-10B, 3.46×10^{-5} m/s in S7-30-10B, 3.35×10^{-5} m/s in S1-35-10B, 4.22×10^{-5} m/s in S5-20-10B to 4.79×10^{-5} m/s in S6-10-10B.

These results show a high correlation with seepage velocity, plotted in Figure C.4. As expected, specimens with lower initial fines content, i.e. S5-10-10B and S6-20-10B showed the highest average permeability of 4.22×10^{-5} m/s and 4.79×10^{-5} m/s, respectively. On the other hand, specimens with higher initial fines content, i.e. S8-40-10B and S9-50-10B presented lower average permeability of 3.01×10^{-5} m/s and 2.73×10^{-5} m/s, respectively. In general, the average permeability value showed an inverse correlation with initial fines content.

A decrease in the permeability during the test progression and with strain is also notable for all the six specimens – typically a drop of around 1.06×10^{-5} m/s, although this change appears to be greater for the specimens with fewer fines (around 1.5×10^{-5} m/s drop for 10% and 20% cases S5-10-10B and S6-20-10B) than more fines (around 0.7×10^{-5} m/s drop for 40% and 50% cases, S8-40-10B and S9-50-10B).
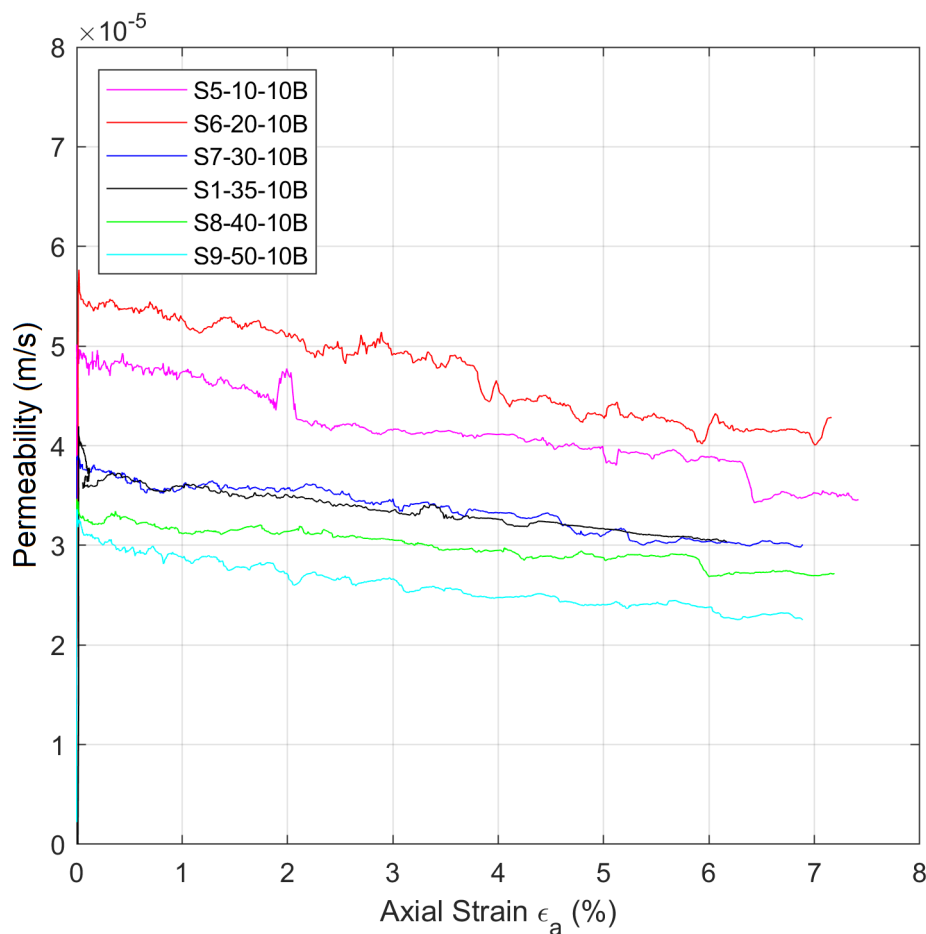
FIGURE 5.8: Relationship between permeability and local axial
strain

5.2.3   Erosion

The accumulated mass erosion in grams versus axial strain is plotted in
Figure 5.9(a) while 5.9(b) presents the relationship between accumulated
erosion mass as a percentage of the original fines content mass. As shown
in both (a) and (b), the rate of fines erosion increases with the increase
of fines content until reaching 35% and then starts to decrease. Hence,
the accumulated erosion increases significantly from test S5-10-10B at 10.8g

(8.5%), reaching 66.8g (13.9%) for test S1-35-10B. The erosion rate then tends to decrease with the threshold percentage and goes down to 18.3g (2.7%) for the specimen S9-50-10B. The same behaviour can be seen analysing the erosion rate versus axial strain graph, Figure 5.10.
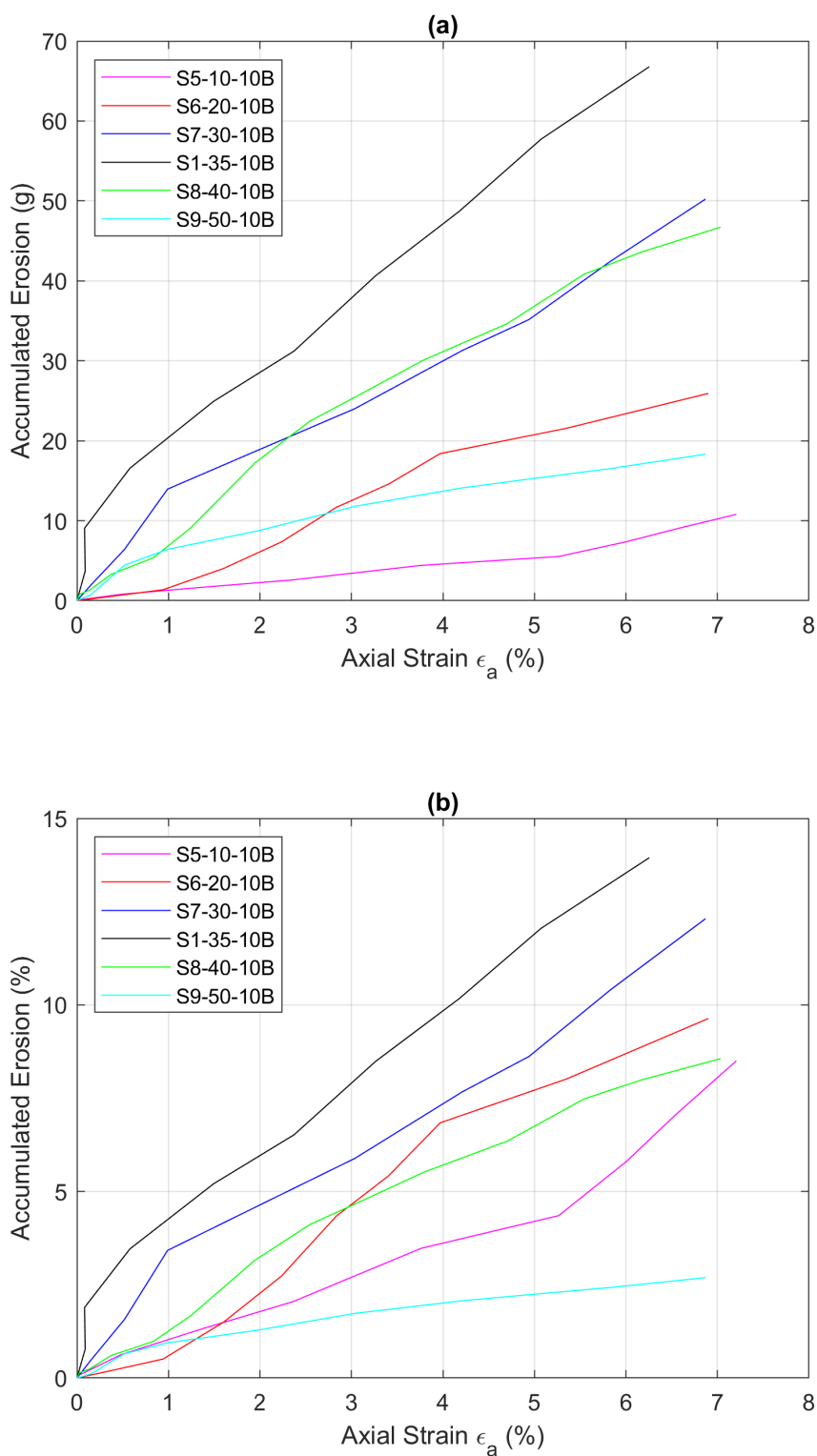
FIGURE 5.9: Accumulated erosion versus local axial strain under different hydraulic gradient, with erosion presented (a) in grams and (b) as a percentage of the initial fines content
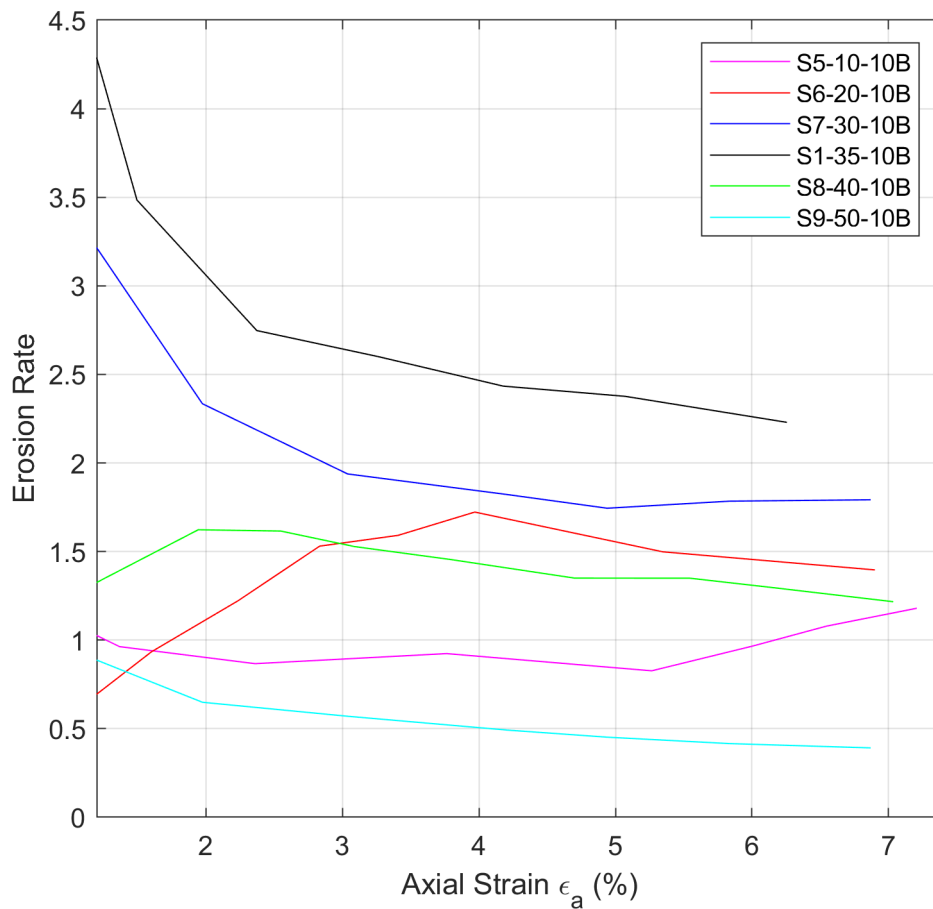
FIGURE 5.10: The erosion rate (accumulated erosion % / axial strain %) versus local axial strain

5.3 Discussion and interpretation

The influence of fines content on the onset and the development of internal erosion was apparent in the conducted tests. A program of erosional tests was conducted, six tests were performed under the same hydro-mechanical conditions on six samples with different fines content at 10%, 20%, 30%, 35%, 40%, and 50%.

From a hydraulic perspective, the initial permeability and seepage velocity values decrease with the initial fines content. With the progression of each test, it can be seen that the seepage velocity and permeability values exhibited a moderate decrease across all tested specimens. This decrease was also noted by previous research by Shwiyhat and Xiao (2010), among others and was explained by the clogging of the transported particles within the constrictions.

Regarding the stress-strain behaviour, the results of the tests revealed that the peak deviatoric stress value under the same hydraulic gradient and imposed stress path reduces with fines content. This reduction of the peak stress is linked to the loss of fines. Hence, specimens that have subjected to higher fines loss recorded the lowest peak angle of shearing resistance or peak stress ratio.

The peak stress ratio envelope clearly demonstrates a strong relationship between fines loss and peak stress ratio. The most notable aspect of the data is that the highest two peak stress ratio values reported for S5-10-10B and S9-50-10B with 1.98 and 2.00. Those two tests experienced the least accumulated erosion mass loss percentage at 8.5% and 2.7%, respectively. Also striking is that the lowest two peak stress ratio values were found for S1-35-10B and S7-30-10B at 1.82 and 1.85. Those two tests experienced the most accumulated erosion mass loss percentage at 13.9% and 12.3%, respectively. Overall, the loss of fines and loss of peak strength ratio were found to be greatest at a fines content of 35% - which may be considered to be a transition fines content between under and overfilled according to Skempton and Brogan (1994). However, this was not clearly reflected in

the volumetric strain data for which did not show a clear trend. A possible explanation for these results may be linked to how fine particles loss can affect the internal structure of the soil. This loss of fine particles disturbed the force chains by removing fine particles which were part of the lateral support fabric.

This conclusion is consistent with what has been found in several previous studies wherein, Shuler (1995), Chang and Zhang (2011), and Ke and Takahashi (2014) who have concluded that the loss of fines can lead to the reduction of the shear strength of the soil. Wautier (2018) has explained this behaviour by the weakening of the soil's skeleton by the loss of rattlers that provide lateral support for force chains leading to their failure under an incremental loading. Hence, plastic strain occurs in the non-cohesive granular material.

As for the volumetric strain, all the tested specimens exhibited a contractive behaviour at the first stages of the tests, followed by significant dilation. The exhibited dilative behaviour shows a slight increase with fines content.

On the other hand, in this chapter, it was also concluded that increasing the initial fines content percentage led to an increase in the amount of eroded fines. However, by surpassing the threshold value from 35% to 50% fines, no increase in erosion rate was detected. On the contrary, when the amount of initial fines increases above 35%, the erosion rate generally decreases with the increase of the initial fines content.

These experimental results found clear support for previous researches of

Ke and Takahashi (2014), who stated that increasing the percentage of initial fines would increase the amount of eroded fines. However, soil mixtures used in their experiments did not exceed 35%.

The observed behaviour of the erosional process could as well be explained by the participation of fines in the stress transfer hypothesis proposed by Skempton and Brogan (1994). They defined 35% as a critical fine fraction under which fine particles would play a diminished role in stress transfer and above which fines would completely separate coarse particles. Indeed, the participation of fines particles in the strong force chains and their participation in stress transfer would increase their resistance to the internal erosion process. Also this could be the result of blocking the erosion path when increasing the fines content above 35%. Hence, the amount of eroded particles would decrease, as reported by the erosional results above.

Chapter 6

Stress Path Study

6.1 Introduction

The internal erosion process in soils is significantly controlled by the state of stress. That internal erosion is stress state dependent has been recently recognised and reported by previous works including Bendahmane et al. (2008), Garner and Fannin (2010), Moffat et al. (2011), Chang and Zhang (2013), and Luo et al. (2013).

However, none of the previous researches have investigated internal instability while changing the stress state (continuously shearing while eroding). As a result, this chapter will discuss the influence of shearing by studying the internal erosion process under three different stress paths.

This chapter's main objective is to investigate the effect of the stress path on the onset and the progression of internal erosion on a dense gap-graded soil. A set of experiments was carried out on six samples under three different stress paths, hence with two repeats per stress path.

Figure 6.1 illustrates the stress paths used in this research, all three stress paths are typical conventional paths used in geotechnical engineering. Stress path 'A' where the radial pressure was decreasing, and axial stress was maintained so as to decrease the total mean stress p while increasing the deviatoric stress q. Stress path 'B', where the radial pressure was decreasing, the axial stress increasing, and hence, deviatoric stress increased while keeping the total mean stress constant (taking a vertical stress path). Stress path 'C', where the radial pressure was kept constant, increasing the axial stress and hence, total mean stress while increasing the deviatoric stress (a typical stress path used in triaxial testing).
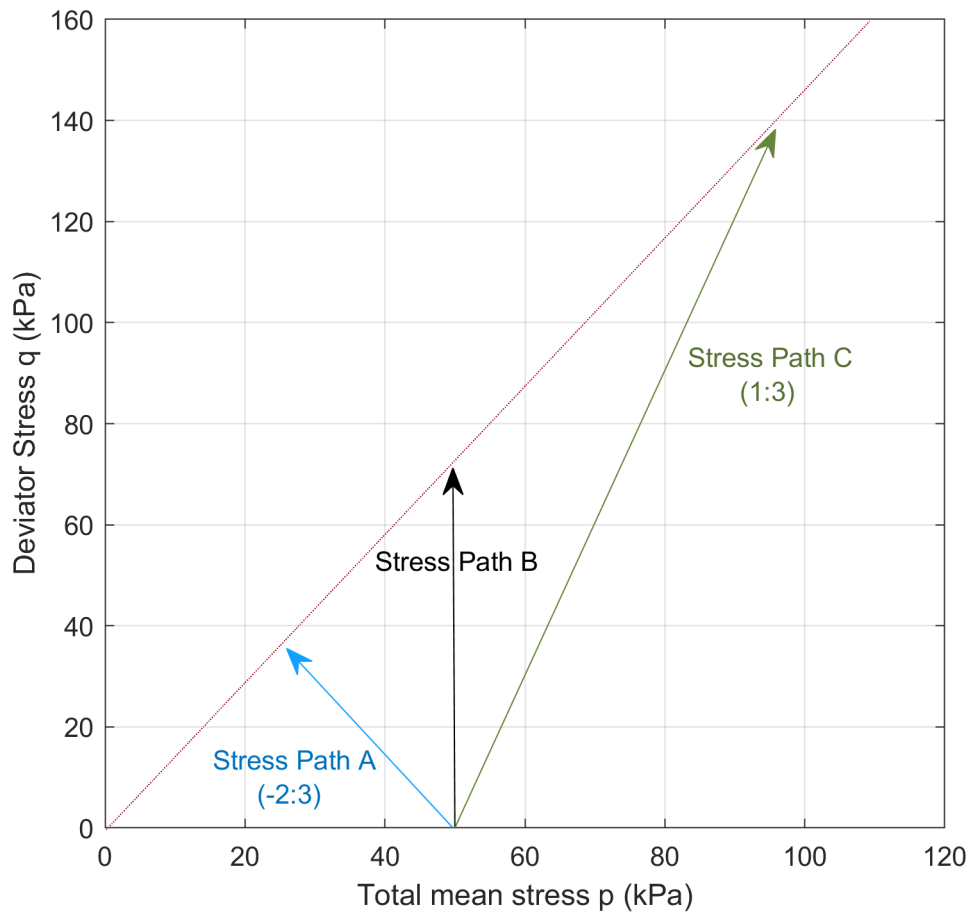
FIGURE 6.1: An illustration of the stress paths used in this thesis

6.2   Results of stress path study

The pore pressure differential across the sample, volume change, outflow rate of water and the mass of eroded particles were recorded during all six tests. This allowed the hydro-mechanical parameters including hydraulic gradient, seepage velocity, permeability and the internal erosion rate to be determined. The obtained results are presented and discussed below. A summary of the testing conditions is shown in Table 6.1.

TABLE 6.1: Summary of the testing program and results for stress
path study.

Test Name*	S10	S11	S12	S1	S13	S14	B1	B2	B3
Finer fraction (%)	35	35	35	35	35	35	35	35	35
Axial displacement rate (mm/min)	0.1	0.1	0.1	0.1	0.1	0.1	0.1	0.1	0.1
Gap ratio	5.57	5.57	5.57	5.57	5.57	5.57	5.57	5.57	5.57
Intended relative density, D_R (%)	70	70	70	70	70	70	70	70	70
Initial relative density, D_{Ri} (%)	71.6	69.3	72.4	70.9	68.9	71.2	70.4	71.3	70.8
Intended void ratio, e	0.472	0.472	0.472	0.472	0.472	0.472	0.472	0.472	0.472
Initial void ratio, e_0	0.467	0.474	0.464	0.469	0.476	0.468	0.471	0.468	0.469
Coarse particles initial mass, m_{ci} (g)	889	889	889	889	889	889	889	889	889
Fine particles initial mass, m_{fi} (g)	479	479	479	479	479	479	479	479	479
Intended Hydraulic Gradient i	10	10	10	10	10	10	-	-	-
Mean hydraulic gradient i_m	11.4	10.9	11.5	11.2	11.9	10.7	-	-	-
Initial total mean stress, p_i (kPa)	50	50	50	50	50	50	50	50	50
Max Deviatoric stress, q_{max} (kPa)	34.9	31.4	84.1	86.4	175.3	185.4	46.3	102.8	201.6
Mean effective stress at q_{max}, p'_{qmax} (kPa)	20.1	20.3	46.8	47.4	92.1	96.2	22.6	51.4	98.9
Shearing resistance internal angle, $\phi_{peak'}$	42.4°	38.1°	43.8°	44.3°	46.1°	46.8°	49.8°	48.6°	49.3°
Accumulated erosion mass, m_{fa} (g)	60.5	76.2	62.2	66.8	46.9	36.9	-	-	-
Accumulated erosion percent, m_{fap} (%)	12.6	15.9	13.0	13.9	9.8	7.7	-	-	-

*S10=S10-35-10A, S11=S11-35-10A, S12=S12-35-10B, S1=S1-35-10B, S13=S13-35-10C, S14=S14-35-10C, B1=B1-35-10A, B2=B2-35-10B, and B3=B3-35-10C.

6.2.1   Drained shear strength

Figure 6.2 demonstrates the stress condition at the beginning and the end
of tests for stress path 'A', 'B' and 'C'. This figure shows the relation be-
tween total mean stress p, seepage flow u, and the mean effective stress
p'. It must be mentioned that at the end of tests for stress path 'A', the
effective stress p' reached as low as 15 kPa at the top of the sample, at

this low-stress level, there was a concern about the potential for hydraulic fracturing (reaching the no-tension criterion), hence all tests in stress path 'A' were terminated sooner than other stress paths. As it can be seen in the calculation below, the difference between the radial stress, σ_r and the pore pressure, u is only 2.5 kPa, hence the radial effective stress σ_r' is 2.5kPa:

$$p = 25 \ kPa \quad (from \ \frac{2}{3}) \quad q = 37.5 \ kPa \tag{6.1}$$

$$p = \frac{2\sigma_r + \sigma_a}{3} = \frac{2\sigma_r + (\sigma_r + q)}{3} = \frac{3\sigma_r + q}{3} \tag{6.2}$$

$$25 = \frac{3\sigma_r + 37.5}{3}, \quad \sigma_r = 12.5 \ kPa, \quad u = 10 \ kPa, \quad \sigma_r' = 2.5 \ kPa \tag{6.3}$$

Figure 6.3 presents all nine tests sheared using stress path 'A', 'B' and 'C'. Two specimens were used for each stress path to validate the erosional test results. Tests using the same stress path showed a high correlation between results. Figure 6.4 illustrates the mean effective stress, p' which was estimated by deducting the average seepage flow pressure across the sample (the pore pressure at mid-point) from the total mean stress, p.

Notably, the baseline tests B1-35-0B, B2-35-0B and B3-35-0B displayed a more consistent and less 'noisy' stress path than the other tests due to the hydraulic controllers being able to maintain the aimed-for stress path far more easily without seepage and erosion taking place.
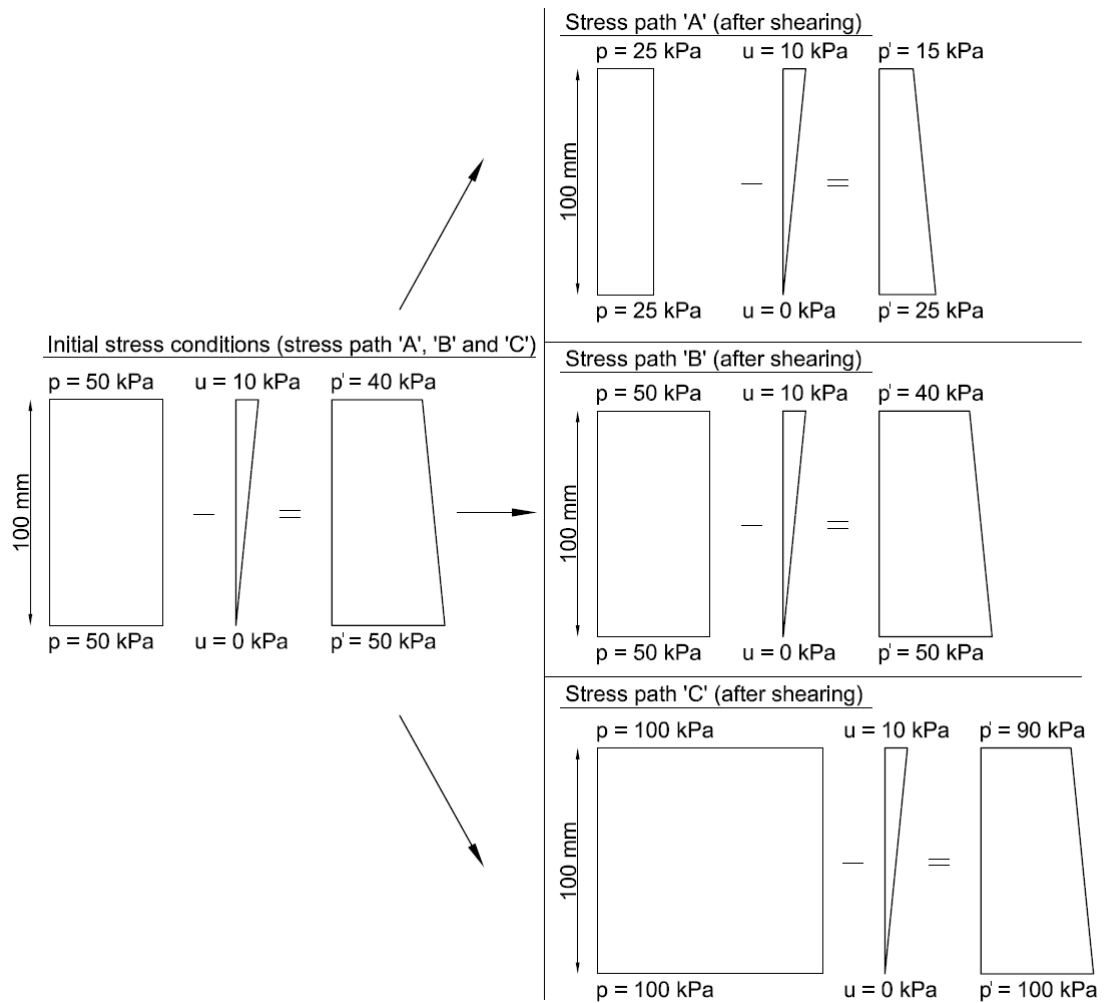
FIGURE 6.2: An illustration of the stress conditions at the beginning and end of tests for stress path 'A', 'B' and 'C'
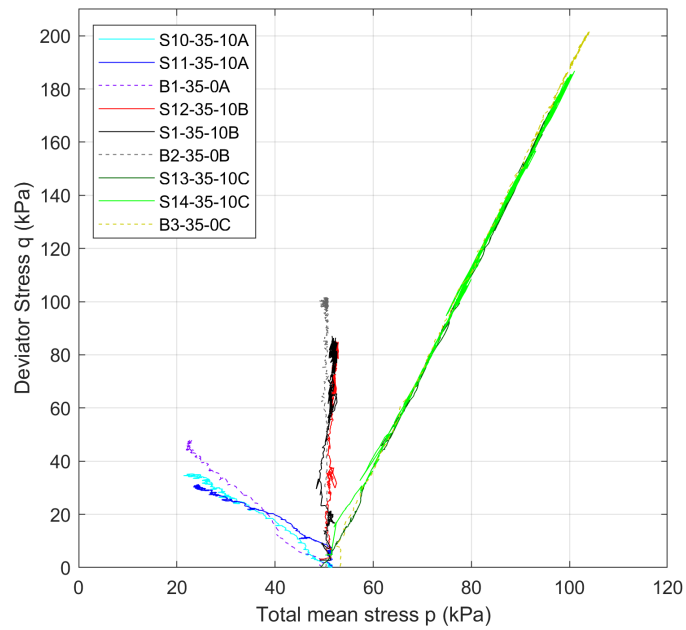
FIGURE 6.3: Deviator stress, q versus total mean stress, p
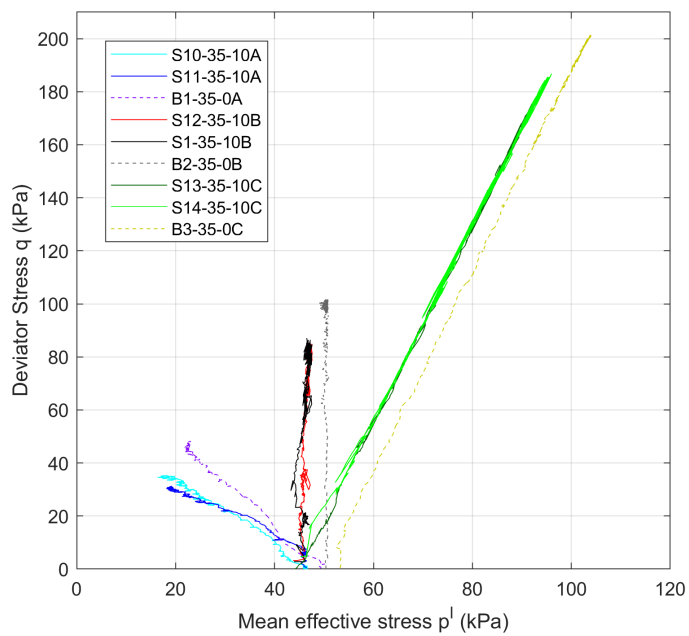
FIGURE 6.4: Deviator stress, q versus mean effective stress, p'

Figure 6.5(a) presents the relationship of deviatoric stress, q against axial strain, ϵ_a. As expected, the maximum deviatoric stress, q_{max} values varied between the three stress paths. Stress path 'A' recorded maximum deviatoric stress values of 34.9 kPa and 31.4 kPa for tests S10-35-10A and S11-35-10A, respectively. Stress path 'B' recorded maximum deviatoric stress values of 84.1 kPa and 86.4 kPa for tests S12-35-10B and S1-35-10B, respectively. Finally, stress path 'C' recorded the highest maximum deviatoric stress values of 175.3 kPa and 185.4 kPa for tests S13-35-10C and S14-35-10C, respectively. In general, all erosion tests have recorded lower peak deviatoric stress values comparing to the baseline test (without erosion) sheared using the same stress path.

Figure 6.5(b) presents the volumetric strain curves of the tested specimens. All the specimens exhibit contractive behaviour at the first stage of the erosion tests but latter on changes to be more dilative. At the first stages of the tests, the specimens S13-35-10C and S14-35-10C have recorded the largest contractive behaviour under stress path 'C'. As for stress path 'B', specimens recorded a mean contractive behaviour ranging from -0.2% for specimen S1-35-10B to 0.5% for specimen S12-35-10B. With the progression of the erosion tests, the contractive behaviour turns into dilative behaviour. However, specimens S13-35-10C, S14-35-10C, S12-35-10B and S1-35-10B have recorded the largest dilative behaviour for the erosion tests. Whereas, specimens S10-35-10A and S11-35-10A displayed less dilative behaviour at 0% for the former and -2% for the latter. Baseline tests showed more dilative behaviour in comparison to all erosion tests apart from baseline test B1-35-0A which showed somewhat anomalous volumetric strain results.
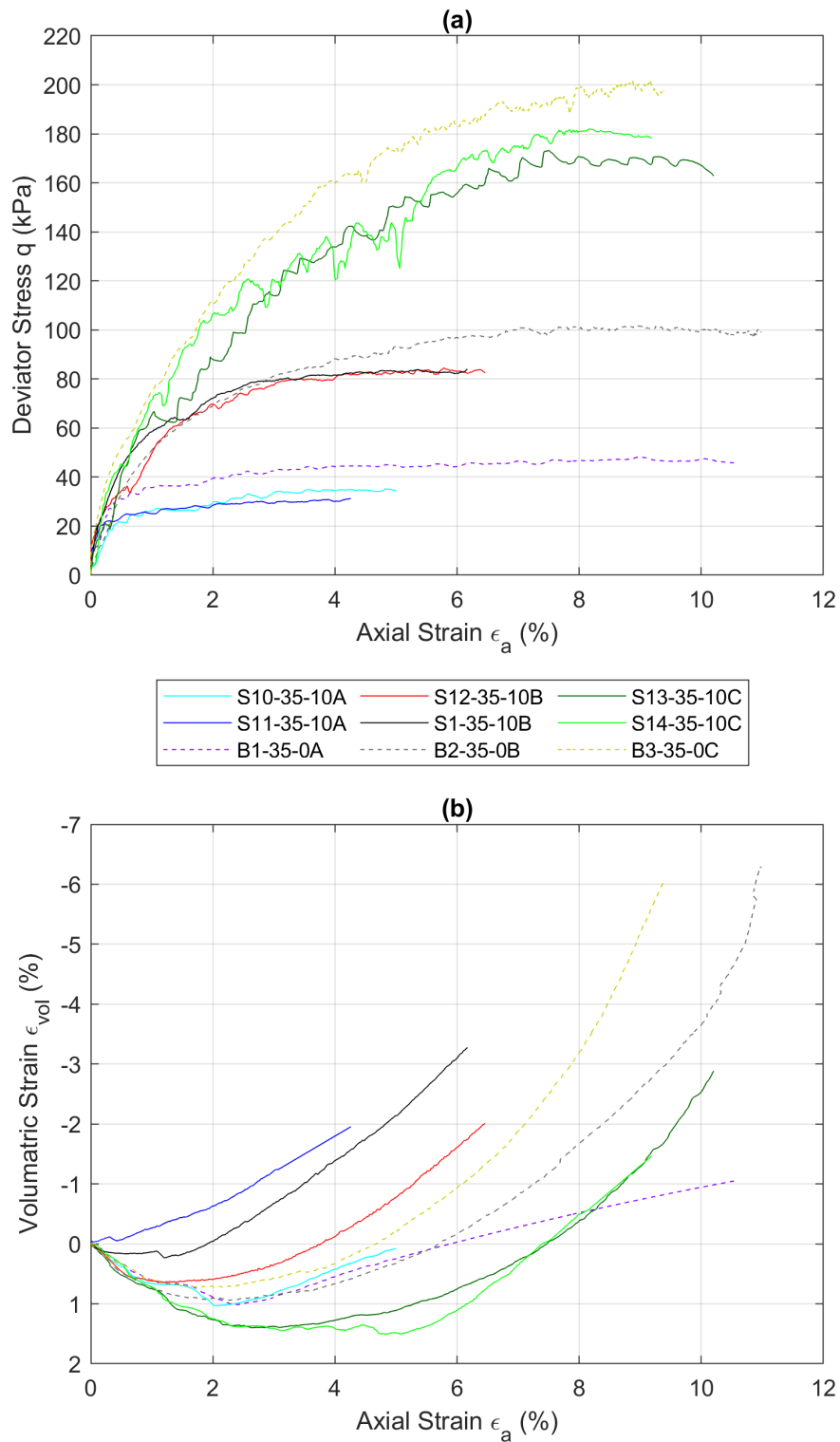
FIGURE 6.5: Relationship between deviatoric stress and volumetric strain vs local axial strain

Figure 6.6(a) demonstrates the normalised deviatoric stress, q_n (q/p') against the local shear strain, ϵ_s for the tested specimens. In general baseline tests showed a higher peak normalised deviatoric stress, q_n. In terms of erosional tests, S13-35-10C and S14-35-10C showed the highest peak normalised deviatoric stress, q_n. It is worth mentioning that those two tests have recorded the least accumulated erosion mass with an average for stress path 'C' of 41.9 g (12.6%).

In contrast, tests S10-35-A and S11-35-10A recorded the lowest peak normalised deviatoric stress and the highest accumulated erosion mass with an average between them for stress path 'A' of 68.3 g (20.5%). Stress path 'B' lies in between with an average accumulated erosion of 64.5 g (19.4%).

Figure 6.6(b) illustrates the variation of the volumetric strain , ϵ_v with respect to shear strain, ϵ_s. All the specimens experienced contractive behaviour followed by dilative behaviour.
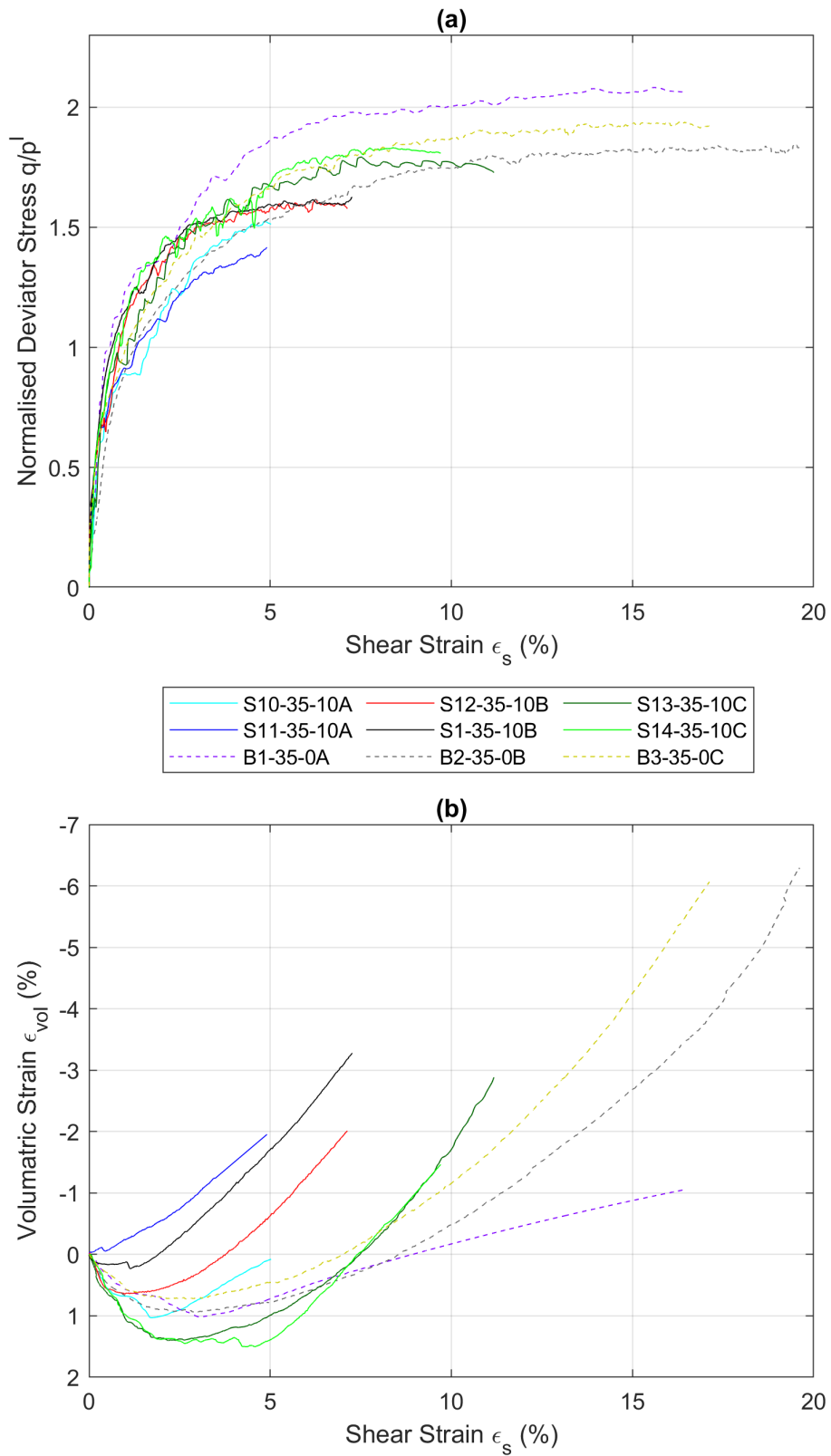
FIGURE 6.6: Relationship between normalised deviatoric stress
and volumetric strain with local shear strain

Figure 6.7 illustrates the average peak strength line for all three stress paths and the baseline tests' average value. The peak stress ratio, η_{peak}, has dropped from 2.02 for the average baseline test values to 1.92 for the average η_{peak} for stress path 'C', a drop of 0.1 (4.9%). Stress path 'B' experienced a drop of 0.21 (10.4%) in η_{peak}. Stress path 'A' has recorded the highest drop of 0.37 (18.3%) in the peak stress ratio, η_{peak}.

This behaviour can also be seen using the internal angle of shearing resistance, $\phi_{peak'}$. The value was 49.2° for baseline tests (tests without erosion). This value has dropped for all erosional tests. Stress path 'A' recorded 40.3° a drop of 8.9°, stress path 'B' recorded 44.1° a drop of 5.1° and stress path 'C' recorded 46.5° the least drop of 2.7°. Figure 6.8 presents the peak strength line for each stress path individually.
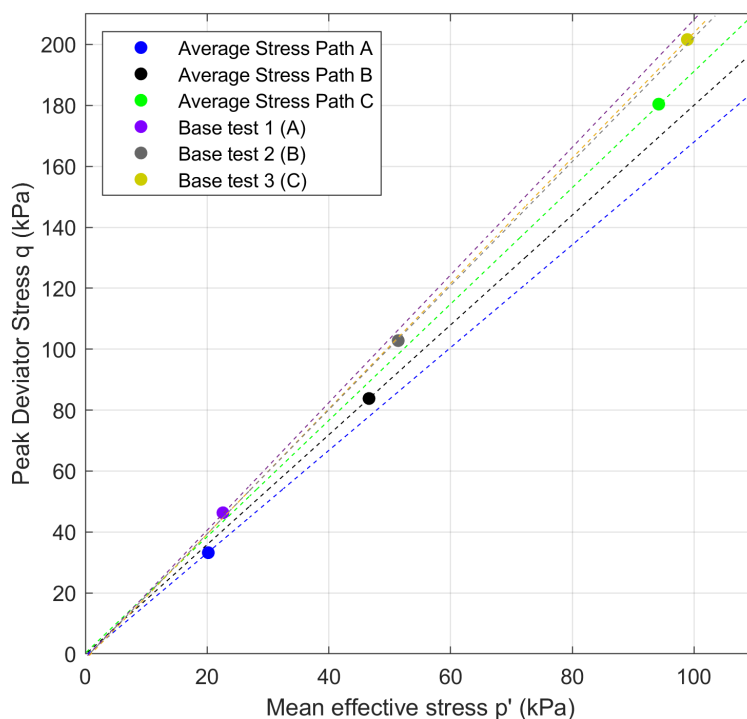
FIGURE 6.7: Illustration of the average peak strength line
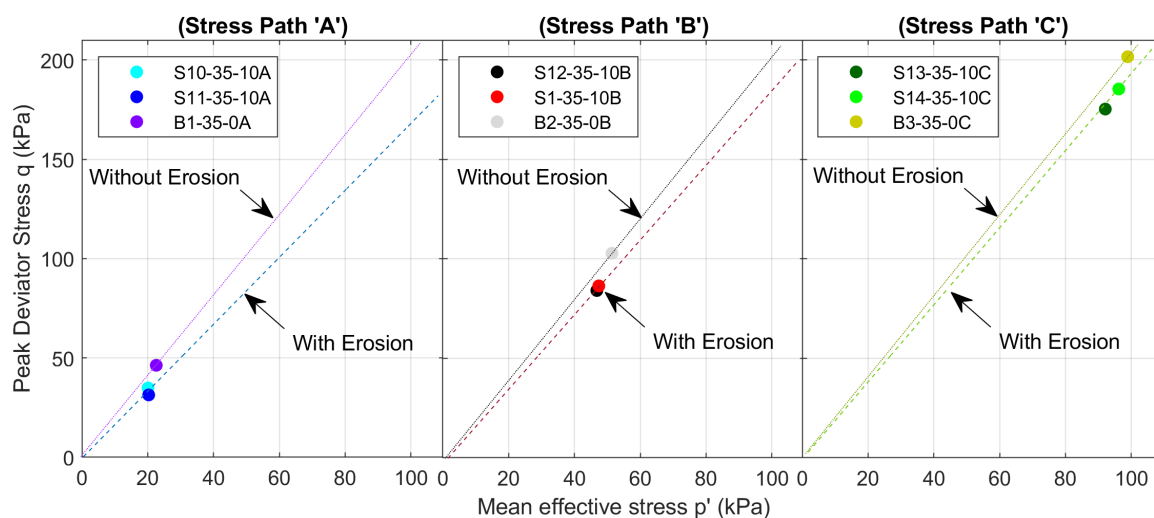
FIGURE 6.8: Illustration of the peak strength line for each stress
path individually

6.2.2 Permeability

Figure 6.9 plots the coefficient of permeability determined for all three stress paths (six tests). The average permeability ranges from 2.63×10^{-5} m/s in S12-35-10B, 2.77×10^{-5} m/s in S14-35-10C, 2.89×10^{-5} m/s in S13-35-10C, 3.35×10^{-5} m/s in S1-35-10B, 3.98×10^{-5} m/s in S10-35-10A to 4.87×10^{-5} m/s in S11-35-10A. Specimens sheared using stress path 'A' recorded the highest coefficients of permeability.

These results show a high correlation with seepage velocity, plotted in Figure C.5. Similar to the seepage flow velocity, all specimens experienced a slight decrease in permeability during the erosional tests. The results show some differences in the determined permeabilities with a maximum average permeability difference of 2.24×10^{-5} m/s.
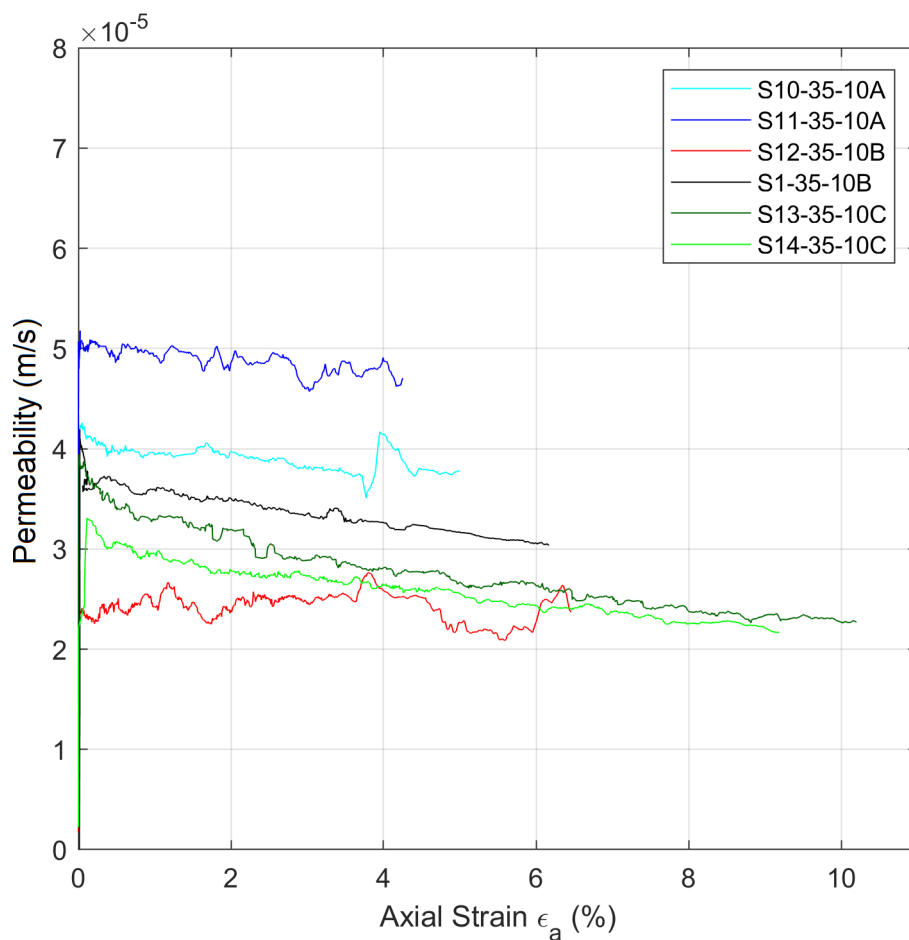
FIGURE 6.9: Relationship between permeability and local axial
strain

6.2.3   Erosion

The accumulated erosion with respect to axial strain is illustrated in Figure 6.10(a). All specimens exhibit the erosion of fine particles with the increase of axial strain. The results showed an interesting relation between the stress path used to shear the specimens and the amount of fine particles erosion. Before the start of each test, the water flow increased from zero to the targeted hydraulic gradient before shearing the sample, any

erosion at this stage was recorded and considered.

Stress path 'A' recorded the highest average accumulated erosion of 68.3 g (14.3%). On the other hand, stress path 'C' recorded the lowest average accumulated erosion of 41.9 g (8.8%). Stress path 'B' lies in between with an average accumulated erosion of 64.5 g (13.5%).

Another way to study accumulated erosion by presenting the data as a percentage from the original fines content mass, Figure 6.10(b). The highest accumulated erosion value at 22.9% was presented by specimen S11-35-10A. Whereas, the lowest accumulated erosion value at 11.1% was presented by specimen S14-35-10C. Similar observations can be seen analysing the erosion rate for the six tested samples, Figure 6.11.

(a)

(b)
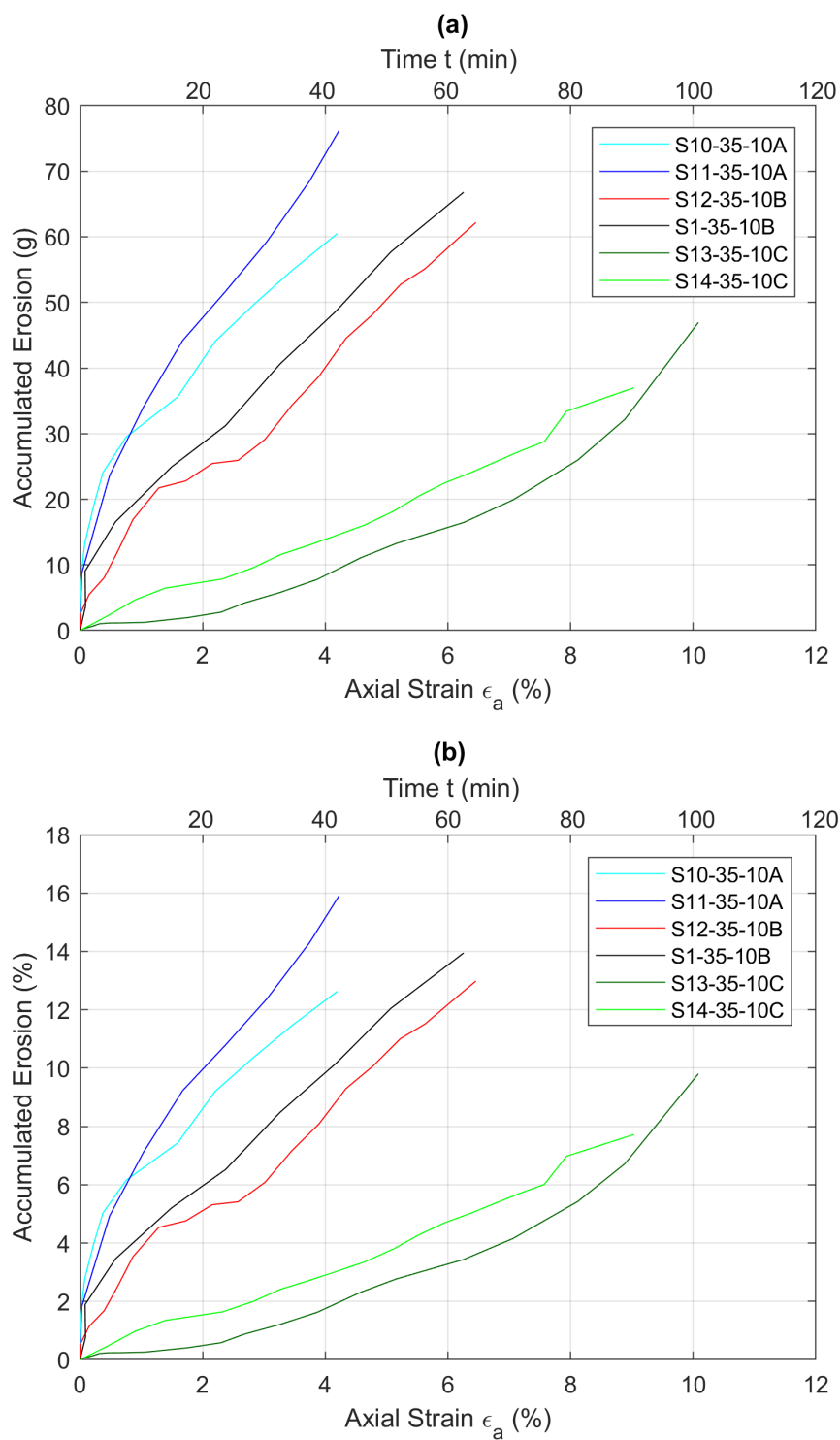
FIGURE 6.10: Accumulated erosion versus local axial strain under different hydraulic gradient, with erosion presented (a) in grams and (b) as a percentage of the initial fines content
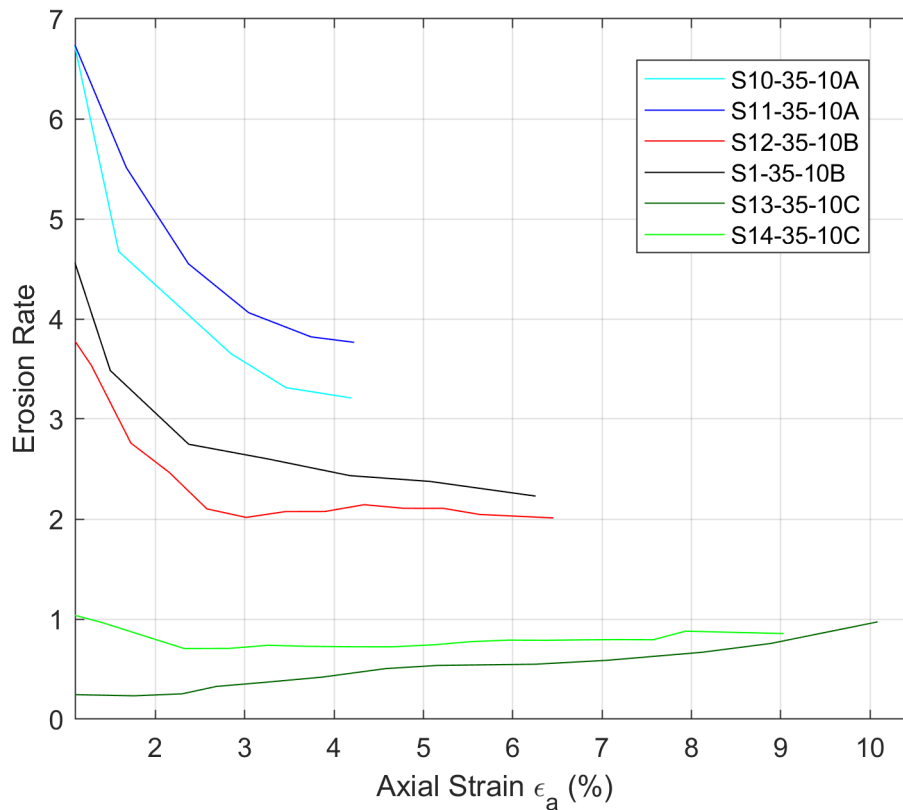
FIGURE 6.11: The erosion rate (accumulated erosion % / axial strain %) versus local axial strain

6.3 Discussion and interpretation

The onset and the development of internal erosion within gap-graded soils are investigated using a stress-controlled erosion apparatus. A series of laboratory experiments was carried out on six specimens under three different stress paths; stress path 'A', 'B' and 'C'. The purpose of this investigation is to understand the effect of these stress paths on the triggering and the development of internal erosion.

To quantify the influence of erosion on the strength of the soil, baseline

tests at the same initial fines content were performed. Figure 6.6 illustrates the normalised deviator stress of the test specimens as well as the baseline tests. The results revealed a clear relationship between the amount of eroded fine particles and the peak normalised deviator stress. It seems that the more fine particles lost, the more significant the drop in peak normalised deviator stress value from the baseline tests. Stress path 'C' presented by S13-35-10C and S14-35-10C recorded the highest peak normalised deviator stress value compared to stress path 'A' and 'B'. The two tests (stress path 'C') showed the lowest drop in the peak normalised deviator stress value from the baseline tests. In contrast to stress path 'A'.

The same behaviour can also be seen using the internal angle of shearing resistance, ϕ'_{peak}. Stress path 'C' recorded 46.5° , the highest value (the least effected value by erosion) compared to the baseline tests, 49.2°. Stress path 'A' and 'B' recorded 40.3° and 44.1°, respectively. A possible explanation for these results may be linked to how the loss of fine particles could affect the internal structure of the soil. This loss of fine particles could disturb the force chains, by removing fine particles which were part of the lateral support fabric. These results are consistent with the findings of other researchers wherein Chang et al. (2012), Chang and Zhang (2013), Ke and Takahashi (2014), and Wautier (2018) among others which stated that the internal erosion weakens the soil strength.

Regarding volumetric strain, all specimens exhibited a contractive behaviour at the first stages of the tests. However, with the progression of the erosion tests, the contractive behaviour turns into dilative behaviour. With the massive loss of fines during the first stages of the erosion tests, specimens tested under the stress path 'A' (S11-35-10A and S10-35-10A) exhibited the

least dilative behaviour followed by those of the stress path 'C', whereas the specimens tested under the stress path 'B' exhibited the most significant dilative behaviour. These results are in perfect concordance with previous researches of Chang et al. (2012), Chang and Zhang (2013), Ke and Takahashi (2014), and Slangen and Fannin (2017).

These occurring differences between the amounts of erosion among as well as the hydraulic and the mechanical behaviours of the specimens under the three stress paths can be explained by the different mean stress under which the tests were performed. The mean stress is a stabilisation factor that slows down the progression of the erosion. By providing lateral support for the force chains, mean stress strengthens these chains, which are oriented vertically under positive deviatoric stress. Thus, fines particles are kept trapped, enhancing the erosion resistance of the soil. Hence, under stress path 'A', specimens were tested under reducing mean stress and displayed the largest loss of fines. Whereas, specimens that were tested under stress path 'C', the mean stress was much constant, and as a result, the specimens exhibited the lowest fine erosion rate. The mean stress was also decreasing in stress path 'B' but not as intensely as for stress path 'A'. Hence, the accumulated eroded fines is a mean value between the previous values.

Using flexible wall permeameters, Chang and Zhang (2011) and Ke and Takahashi (2014) have reached similar conclusion and revealed that the internal erosion potential decreases with the increment of mean stress. Bendahmane et al. (2008) stated that suffusion maximum erosion rate was doubled when the mean stress was decreased from 150 to 100 kPa. This behaviour was explained by the increase of interparticle contacts with the

increment of mean stress intensifying the internal erosion resistance. Chang and Zhang (2011) demonstrated that under the same confining stress, the maximum erosion rate and the cumulative eroded soil shows an increasing trend with the increase of deviatoric stress. Luo et al. (2013) carried out suffusion experiments under different confining pressures, and the tests results revealed that the initial porosity decreases with the increase of the confining pressure. Furthermore, the initial porosity affects the migration of fine particles, a decrease in initial porosity makes it harder for fine particles to migrate through the sample. Furthermore, in their experiments, Ke and Takahashi (2014) found that the percentage of cumulative fines loss was the least under a confining pressure of 200 kPa and the largest under a confining pressure of 50 kPa. They supposed that under larger confining pressure, fines are more densely packed among coarse grains - hence, the interstitial spaces are narrower.

The results show some differences in the determined permeabilities among all six erosional tests. These differences could be due to the non-uniformity of specimens. Despite the permeabilities being different between tests that are repeats of each other, there is no consistent difference in stress-strain behaviour nor in the internal erosion behaviour.

All the specimens display decreasing permeability values during the erosion tests, irrespective of the stress path, including the most dilative one, stress path A. Several researchers report this reduction for the situation where there is not continuous shearing, wherein Shwiyhat and Xiao (2010) and Ke and Takahashi (2014) explained this behaviour by particle redeposition and clogging processes within the soil fabric reducing its porosity.

Chapter 7

Shearing Rate study

7.1   Introduction

Many researchers have asserted that the influence of the shearing rate on soil mechanical behaviour cannot be neglected, mainly on the residual shear strength of soil (Li et al., 2017). However, none of them have so far researched the influence of shearing rate on the hydraulic behaviour of the soil specifically under soil internal erosion.

In the course of this chapter, the results of the study are presented and discussed regarding the influence of different shearing rates on the internal erosion behaviour of different samples of gap-graded soil under downward seepage. In this series of tests, six samples of internally unstable soil were tested in the triaxial permeameter. The samples were prepared with two different fines percentages, three samples at 20% fines content ("underfilled") and the other three samples at 35% fines content ("overfilled"). Samples were tested under a constant downward seepage flow using different shearing rates between 0.05 mm/min and 0.2 mm/min. This was performed while measuring the amount (mass) of particles which were

eroded out under constant hydraulic gradient. The water outflow was measured using an electronic scale to enable permeability to be tracked throughout the test.

7.2   Results of shearing rate study

The six tests included in this chapter were prepared and sheared using the stress path 'B' as explained in Chapter 6 under constant hydraulic gradient, i, of 10. The mean stress was kept constant at 50 kPa taking a vertical stress path to reach failure.

The six erosion tests are named S15-20-0.05, S6-20-0.1, S16-20-0.2, S17-35-0.05, S1-35%-0.1, and S18-35-0.2. The first segment of the name refers to the specimen number followed by fines content percentage and the axial displacement rate in mm/min. Table 7.1 shows a summary of the testing program and key results for this chapter.

Two different fines contents were tested in order to examine the influence of shearing rate on soil erosion at the extremes of fines content. The 20% fines ratio was chosen because it is theoretically underfilled so that the fine particles carry no load/stress and are held in pores between the coarse fabric. On the other hand, the 35% fines ratio was chosen because it is theoretically overfilled by fines so both fine and coarse particles carry the load/stress via force chains (Shire et al., 2014). In both cases, the samples were prone to piping induced by the seepage flow. This concept has been covered in detail in Chapter 3.

The pore pressure differential across the sample, volume change, outflow rate of water and the mass of eroded particles were recorded during all six tests as discussed in Chapter 3. This allowed the hydro-mechanical parameters including hydraulic gradient, seepage velocity, permeability and the internal erosion rate by mass to be determined. The obtained results are presented and discussed below.

TABLE 7.1: Summary of the testing program and results for shearing rate study.

Test Name*	S15	S6	S16	S17	S1	S18
Finer fraction (%)	20	20	20	35	35	35
Axial displacement rate (mm/min)	0.05	0.1	0.2	0.05	0.1	0.2
Gap ratio	5.57	5.57	5.57	5.57	5.57	5.57
Intended relative density, D_R (%)	70	70	70	70	70	70
Initial relative density, D_{Ri} (%)**	71.4	72.3	69.4	71.2	70.9	70.5
Intended void ratio, e	0.499	0.499	0.499	0.472	0.472	0.472
Initial void ratio, e_i	0.495	0.493	0.501	0.468	0.469	0.470
Coarse particles initial mass, m_{ci} (g)	1075	1075	1075	889	889	889
Fine particles initial mass, m_{fi} (g)	269	269	269	479	479	479
Intended Hydraulic Gradient i	10	10	10	10	10	10
Mean hydraulic gradient i_m	10.6	11.2	12.1	11.3	11.2	10.1
Initial total mean stress, p_i (kPa)	50	50	50	50	50	50
Max Deviatoric stress, q_{max} (kPa)	92.9	95.1	88.1	85.3	86.4	79.4
Mean effective stress at q_{max}, p'_{qmax} (kPa)	47.9	48.3	44.9	47.3	47.4	44.9
Shearing resistance internal angle, $\phi_{peak'}$	47.1°	47.9°	47.6°	43.8°	44.3°	43.1°
Accumulated erosion mass, m_{fa} (g)	21.4	25.9	25.6	62.2	66.8	68.9
Accumulated erosion percent, m_{fap} (%)	8.0	9.6	9.5	13.0	13.9	14.4

*S15=S15-20-0.05, S6=S6-20-0.1, S16=S16-20-0.2, S17=S17-35-0.05, S1=S1-35-0.1 and S18=S18-35-0.2.

**Initial relative density was measured just before commencing the erosion stage (testing stages are discussed in Chapter 3).

7.2.1 Drained shear strength

Figure 7.1 illustrates the relation between total mean stress p (50 kPa), seepage flow u (hydraulic gradient of 10), and the mean effective stress p′

for a typical sample.

p = 50 kPa   u = 10 kPa   p' = 40 kPa

100 mm

—   =   p' = 45 kPa

p = 50 kPa   u = 0 kPa   p' = 50 kPa
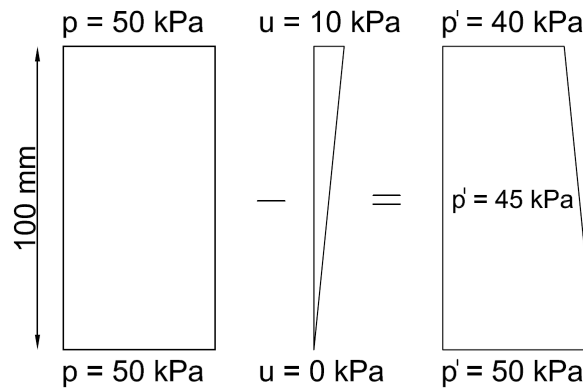
FIGURE 7.1: An illustration of the initial stress conditions

Figure 7.2 presents all six tests results sheared using stress path 'B'. Three tests were used for each fines content, i.e. 20% and 35%. The peak deviator stress values ranged between 79.4 kPa and 95.1 kPa represented by specimens S17-35-0.05 and S6-20-0.1, respectively. Also the mean effective stress p' can be seen in Figure 7.3, which includes the influence of the seepage flow, with pore pressure determined at the midpoint as an average of the top and bottom PPTs.
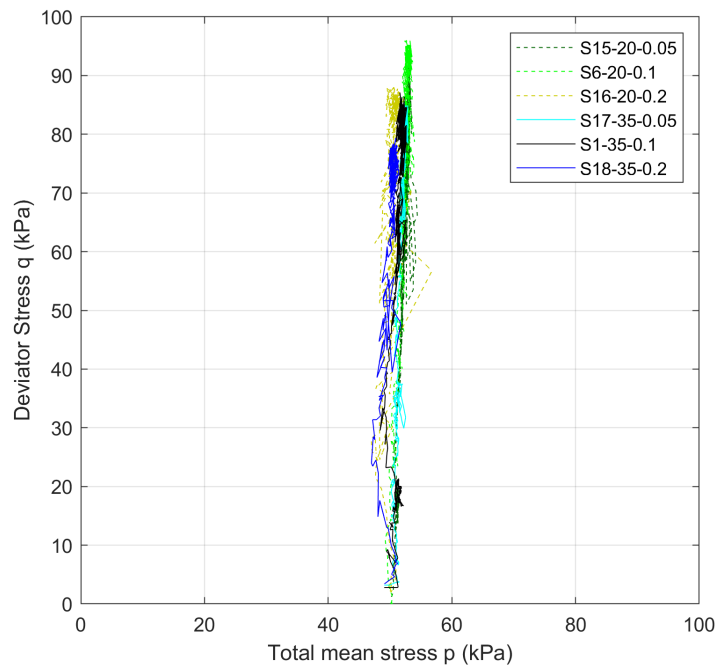
FIGURE 7.2: Deviator stress, q versus total mean stress, p
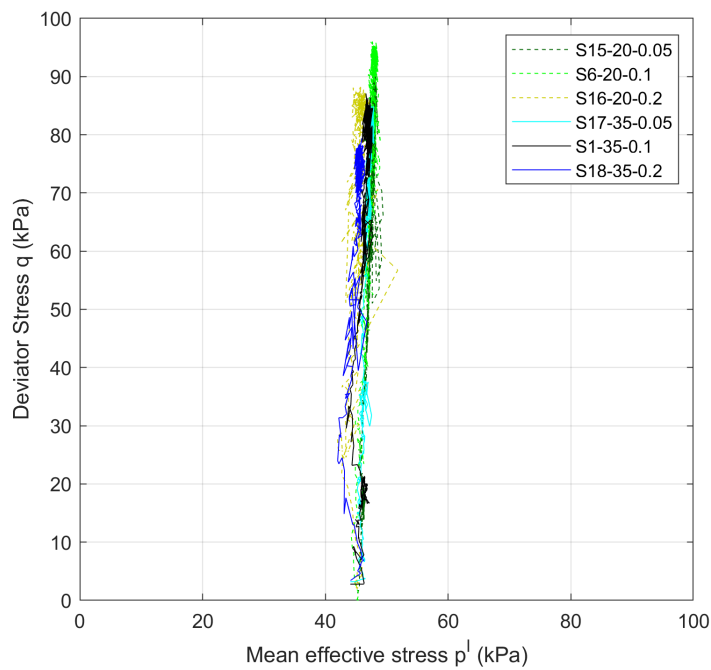
FIGURE 7.3: Deviator stress, q versus mean effective stress, p′

Figure 7.4(a) demonstrates the deviatoric stress q against the local axial strain ϵ_a for the tested specimens. On average, specimens with 20% initial fine particles, S15-20-0.05, S6-20-0.1 and S16-20-0.2, record a higher peak deviator stress values than specimens with 35% initial fine particles. Test S6-20-0.1 recorded the highest peak deviator stress at 95.1 kPa. Test S18-35-0.2 recorded the lowest peak deviator stress at 79.4 kPa a difference of 15.7 kPa (16.5%).

Figure 7.4(b) presents the volumetric strain curves, ϵ_v of the tested specimens. All the specimens exhibit contraction followed by a significant dilation. Specimen S6-20-0.1 recorded the lowest volumetric strain at 1.2%. All six tests showed similar behaviour, with tests at lower fines contents showing slightly more contraction than those at higher contents in the curves up to 1% axial strain.

In general, there is no noticeable correlation between the shearing rate and volumetric strain development, and hence no discernible influence of shearing rate on volumetric strain.
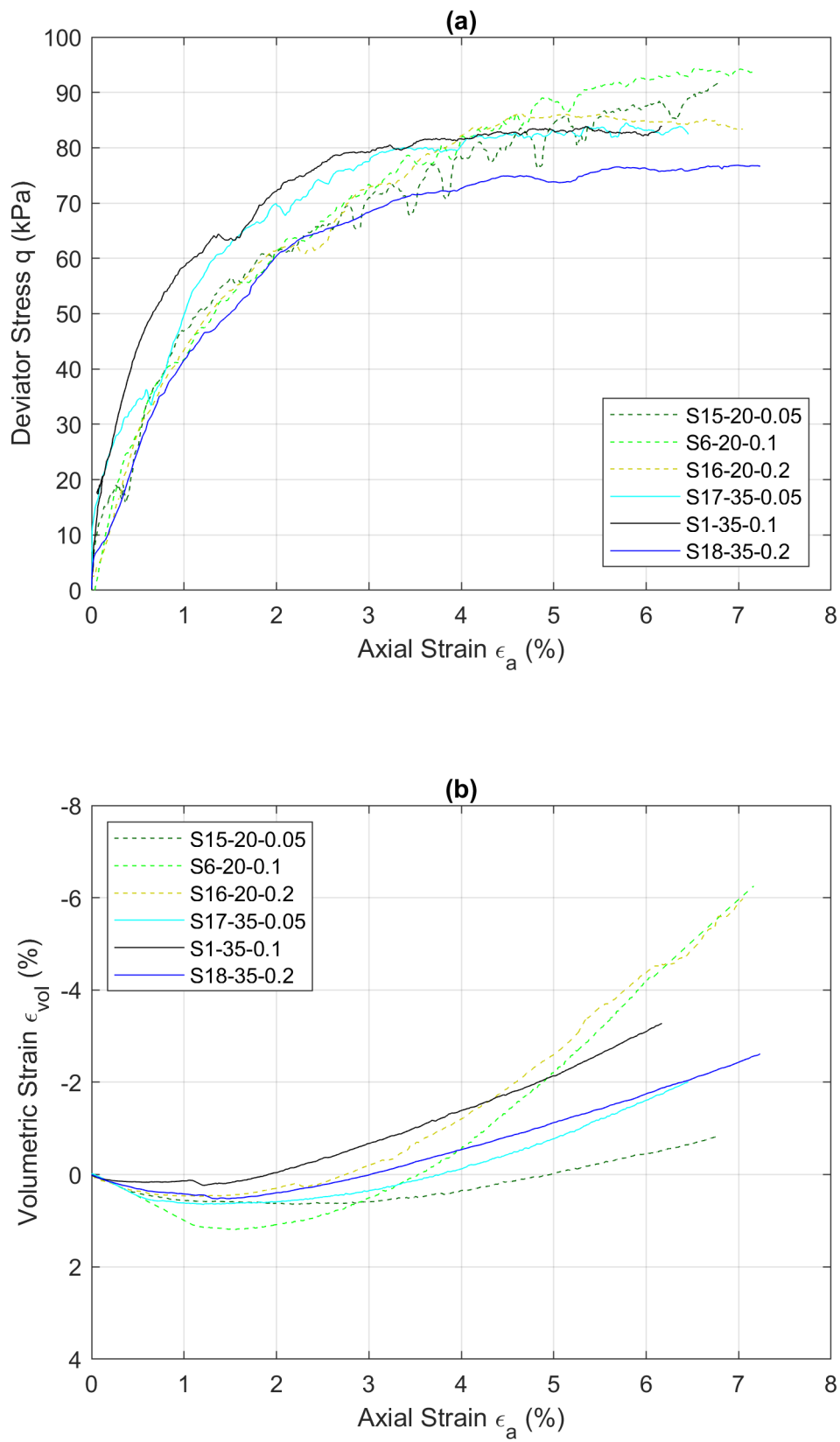
FIGURE 7.4: Relationship between deviatoric stress and volumetric strain vs local axial strain

Figure 7.5(a) shows the normalised deviatoric stress, q_n (q/p') against the local shear strain, ϵ_s for the tested specimens. In general, tests with 20% initial fines developed a higher peak normalised deviatoric stress apart from S15-20-0.05, which showed a slightly lower value. Specimen S18-35-0.2 recorded the lowest peak normalised deviatoric stress at 1.51, interestingly the same test has recorded the highest accumulated fines loss at 68.9 g (14.4%).

Figure 7.5(b) illustrates the variation of the volumetric strain ϵ_v, with respect to shear strain, ϵ_s. All the specimens experienced contractive behaviour followed by dilative behaviour.
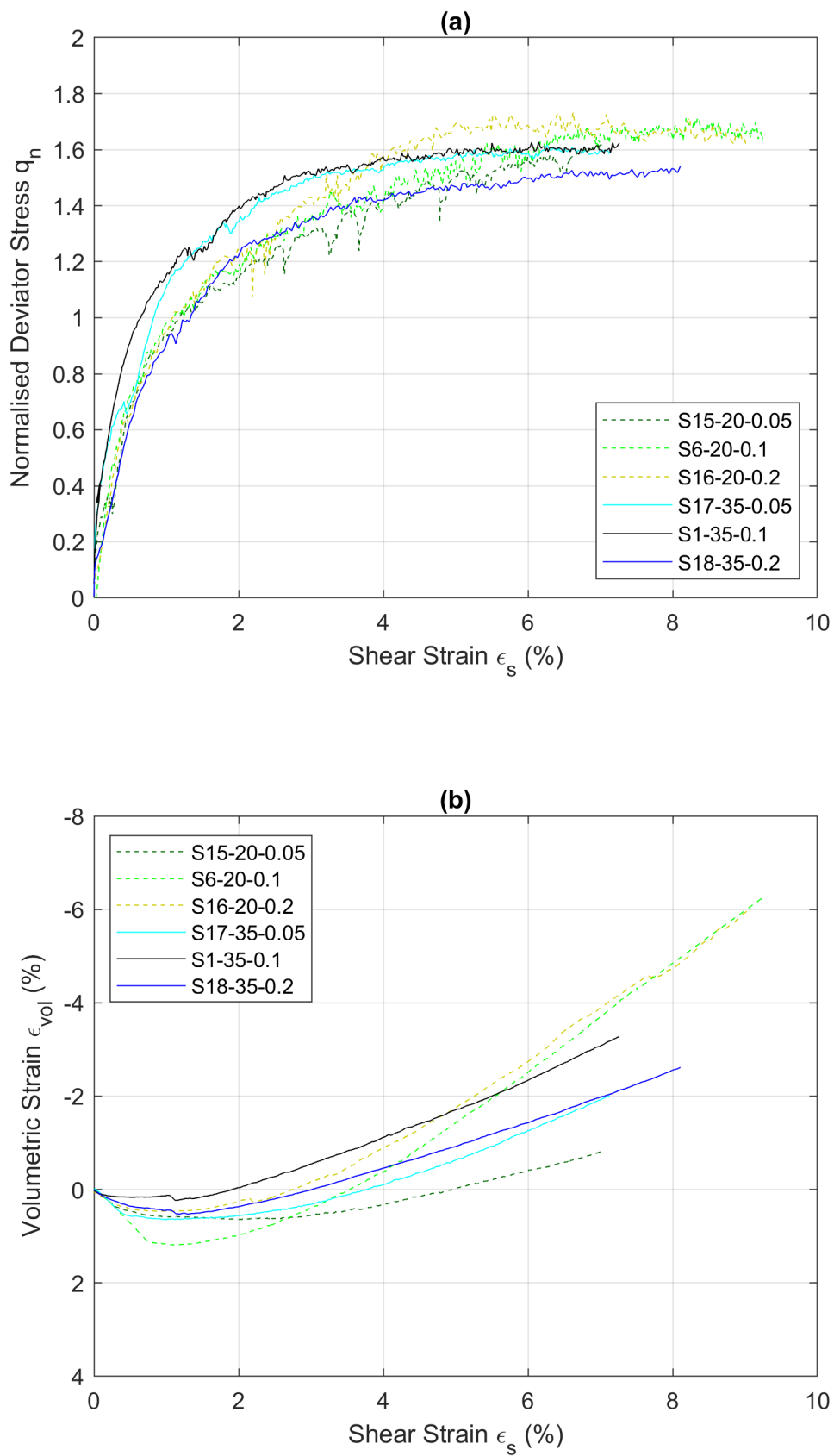
FIGURE 7.5: Relationship between normalised deviatoric stress
and volumetric strain with local shear strain

Figure 7.6 illustrates the average peak strength line for the two initial fine particles groups. The average peak strength line for 20% fines tests recorded 1.96 where as 35% fines tests recorded 1.80 on average between all three tests.

Alternatively, this can also be seen using the internal angle of shearing resistance, ϕ'_{peak}. The former tests at 20% fines developed $47.5°$ on average, whereas the 35% fines tests recorded $43.7°$.
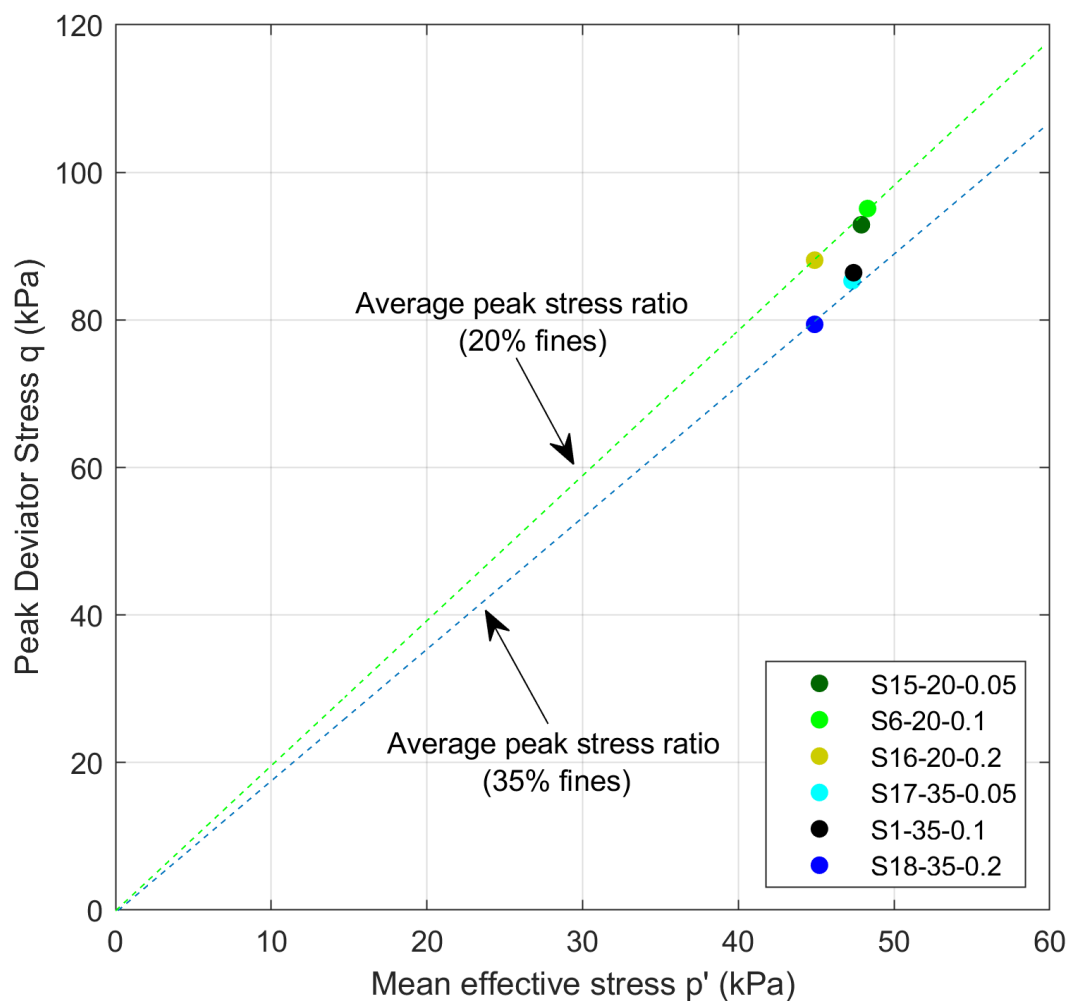
FIGURE 7.6: Maximum deviatoric stress against mean effective stress for sheared and eroded soils. Initial fines contents of 20% and 35% respectively

7.2.2   Permeability

The permeability k is determined from the recorded outflow rate induced by the seepage water flow throughout the tested specimens, and the calculated hydraulic gradient from the difference in the water pressure across

the sample. Figure 7.7 shows the outcome of all six tests where the average permeability ranges from 2.5×10^{-5}m/s for specimen S17-35-0.05 to 5.4×10^{-5}m/s for the specimen S15-20-0.05.

Overall, specimens with 35% fines content had lower initial permeability k when compared with specimens with 20% fines content. This can be attributed to the general behaviour of soils with larger proportions of fines. The difference in permeability between specimens with the same fines content is a result of a slight difference in density within the specimens' layers. Unsurprisingly, these results display a high correlation with the seepage velocity v results, shown in Figure C.6.

Figure 7.7 also demonstrates that all samples exhibit a decrease of permeability k when eroding and shearing, except for specimen S17-35-0.05 that displays a relatively stable permeability.
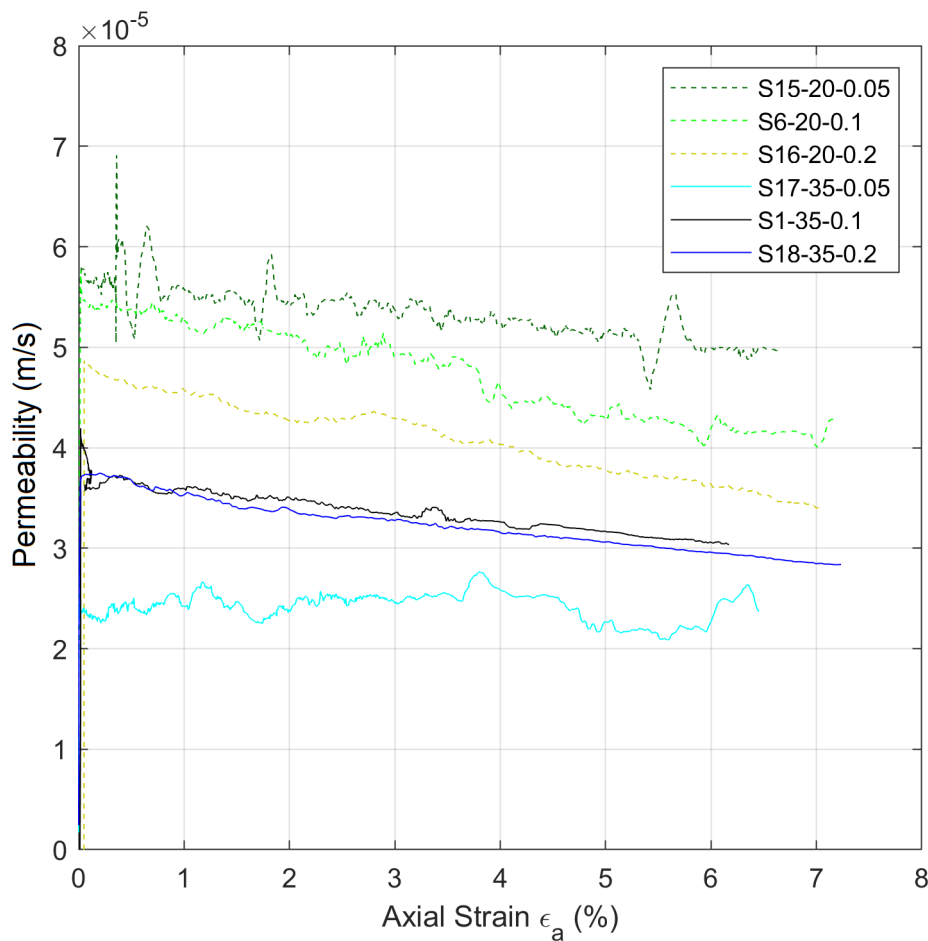
FIGURE 7.7: Relationship between permeability and local axial
strain

7.2.3   Erosion

The progression of internal erosion was determined by collecting the eroded
fines in ten minutes intervals meaning that the slower the shear rate, the
greater the number of individual fines collections with the strain. The
method is described in detail in Chapter 3 under fine particles collection
system section.

Figure 7.8(a) illustrates clearly the effect of the shearing rate on erosion. The most striking result to emerge from the data is that there is no significant difference in the amount of erosion when plotting accumulated erosion against axial strain, even though, for example, tests with 0.05 mm/min shearing rate were half the duration of 0.1 mm/min tests and quarter the duration of 0.2 mm/min tests. This figure suggests that tests with 35% fines content lost a greater amount of fines when compared with 20% fines content tests.

Another way to present the data is as a percentage of the original fines content by mass, Figure 7.8(b). The highest accumulated erosion proportion at 14.4% was developed in specimen S18-35-0.2. Whereas, the lowest accumulated erosion proportion at 8.0% occurred for specimen S15-20-0.05. The same behaviour can be seen analysing the erosion rate versus axial strain graph, Figure 7.9. In this figure, it is clear that for tests conducted with 35% fines, the erosion rate decreases over the tests to approximately 2.2, while for tests with 20% fines, the erosion rate is quite steady at around 1.5 throughout.
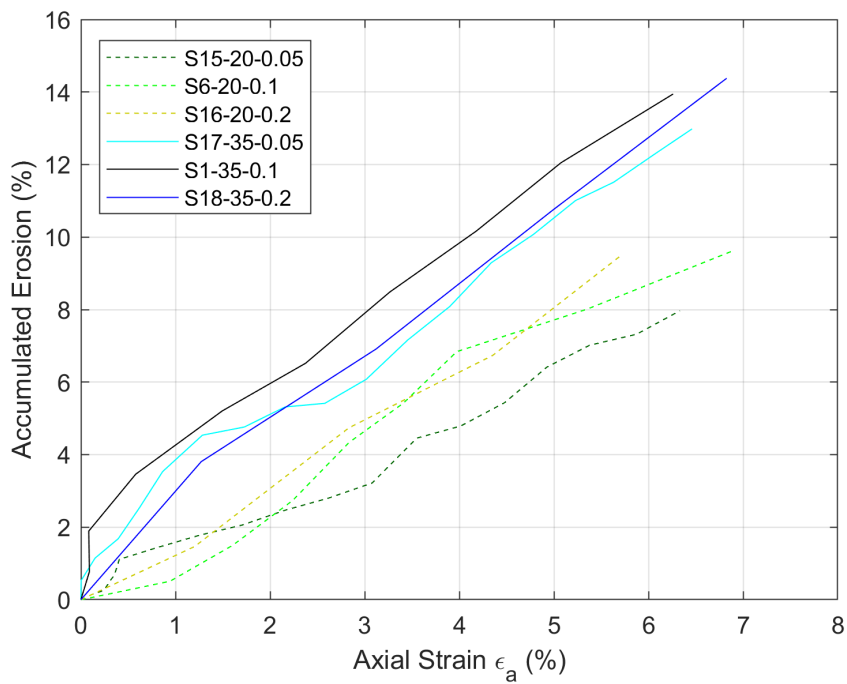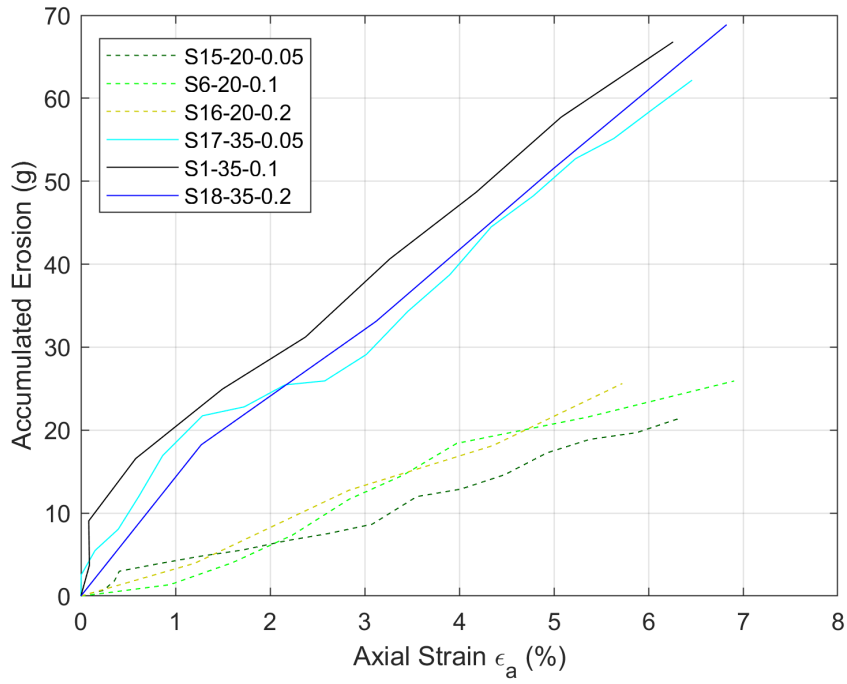
FIGURE 7.8: Accumulated erosion versus local axial strain for
two fines content (20% and 35%) under different shearing rates
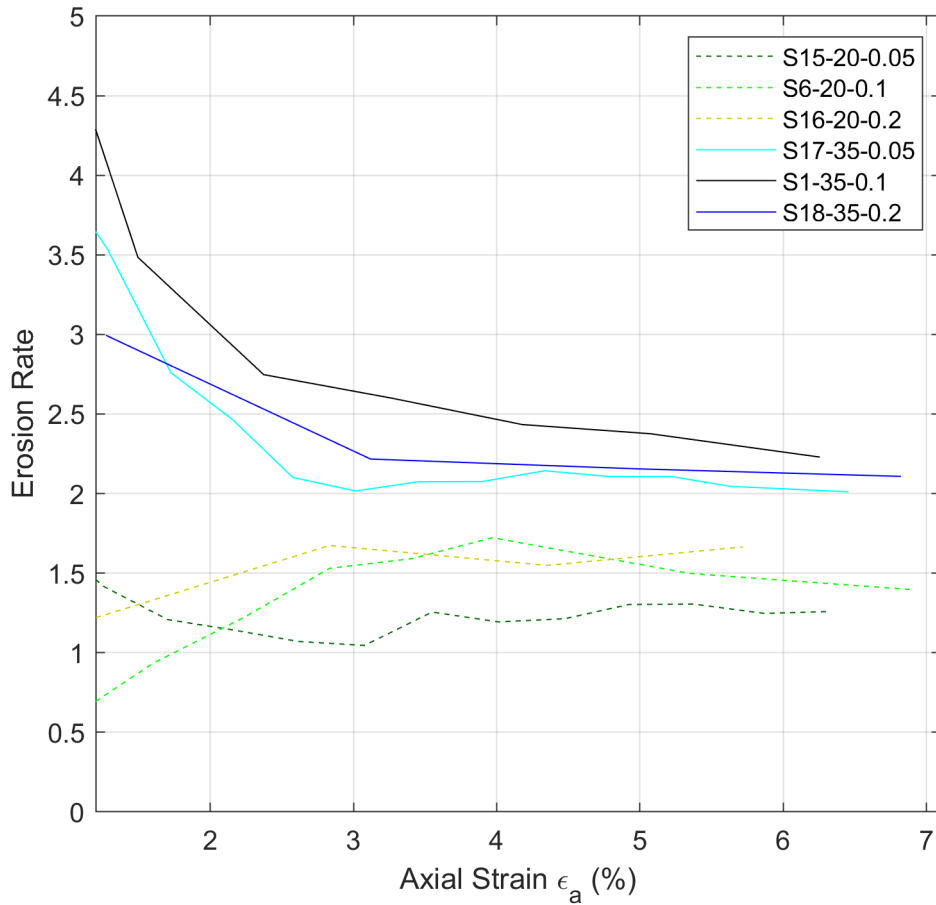
FIGURE 7.9: The erosion rate (accumulated erosion % / axial strain %) versus local axial strain

To draw a theoretical boundary on shear rate results, it is crucial to estimate the time it takes for a particle to move from the top of the sample (in theory) to be eroded out the bottom. This can be calculated using Darcy's velocity, v_D which was calculated using water flow-rate, q and the corrected area, A_c .

$$v_D = q/A_c \qquad (7.1)$$

To better estimate the particle travel time, Darcy's velocity then can be converted to true velocity. The true or tortuous fluid velocity v_T is obtained by dividing the flow-rate q by the cross-sectional area of the voids alone. Assuming that the void ratio for the cross-section is the same as the volumetric void ratio, the cross-sectional area of the voids is smaller than the total area by a factor $e/(1+e)$ (Powrie, 2018).

$$v_T = v_D(1+e)/e \tag{7.2}$$

To demonstrate this, specimen S1-35-0.1 is used as an example. The average velocity determined was 0.38 mm/s, the initial void ratio, e_i was 0.469 and the height of the sample before shearing was 99.3mm.

$$v_T = v_D(1+e)/e = 0.38(1+0.469)/0.469 = 1.19 mm/s \tag{7.3}$$

$$t = x/v_T = 99.3/1.19 = 83.4s = 1.4 min \tag{7.4}$$

Using the same method, The estimated average particle travel time was 1.1 minutes for all three tests at 20% fines. Figure 7.10 illustrates this concept from the top and from the middle of the sample for both cases 20% and 35% fines.

It must be noted that this time (the theoretical time assumed) was calculated assuming a straight flow path travelling from the top to the bottom of the sample, whereas, in the actual sample, the fine particles would take a devious flow path. Additionally, there is most likely to be a delay in travel due to the effect of fine particles blockage.
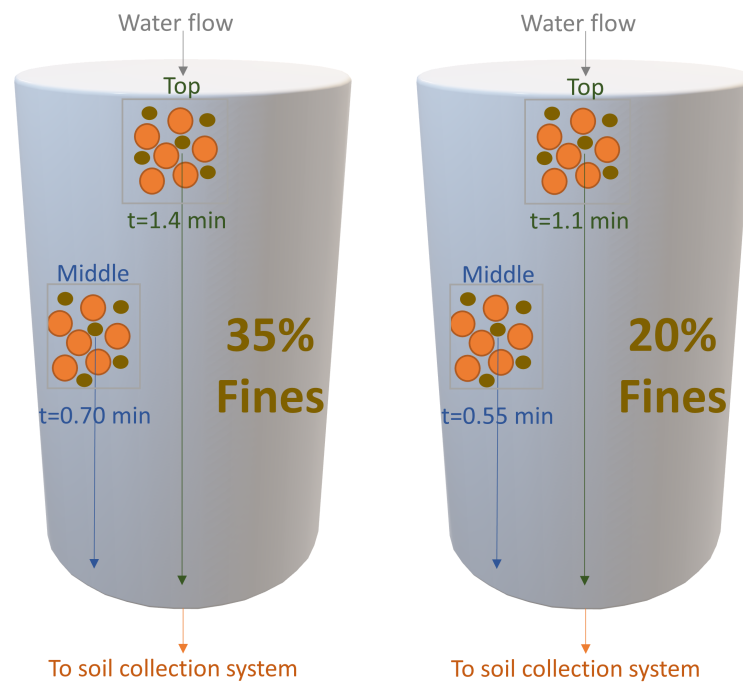
FIGURE 7.10: particle travel time from the top and middle

All tested samples was equally divided into three layers, top, middle and bottom after each test. All layers were oven-dried separately and sieved to analyse the effect of erosion on particle size distribution for each layer.

Figure 7.11 and Figure 7.12 illustrate the variations in the particle-size distributions in different layers of the soil specimen for specimen S1-35-0.1 and S6-20-0.1. The tests presented here as examples, a general trend in all tests is that more fine particles in the top layer are eroded than those in the bottom layer.
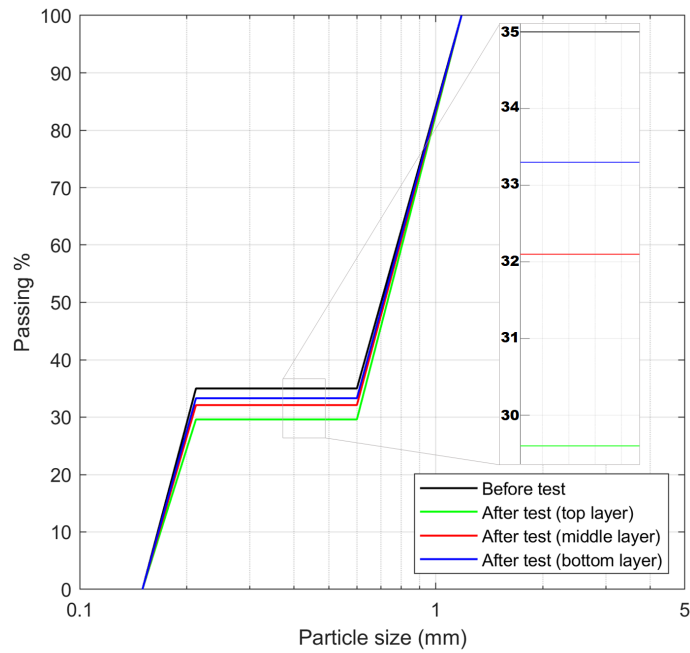
FIGURE 7.11: PSD in different layers, S1-35-0.1
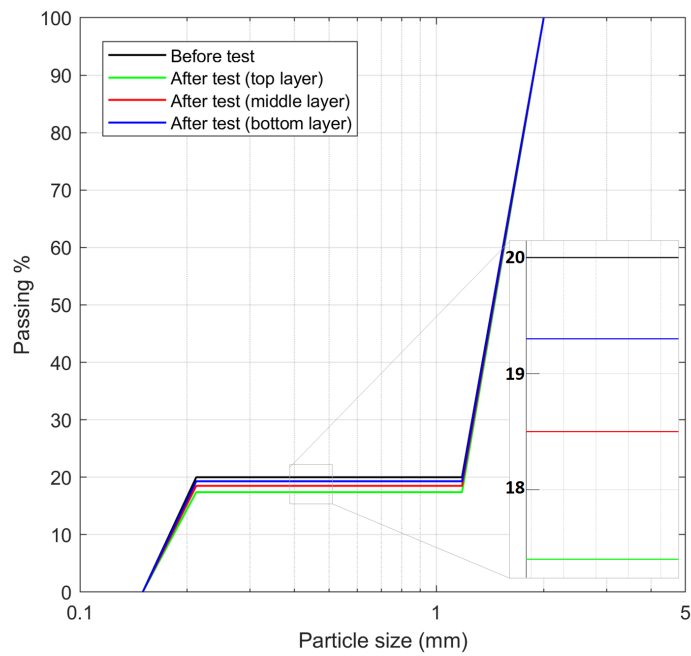
FIGURE 7.12: PSD in different layers, S6-20-0.1

Comparing these results with the fines eroded during the tests, the values were 13.9% and 9.6% (Table 7.1) for samples with initial fines of 35% and 20%, respectively. Considering these values, the percentages of fines left are 30.1% and 18.1% compared to 31.7% and 18.4%, respectively, the average fines left from dissecting the samples (Figure 7.11 and Figure 7.12). The difference between the two methods is small and could be due to fines loss during the preparation, fines collection or when drying the fines.

7.3 Discussion and interpretation

To evaluate the influence of the shearing rate on the internal erosion, a series of laboratory experiments were conducted with a stress-controlled apparatus. This was done on two different mixtures of gap-graded soil containing 20% and 35% initial finer fraction, under three different axial displacement rates 0.05, 0.1 and 0.2 mm/min.

It was found that the increase of the displacement rate from 0.05 mm/min to 0.2 mm/min led to a near linear increase in the erosion rate for both fines contents such that the same amount of erosion occurred with strain developed. The result was somewhat unexpected in two ways: First, it might be predicted that a greater amount of erosion would occur for a longer duration test using the same material and under the same seepage flow (i.e. hydraulic gradient). This indicates a direct positive correlation between the amount of shearing and the amount of fines erosion. From a micromechanical perspective, considering the interaction between particles, It is thought that, in these tests, the continued shearing disturbs the fabric of the sample and continuously frees fines from the force network (force

chains), so they become "rattlers" able to be picked up by the flow. This dominates the erosion compared to a process in which particles initiate movement purely due to seepage flow (e.g. via viscous drag).

As discussed in Chapter 2, recent research by Wautier (2018) on internal erosion in granular material using numerical DEM simulations has revealed that the materials, when exposed to seepage flow accompanied with stress state change, are prone to force chain destabilisation and microstructural anisotropies, leading to structural rearrangements. Therefore, fine particles are prone to be removed from force chains, transported by the seepage flow, and can then result in being either eroded or clogged. This behaviour from the DEM simulation can be seen in the erosion tests conducted, where a continuous erosion was observed as a result of chain destabilisation (chain renewal) and the movement of the coarse particles relative to each other. It was found that this change in condition had a noticeable impact on the distribution of these contacts and provoked important microstructure re-organisation through gain and loss of contacts.

The loss of fine particles weakens the force chains, which become prone to microstructural rearrangements, which favours the development of plastic strain and contractive behaviour. Even if that loss remains localised, this can affect the whole sample by affecting the contact network as stresses are forced to redistribute.

This research can not be certain about the main trigger of fine particles erosion, if it was purely by shear stress (force chain reconfiguration) or shear strain (movement of the coarse particles relative to each other). It was assumed that both actions could lead to fine particles erosion. It must

be mentioned that with erosion, there will be a potential risk of runaway failure (fine particles erosion leads to strain, and strain leads to more fine particles erosion).

The second unexpected outcome was that there appeared to be no difference in the behaviour of the two fines content tests - overfilled (35% fines) and underfilled (20% fines). The accumulated erosion for fines of 35% is almost triple that of initial fines of 20%, as seen also in Chapter 5 (a result which is consistent with the previous work of (Ke and Takahashi, 2014)).

However, again - the shear strain accumulation dominated the erosion process for both fines content, so that the same proportion of fines was eroded, irrespective of shear rate, by the same strain. This suggests that, while it is considered that fines are held between the voids in low fines content gap graded soils, their release may be fundamentally linked to the force chain network and its disruption, rather than viscous shear dislodging particles.

Considering the result that emerged from this chapter, the erosion phenomenon is strain-dependent and not time-dependent. Erosion would stop after the migration of fine particles that not held by the force chains and needs a change in stress state or hydraulic gradient for the erosion to resume again.

The specimens displayed a decrease in the deviatoric stress peak with the increase of the fines content. This behaviour can be seen analysing Figure 7.13 which illustrates the relationship between η_{peak} reduction and

fines loss% for tests from Chapter 6 (stress path study) and for tests from this chapter (shearing rate study). All the compared erosional tests used 35% fines and a hydraulic gradient of 10. A 2nd order polynomial trend-line was added to present the results. It can be concluded that in general there is a positive relationship between η_{peak} reduction and fines loss %, supporting the argument of fines loss can affect the shear strength.

It can be assumed that if the fine particles were to be removed completely in one of the samples, there would be no change in η_{peak} and no fine particles erosion and hence a point at the origin (0,0).
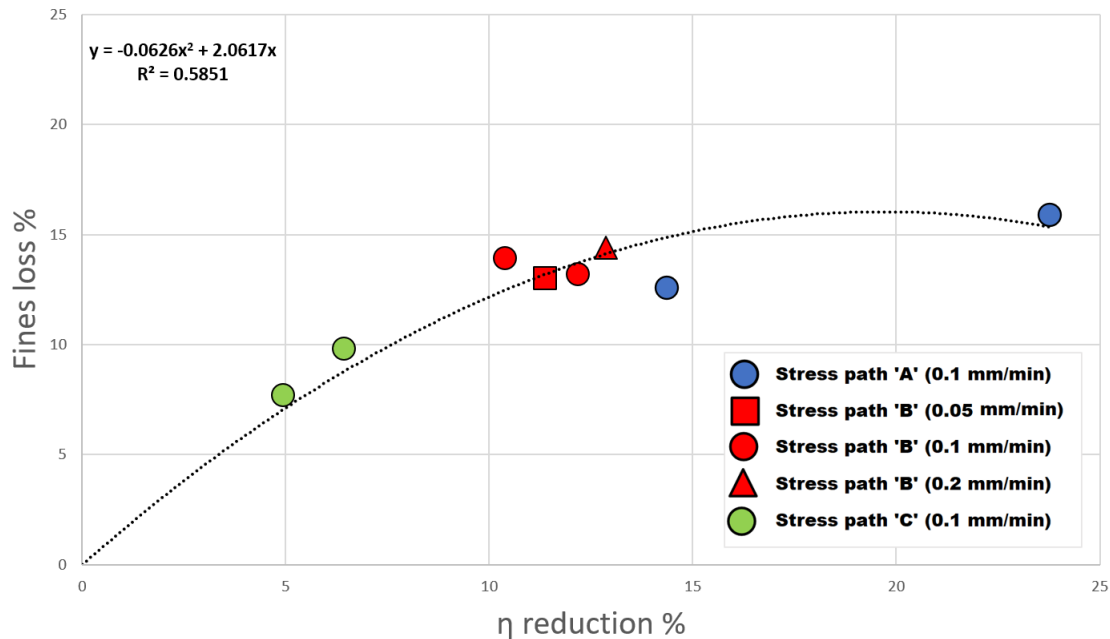
FIGURE 7.13: Relashinship between η_{peak} reduction and fines loss

The nature of these tests does not allow the influence of the erosion on volumetric strain to be clearly ascertained independently of the influence of shearing. That is, the influence of shearing on volume change is con-sidered to be much greater than the effect of fines removal on volume, hence any volume change can be mainly referred to the shearing rather

than fines removal. However, the influence of the change in mean effective stress can be discounted because the vertical stress path ensured that this was kept near constant.

Analysing the erosion across the length of the sample, all tests experienced more fines loss from the top layer compared to middle and bottom layer. This is because the fine particles lost in the top layer under seepage force and self-weight can be transferred to or captured in the bottom layer. In their tests, when erosion developed, Moffat et al. (2011) also observed that the local hydraulic gradient in the top layer to become higher than that in the bottom layer under downward seepage flow, this could induce more fine particles being eroded in the top layer. Figure 7.1 highlighted the minor non-uniform effective stress within the sample from top to bottom with more effective stress at the bottom, and that can play a stabilising factor leading to more fine particles getting trapped at the bottom compared to the top. Finally, the longer the erosion path, the more chances for fine particles from the top to get trapped. All the above three reasons could lead to more fine particles blockage at the bottom of the sample than at the top.

Under a constant hydraulic gradient the permeability and the seepage flow velocity exhibit a decrease with the progress of the internal erosion testing. Several researchers have reported this decrease in permeability in experiments conducted under downward seepage. Shwiyhat and Xiao (2010) have explained this behaviour by the clogging of the downstream soil layer by the eroded fine particles. This appears to be a factor for both 35% and 20% fines cases, with the permeability decreasing more for the 20% fines tests overall. Given that all soil layers, including the bottom

layers, lost fines during testing, this suggests that clogging must be a very localised phenomenon. There may be other factors contributing to this reduction, like the internal rearrangement of particles during the shearing phase i.e. contraction of the sample as a result of shearing, although this is then followed by dilation.

Furthermore, Chang et al. (2012) have concluded that the skeleton deformation hydraulic gradient under an anisotropic stress state is much lower than that under isotropic stress. This was explained by the buckling potential of force chains in the soil being much larger under an anisotropic conditions.

From this prospect, the observed increasing loss of fine particles by increasing the amount of shear in this research can be attributed to the influence on the internal stability of the soil. This originates by acting directly on the force chains. As a result of these force chain destabilisations, more fine particles are removed from their stable positions in the skeleton and released from the stress chains. Hence, more fines are prone to be transported and eroded from the specimens before the new force chain is established.

This is a promising finding in the understanding of the progression of internal erosion in soil under critical stress conditions.

Chapter 8

Conclusions and Further Work

There are many embankment dams around the world that are deemed to be unstable based on the investigation of their material susceptibility and hydraulic conditions. As a result, they are continuously subjected to internal seepage flow that can affect their internal structure through internal erosion.

These processes may generate mechanical instabilities that will lead to unexpected failures in case of sudden changes in the loading conditions. The research presented in this thesis is centred around developing an understanding of the role of seepage flow on internal instability in dense gap-graded soils under complex states of stress in geotechnical structures.

8.1   Major contributions

- A triaxial permeameter has been developed to study the effect of seepage flow through a gap-graded soil under continuous shearing stress. A Bishop and Wesley stress path cell has been adapted to create the triaxial permeameter. It is equipped by (i) a pressurised water supply system, which allows the hydraulic head to be controlled.

(ii) A fine particles collection system, which enables the erodibility and the accumulated erosion to be determined during erosion experiments. (iii) A water collection system, which allows the discharge flow rate as well as the permeability of the sample to be determined. More on the design of the triaxial permeameter was discussed in detail in Chapter 3.

- For the first time, the internal erosion process was studied under three different stress paths named "A", "B", and "C". For stress path 'A', the radial pressure was decreasing, and axial stress was maintained so as to decrease the total mean stress p while increasing the deviatoric stress q. For stress path 'B', the radial pressure was decreasing, the axial stress increasing, and hence, deviatoric stress increased while keeping the total mean stress constant (taking a vertical stress path in p-q space). In stress path 'C', the radial pressure was kept constant, increasing the axial stress and hence, total mean stress while increasing the deviatoric stress (a typical conventional stress path used in triaxial testing). Analysing the results, it can be concluded that greater fine particles erosion was recorded for the samples tested under the stress path "A" followed by the stress path "B". Whereas stress path "C" recorded the least fine particles erosion.

- The influence of the shearing rate on internal erosion was investigated for the first time. Two different mixtures of gap-graded soil containing 20% and 35% of initial finer fraction were tested under three different axial displacement rates 0.05, 0.1, and 0.2 mm/min. The test results revealed a direct positive correlation between the amount of shear and the amount of fines erosion.

8.2 Conclusions

Series of triaxial tests were performed on dense gap-graded soil in order to investigate the influence of varying the hydraulic gradient, the effect of different initial fines contents, the impact of different stress paths and finally, this research studied the role of the rate of shearing on fine particles erosion.

- The contribution of the seepage flow on erosion was investigated. The tests' results revealed that increasing the hydraulic gradient from 10 to 25 led to an increase in the amount of eroded fines. The seepage flow study is discussed in detail in Chapter 4.

- The increase of initial fines content percentage led to a significant increase in the amount of eroded fines when initial fines content was increased from 10% to 35%. However, by surpassing the threshold value (35%) to 50%, no increase in erosion was detected. On the contrary, when the amount of initial fines was increased above this value, the amount of eroded fines decreased with the increase of the initial fines content. This could be the result of blocking the erosion path when increasing the fines content by more than 35%. The initial fines content is discussed in detail in Chapter 5.

- Analysing all erosional tests, it can be concluded that, in general, the shear strength of the soil decreases with the increase of the amount of eroded fine particles. Fine particles loss can affect the internal structure of the soil. This loss of fine particles disturbed the force chains by removing fine particles which were part of the lateral support fabric. As for the volumetric strain, during the erosional tests, all samples exhibited contractive behaviour at the first stages of the

tests. However, with the progression of erosion, this behaviour changed into dilative behaviour.

- All erosional test samples were equally divided after each test into three layers, top, middle, and bottom, to analyse the effect of erosion on each layer's particle size distribution. A general trend in all tests is that more fine particles in the top layer are eroded than those in the bottom layer.

- The permeability deceased in all tests, despite the loss in fines in all parts of the sample. It is possible that local clogging of one or more thin layers could have reduced the permeability, despite the overall fines reducing.

8.3   Real-world engineering implications

Embankment dams can be of virtually any height up to 300 m (i.e. the highest embankment dam in the world, currently, is the Nurek dam in Tajikistan at 300 m (Charles, 2005)). Assuming an earth or rockfill dam has soil with a unit weight of 20 kN/m^3 (typically), this equates to a maximum total vertical stress of $20 \times 300 = 6000$ kPa at the base and centreline of the dam. The maximum effective stress would be somewhat less than this due to pore pressure influence. The highest of the approximately 2,800 embankment dams in Great Britain (BBC, 2019) is the 76 m high Scammonden dam in Yorkshire (Charles, 2005). Most dams are considerably smaller, while stresses vary more-or-less linearly with depth.

For dams to be considered a "large" dam, and therefore to be regulated by ICOLD (International Consortium on Large Dams), it needs to be greater

than 15 m high (i.e. maximum total stress in a 15 m high dam would be 300 kPa). There are approximately 58,000 of these large dams globally (ICOLD, 2014). Hence, the stresses used in this thesis are at the "low" end for a large embankment dam but may be considered to represent a typical value at the base of a small dam (of which there hundreds of thousands globally, most of which are unregulated) or at the middle or upper portion of a large dam as designated by ICOLD.

This thesis aims to offer a better understanding of internal erosion behaviour and to shed light on the reason for the distress seen in some dams and the ongoing stability of others. The seepage flow rate study showed that a higher hydraulic gradient (equivalent in real geotechnical structures to higher reservoir water levels) in a densely compacted internally erodible soil at 35% fines undergoing shearing does not lead to a significantly greater rate of erosion within the soil, except at the commencement of flow (which is similar to the behaviour without shearing). This suggests that for a given well-constructed dam, whether the reservoir level is relatively high or low, if it is undergoing monotonic shearing (e.g. due to seismic displacement or by adding height to the embankment), this will not significantly alter the amount of soil eroded.

The fines content study was conducted to ascertain the influence of the initial fines content on internal erosion. In addition, by studying a range of dense soil mixtures (from under to over filled), this study can relate to broader material types used in geotechnical structures. This thesis commenced a stress path study where the influence of different stress paths on internal erosion was studied as well as commencing shear rates study where the influence of the shear rate on internal erosion was investigated by shearing the testing samples using different axial displacement rates.

This can model the change in stress state under constant fluid flow in a geotechnical structure, which could be experienced during an earthquake or if the geotechnical structure was altered (loaded/unloaded) externally via, for example, excavation or wall height increase which applies to tailings dams (since they are built continuously upwards). This change in stress state could also occur due to changes in water level behind the geotechnical structure. During those cases, it is vital to understand the erosion behaviour and hence the behaviour of the whole geotechnical structure.

The results revealed that strain rate did not affect the amount of erosion, but overall shearing displacement did - denoting that monitoring of a dam for displacements may allow an engineer to work out how much displacement-induced internal erosion has taken place for a given soil (i.e. if there is internal shearing during an earthquake) if specific displacement-focused lab testing is done on the soil in question.

This research concentration was on studying the behaviour of internal erosion under a continuous change of stress state. Other researchers (as the comprehensive literature review discussed) have investigated the effect of stress state change prior to water flow, i.e. if the water flow stopped, stress state changed, and then water flow re-imposed. The influence on internal erosion would vary depending on the intensity of the stress state change. In general, higher deviatoric stress would lead to lower critical hydraulic gradients and an increase in internal erosion.

Indeed, by investigating the effect of seepage flow, initial fines content, stress path and shearing rate on the onset and progression of internal erosion, this research aimed to lay out a practical knowledge for real-world engineering to use when approaching internal erosion phenomenon.

8.4   Recommendations for further work

- The erosional tests conducted under different shear rate revealed fresh insights into the role played by shear in the internal erosion process. However, the research restricted to limited shear rates. Hence, it is important to investigate the impact of this factor under lower rates perhaps comparable to the time for particles to be driven out from the sample, to examine the influence of path length. The challenge in using lower shearing rates is that the experiments' duration will be increased, and hence more seepage flow de-aired water supply could be needed.

- Coloured soil can be used to study soil erosion in distinguishable colours to ensure that the eroded particles are from the original fines content and not a product of crushing within the coarse matrix and to use different fine particles colour in each layer to be able to visually investigate the soil erosion process (Appendix A).

- In all of the main series of tests, the hydraulic gradient i was above 10. This is because very little erosion was detected in a static (no shear) situation at gradients lower than this (Appendix B). It would be interesting to see how the critical hydraulic gradient is influenced by shear - in other words, conduct shearing tests at lower hydraulic gradients in future.

- The triaxial permeameter can be used for different erosional testing applications. Different soil type, gap ratio, fines content or density (e.g. loose soils) can be studied using the triaxial permeameter. Furthermore, the triaxial permeameter can be used for tests conducted

at a constant q and p′ (e.g. following the stress path B but without flow and starting seepage at values along the stress path).

- Although the factor of time is rarely taken into account in the majority of literature, it constitutes an important agent controlling the erosion process. The majority of laboratory permeameter tests are relatively short with respect to embankment dams loading and unloading periods. Therefore, it is very important to develop new concepts of long-term erosional experiments in order to shed light on this neglected factor of time.

Appendix A

Previous trial of coloured model soil samples

Model soil samples of aquarium sand and gravel, Figure A.1, with a specific gravity, Gs, of 2.72 were used initially to study soil erosion in distinguishable colours to ensure that the eroded particles are from the original fines content and not a product of crushing within the course matrix and to use different fine particles colour in each layer to be able to visually investigate the soil erosion process.

FIGURE A.1: Model soil samples
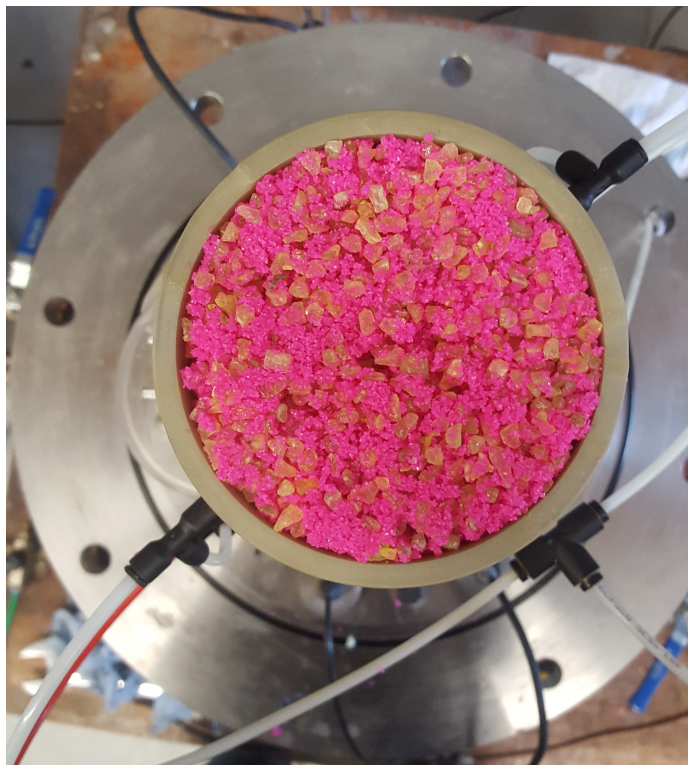
FIGURE A.2: Model soil samples

The fine particles were not eroding at the expected hydraulic gradient. A microscopic investigation reveals the reason, Figure A.3. The fine particles were shaped as cubes, and this did affect the soil erosion progress. The particle size distribution used for the coloured soil is illustrated in Figure A.4.
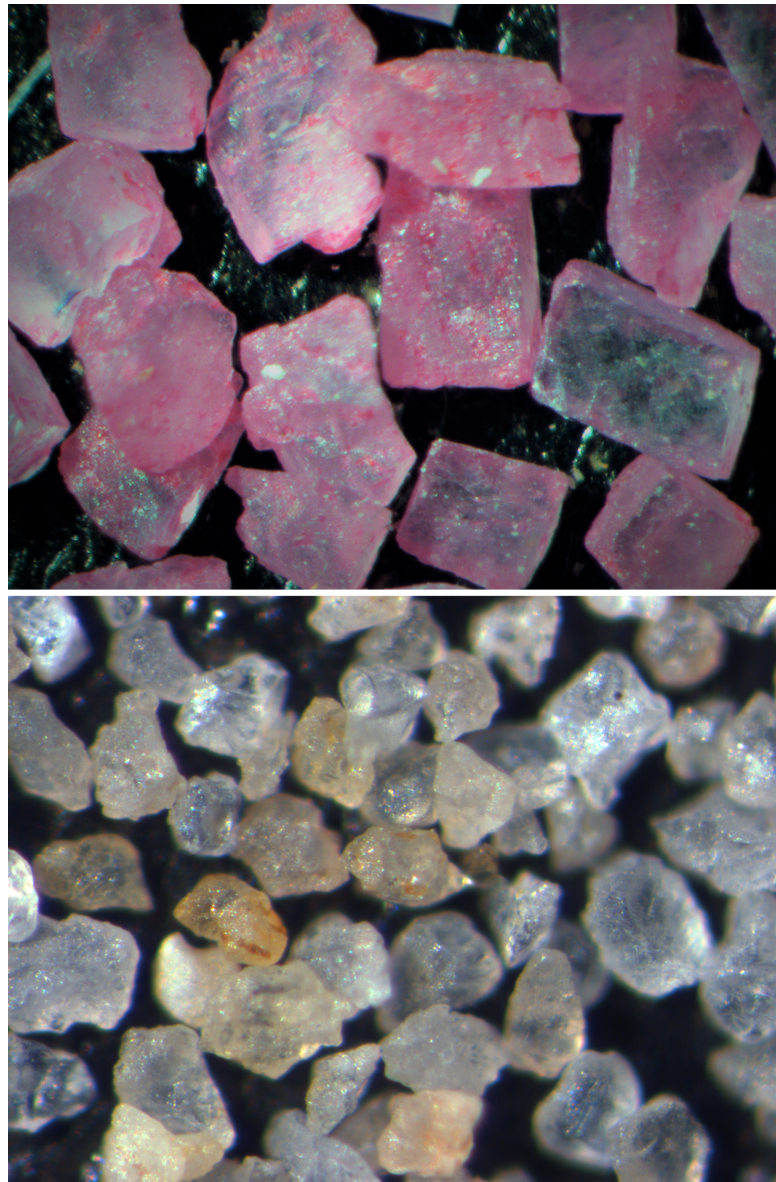
FIGURE A.3: Microscopic image of the model soil (top) and Leighton Buzzard sand fraction D (bottom)
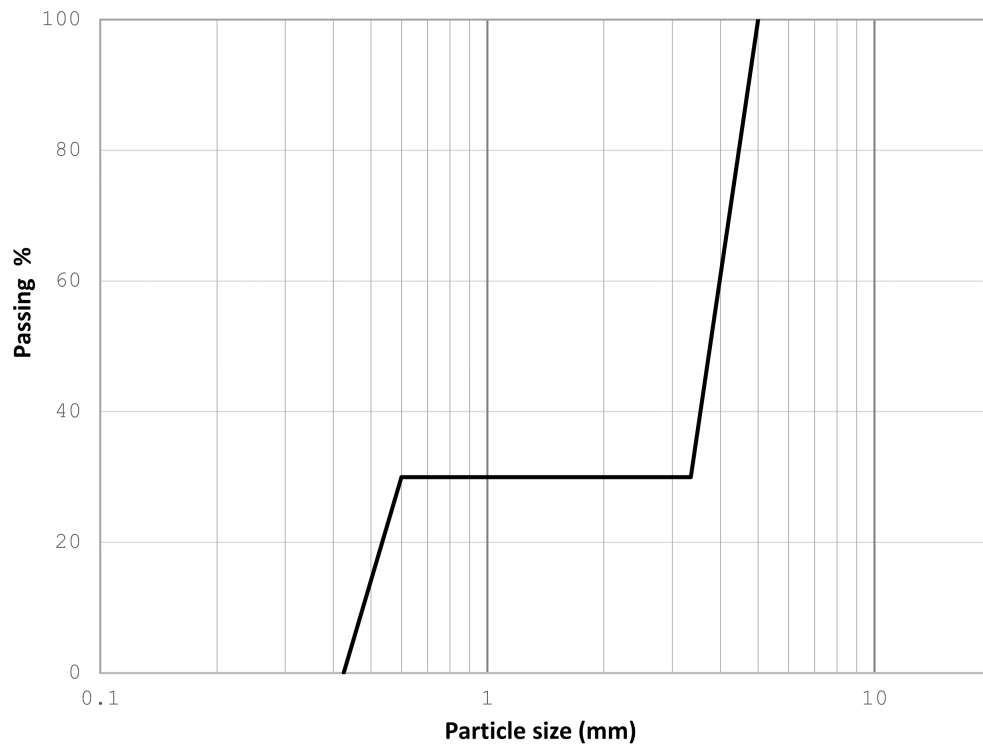
FIGURE A.4: Particle size distribution used for coloured soil

Appendix B

Observational tests

Observational tests were needed to identify the ideal range of hydraulic gradients to study the behaviour of internal erosion in dense gap-graded soil.

B.1   Seepage flow while shearing

The initial observational test was conducted while shearing the sample to determine the ideal range of hydraulic gradients to study the seepage flow behaviour for the soils examined in the thesis at the initial stress state chosen. A soil with 35% initial fines content was tested, the sample was prepared, saturated and consolidated using the method described in Chapter 3. The test was commenced by shearing the sample (0.1 mm/min), while the hydraulic gradient was increased in stages to the final value of 26 (i.e., 2 per 5 minutes).

A hydraulic gradient of 10 was found to be the minimum sufficient gradient to cause measurable fines loss under the initial conditions (Figure B.1).

Also, it was observed that a step of 4 to 6 in hydraulic gradient would be adequate to observe a physical change in erosional behaviour.
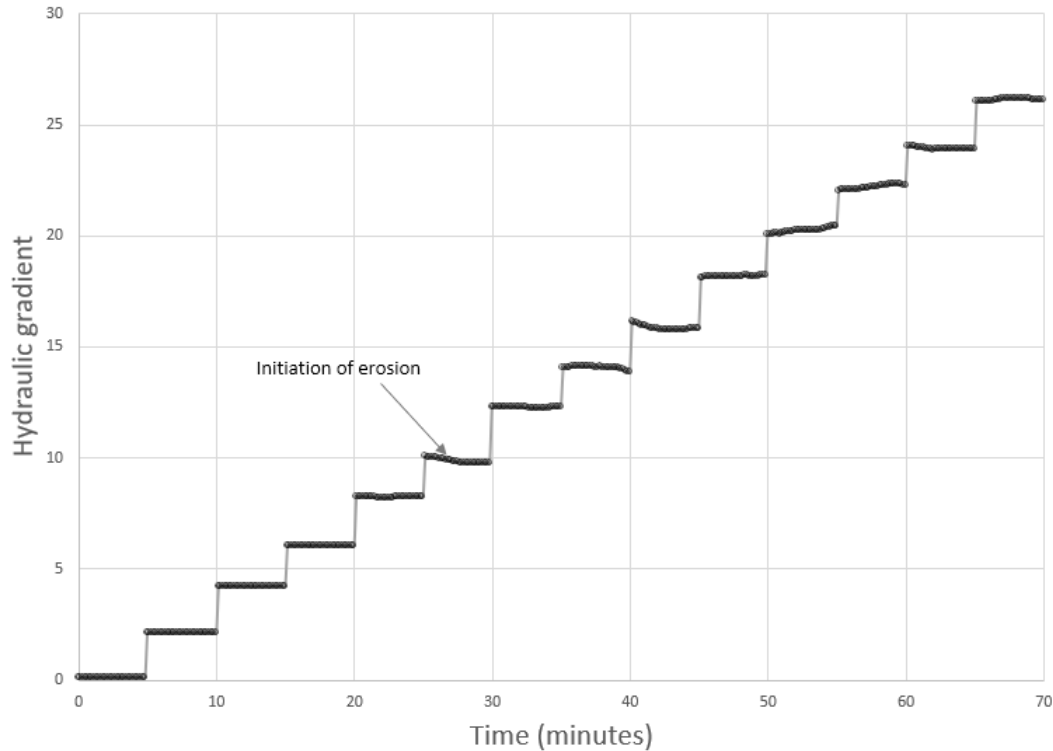
FIGURE B.1: Hydraulic gradient vs time for the observational test

B.2   Seepage flow no shearing

The same experiment was repeated without shearing the sample, and there was no measurable fines loss until the hydraulic gradient of 14 was reached, but the soil erosion was stopped after about 1 minute. There were fines loss with each hydraulic gradient increment, but this loss was in general ending after about 1 minute. The erosion rate decreased to zero before the hydraulic gradient was increased in a stepwise procedure.

Analysing the results from the observational tests, there were two choices to get a continuous erosion (for the chosen initial conditions), either by increasing the hydraulic gradient in stepwise procedure or conduct the erosional tests while shearing. For the purpose of this research, it has been decided to shear all samples while conducting the erosion testing.

Appendix C

Additional Graphs

C.1   Hydraulic gradient
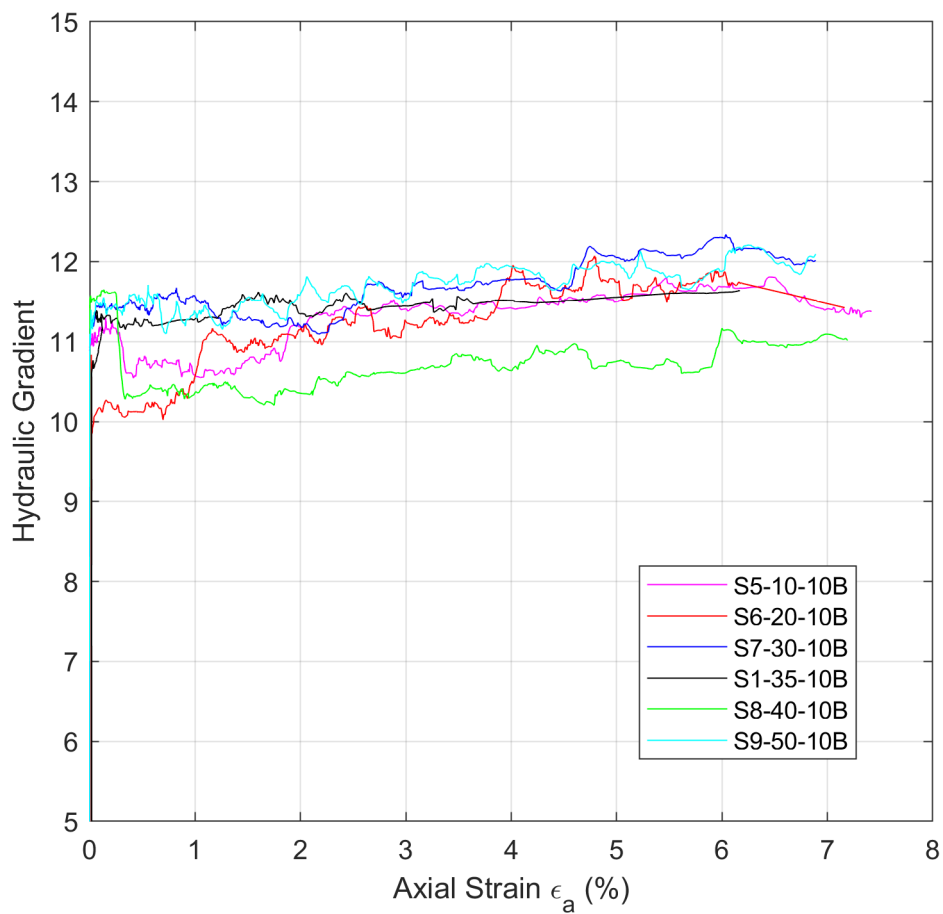
FIGURE C.1: Relationship between hydraulic gradient and local
axial strain
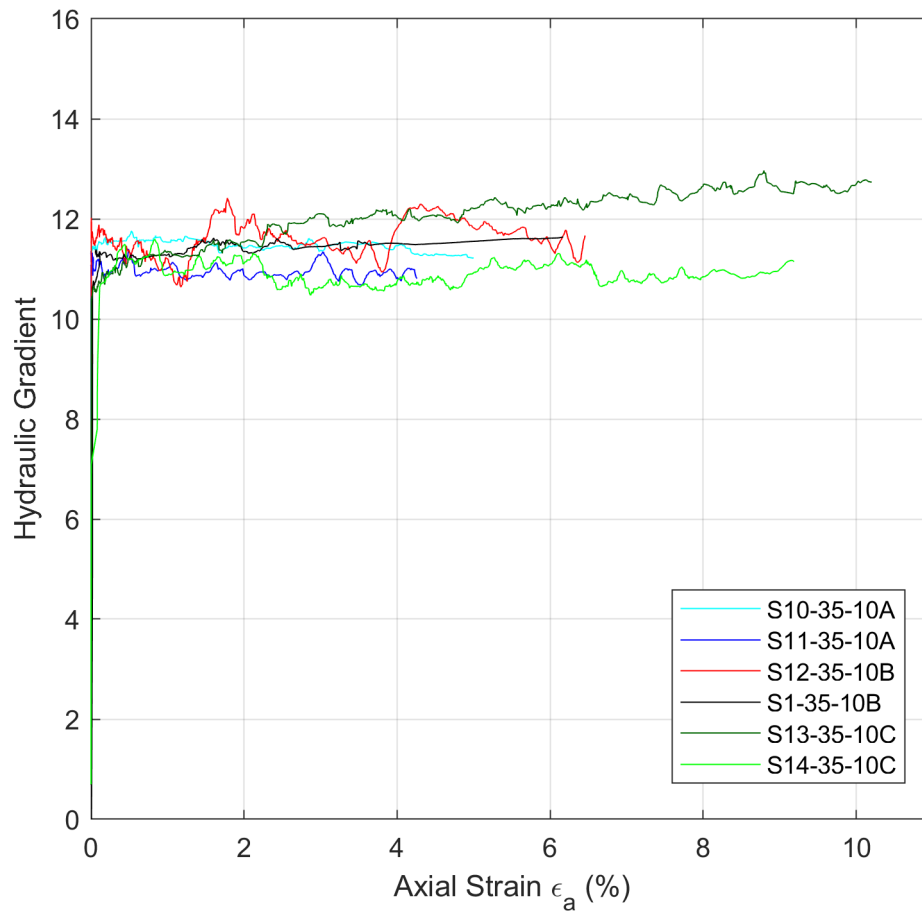
FIGURE C.2: Relationship between hydraulic gradient and local axial strain
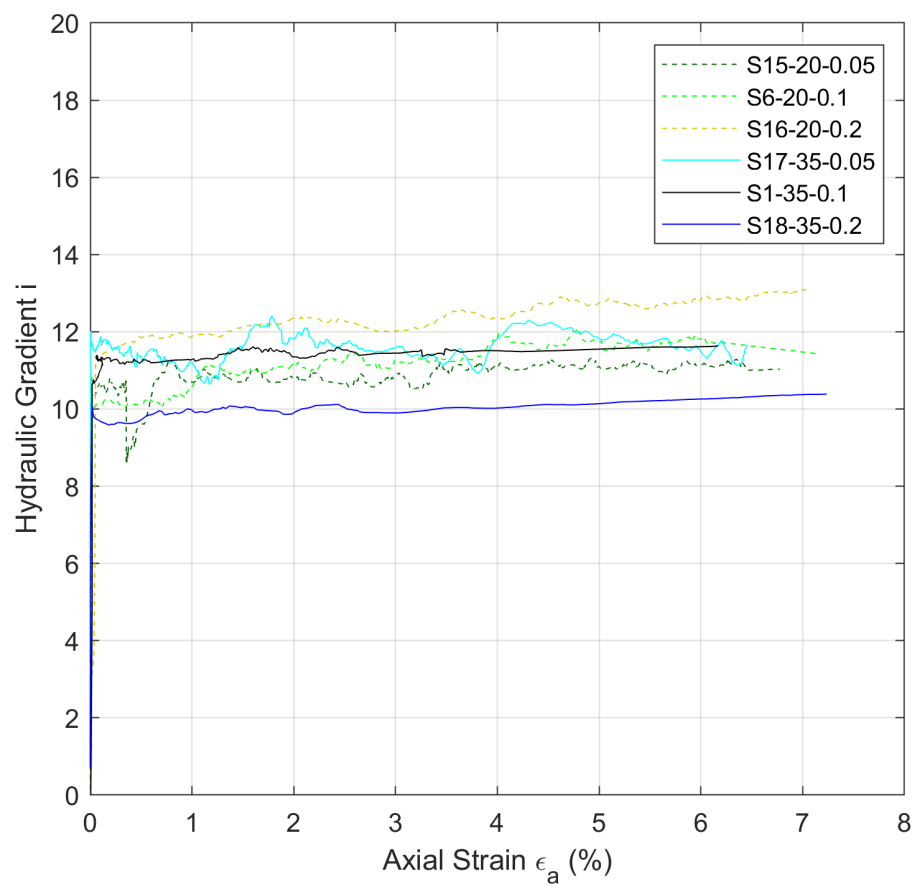
FIGURE C.3: Relationship between hydraulic gradient and local
axial strain

C.2 Seepage velocity
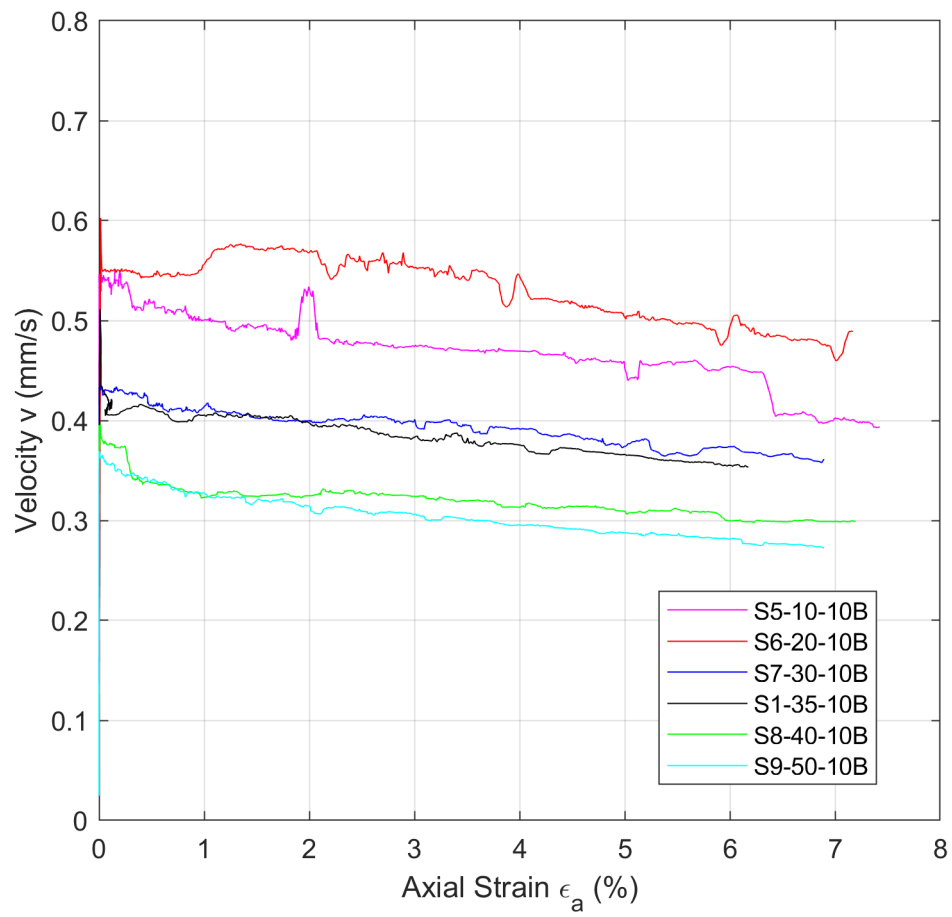
FIGURE C.4: Seepage velocity versus local axial strain
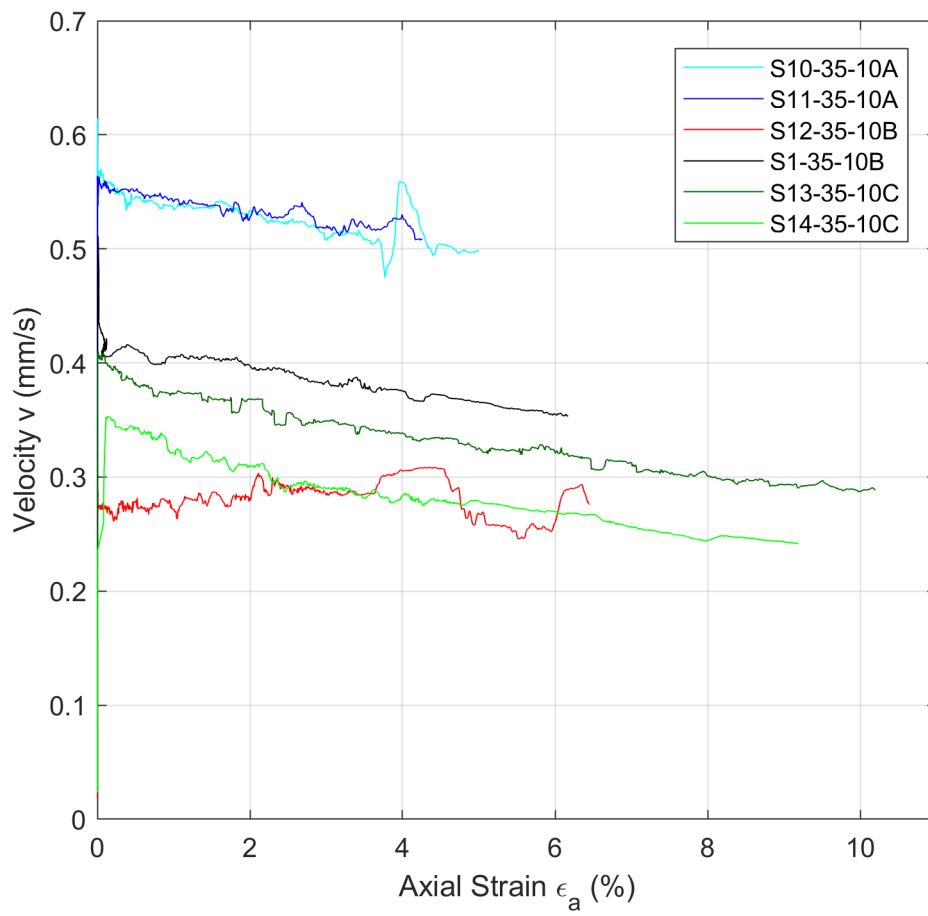
FIGURE C.5: Seepage velocity versus local axial strain
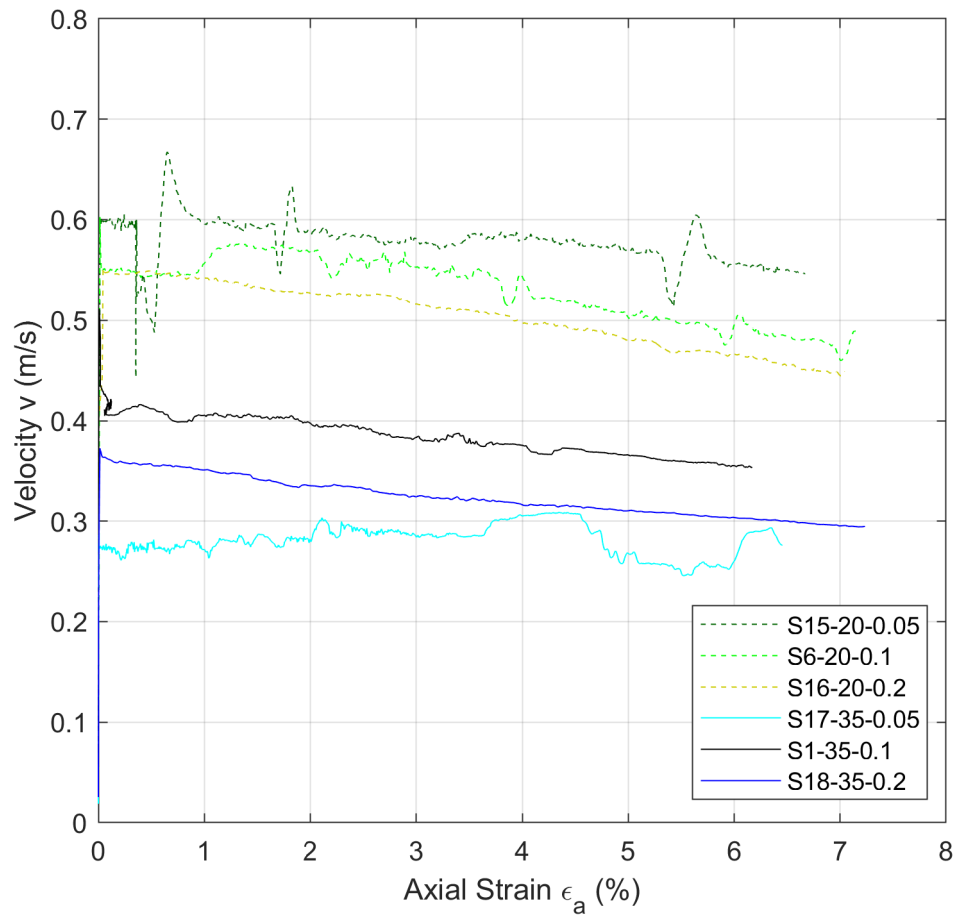
FIGURE C.6: Seepage velocity versus local axial strain

Bibliography

BBC (2019). "Whaley bridge: How safe ARE BRITAIN'S DAMS?" In: *BBC News*. URL: https://www.bbc.co.uk/news/uk-england-derbyshire-49196766.

Bendahmane, Fateh, Didier ot, and Alain Alexis (2008). "Experimental parametric study of suffusion and backward erosion". In: *Journal of geotechnical and geoenvironmental engineering* 134.1, pp. 57–67.

Bishop, Alan W and Gordon E Green (1965). "The influence of end restraint on the compression strength of a cohesionless soil". In: *Geotechnique* 15.3, pp. 243–266.

Bonelli, Stéphane (2013). *Erosion in geomechanics applied to dams and levees*. John Wiley & Sons.

Brown, AJ and RC Bridle (2008). "Progress in assessing internal erosion". In: *Ensuring reservoir safety into the future: Proceedings of the 15th Conference of the British Dam Society at the University of Warwick from 10–13 September 2008*. Thomas Telford Publishing, pp. 29–38.

Burenkova, VV (1993). "Assessment of suffusion in non-cohesive and graded soils". In: *Filters in geotechnical and hydraulic engineering. Balkema, Rotterdam*, pp. 357–360.

Carraro, J Antonio H, Monica Prezzi, and Rodrigo Salgado (2009). "Shear strength and stiffness of sands containing plastic or nonplastic fines". In: *Journal of geotechnical and geoenvironmental engineering* 135.9, pp. 1167–1178.

Cavallaro, Antonio, Michele Maugeri, and Rosalia Mazzarella (2001). "Static and dynamic properties of Leighton Buzzard sand from laboratory tests". In:

Chang, Dong Sheng and Li Min Zhang (2013). "Critical hydraulic gradients of internal erosion under complex stress states". In: *Journal of Geotechnical and Geoenvironmental Engineering* 139.9, pp. 1454–1467.

Chang, DS and LM Zhang (2011). "A stress-controlled erosion apparatus for studying internal erosion in soils". In: *Geotechnical Testing Journal* 34.6, pp. 579–589.

Chang, DS, Limin Zhang, and TH Xu (2012). "Laboratory investigation of initiation and development of internal erosion in soils under complex stress states". In: *ICSE6 Paris*.

Charles, J.A. (2005). "ENGINEERING GEOLOGY | Made Ground". In: ed. by Richard C. Selley, L. Robin M. Cocks, and Ian R. Plimer, pp. 535–542. DOI: `https://doi.org/10.1016/B0-12-369396-9/00218-5`. URL: `https://www.sciencedirect.com/science/article/pii/B0123693969002185`.

Chen, Chen, Li Min Zhang, and Dong Sheng Chang (2016). "Stress-strain behavior of granular soils subjected to internal erosion". In: *Journal of Geotechnical and Geoenvironmental Engineering* 142.12, p. 06016014.

Crawford-Flett, Kaley A (2014). "An improved hydromechanical understanding of seepage-induced instability phenomena in soil". PhD thesis. University of British Columbia.

Cundall, Peter A and Otto DL Strack (1979). "A discrete numerical model for granular assemblies". In: *geotechnique* 29.1, pp. 47–65.

Deutsches-Talsperrenkomitee (2007). "Assessment of the Risk of Internal Erosion of Water Retaining Structures: Dams, Dykes and Levees". In: *Intermediate Report of the European Working Group of ICOLD Symposium*.

Fannin, Jonathan (2008). "Karl Terzaghi: from theory to practice in geotechnical filter design". In: *Journal of geotechnical and geoenvironmental engineering* 134.3, pp. 267–276.

Fell, Robin and Jean-Jacques Fry (2007). *Internal Erosion of Dams and Their Foundations: Selected and Reviewed Papers from the Workshop on Internal Erosion and Piping of Dams and their Foundations, Aussois, France, 25-27 April 2005.* CRC Press.

Garner, SJ and RJ Fannin (2010). "Understanding internal erosion: a decade of research following a sinkhole event". In: *The international journal on hydropower & dams* 17.3, p. 93.

Honjo, Y, MA Haque, and KA Tsai (1996). "Self-filtration behaviour of broadly and gap-graded cohesionless soils". In: *Proceedings of Geofilters.* Vol. 96, pp. 227–236.

ICOLD (2014). "A dam with a height of 15 metres". In: *ICOLD.* URL: `https://www.icold-cigb.org/GB/dams/definition_of_a_large_dam.asp`.

Ke, Lin and Akihiro Takahashi (2014). "Triaxial erosion test for evaluation of mechanical consequences of internal erosion". In: *Geotechnical Testing Journal* 37.2, pp. 347–364.

Kenney, TC and D Lau (1985). "Internal stability of granular filters". In: *Canadian geotechnical journal* 22.2, pp. 215–225.

– (1986). "Internal stability of granular filters: Reply". In: *Canadian Geotechnical Journal* 23.3, pp. 420–423.

Kézdi, A (1979). *Soil physics-selected topics-developments in geotechnical engineering-25.* Tech. rep.

Ladd, RS (1978). "Preparing test specimens using undercompaction". In: *Geotechnical testing journal* 1.1, pp. 16–23.

Li, Deying et al. (2017). "Effect of over-consolidation and shear rate on the residual strength of soils of silty sand in the Three Gorges Reservoir". In: *Scientific Reports* 7.1, pp. 1–11.

Li, M and RJ Fannin (2012). "A theoretical envelope for internal instability of cohesionless soil". In: *Géotechnique* 62.1, pp. 77–80.

Li, Maoxin (2008). "Seepage induced instability in widely graded soils". PhD thesis. University of British Columbia.

Li, Maoxin and R Jonathan Fannin (2008). "Comparison of two criteria for internal stability of granular soil". In: *Canadian Geotechnical Journal* 45.9, pp. 1303–1309.

Liang, Yue et al. (2017). "Onset of suffusion in upward seepage under isotropic and anisotropic stress conditions". In: *European Journal of Environmental and Civil Engineering* 23.12, pp. 1520–1534.

Luo, Yu-long et al. (2013). "Hydro-mechanical experiments on suffusion under long-term large hydraulic heads". In: *Natural hazards* 65.3, pp. 1361–1377.

Marot, Didier, Pierre-Louis Regazzoni, and Tony Wahl (2011). "Energy-based method for providing soil surface erodibility rankings". In: *Journal of Geotechnical and Geoenvironmental Engineering* 137.12, pp. 1290–1293.

Moffat, Ricardo (2005). "Experiments on the internal stability of widely graded cohesionless soils". PhD thesis. University of British Columbia.

Moffat, Ricardo and R Jonathan Fannin (2011). "A hydromechanical relation governing internal stability of cohesionless soil". In: *Canadian Geotechnical Journal* 48.3, pp. 413–424.

Moffat, Ricardo, R Jonathan Fannin, and Stephen J Garner (2011). "Spatial and temporal progression of internal erosion in cohesionless soil". In: *Canadian Geotechnical Journal* 48.3, pp. 399–412.

Moffat, Ricardo A and R Jonathan Fannin (2006). "A large permeameter for study of internal stability in cohesionless soils". In: *Geotechnical Testing Journal* 29.4, pp. 273–279.

O'Sullivan, Catherine (2011). "Particle-based discrete element modeling: geomechanics perspective". In: *International Journal of Geomechanics* 11.6, pp. 449–464.

Ouyang, Mao and Akihiro Takahashi (2015). "Optical quantification of suffosion in plane strain physical models". In: *Géotechnique Letters* 5.3, pp. 118–122.

Powrie, William (2018). *Soil mechanics: concepts and applications*. CRC Press.

Prasomsri, Jitrakon and Akihiro Takahashi (2020). "The role of fines on internal instability and its impact on undrained mechanical response of gap-graded soils". In: *Soils and Foundations* 60.6, pp. 1468–1488.

Richards, Kevin S and Krishna R Reddy (2007). "Critical appraisal of piping phenomena in earth dams". In: *Bulletin of Engineering Geology and the Environment* 66.4, pp. 381–402.

Shire, Thomas et al. (2014). "Fabric and effective stress distribution in internally unstable soils". In: *Journal of Geotechnical and Geoenvironmental Engineering* 140.12, p. 04014072.

Shuler, U (1995). "How to deal with the problem of suffusion". In: *Research and development in the field of dams, Swiss National Committee in Larges Dams*.

Shwiyhat, Nathan and Ming Xiao (2010). "Effect of suffusion on mechanical characteristics of sand". In: *Scour and Erosion*, pp. 378–386.

Skempton, AW and JM Brogan (1994). "Experiments on piping in sandy gravels". In: *Geotechnique* 44.3, pp. 449–460.

Slangen, P and RJ Fannin (2017). "A flexible wall permeameter for investigating suffusion and suffosion". In: *Geotechnical Testing Journal* 40.1, pp. 1–14.

Terzaghi, Charles (1935). "discussion of Uplift and Seepage Under Dams on Sand". In: *Trans. ASCE* 100, p. 1395.

Terzaghi, Karl (1939). "45th james forrest lecture, 1939. soil mechanics-a new chapter in engineering science". In: *Journal of the Institution of Civil Engineers* 12.7, pp. 106–142.

Thevanayagam, S (1998). "Effect of fines and confining stress on undrained shear strength of silty sands". In: *Journal of Geotechnical and Geoenvironmental Engineering* 124.6, pp. 479–491.

Tomlinson, Scott Stewart and YP Vaid (2000). "Seepage forces and confining pressure effects on piping erosion". In: *Canadian Geotechnical Journal* 37.1, pp. 1–13.

Wan, Chi Fai and Robin Fell (2004). "Investigation of rate of erosion of soils in embankment dams". In: *Journal of geotechnical and geoenvironmental engineering* 130.4, pp. 373–380.

– (2008). "Assessing the potential of internal instability and suffusion in embankment dams and their foundations". In: *Journal of geotechnical and geoenvironmental engineering* 134.3, pp. 401–407.

Wautier, Antoine (2018). "Micro-inertial analysis of mechanical instability in granular materials with application to internal erosion." PhD thesis. Diplôme de doctorat de l'université d'Aix Marseille.

Wood, David Muir (1990). *Soil behaviour and critical state soil mechanics*. Cambridge university press.

Xiao, Ming and Nathan Shwiyhat (2012). "Experimental investigation of the effects of suffusion on physical and geomechanic characteristics of sandy soils". In: *Geotechnical Testing Journal* 35.6, pp. 890–900.

Zou, Yu-Hua, Qun Chen, and Chang-Rong He (2013). "A new large-scale plane-strain permeameter for gravelly clay soil under stresses". In: *KSCE Journal of Civil Engineering* 17.4, pp. 681–690.